Insights into the design of an improved PfRH5 malaria immunogen using vaccine-induced monoclonal antibodies

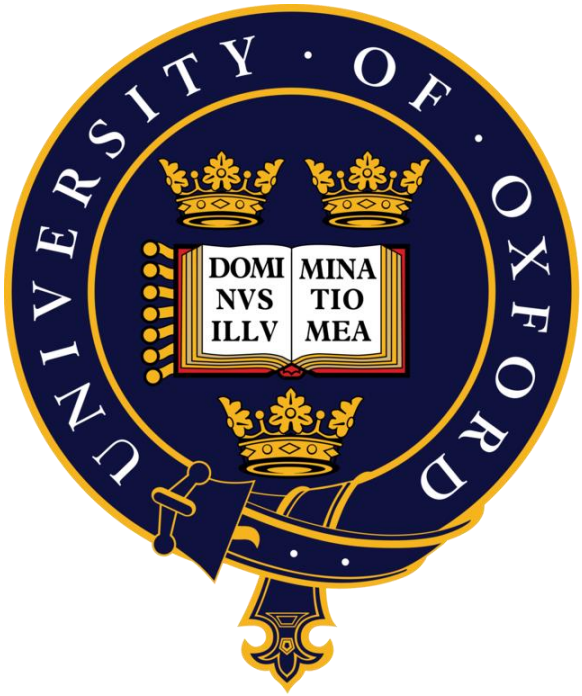

A thesis submitted in fulfilment of
the requirements for the degree
of Doctor of Philosophy

Daniel G. W. Alanine

Linacre College, University of Oxford

October 2017

Word count: circa 43,000 words excluding bibliography and figure legends.

University of Oxford

Abstract

Nuffield Department of Medicine
The Jenner Institute

Doctor of Philosophy

Insights into the design of an improved PfRH5 malaria immunogen using vaccine-induced monoclonal antibodies

By Daniel G. W. ALANINE

The causative agent of the most deadly form of malaria, *P. falciparum*, was identified over 130 years ago, yet this disease still causes 430,000 deaths each year. Although naturally-acquired immunity exists, it requires a heavy and sustained exposure to the parasite, with most succumbing as young children, before this immunity has fully developed. Effective treatments exist but with small-molecule drug resistance on the rise and little in the way of affordable alternatives, the need for an efficacious malaria vaccine is as great as ever. A successful malaria vaccine is likely to necessitate targeting each stage of the parasite's lifecycle. Immunity directed to the blood-stage, the stage which causes all the symptoms of malaria, is unique in that it would allow for a concomitant development of naturally-acquired immunity along with a reduction in morbidity and mortality. To date, antibody-mediated immunity to the blood stage requires intractably high levels of antibody and this problem is compounded by a paucity of viable candidates with which to effectively target different strains. Other fields of vaccinology, over the past decade, have been employing various structure-based strategies to increase the specific activity of the immune response thus lowering the antibody levels required for protection. However, very few detailed investigations of this kind have been conducted on a *P. falciparum* vaccine candidate, and certainly none as promising as PfRH5. In a world's first, fully-human antibodies raised in response to PfRH5 vaccination were isolated and extensively characterised, both functionally and structurally with the intention of elucidating the important features necessary to inform the design of an improved PfRH5-based vaccine. Synergistic and antagonistic effects of antibody combinations were noted and highlight new complexities of the immune response to PfRH5, opening the door to unanticipated potential for rational vaccine design.

Acknowledgements

I write this section with the intent of being more thorough than succinct. Firstly and foremost, as etiquette rightly dictates, I'd like to thank my supervisors Simon Draper and Matt Higgins. Simon, as a supervisor striking that balance between guidance and freedom is no mean feat, but one which you mastered with me. The precision, rigour and structure with which you approach science are exemplary and the amount by which your group has grown during my time here in Oxford (in numbers and breadth of expertise) is a testament to your exceptional managerial qualities (and your impressive hit-rate when it comes to securing grant money!). I am grateful for having been chosen to do my DPhil in this stimulating environment. I'd like to express a separate thanks to you also for being the only person (with the exception of Chapter V) willing to proof-read this thesis, even taking the time to read a chapter less than a week before the submission deadline! Matt, your affinity for order is reflected (yes, pun intended) both in your crystallography expertise and the tidiness of your office. Your relaxed demeanour, patience, drive and aversion for the insipid are all academic ideals. Both of you will have a lasting effect on the trajectory of my future career.

I must thank Julie Furze, Drew Worth, Geneviève Labbé, Rebecca Brown, Jennifer Marshall and Doris Quinkert for their practical and technical support as well as the students (Francesca Donnellan in particular) who spent their Part IIs or DPhil rotations helping my project along.

My gratitude also extends to external collaborators; namely Kazutoyo Miura for his work with the GIA assays, Lander Foquet for so gladly conducting a passive transfer study in his humanised mouse model and Shahid Mehmood for his help with the HDX-MS work. A special shout out goes to Joe Illingworth, not so much for his wilful and sustained criticism of this work but for taking me under his wing since day one at the Jenner Institute. You have earnt my respect as a friend and colleague, and your scepticism and healthy anti-establishmentarian stance on science has certainly shaped me as a scientist.

To my office-mates: Sarah, Rachel (K) and Rachel (T), you all succeeded in making our office area fun, convivial and, for a while, the social hub of the Jenner. Here's to "Matching Mondays", inappropriate workplace chat, cake, and gossip. A special mention goes to Rachel Tanner for being an entertaining desk mate and friend, once you got the first six months of ignoring me out of the way. Warm thanks also go to various Jenner colleagues past and

present: Lynda, Daria, Anita, Kathryn, Danny, Jonathan, Sean, Florian, Carolyn, Tom, Martino and Iona. I'm sure I will look back fondly on my time here in years to come.

Outside of the Jenner bubble, I'd also like to thank the cycling gang of Al, Ben, Isaac, Jakub, James and Angus for making the Oxford University Cycling Club an always fun, usually healthy and sometimes dangerous pastime and an ever-welcome break from academic life.

Thank you Hannah for being infinitely accommodating with me when I (predictably) left most of the thesis writing until the last minute, for reminding me not to come home too late and for your useful essay-writing pointers…

My last thanks go, with love, to those two who have known me the longest: Mum and Dad; for their constant support, for giving me the freedom to make my own mistakes and for trusting me to eventually turn out OK.

Table of contents

List of figures

List of tables

List of appendices

List of acronyms and abbreviations

AAV: Adeno-associated virus

Ab: Antibody

ADCC: Antibody-dependent cell-mediated cytotoxicity

ADRB: Antibody-dependent respiratory burst

ASC: Antibody-secreting cell

AVEXIS: Avidity-based extracellular protein interaction screen

BCIP/NBT: 5-bromo-4-chloro-3'-indolyphosphate / nitro-blue tetrazolium

BCR: B cell receptor

BLI: Bio-Layer interferometry

CD: Cluster of differentiation

CDC: Complement-dependent cytotoxicity

CDR: Complementarity-determining regions

CFCA: Calibration-free concentration analysis

ChAd63: Chimpanzee adenovirus serotype 63

CHMI: Controlled human malaria infection

CPEC: Circular polymerase extension cloning

DMEM: Dulbecco's modified Eagle medium

DNA: Deoxyribonucleic acid

DTT: Dithiothreitol

DVD-Ig: Dual variable domain Immunoglobulin

EC_{50}: Effective concentration to achieve 50% of maximal effect.

ELISA: Enzyme-linked immunosorbent assay

ELIspot: Enzyme-linked immuno spot (assay)

ESI-TOF MS: Electrospray ionisation-tome-of-flight mass spectrometry

Fab: Fragment antigen binding

Fc: Fragment crystallisable

fHbp: Factor H binding protein (*N. meningitidis*)

FPLC: Fast protein liquid chromatography

GIA: Growth inhibitory activity

GPI: Glycosylphosphatidylinositol

HC: Heavy chain

HDX-MS: Hydrogen-deuterium exchange mass spectrometry

HEK293: Human embryonic kidney cell 293

HEPES: (4-(2-hydroxyethyl)-1-piperazineethanesulfonic acid

HIV: Human immunodeficiency virus

IgG: Immunoglobulin G

iRBC: Infected red blood cell

kDa: Kilodalton

LB: Lysogeny broth

LC: Light chain

mAb: Monoclonal antibody

MAC: Membrane attack complex (of complement)

MES: 2-(N-morpholino)ethanesulfonic acid

ME-TRAP: Multiple epitope-thrombospondin-related adhesion protein

MHC: Major histocompatibility complex

MPD: 2-Methyl-2,4-pentanediol

MVA: Modified vaccinia Ankara

MW: Molecular weight

NAI: Naturally acquired immunity

NK: Natural killer (cell)

NMR: Nuclear magnetic resonance

O.D: Optical density

ORF: Open reading frame

pAb: Polyclonal antibody

PABA: 4-aminobenzoic acid

PBMC: Peripheral blood mononuclear cell

PBS: (Dulbecco's) phosphate-buffered saline

PBS-T: (Dulbecco's) phosphate-buffered saline + 0.005% Tween20.

PCR: Polymerase chain reaction

PEG: Polyethylene glycol

PEI: Polyethylenimine

PfAARP: *Plasmodium falciparum* apical asparagine-rich protein

PfAMA-1: *Plasmodium falciparum* apical membrane antigen 1

PfCSP: *Plasmodium falciparum* circumsporozoite protein

PfCyRPA: *Plasmodium falciparum* cysteine-rich protective antigen

PfEBA-175: *Plasmodium falciparum* erythrocyte binding antigen 175

PfEBL-1: *Plasmodium falciparum* erythrocyte binding-like (protein)

PfEMP-1: *Plasmodium falciparum* erythrocyte membrane protein

PfGLURP: *Plasmodium falciparum* glutamate-rich protein

PfMSP-1: *Plasmodium falciparum* merozoite surface protein 1

PfRH5: *Plasmodium falciparum* reticulocyte-binding protein homologue 5

PfRH5ΔNL: *Plasmodium falciparum* reticulocyte-binding protein homologue 5 with the N-terminus (N) and internal loop (L) deleted.

PfRIPR: *Plasmodium falciparum* RH5-interacting protein

PfRON1/2: *Plasmodium falciparum* rhoptry neck (protein)

PfS-antigen: *Plasmodium falciparum* surface-antigen

PfSEA-1: *Plasmodium falciparum* schizont egress antigen-1

PfSERA: *Plasmodium falciparum* serine repeat antigen

PMR: Parasite multiplication rate

PNPP: p-Nitrophenyl phosphate

PvDBP: *Plasmodium vivax* Duffy-binding protein

RBC: Red blood cell

RMSD: Root-mean-square deviation

RNA: Ribonucleic acid

RPMI medium: Roswell Park Memorial Institute medium

RSV: Respiratory syncytial virus

RT-PCR: reverse-transcriptase-polymerase chain reaction

SDS-PAGE: Sodium dodecyl sulphate polyacrylamide gel electrophoresis

SEC: Size-exclusion chromatography

SHM: Somatic hypermutation

SNP: Single nucleotide polymorphism

SPR: Surface plasmon resonance

TBE: Tris/borate/ethylenediaminetetraacetic acid

TCR: T cell receptor

TFF: Tangential flow filtration

T_{FH} cell: T follicular helper cell

TROSY NMR: Transverse relaxation-optimised spectroscopy nuclear magnetic resonance

V_H: Variable heavy region, used interchangeably with Vγ in less specific contexts

V_L: Variable light region. This is an umbrella term for Vκ and Vλ.

VSA: Variant surface antigen

Vγ: Gamma (heavy)-chain variable region

Vκ: Kappa (light)-chain variable region

Vλ: Lambda (light)-chain variable region

WHO: World health organization

Chapter I: Introduction

1.1 Antibodies and immunity

Immunoglobulin molecules, also known as antibodies, are one of the major driving forces of immunity in mammals. Antibodies exist in abundance in extracellular fluids such as blood, lymph, cerebrospinal fluid and mucosal secretion and are the primary defence mechanism against many extracellular pathogens. Antibodies are expressed exclusively by the B cell lineage and the vast majority of serum immunoglobulin is expressed by specialised terminally differentiated B cells called plasma cells found in the bone marrow. Immunoglobulins serve their immunological function through several mechanisms:

-Opsonisation, whereby antibody recognises pathogenic determinants, directing immune cells to the pathogen via the Fc (fragment crystallisable) to mediate phagocytosis by macrophages, dendritic cells and neutrophils or degranulation of lytic mediators mainly by neutrophils, eosinophils and natural killer (NK) cells.

-Complement lysis of pathogens in the classical pathway by fixing C1q, again via the antibody Fc, triggering an enzymatic cascade resulting in the pore-forming membrane attack complex (MAC).

-Neutralisation of toxins or pathogen ligands by trapping or agglutinating them in immune complexes and interfering with interactions critical for the pathogen's survival.

Immunoglobulin G (IgG) comprises the majority of serum antibody of which there are four subclasses in humans (IgG1, 2, 3 and 4) each with a unique combined phenotype with respect to serum abundance, Fcγ-receptor binding affinity, complement activation, protein sequence,

hinge flexibility and ability to cross the placenta amongst other characteristics. IgG molecules are abundant serum glycoproteins with a global "Y"- or "T"-shaped 3-domain architecture composed of two highly variable antigen-binding domains (Fab) connected to an effector function-transducing constant region (Fc) by a flexible hinge region (see Figure 1.1). IgG molecules are highly dynamic and flexible proteins; electron microscopy and cryo-electron tomography have revealed the breadth of conformations the protein can adopt. Each Fab arm is able to rotate about its axis with up to 160° of freedom and Fab-Fab/Fab-Fc angles can both reach 60° in a bound state[1,2]. IgG are c. 150kDa heterodimers of disulphide bonded heavy- and light-chain proteins of approximately 50kDa and 25kDa, respectively.

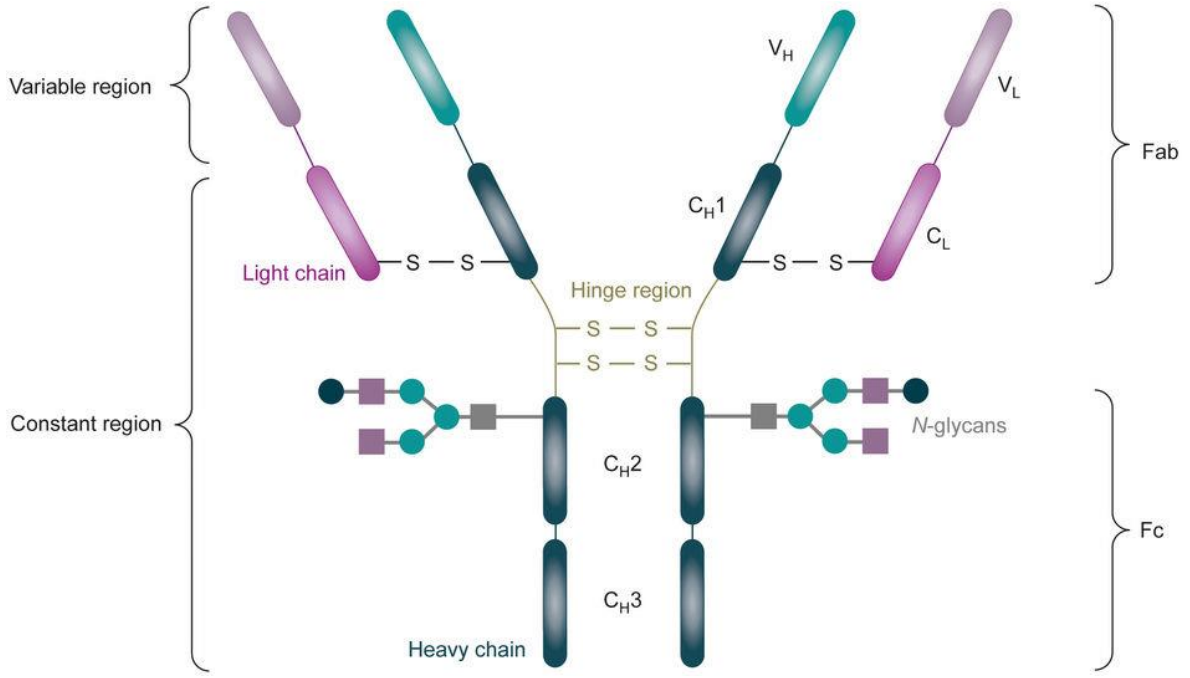

Figure 1.1: Diagram of IgG1. Nomenclature and abbreviations relating to the different antibody protein domains are also shown. Figure taken from Chudasama *et al*[3].

1.1.1 The antibody-coding transcript

The strength of antibodies lies in the breadth of different epitopes they are theoretically able to bind. The strategy employed by the humoral arm of the immune system is to cover a vast array of possible epitopes, negatively select against host epitopes in the bone marrow and allow non-reactive B cells to enter the lymphatic system. The ways B cells generate antibody diversity was elucidated by Susumu Tonegawa and others in the late 1970s and early 1980s, earning him sole receipt of the Nobel Prize for Physiology and Medicine in 1987.

Antibody heavy chains and light chains are encoded by different multigene families but the genetic rearrangement processes that generate diversity, as well as their final genetic organisation, are very similar. The variable heavy (V_H) and variable light (V_L) domains are the sole contacts with the target and therefore are wholly responsible for antigen binding. These domains are, as their names suggest, highly diverse in sequence due to four major diversity generation processes, three early in the development of a B cell and another in activated B cells. In early naïve B cells, an antibody V_H domain transcript is assembled from one of 65 variable heavy exons (V_H), one of 27 diversity exons (D) and one of 6 joining heavy exons (J_H). Likewise V_L domain transcripts are assembled from one of 70 variable light exons (V_L) and one of 9 joining light exons (J_L) in what is termed "combinatorial diversity"[4]. Furthermore, at the junction between any two variable exons containing recombination signal sequences, up to 20 so-called P- and N-nucleotides can be added by the careful action of enzymes RAG-1/2 and TdT to generate further "junctional diversity". Any given antigen binding site is a complex spatio-chemical environment composed most commonly of both the V_H and V_L domains. The third type of diversity arising in early B cell development is heavy chain (HC) and light chain (LC) pairing which will give rise to as many additional binding sites as there are HCs and LCs which are able to functionally pair.

The estimated pre-immune repertoire of human B cells is upwards of 100 billion[5,6]. The final major source of sequence diversity in antibody paratopes is somatic hypermutation (SHM). Although this process rarely changes the specificity of binding, it is usually viewed as a procedure for enhancing pre-existing affinity for a target. SHM takes place in activated B cells at lymphoid sites called germinal centres, whereby point mutations are accrued preferentially in certain variable region zones due to the action of the Activation Induced cytidine Deaminase (AID) enzyme and an error-prone base pair excision and DNA polymerase repair process. The mutations happen non-specifically and most result in either no enhancement in affinity or a non-productive mutation. The B cells which do get an increase affinity for the target through SHM are positively selected by clonal expansion. The combination of these processes is responsible for the 3 spikes in amino acid diversity observed at each of the antibody's four variable domains; these are the complementarity determining regions (CDRs) which play the major role in determining binding specificity. The variable domain regions which flank the CDRs are known as framework regions (FWR) and are much more conserved in sequence; they are crucial regions in the molecule as their name suggests, providing a platform to orient the CDRs outwards. The constant domain of a heavy chain (C_H1, C_H2 and C_H3 in Figure 1.1) or light chain (C_L in Figure 1.1) is encoded by a single exon in every B cell. In the case of the heavy chain, one of 9 exons (Cμ, Cδ, Cγ3, Cγ1, Cα1, Cγ2, Cγ4, Cε and Cα2) is selected and in the case of the light chain one of 5 exons (Cκ, Cλ1, Cλ2, Cλ3 and Cλ4) is selected. Although all B cells begin with Cμ or Cδ constant domains, these are usually substituted for another of the remaining 7 constant domain exons by splicing during isotype class-switching which occurs after the variable region exons have been irreversibly recombined in activated B cells. A typical example of a mature secreted IgG1-Kappa heavy chain and light chain open reading frames (ORF) are depicted in Figure 1.2.

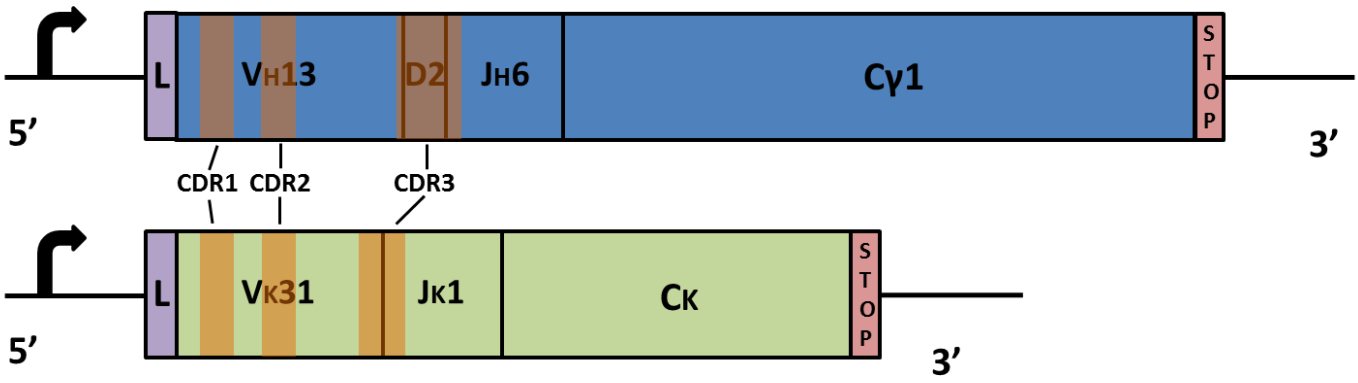

Figure 1.2: Schematic of an IgG1 heavy and light chain ORFs. A diagram of a gamma heavy ORF (top) and a kappa light chain ORF (bottom) are shown. The purple "L" at the 5' end denotes the secretory leader peptide.

1.2 Malaria

Malaria is an ancient disease, almost certainly older than mankind, and many civilisations over the ages have been afflicted by this disease. From the ancient Greeks through the Huns to modern day man, it is thought that malaria has played a role in shaping history for millennia. More recently, in 1996, the director of the US Navy malaria research program Dr. (Capt.) S. Hoffman remarked that "In every military campaign this century, we lost more casualties to malaria than bullets. During World War II and the Vietnam War entire divisions ceased to be effective combat units due to malaria". Even today malaria remains the biggest parasitic killer on earth and the importance of malaria as a human disease has been acknowledged by the award of five Nobel prizes for research into combatting it and by it being the focus of a WHO world eradication campaign since 1955.

Malaria's modern English name was taken from medieval Italian meaning "bad air", betraying an assumption that the disease was transported through the air. It wasn't until the late 1890s that this assumption was shown to be rather prescient when Ronald Ross and Giovanni Grassi first conclusively showed that the *Anopheles* mosquito was responsible for

transmitting the disease in humans. Like most microbial diseases it wasn't until the germ theory revolution in the second half of the 19th century that malaria began to be studied and characterised further than just the symptoms it caused. It was Charles Laveran, a French army surgeon who first linked a blood-borne parasite he observed in the blood of a soldier in Algeria with the malaria disease in 1880 and the still relatively unknown Camillo Golgi who first noted the existence of morphologically different malaria parasites a few years later. Today, there are six species of *Plasmodium* parasites known to cause malaria in humans: *P. falciparum*, *P. ovale curtisii*, *P. ovale wallikeri* (*P. ovale* has recently been shown to consist of two sympatric subspecies[7]), *P. vivax*, *P. malariae* and *P. knowlesi*. Each of these species exist as multiple related strains but by far the most deadly of those are the *falciparum* strains of malaria; any further reference of "malaria" will be implicitly understood to be of the *falciparum* species, unless stated otherwise.

The latest reports by the WHO estimate 212 million cases of malaria (all species) resulting in 429,000 deaths a year. The world-wide distribution of malaria (Figure 1.3) follows tropical climatic conditions that favour the survival and proliferation of *Anopheles* mosquitoes but also negatively correlates with the distribution of global wealth[8].

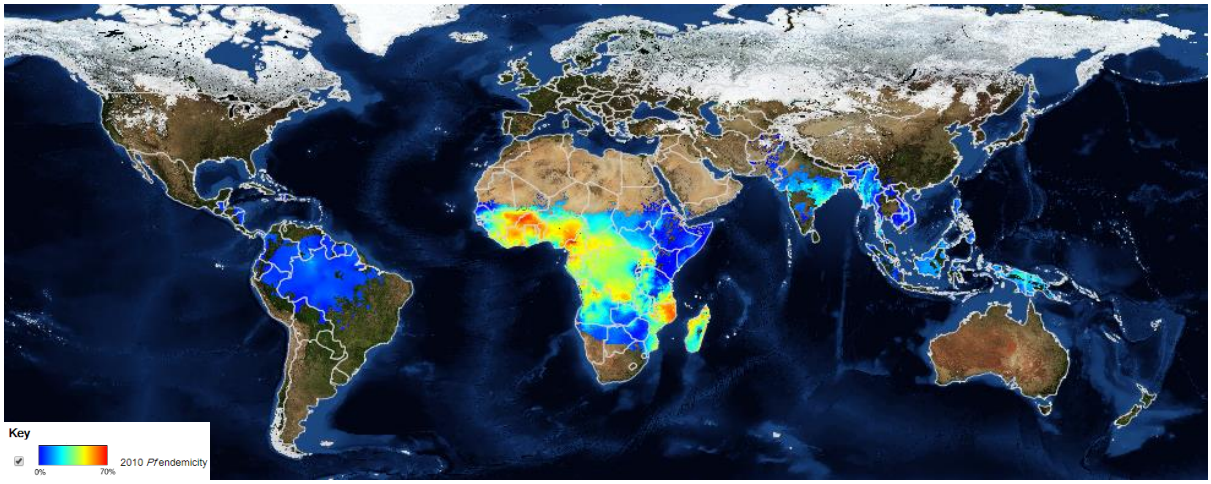

Figure 1.3: Global distribution of *P. falciparum* malaria in 2010 (http://map.ox.ac.uk/explorer/)

1.2.1 The *P. falciparum* lifecyle

The malaria lifecycle is complex and multifaceted (Figure 1.4). The lifecycle can be naturally split into three main stages: The liver- or pre-erythrocytic stage and the blood- or erythrocytic stage in the human host and the sexual- or sporogonic-stage in the mosquito host (Figure 1.4).

The liver-stage begins with the bite of an infected female *Anopheles* mosquito where around 15 or more[9] haploid parasites called sporozoites are injected into the dermis[10,11] or bloodstream. Highly motile, these cells migrate from the dermis to the blood and via the central circulation system to the liver where they infect hepatocytes in a matter of minutes from entering the blood[12]. Here the sporozoites traverse several hepatocytes including liver-resident Kupffer cells before coming to a halt. The specific invasion process is still incompletely understood but is thought to involve PfCSP, and PfP36 on the sporozoite and highly-sulfated heparan sulfate proteoglycans, SR-BI, CD81 and EphA2 on the hepatocyte[13–15]. Within the protective confines of a parasitophorous vacuole which keeps plasmodial proteins from entering the class-I MHC processing pathway, the parasite divides and differentiates over the course of 6-7 days in the case of *P. falciparum*. After this time, buds of thousands of merozoites coated in host membrane (merosomes) are released through the layers of hepatoyctes traversed during infection so as to evade destruction by macrophage-like Kupffer cells[16]. Several thousands of merozoites enter the bloodstream from the infection of a single hepatocyte[13].

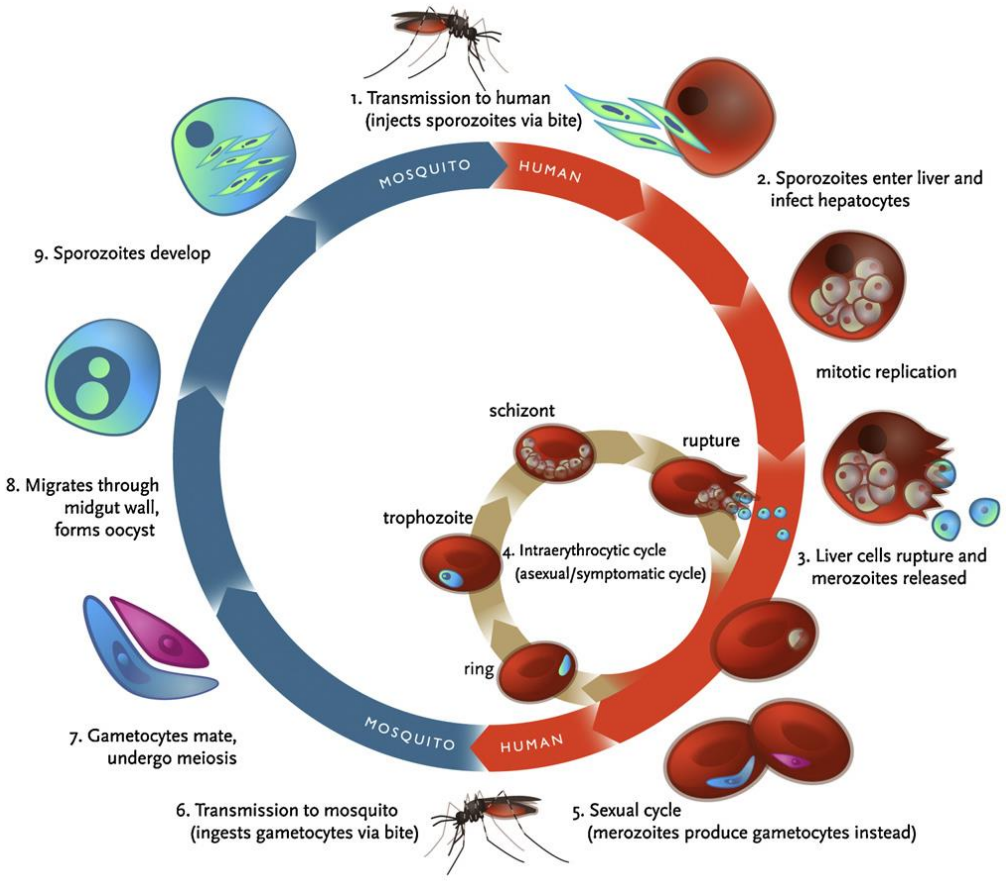

Figure 1.4: *P. falciparum* life cycle diagram. Sexual replication occurs only in the invertebrate host (blue) and asexual replication occurs exclusively in the vertebrate host (red). Figure taken from Klein *et al*[17].

In the blood, the merozoite form of the parasite invades red blood cells (RBCs) in 48h invasion cycles causing the cyclical waves of fever associated with malaria. Through a set of redundant invasion pathways the merozoite is capable of invading reticulocytes and mature RBCs alike[18]. The parasite initiates a complex active invasion process upon contact with RBCs which will be discussed in further detail in section 1.2.4. Upon entry the merozoite undergoes differentiation into three morphologically distinct forms identifiable under magnification with contrast staining. For the first 16 hours the parasites take the form of a ring before the cytoplasm densifies and broadens into a trophozoite. After this the parasite undergoes schizogony to produce a schizont—essentially a RBC sac full of teardrop-shaped merozoites— in the 10-14 hours preceding rupture. It is during this stage that all symptoms

associated with malaria occur. The parasite multiplication rate (PMR) is linked to disease severity[19] and is determined by several factors including the efficiency of invasion and the average number of merozoites each schizont yields (typically 16-32[20]). When the schizont matures and ruptures, most of the products are infectious merozoites entering the quasi-exponential asexual replication phase but around 0.1%[21,22] develop into the sexual form called a gametocyte in response to increased levels of transcription factor PfAP2-G[23]. This central event in assuring the continuity of the life cycle is controlled by exosome-like microvesicle signalling between iRBCs[24].

The final segment of the lifecycle occurs in the mosquito host where again the parasite exists in several distinct forms. When a blood meal contains gametocytes, the increase in pH and decrease in temperature leads to their exflagellation[25,26] (emergence from their RBC coat) into mature sexual gametes. As is the case in human reproduction, the male gamete only is endowed with motility and travels to the female gamete for fertilisation. The resulting zygote matures into an ookinete and, also motile, is able to burrow into the wall of the mosquito midgut where it becomes one of a small number of oocysts producing thousands[27] of genetically recombined sporozoites after approximately 8 days of meiotic activity. These sporozoites migrate to the mosquito's salivary glands, ready to infect the next vertebrate host and complete the lifecycle.

1.2.2 The pathogenesis of malaria

Febrile malaria patients typically present with high fever, headache, nausea, myalgia, vomiting, diarrhoea and anaemia which may progress to localised organ failure, convulsions and death in more extreme instances. The symptoms of uncomplicated malaria are generally non-specific and typical of many infections, thus complicating its rapid diagnosis; typically

malaria infection is confirmed by microscopy on a blood film and/or by PCR. Outside of laboratory settings, so-called rapid diagnostic tests (RDT) based on simple immuno-chromatographic principles can be used for rapid parasite antigen detection. The aetiology of malaria originates entirely from blood-stage infection with the pre-erythrocytic stage being asymptomatic. The various symptoms of acute and severe malaria infection are caused by two main disease processes: the host cytokine response to malaria infection and the sequestration of iRBC in the microvasculature of vital organs. High parasitaemias are of course associated with large quantities of malarial pathogen-associated molecular patterns (PAMP) such as haemozoin[28,29] and GPI[30], waste products from the asexual replication cycle. The systemic inflammatory response to these PAMPs in the form of pro-inflammatory cytokines such as IL-6, IL-1RA, IL-12 and TNFα are thought to be largely responsible for malarial fever[31–34]. In addition, IL-6 and TNFα are known to downregulate erythropoiesis through iron regulation[35] and erythroid transcription factor cleavage[36] respectively, which along with splenic iRBC clearance cause the severe anaemia associated with malaria infection. The infection of erythrocytes causes a number of functional and morphological changes in the host erythrocyte, namely the insertion of cytoadherent knob-like structures composed of highly variable antigens such as the PfEMP-1 family whose function is to sequester the iRBC on endothelia and away from the spleen as an important survival strategy[37]. The most affected organs are the lungs, kidneys, brain, and placenta, probably due to relatively high levels of host receptors for PfEMP-1 variants (CSA, CD36, EPCR, ICAM-1, VCAM-1, TSP) and the low shear force environments in the capillaries of these highly vascularised structures. The systemic and localised cytokine-induced inflammation in these sensitive organs and the ischaemic complications that accompany the blockade of the deep capillaries are the source of most symptoms in complicated malaria infection.

1.2.3 Naturally-acquired immunity to malaria

At the turn of the 20th century, Robert Koch was the first person to describe natural immunity to malaria in a landmark study conducted in Papua New Guinea. In this study, he used blood-films to investigate the different parasite burdens of adults and children local to areas of high and low malaria transmission as well as new arrivals to those areas. The knowledge gained from this study was that adults in high-transmission areas, with evidently equal malaria exposure to children in the same areas, harboured lower levels of blood-stage infection and an absence of malaria symptoms whereas the children harboured high blood-stage parasitaemias and suffered from acute malaria. In low-transmission areas, the parasite burden was more uniform across age groups. The conclusions which emerged from this work clearly showed that there is a naturally-acquired immunity to malaria which is developed over the course of many repeated sub-lethal malaria infections in a species-specific way. Immunity is developed continuously with a gradual decrease in both blood-borne parasite load and symptom severity. Severe malaria is uncommon in endemic settings past late childhood[38]. Hyper-immune adults living in high-transmission areas show sub-patent levels of blood-stage infection and are asymptomatic[39]. Since the seminal work by Cohen *et al.* in the early 1960s[40], it has been known that passively-transferred antibody from naturally immune individuals is sufficient for the conferral of immunity to acute malaria infection. Subsequently it was shown that anti-sporozoite[41] and anti-infected hepatocyte[42] naturally acquired immunity were negligible contributors, confirming that antibody-mediated immunity to the blood-stage was both necessary and sufficient to explain naturally-acquired immunity to malaria. Although these studies showed that immunity to malaria is resolutely to the blood-stage (anti-gametocytic activity was excluded however), the question of what the protective antibodies targeted remained unanswered.

Since the 1980s studies showed that iRBC proteins are recognised in a homologous manner by children but in a heterologous manner by adults. Later, a major virulence factor was identified as PfEMP-1[43], a family of surface iRBC proteins intimately implicated in mediating adhesion to the vascular lining by binding to EPCR[44] in severe cases of malaria. Three other multigene families RIFINs[45], STEVORs[46] and SURFINs[47] (collectively termed variant surface antigens (VSAs) along with PfEMP-1), have more recently been described, some of which also promote RBC rosetting and microvascular binding, although their association with severe pathogenesis is less clear than for PfEMP-1. Immune individuals are protected from malaria carrying homologous PfEMP-1 variants and disease can arise from parasites expressing a PfEMP-1 not covered by the individual's antibody repertoire[48]. Further evidence for PfEMP-1 being the most likely target for blood-stage naturally-acquired immunity is provided by the observation that immune women who become pregnant for the first time redevelop acute malaria symptoms in concurrence with the expression of the placenta-specific PfEMP-1 variant VAR2CSA[49,50]. PfEMP-1 proteins are extremely variable. Over 60 so-called *var* genes have been characterised, each able to recombine[51,52], with the potential to generate large diversity both within a single *falciparum* genome as well as across strains. This extensive variability is likely to be the explanation for the slow acquisition of immunity. Although antibody titers to the merozoite are generally high and there have been many reported epidemiological correlations between merozoite antigen levels and protection[53,54], there is little evidence to elevate these co-correlations from markers of exposure to causally linked events in a *naturally acquired in vivo* setting. In addition to PfEMP-1 targeting on iRBCs, it is clear that other mechanisms of natural-acquired immunity are also possible and likely make small contributions. For instance, antibodies to reticulocyte-binding protein homolog 5 (PfRH5) isolated from malaria-infected people do have the capacity to inhibit invasion *in vitro*[53,55], and other merozoite-reactive antibodies are thought

to have *in vivo* merozoite-killing properties by antibody-dependent respiratory nurst (ADRB[56]), antibody-dependent cell-mediated cytotoxicity (ADCC[56,57]) and complement activation[58,59]. The fact that merozoites have overt complement evasion mechanisms[60] further suggests a credible involvement of merozoite complement fixation in immunity. To summarise, naturally-acquired immunity to *P. falciparum* malaria is thought to be multi-factorial with contributions of immunity across the malaria lifecycle but the major mechanism of immunity is mediated mainly by antibodies to an extremely variable antigen family called PfEMP-1 which is responsible for endothelial adherence, a major event in disease pathogenesis. Protective immunity against these targets is developed over time after multiple infections and can be lost following lack of exposure.

1.2.4 Erythrocyte invasion by *P. falciparum* merozoites

In order for the merozoite to thrive it seeks refuge from the host immune system within a RBC, encapsulated within a parasitophorous vacuole where it can regulate the conditions optimal for survival. To achieve this, the merozoite embarks on a highly complex sequence of protein-protein interactions and signalling events which result in RBC remodelling, forced entry and the creation of a parasitophorous vacuole all in the space of around one minute[61]. The invasion process has been extensively studied in real time by microscopy[62] and shows three main invasion events: 1) initial attachment, 2) reorientation and tight attachment and 3) invasion. Initial attachment is thought to be weak and reversible and conducted by highly abundant GPI-linked and associated proteins which form the protein-dense coat on the merozoite's surface. Several proteins including the PfMSP family of proteins, the PfSERA family of proteins, PfS-antigen and PfGLURP among others are known to populate the surface of the merozoite but the key players and mechanisms by which this phase of invasion

occurs is incompletely understood. Several merozoite surface proteins are refractory to genetic deletion[63] or susceptible to neutralising antibody[64–67] and thus must be part of essential processes. PfMSP-1 has long been associated with this stage of invasion[68,69] although more recently doubt has been cast over its direct involvement in erythrocyte binding[70]. After this initial attachment, significant erythrocyte membrane deformation causes the reorientation of the merozoite leading to an apically-abutted merozoite against the RBC membrane[71]. Critical invasion ligands are expelled from the merozoite's apical organelles: the micronemes and rhoptries. Upon first contact, the micronemal contents are expelled then the rhoptries discharge following reorientation, allowing them to create high-affinity and irreversible contacts with host cell receptors. Here, DBL-family proteins (PfEBA-175, PfEBA-140, PfEBA181 and PfEBL-1) and RH-family proteins (PfRH1, PfRH2a, PfRH2b, PfRH4 and PfRH5) interact with their cognate RBC receptors to specifically determine tropism to RBCs and create a tight attachment. First PfRH1 engagement triggers a Ca^{2+} signalling event leading to the release of more micronemal proteins including PfEBA-175[72,73]. The other adhesins, with the exception of PfRH5 which will be discussed later, act with seemingly high redundancy to exert their function[74]. The following sequence of molecular events that ensues includes the formation of the tight junction. Here, two proteins, PfRON1 and PfRON2 are translocated from the rhoptry neck into the RBC membrane where they specifically act with the essential invasin PfAMA-1 serving as an anchor with which to force entry into the RBC[75]. Concurrently, rhoptry bulb contents are released to form the bulk of the nascent parasitophorous vacuole. As the merozoite enters the RBC, a number of surface proteins are selectively cleaved including PfMSP-1 and PfEBA-175 by the action of PfSUB1/2 and PfROM1/4 proteases[76]. This shedding step is both essential for invasion and hypothesised to create a rapid protein-rich immune diversion from tight junction proteins. The merozoite is pulled through the tight junction, into a parasitophorous vacuole under the

action of a molecular complex termed “glideosome”; at its core a molecular actin-myosin-like motor. An in-depth review of the merozoite invasion process was recently published by Cowman *et al*[77] (Figure 1.5).

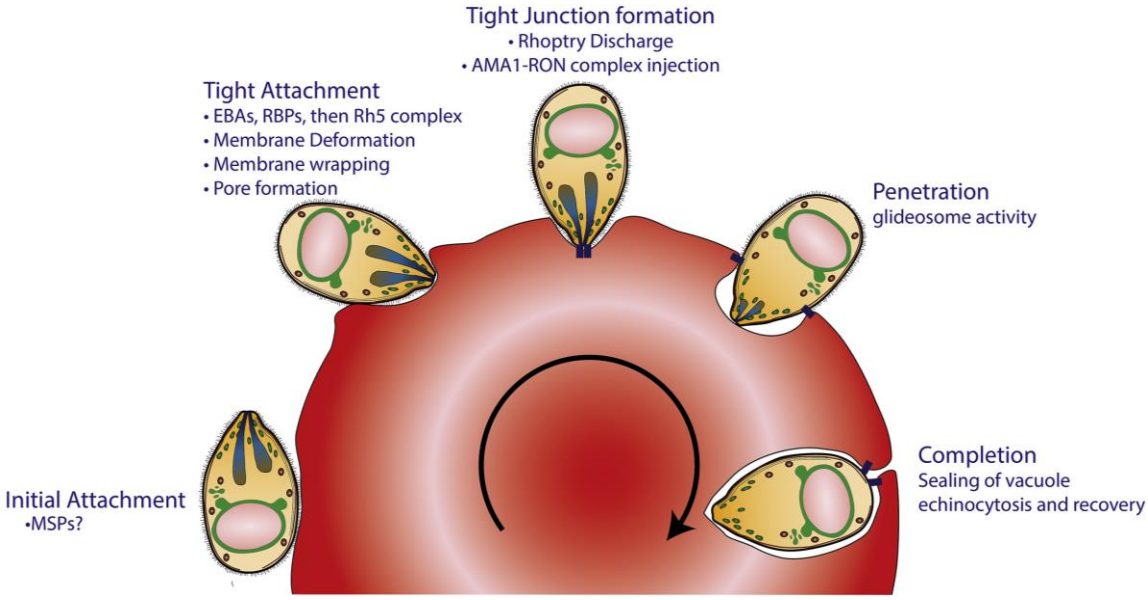

Figure 1.5: Illustration of the merozoite invasion process into a human erythrocyte. Figure adapted from Cowman *et al.*[77]

1.3 Malaria vaccines past and present

1.3.1 Vaccines targeting infected red blood cells

When it became clear that a large part of malaria’s pathogenesis is caused by iRBC sequestration and that naturally-acquired immunity appears to act largely through inhibiting this process, eliciting immunity to VSAs became an obvious path to explore. Further bolstering the hypothetical potential of iRBC-targeting vaccines, VSAs present static targets for complement-activating or cytophilic antibodies unlike merozoites which are only transiently exposed to immune recognition. Antibodies to iRBC therefore may not need to be

required to inhibit a specific interaction to be efficacious. Despite the theoretical promise, vaccines targeting PfEMP-1 haven't gained much traction, falling to the huge variability shown by these proteins[52]. Although strain-specific protection can be achieved[78,79], this protection will not be relevant in endemic settings where most infections are mixed[80,81]. The theoretical diversity of these protein families is also constrained as they must retain the ability to bind host receptors. The proof of this is in that sufficient immunity from severe malaria by targeting these proteins is gradually developed, and sometimes after only a few infections[82,83]. Replicating the diversity of natural infection with a vaccine is a difficult task. Apart from the obvious technical challenges of producing a multi-component vaccine, previous attempts to elicit multi-strain immunity have ultimately been counter-productive due to immune interference[84–86]. In the past few years, vaccine efforts have shifted to tackling the diversity issue by using rationally-designed structural mimics to replicate the functional shape of a PfEMP-1[87].

1.3.2 Pre-erythrocytic vaccines

Every stage of the parasitic lifecycle is theoretically susceptible to host immunity. Successfully inducing immunity to the liver-stage is particularly alluring as it would result in asymptomatic sterile (with respect to disease-causing merozoites, at least) immunity at stages of low parasite burden relative to the ensuing blood-stage. Naturally acquired and induced immunity to the pre-erythrocytic stages has been described against both sporozoites[88] and infected hepatocytes[42,89] but it is widely accepted that their contribution to protection in naturally-acquired settings is minimal probably due to the small amount of antigen exposure to these antigens. Pre-erythrocytic vaccines are currently leading the way for malaria vaccines with RTS,S/AS01 (Mosquirix®) the parasitic vaccine closest to achieving licensure

and whole-sporozoite vaccines showing sterile protection following mosquito-bite challenge[90]. Concerted effort to target infected hepatocytes gained traction on the one hand from early success inducing this type of immunity against the murine malaria model *P. yoelii*[91] and on the other hand from the realisation that immunity developed following vaccination with attenuated sporozoites was mainly $CD8^+$ T cell-mediated[92,93]. Another type of pre-erythrocytic immunity would aim to elicit antibodies targeting sporozoites to neutralise them before they infect hepatocytes. Whole-sporozoite vaccines from Sanaria currently require four vaccinations of a large dose of sporozoite to be efficacious. A successful means of culturing sporozoites has not been developed and their current generation relies on isolating them from mosquito salivary glands. Despite attempts to automate the dissection of infected mosquitoes, feasibility in terms of vaccine product cost and deployment as cryopreserved products is far-fetched, certainly not at a cost which is realistic for a vaccine whose target population mostly resides in the third-word. Subunit vaccine counterparts such as ME-TRAP have been proposed as alternative means of inducing this type of immunity but their efficacy is insufficient[94]. The other line of pre-erythrocytic vaccine research aims to generate antibodies to neutralise the sporozoite before it reaches the liver. Namely, the major sporozoite surface protein PfCSP has been the focus in these vaccines because of efficacy against its orthologue in the *P. berghei* mouse malaria model. RTS,S (produced by GlaxoSmithKline) is composed of a repeating set of B cell and T cell epitopes identified from PfCSP expressed as a fusion protein with hepatitis B surface antigen which assembles to form a virus-like particle (VLP) displaying PfCSP epitopes and is formulated in the potent AS01 adjuvant. Despite this vaccine being on the cusp of licensure, this vaccine has modest efficacy beyond the first month after administration with a disease protection rate of around 1/3 in malaria-endemic populations[95,96]. The success of this vaccine is also its downfall. Efficacy of the RTS,S vaccine is due to the high titers of anti-PfCSP antibodies produced by

this vaccine[97], which is only maintained for a short period of time, resulting in waning efficacy[96].

1.3.3 Vaccines that interrupt malaria transmission (VIMT)

Vaccines of this kind target proteins from the sexual stage, i.e parasitic targets which are available for and susceptible to neutralisation within the mosquito midgut. Inducing immunity of this type targets gametocytes, gametes or ookinetes (or indeed certain mosquito proteins[98,99]) which have evidently different protein expression profiles to the merozoite and sporozoite. As a result, there is likely to be very little functional overlap with vaccine targets present in the liver and blood-stages. This means that functional immunity elicited here would serve only to interrupt the transmission of malaria between human hosts but serve no direct purpose in protecting the vaccinee. Furthermore, unlike vaccines targeting the human-stages where children would be the only age group in need of vaccination, transmission-blocking vaccines would require the vaccination of all age groups including immune adults. An advantage of transmission-blocking vaccines is that they target proteins with limited polymorphism due to their loci not being under the selective pressure of an immune system capable of generating the large diversity seen in human BCRs and TCRs[100,101]. Much of the research to date has focussed on Pfs25, Pfs230 and Pfs48/45, proteins known to play key roles in sexual stage processes[102]. The first *P. falciparum* sexual stage antigen to have entered human clinical trials is Pfs25 but the trial was foreshortened due to safety concerns though to be caused by the particular protein-adjuvant formulation[103]. Pfs25 entered a second Phase I trial at the Jenner Institute in late 2015 and showed an improved safety profile (manuscript in preparation).

1.3.4 Vaccines targeting merozoites

The pursuit of this type of vaccine is predicated on the assumption that merozoites can be the target of protective immunity. The evidence supporting the idea of neutralising merozoites with antibody is strong. Merozoite protein vaccination has widely been shown to cause *in vitro* invasion inhibition[104–108] and *in vivo* protection in challenge models[109–111]. There are two major functional mechanisms for anti-merozoite antibody to have an effect: Fab-mediated effects caused by antibody binding to susceptible epitopes, inhibiting essential interactions from taking place or Fc-mediated effects caused by opsonisation and complement activation where antibody binding location on the merozoite is secondary to the effect transduced by the Fc. Unlike VIMTs, blood-stage vaccines would serve to reduce morbidity in the host, as symptoms are caused exclusively in the blood stage and, unlike pre-erythrocytic vaccines, sterile immunity is not a necessary requirement. In fact, blood-stage vaccines could benefit from natural boosting by repeated infection. These vaccines can be viewed as a crutch to reduce symptom severity and mortality in early life, all the while allowing for the development of naturally-acquired immunity in parallel. On the other hand, merozoite proteins are often highly polymorphic[112–114], slowing the development and progress of blood-stage vaccines. Moreover, because merozoites are highly targeted by antibody in natural infection, it isn't clear that vaccine-induced antibodies will be as potent in that setting as they are *in vitro* or in early-phase trials in non-exposed volunteers[115]. Mirroring many successful whole-organism vaccines, and with little knowledge of the susceptible targets of the merozoite, blood-stage vaccines began with the immunisation of adjuvanted whole cell preparations[116]. There are several drawbacks associated with this type of vaccine; a practical one is that although it is straightforward to culture blood-stage *P. falciparum* parasites, it requires the use of human blood which poses blood-borne infection risks. Furthermore, simply generating the volume of material will be more challenging than recombinant

proteins. A conceptual drawback is the concern that a killed or attenuated parasite without the ability to invade may never trigger the sequence of events necessary for the exposure of critical ligands, regardless of how well-synchronised the parasites are. The abundance of certain antigens thought to have the potential to be protective is so low (such as PfRH5 for example) that the dose of parasite needed to overcome this is unrealistic and dangerous in equal measure. Since then the mainstream of blood-stage vaccine research has focussed on subunit vaccines of invasion ligands thought to be the target of protective antibody from naturally-acquired immune responses. Merozoite surface antigens PfMSP-1, PfMSP-3 and PfGLURP have been identified on this basis and have been involved in human clinical trials. PfMSP-1 has long been the focus of blood-stage vaccine attention due to its immunogenicity, susceptibility to antibody and inability to be genetically deleted[117]. In a 2009 Phase IIb clinical trial it was shown that despite the use of a potent adjuvant (AS02), the antibodies failed to have any significant protective impact[118]. GMZ2, a fusion protein of a fragment of both PfMSP-3 and PfGLURP was also recently progressed to a Phase IIb trial in Africa. Again, despite the immunogenicity performing as expected, efficacy was a disappointing 11%[119]. Several apical invasion ligands have shown considerably more pre-clinical promise than most merozoite surface antigens; the leading candidate of this type of antigen was PfAMA-1. Subsequent efficacy trials both in African children[120] and healthy UK adults[121] have since cast doubt over its inclusion in any future malaria vaccine. The introduction of more reliable correlates of protection[111,122] in the form of standardised growth inhibition assays[123] (see Chapter IV) has brought renewed hope in blood-stage vaccines by ushering in the next wave of promising new blood-stage antigens such as PfSEA-1[124], PfAARP[104] and PfRH5[125].

1.3.5 PfRH5

Unlike other blood-stage invasion ligands, PfRH5 is unique in that it plays an undisputedly essential role in the RBC invasion process, is refractory to genetic deletion, is genetically well-conserved and is susceptible to strain-transcending antibody-mediated immunity[125–127]. Antibodies to PfRH5 are raised in endemic malaria infections[53,55] and correlate with protection[53,128] although the low antibody titers are not thought to meaningfully contribute to protection. The observation that PfRH5 titers elicited during natural infection are low[53] is indicative of low immune exposure, either because of the transient nature of PfRH5 exposure or its low abundance or a combination of both factors. Low immune exposure means low selection pressure which is congruent with PfRH5 showing limited polymorphism in contrast to highly polymorphic PfAMA-1 and PfMSP-1 which both generate high antibody titers. PfRH5 was shown to bind erythrocyte receptor basigin (aka EMMPRIN or CD147) and that disrupting this interaction is a basis for neutralisation of PfRH5 with antibodies[129]. In 2014, the structure of a truncated version of PfRH5 (named PfRH5ΔNL) bound to basigin and two mouse monoclonal antibodies was reported, revealing neutralising epitopes at the tip of the "kite-like" structure[130] (Figure 1.6).

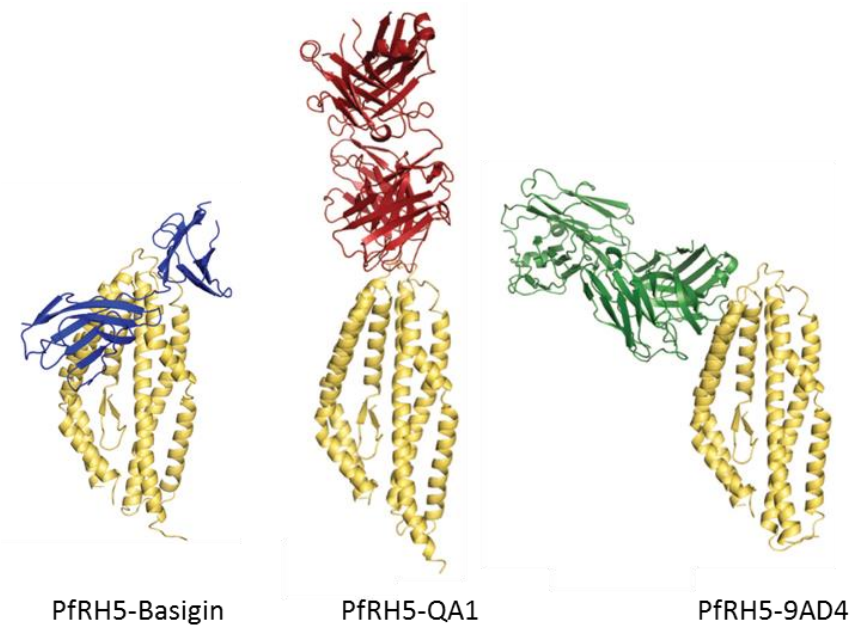

Figure 1.6: Structure of PfRH5 in complex with basigin (left), QA1 (middle) and 9AD4 (right) mAb Fab fragments. QA1 and 9AD4 are both inhibitory mouse mAbs. Figure adapted from Wright *et al*[130].

Over the past few years, mechanistic insights have been gained relating to the biological processes surrounding PfRH5 at play during the invasion process. PfRH5 lacks a transmembrane domain and so must be tethered to the membrane via association with other proteins. PfRIPR, a cysteine-rich EGF-like protein and PfCyRPA a cysteine-rich six-bladed β-propeller protein whose structure was recently described[131,132], have both been described as components of a PfRH5 invasion complex by co-immunoprecipitation[133,134] but the membrane anchor remains a source of debate. First, PfCyRPA was reported to tether PfRH5 to the surface via GPI-linkage. More recently however, another GPI-linked protein PfP113 has been reported to tether PfRH5 by its N-terminus[135]. It's unlikely but not impossible that PfRH5 interacts with two GPI-linked proteins, one via its N-terminus and via its C-terminus. Although clearly more work must be done to elucidate the PfRH5 complex invasion process, the current model proposed by Galaway *et al*.[135] is as follows: PfRH5 is locally clustered by PfP113 tetramerisation; these heterodimers then bind basigin after which secreted PfCyRPA-PfRIPR bind the complex, releasing PfP113 from PfRH5 possibly by recruiting a protease or

simply by mutually-exclusive binding to PfRH5 (see Figure 1.7). The role played by this invasion complex is beginning to be understood; PfRH5/PfCyRPA/PfRIPR binding to basigin mediates Ca^{2+} release from the merozoite into the RBC[73]. It is not known whether this Ca2+ influx is a cause or a symptom of invasion but either way, it is known to be an essential characteristic of the establishment of the irreversible PfAMA-1/PfRON complex tight junction, without which the PfRH5/PfCyRPA/PfRIPR-basigin binding event cannot occur[136].

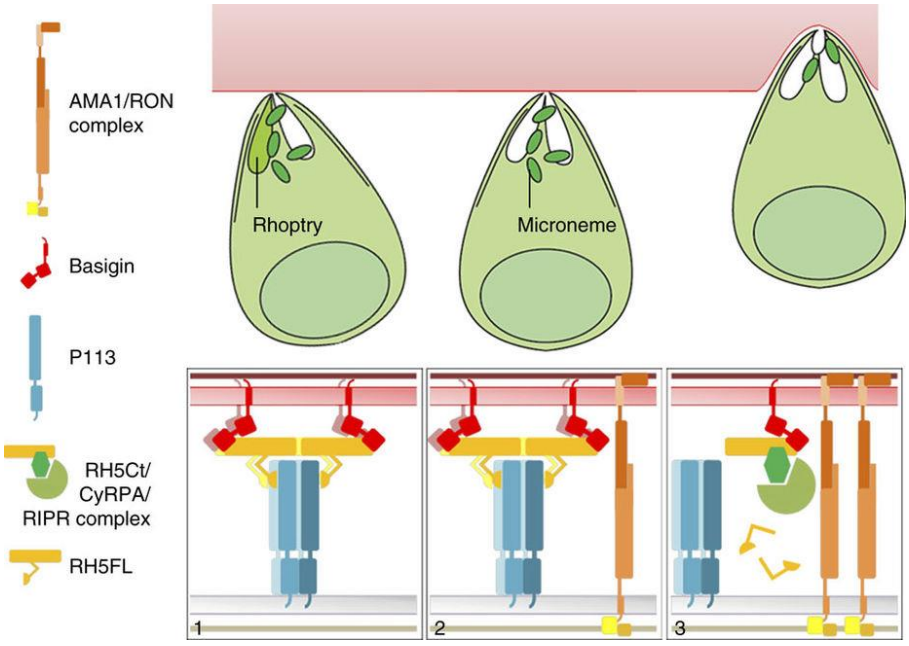

Figure 1.7: Model of the PfRH5 invasion complex as proposed by Galaway *et al*. "RH5FL" refers to full-length PfRH5 and "RH5Ct" refers to the processed 45kDa fragment of PfRH5 lacking 15kDa at the N-terminus. Figure taken from Galaway *et al*.[135]

On the vaccine front, the excitement surrounding the discovery of PfRH5 translated in a quick transition from pre-clinical validation to a non-human primate challenge trial[111]. This study in which 6/6 monkeys were protected following PfRH5 vaccination in Freund's adjuvant and 4/6 were protected following viral-vector immunisation, provided proof-of-concept that vaccination with PfRH5 alone is sufficient to protect the host from a lethal

challenge of heterologous FVO-strain *P. falciparum* malaria in an *Aotus* primate model. This trial also validated the use of the growth inhibitory activity (GIA) assay as a correlate of protection, establishing a quantitative link between GIA and protection and showed that invasion-blocking antibodies are capable of causing *in vivo* growth inhibition. A major hurdle in malaria vaccine development has been the difficulty in expressing functional recombinant protein in sufficient quantities[137,138]. The recombinant expression of a clinically-compatible form of PfRH5 from HEK293 cells was challenging (Draper group, unpublished data), however other groups had successfully expressed the protein in *E. coli*, although it necessitated refolding[126]. The adoption of a rarely-used *Drosophila* S2 cell line allowed for high-level production of protein in a eukaryotic system, capable of expressing soluble secreted protein with oxidised disulphide bonds and represented a step forward in vaccine clinical development[139]. PfRH5 has since advanced to human clinical trials; a Phase Ia trial using viral-vectored delivery (which will be discussed in more detail in Chapter III), and currently underway is a Phase I/IIa efficacy trial consisting of AS01B-adjuvanted recombinant PfRH5 vaccination followed by a blood-stage challenge.

Pre-clinically, efforts remain on-going to reduce the concentrations of anti-PfRH5 IgG needed for neutralisation and alleviate the selection pressure imposed by targeting a single protein by vaccination. Therefore, the potential for synergy by simultaneously targeting other invasion proteins is being explored. Another member of the RH-family, PfRH4, and PfCyRPA have been reported to elicit antibodies which synergise with PfRH5 antibodies[133,140]. Two published studies have produced PfRH5-specific mAbs isolated from mice, in both cases they obtained mAbs with very high growth inhibitory properties and others with very detectable activity[127,141]. These mAbs provide valuable tools to understand the basis of the vaccine-induced polyclonal antibody response. An attractive alternative vaccine or mAb therapy strategy would be to target basigin. *In vitro* studies have shown that

small quantities of anti-basigin mAb can be exceptionally potent in inhibiting parasite growth[127,129,142], probably because blocking antibodies are afforded the time to reach equilibrium and therefore maximal saturation in the context of a permanently exposed target. However, these growth inhibition assays are not conducted at physiological haematocrit, nor do they include lymphocytes or endothelial cells, both of which express basigin. The widespread expression of basigin reflects a multi-functional protein. Indeed, basigin is known to have functions in spermatogenesis[143], embryonic development[143,144], lymphocyte activation[145] and neural function[145]. Furthermore, although anti-basigin mAb has been given to humans in the context of a clinical trial[146], the risk of interfering in essential human processes mediated by basigin and the risk of inducing autoimmunity would be too great, consequently this approach is not actively being pursued clinically.

1.3.6 Next-generation vaccines

The concept at the heart of any vaccine is that of priming the immune system to respond in a certain way upon encounter with a disease-causing pathogen by exposing it to a mimic incapable of causing disease. There is evidence of so-called "variolation" in medieval China; that is the practice of nasally-administering dried scabs from infected smallpox-sufferers in otherwise healthy patients to protect them from that disease. It apparently didn't gain widespread usage, probably because the application of live virus often led to symptomatic disease. The etymological origin of the word "vaccine" comes from the Latin "*vacca*" meaning cow, a sign of the roots of modern vaccinology. Edward Jenner, a physician from rural England, knew of the widely-held belief that milkmaids never caught smallpox and supposed that the pus contained in their cowpox blisters, was protecting them from the similar but more deadly smallpox disease. Proof-of-concept for vaccinology in modern

medicine was made in a ground-breaking but ethically barren experiment where a young boy named James Phipps was inoculated with cowpox-containing pus and subsequently exposed to smallpox several times, exposures from which he thankfully survived. Throughout much of the 20th century vaccinology has followed the "isolate, inactivate, inject" paradigm pioneered by Louis Pasteur in the late 19th century. This was used to great effect to vaccinate against mumps, measles, rubella, poliomyelitis and many other diseases reducing the number of new cases of disease from millions to dozens in 50 years or less[147]. The culmination of vaccinology applying Pasteur's general method was of course the eradication of smallpox in 1980 following a WHO-led worldwide vaccination project which lasted only 22 years[148]. Traditionally, vaccines have been formulations of complete organisms or toxins either live and attenuated by passages through a foreign host to reduce virulence or killed with chemicals, radiation or heat. However these unreliable and unpredictable methods of attenuation means that whole-organism vaccines must find a balance between over- and under-attenuation to be successful and have, on occasion, led to adventitious consequences, mainly through genetic reversion to a virulent form[149]. The oral polio vaccine which consists of three live attenuated serotypes is one such example, where around 1 in 750,000 first-time vaccinations resulted in vaccine induced poliomyelitis[150,151]. Similarly, early inactivated whole-virion RSV vaccines actually enhanced infection[152]. An increase in the safety standards (or decrease in tolerance for adverse side-effects) imposed on medicines over the course of the last 60 years likely played a part in whole-organism vaccines being phased out in favour of simpler subunit vaccines such as those to vaccinate against pertussis or hepatitis B. By the end of the 20th century, the major diseases of human concern had either had a vaccine developed or had proven refractory to the standard vaccine development approaches. The latter stages of the 1900s saw the explosion of the genomic and biotechnological era, offering new tools and new hope for difficult pathogens.

Since the year 2000, reverse vaccinology emerged as a key alternative approach to the largely empirical vaccine discovery methods used before. This approach consists of searching the genome for potential vaccine targets, expressing them as recombinant proteins and screening their efficacy as vaccines in animal models. Meningococcal serogroup B (MenB) infections were not remedied by whole bacterium immunisation because of extensive surface protein polymorphism coupled with low immunogenicity due to tolerance of a polysaccharide which resembles a host epitope. In 2012, Bexsero®, a MenB vaccine composed of four antigens (fHbp, NadA, NHBA, and PorA P1.4), identified using reverse vaccinology, was licensed for human use[153].

Almost all currently licensed infectious disease vaccines are thought to serve their protective function by inducing antibodies capable of neutralising the disease-causing pathogen[154]. As we gain insight into the mechanisms of protection from infectious diseases, vaccines have become progressively simpler mixtures as they aim to elicit increasingly focussed and increasingly predictable antibody responses. Most pathogens have co-evolved with their host for long periods of time and their components have evolved methods to escape immunity. Trends in vaccinology over the past 10 years point to next-generation vaccines being rationally engineered immunogens in an attempt to overcome a variety of hurdles still faced by vaccinologists, such as low immunogenicity, high polymorphism and unstable immunogens (Figure 1.8).

Structural vaccinology refers to the utilisation of structural information to optimise immunogens with more desirable immunological properties. HIV research has led the field in structural vaccinology over the past decade. Broadly neutralising mAbs (bnAbs) to HIV-1 infection are rare and only arise after several years of ongoing infection[155]. One such anti-gp41 bnAb called 4E10 has been shown to bind an epitope only transiently-exposed during viral fusion, possibly explaining the time taken for this type of bnAb to arise. One strategy

employed to overcome this poor immunogenicity is the design of computationally-designed scaffolds permanently presenting the 4E10 epitope. Although this attempt did elicit 4E10-like antibodies, it failed to elicit bnAbs (probably owing to a technical oversight by incompletely including the whole neutralising epitope in the scaffold[156]). This work nevertheless showed that it is feasible to elicit antibodies of a pre-defined specificity with computationally-designed synthetic scaffolds. Such advances led the way for several other antigen minimisation attempts in targets of other diseases[87,157–159]. Another structural approach to increasing bnAb immunogenicity was pioneered by Jardine *et al*[160,161]. The rare VRC01-class of HIV Env-binding bnAbs arose from the same germline B cell precursors with common features; namely the same VH exon usage (VH1-2*02) and short LC CDR3 domains (5 amino acids or less). However, the predicted germline B cell precursors of these highly-mutated bnAbs had barely detectable affinity for wild-type Env meaning their activation would be a rare event[162]. Using molecular interface modelling using the Rosetta package[163], the authors designed a mutant Env (eOD-GT6) with high-affinity for the VRC01-class bnAb B cell precursors in an attempt preferentially trigger these B cells to guide quicker mutation towards the bnAbs. One of the components of Bexsero® –fHbp, is a highly variable MenB protein whose variants are groups into three classes of proteins which fail to elicit cross-reactive antibodies[164]. In a feat of structural engineering, Scarselli *et al*. engineered epitopes from the three variant families into a single molecule and this chimera was able to elicit cross-reactive neutralising antibodies of comparable potency to homologous vaccination in mice[165].

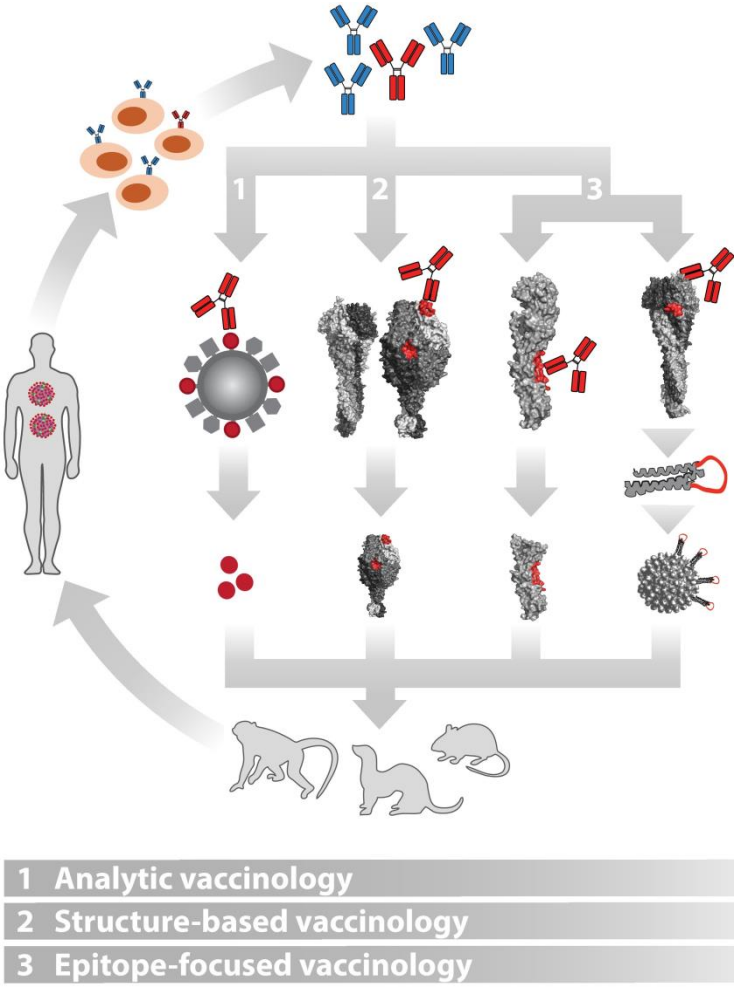

Figure 1.8: The present and future of vaccinology: using antibodies to identify protective antigens (path 1), antigen conformations (path 2) or antigen epitopes (path 3). Figure taken from Lanzavecchia et al.[166]

In malaria, rationally-designed vaccines are slowly beginning to emerge. An N-glycan-engineered version of the *P. vivax* invasion ligand PvDBP has been described to increase the immune focus on predicted neutralising epitopes. The results were encouraging in one of the two inhibitions assays for two of the three glycan-masked variants tested which showed increased binding inhibition with similar titers of specific antibody, thus suggesting a qualitative improvement in antibody response[167]. In *P. falciparum*, the only progress to date has been the development of a heat-stable variant of a PfRH5 truncation construct. The mutations made were designed with the sole intention of increasing stability, hence

enhancing its potential as a real-world vaccine candidate, and were not informed by immune guidance leading to no increase in vaccine potency[168]. With no new merozoite invasion ligand vaccine candidates on the horizon (Illingworth *et al*., submitted), improved vaccines based on existing candidates are essential for progressing the malaria vaccine field. Inroads have been made to structurally define neutralising epitopes on PfAMA1[169], PfRH5[130], and PvDBP[170], but there is a lack of information about neutralising antibody responses hampering second-generation vaccine development. Notably, almost all structural antigen characterisation in the malaria field has come from the blood-stage vaccine field; this is surely due to the increased challenge of developing a vaccine against this stage, forcing this field to explore "higher"-hanging fruit at an earlier stage. Without a doubt, the virus pathogen field of research has led the way in structural vaccinology, with arguably many of the most seminal advances stemming from HIV research. Rational vaccinology in the malaria field is thus truly still in its infancy and no investigations so far have aimed to explore which features are needed to increase functional/protective antibody responses to a *P. falciparum* protein.

1.4 Thesis outline and aims

Successful vaccines have in common that the antibody response they elicit causes sufficient neutralisation to achieve protection. The aims of this thesis were to characterise what features and attributes neutralising anti-PfRH5 mAbs have over non-neutralising anti-PfRH5 mAbs, and to use that information to explore the possibility of rationally-designing an enhanced PfRH5 immunogen.

Chapter III describes the protocol and techniques I set up to isolate antibody-coding genes from human vaccine-induced B cells in the world's first PfRH5 vaccine clinical trial.

Seventeen mAbs were successfully isolated and expressed as recombinant proteins. In this chapter I also describe some basic binding characteristics of all the mAbs.

Chapter IV describes the functional properties of the seventeen mAbs in terms of their ability to neutralise *P. falciparum* growth *in vitro* against multiple strains. I also begin trying to understand the mechanism by which anti-PfRH5 mAbs exert their neutralising effect both as mAbs and within a polyclonal mix as would be elicited by a vaccine.

Chapter V describes the efforts made to define the binding location of the mAbs on PfRH5 and, from this, to distinguish "neutralising" from "non-neutralising" epitopes which are probed by human mAbs following vaccination with PfRH5. The panel of mAbs are clustered by binding location which is reflected by functional similarities including their growth inhibitory properties. This chapter also describes the pre-clinical testing of the construct designed for crystallisation in a rabbit immunisation experiment. The "modified" vaccine candidate proves to only be a minor improvement.

Chapter VI describes instances of functional interplay which are observed within this panel of mAbs leading to a re-assessment of what constitutes a neutralising epitope.

Chapter VII summarises the output of this thesis and discusses future directions of work following-on from the project outlined this thesis.

Chapter II: Materials and methods

2.1 Chapter III methods

2.1.1 Cell sorting

Volunteers from a phase Ia safety and immunogenicity trial named VAC057[171] (clinicaltrials.gov identifier: NCT02181088) were bled seven days after the second immunisation using MVA (modified vaccinia Ankara) encoding PfRH5. Blood was collected from volunteers in heparinised tubes and centrifuged in Leucosep tubes (Greiner Bio one) to separate the PBMC. The PBMC was enriched for B cells using a human pan-B cell enrichment kit (Easysep) and resuspended in DMEM before staining with a $CD19^+$, $CD10^-$, $CD21^-$, $CD27^+$, $CD20^-$, $CD38^+$, IgG^+ fluorophore-conjugated antibody panel. Plasmablasts were single-cell sorted using a MoFlo cell sorter (Dako cytomation) into 96-well PCR plates containing 10µL of 10mM Tris HCl buffer containing 40U/mL of RNase inhibitor (Promega).

2.1.2 Variable region PCR

In each well of a 96-well plate containing a single antibody-secreting cell (ASC), a one-step RT-PCR was carried out with a QIAGEN Sensiscript RT kit (Qiagen) using primers 1-17 (see Appendix 2.1). Next, a PCR beginning with a nested cDNA amplification PCR step (PCR1) is carried out using 1µL of product from the RT-PCR using the same set of degenerate primers used before which cover the diversity of all Vγ, Vκ and Vλ sequences using Phusion

HF master mix (New England Biolabs). Following this, 1µL of the previous product diluted 1/100 is used as template for the insert PCR (PCR 2) using primers 18-51 (see Appendix 2.1) to amplify inserts with plasmid-homologous extensions for CPEC, again using Phusion HF polymerase master mix. Agarose gels were made at 1% and run at 150V in TBE buffer. DNA size was estimated using Generuler DNA 1kb ladder (Thermofisher) with a range of 250-10,000bp.

Thermal cycling conditions

RT-PCR: 40 min at 37°C, 10min at 43°C, 10min at 50°C, 4°C hold.

PCR1: 98°C for 30s, 15 cycles [98°C for 10s; 72°C for 1min], 15 cycles [98°C for 10s; 68°C for 30sec, 72°C for 1min], 72°C for 10min, 4°C hold.

PCR2: 98°C for 30s, 40 cycles [98°C for 10s; 72°C for 1min], 72°C for 10min, 4°C hold.

2.1.3 Variable region cloning

The AbVec-hIgG1/AbVec-hIgKappa/AbVec-hIgLambda expression plasmids were obtained from Patrick C. Wilson (University of Chicago). These plasmids were 5' digested using BshTI and at the 3' using SalI (AbVec-hIgG1), XhoI (AbVec-hIgLambda) and Pfl23II (AbVec-hIgKappa) to yield linear products. CPEC assembly was done by mixing 100ng of a 1:1 molar ratio of insert:plasmid in 20µL containing 1X Phusion HF polymerase master mix and assembled using an 8-cycle CPEC protocol (8 cycles: 98˚C 10s, slow ramp anneal 70˚C ➔55˚C at 0.1˚C/s, 72˚C 35s). Full nicked plasmids were subsequently transformed into Zymo 5α Mix & go competent *E.coli* (Zymo research) according to manufacturer's instructions, streaked on LB agar petri dishes containing 100µg/mL carbenicillin and grown at 37°C overnight in a static incubator.

2.1.4 High-throughput mAb expression for screening purposes

Exponential growth-phase adherent HEK293 cells (HEK293A) were resuspended in DMEM (Sigma-Aldrich) supplemented with 2mM L-glutamine, 1mM sodium pyruvate, 100U/mL penicillin, 0.1mg/mL streptomycin and 10% ultra-low IgG foetal bovine serum (all Thermofischer) and seeded at 4E4 cells/well in 100µL 24 hours prior to transfection in Costar 96-well cell culture plates (Corning). On the day of transfection, for each well, 50µL of 60µg/mL linear 25kDa PEI (Alfa Aesar) was mixed with 200ng of cognate heavy- and light-chain coding plasmid in a volume of 50µL and shaken at room temperature for 30 minutes. The DNA-PEI complexes were the added to the HEK293A cells. The next day, an additional 50µL of supplemented DMEM (as described above) was added to each well. All transfections were done in triplicate wells. Three wells were transfected with PEI but no DNA as a negative control termed (Mock transfection). Four days post-transfection, the supernatants were harvested.

2.1.5 Recombinant PfRH5 expression

The production of recombinant PfRH5 from *Drosophila* S2 cells has been previously described[139]. The sequence used here was identical to the VAC057 vaccine sequence with the addition of a four-amino acid purification tag (c-tag: EPEA). The sequence was based on the 3D7 reference sequence and encoded amino acids E26-Q526 with four mutations to remove glycosylation sequons (T40A, T216A, T286A and T299A). This protein was affinity purified using CaptureSelect c-tag affinity matrix (Thermofischer). A further SEC polishing step was done to separate monomers from oligomers and contaminants as well as to buffer-exchange the protein into 20mM Tris, 150mM NaCl, pH 7.5. All purification steps were carried out on

an ÄKTA Pure FPLC system (GE Healthcare). The pure, recombinant protein was stored at -80°C and at -20°C after first use.

2.1.6 Screening ELISA

Here an indirect ELISA was carried out by coating PfRH5 on Maxisorp flat-bottom 96-well ELISA plates (Nunc) at 2µg/mL in 50µL at 4°C overnight. Wells were washed twice with PBS-T and blocked with 200µL of Blocker™ Casein (Thermofisher) for 1 hour. Plates were then coated with neat HEK293F culture supernatant 1 hour at room temperature then washed 4 times with PBS-T before the addition of 50µL of goat anti-human gamma-chain alkaline phosphatase-conjugated secondary antibody (goat anti-mouse IgG alkaline phosphatase-conjugated secondary antibody for QA1) (both Sigma-Aldrich) for 45 minutes at room temperature. Wells were then washed 6 times with PBS-T and developed with 100µL of PNPP substrate at 1mg/mL (Sigma-Aldrich) and read on an Infinity F50 plate reader at 405nm (Tecan).

2.1.7 *E. coli* culture and plasmid DNA preparation

Transformed *E. coli* cultures were seeded in appropriate volumes of LB + antibiotic and grown at 37°C in an orbital shaking incubator at 225rpm for approximately 18 hours. All plasmids DNA preparations were made with Plasmid *Plus* midi, maxi or mega silica-based anion-exchange kits (Qiagen) as per the manufacturer's instructions. All DNA was eluted in deionised H_2O rather than elution buffer.

2.1.8 Large-scale mAb expression

Recombinant monoclonal antibodies were transiently expressed in HEK293F cells using the Expi293F expression system (Thermofischer) according to the manufacturer's recommendations. Briefly, HEK293F cells diluted to 1E6 24 hours prior to transfection in Expi293 Expression medium (Thermofischer). On the day of transfection, for each 100mL of culture to transfect, 100µg of cognate heavy chain/light chain mix was mixed with Expifectamine 293 transfection reagent in 10mL of Gibco Opti-MEM™ I Reduced Serum Media (Thermofischer), incubated at room temperature for 20 mins and added to the culture which was left to incubate in an orbital shaking incubator at 37°C for 72 hours. Enhancers 1 and 2 were added as recommended in the manufacturer's instructions 16 hours after transfection. Supernatants were harvested by centrifuging the culture at 2500g for 15 mins and filtering the supernatant with a 0.22µm vacuum filter.

2.1.9 mAb purification

The mAbs were purified using a 5mL Protein G HP column (GE Healthcare) on an ÄKTA start FPLC system or an ÄKTA Pure FPLC system, (both GE healthcare). Equilibration and wash steps were performed with Dulbecco's PBS and mAbs were eluted in 0.1M glycine pH 2.7. The eluates were pH equilibrated to 7.4 using 1.0M Tris HCl pH 9.0 and immediately buffer-exchanged into Dulbecco's PBS and concentrated using an Amicon ultra centrifugal concentrator (Millipore) with a molecular weight cut-off of 10kDa or 30kDa.

2.1.10 SPR for affinity determination

The production of recombinant PfRH5 was the same as described above. Data were collected on a Biacore X100 (GE healthcare). Experiments were performed at 25°C in Dulbecco's PBS + 0.005% Polysorbate-20 (GE healthcare). A protein A-coated sensor chip (GE healthcare) was used to capture ≈ 50RU of purified antibody diluted in SPR running buffer at a flow rate of 5µL/min. Next, an appropriate range (typically 20nM-0.625nM) of six 2-fold dilutions of PfRH5 with one replicate was injected for 90s at 60µL/min and dissociation was measured for 1600s (this was extended up to 7200s when necessary). Specific binding of the PfRH5 protein to mAb was obtained by reference-subtracting the response of a blank surface from that of the mAb-coated surface. Sensorgrams were fitted to a global Langmuir 1:1 interaction model, allowing determination of the kinetic association and dissociation rate constants using Biacore X100 evaluation software.

2.1.11 *P. falciparum* culture supernatant dot blot

Briefly, 1.5µL of anti-PfRH5 mAb, a human anti-*Zaire Ebolavirus* GP IgG1 mAb, recombinant PfRH5 (all at 1mg/mL) and PBS was spotted onto 0.2µm nitrocellulose membrane and air-dried for 10 mins. Afterwards, the membrane was blocked in 3% BSA + 3% skimmed milk in PBS for 1 hour and washed in PBS. It was then immersed in *P. falciparum* 3D7 culture supernatant for 1 hour and washed again in PBS. Bound PfRH5 was detected by incubating the membrane in PfRH5-immunised rabbit serum diluted 2000-fold in PBS followed by an alkaline phosphatase-conjugated anti-rabbit IgG mAb (clone RG-96, Sigma-Aldrich) also diluted 1:2000, separated by two wash steps in PBS. After a final series of five PBS washes, the dot blot was developed with Sigmafast BCIP/NBT alkaline phosphatase substrate at 1mg/mL (Sigma-Aldrich).

2.1.12 BLI-based PfRH5 polymorphism binding assay

Assays were carried out on an OctetRED384 (FortéBio) using streptavidin-coated biosensors (FortéBio) and black 96-well plates (Greiner). The biosensors followed a four-step sequential assay: Baseline (PBS, 30s), Protein immobilisation (neat supernatant, 180s), Wash (PBS, 60s), MAb binding (150nM mAb, 120s). The PfRH5 protein sequences used here were based on the 3D7 reference sequence (amino acids 26-526) with mutations N39Q and N214Q to delete glycosylation sequons. The proteins also contained an AviTag™ biotin acceptor peptide followed by a Strep-Tag II™ at the 3' end of the PfRH5-coding sequence. The proteins were expressed as secreted proteins in HEK293F cells, co-expressed with the bacterial BirA biotin ligase for efficient site-specific biotinylation. 72 hours after transfection, supernatants were centrifuged and filtered to remove cell material and then extensively dialysed in PBS to remove free biotin.

Data presentation

Data in Figure 3.11 shows the fold-change in binding of each mAb to the 3D7 PfRH5 reference protein relative to the binding of each mAb to each mutant protein after correction for PfRH5 immobilisation level on each biosensor. The fold-change values which were inferior to 1 were plotted as their inverse to avoid skewing in their representation compared to fold-change values greater than 1. mAb signal/RH5 bound signal =X and if X>1 plotted data =X; if X<1 plotted data =1/X.

2.1.13 ELISA for determining linear epitopes

Here an indirect ELISA was carried out by coating PfRH5 previously heat-treated at 90°C for 300s on Nunc MaxiSorp flat-bottom 96-well ELISA plates (Thermofischer) at 2µg/mL in 50µL at 4°C overnight. Plates were washed twice with PBS-T and blocked with 200µL of

Blocker™ Casein (Thermofisher) for 1 hour. Wells were then coated with mAb at 0.5µg/mL for 1 hour at room temperature then washed 4 times with PBS-T before the addition of 50µL of goat anti-human gamma-chain alkaline phosphatase-conjugated secondary antibody (goat anti-mouse IgG alkaline phosphatase-conjugated secondary antibody for QA1) (both Sigma-Aldrich) for 45 minutes at room temperature. Wells were then washed 6 times with PBS-T and developed with 100µL of PNPP substrate at 1mg/mL (Sigma-Aldrich) and read on an Infinity F50 plate reader at 405nm (Tecan).

2.2 Chapter IV methods

2.2.1 Assay of growth inhibitory activity (GIA)

***In vitro* parasite culture**

Parasites were grown according to standard procedure[172]. Briefly, parasites were grown at 2% hematocrit in O^+ red blood cells, which were changed twice monthly. Culture medium contained 10% heat-inactivated pooled human serum mixed with RPMI 1640 supplemented with 25mM HEPES, 35µM hypoxanthine, 2mM L-glutamine and 20 µg/mL gentamycin. 3D7 clone parasites were used unless otherwise stated.

Synchronisation

Parasite cultures were synchronized using a 65% Percoll solution acting as a density gradient. Because late trophozoites and schizonts are more buoyant than 65% Percoll, these remain on top of the layer while the other cells pass through the Percoll. 24 h after Percoll synchronisation the culture will contain mostly ring stages and young trophozoites. A 5% sorbitol solution is used to kill late stage parasites by osmotic lysis, with younger parasites

unaffected. The late trophozoites and schizonts were then removed with a pipette, washed in warm medium (without gentamycin or serum) and returned into culture.

***In vitro* assay of growth inhibitory activity (GIA assay)**

GIA assays were performed to the protocol of the Path-MVI international GIA reference centre[173]. Sorbitol and Percoll synchronised parasite cultures (3D7) at the trophozite phase were cultured for approximately 40-44 hours at 1% haematocrit at a starting parasitaemia of 0.2-0.4%. Endpoint parasitaemia was quantified by measurement of parasite lactate dehydrogenase activity and samples were read in a Varioskan flash plate reader (Thermofisher) at a 650nm wavelength. Percent GIA was calculated following the equation below.

$$\%\ \mathrm{GIA} = 100 - \frac{100(\mathrm{Sample}_{\mathrm{A650}} - \mathrm{Uninfected\ RBC}_{\mathrm{A650}})}{(\mathrm{Infected\ control}_{\mathrm{A650}} - \mathrm{Uninfected\ RBC}_{\mathrm{A650}})}$$

Assays were quality-controlled by typically including BG98 (anti-PfAMA-1 reactive polyclonal IgG), anti-PfRH5 mAb 2AC7 and 5mM EDTA as positive controls and a *Zaire Ebolavirus* glycoprotein-reactive IgG1 mAb as a negative isotype control for mAb samples.

2.2.2 Nucleotide sequencing

All sequencing was carried out by GATC-biotech by Sanger (dye-termination) sequencing.

2.2.3 Mouse model for mAb passive transfer

P. falciparum sporozoite production and mouse infection

The luciferase expressing strain *P. falciparum* NF54HT-GFP-luc was maintained in RPMI 1640 supplemented with 25mM HEPES, 2mM L-glutamine, 50µM hypoxanthine, 10% human serum and subcultured in 5% O+ human erythrocytes. Briefly, asexual cultures were inoculated at 1% parasitaemia with no further subculturing and daily media changes to induce gametocytogenesis. Mature gametocytes were fed to 4-day old *Anopheles stephensi* mosquitoes to initiate infection. Mosquitoes were incubated at 27°C and 75% humidity for 14 days and given 8% dextrose + PABA to foster parasite growth. Liver humanized FRGN KO mice were purchased from Yecuris Corp. and showed human hepatocyte repopulation levels above 70% determined by human serum albumin levels. Liver humanized mice were cycled on NTBC once a month for 3 days at 8µg/mL in the drinking water to maintain health. Animals did not receive NTBC three weeks prior to and during the infection study. For mosquito bite infection, 3-5 liver humanized FRGN mice were anesthetised and placed on top of a mosquito cage containing 150 - 250 infected mosquitoes for 20 minutes.

P. falciparum liver-to-blood stage transition

On the day of challenge, liver humanized FRGN mice were injected both in the retro-orbital plexus and the peritoneal cavity with 50µl clodronate-containing liposomes (Clophosome®-A, Liposomeexpert.com), 100mg/kg cyclophosphamide (Sigma-Aldrich). Five days after challenge, the animals were bled a volume of approximately 200µl, and 500µl hRBC was injected in the retro-orbital plexus (70% O+ human erythrocytes in RPMI 1640 supplemented with 25mM HEPES, 2mM L-glutamine, 50µM hypoxanthine and 10% human serum). The next day, mice were bled 200µl and received an intraperitoneal injection of 700µl hRBC. Mab transfer was done on day 7 to coincide with the establishment of blood-stage infection. Dosage was 100mg/kg (approximately 2.5mg/mouse) formulated in PBS and delivered

intravenously. The clodronate liposome and cyclophosphamide injections were repeated on days 5, 9, 11, 13. Human RBC was injected daily in a volume of 300-700µl to keep the percentage of hRBC stable between 50% and 70%. If the percentage reached more than 70%, the mice were not injected with hRBC to limit morbidity. On days 7, 9, 11 and 13 each mouse was bled 100µl from the retro-orbital plexus to sample antibody levels.

Quantification of parasite burden

Luciferase activity was measured in the mice using the IVIS Lumina II animal imager (Perkin Elmer). The abdomen of mice was shaved to enhance detection. Mice were injected intraperitoneally with 100µl of luciferase substrate RediJect D-Luciferin (Perkin Elmer) to quantitate specific enzymatic activity. Animals were anesthetized and imaged within 5 minutes of substrate injection. Signal was acquired for 5 minutes using a field of view of 10cm and medium binning factor. Living Image 3.0 software was used to measure total flux (photons/second) of a region of interest, which was placed around each mouse.

2.2.4 Avidity-based extracellular protein interaction screen (AVEXIS)

Biotinylated monomeric bait protein (here PfRH5 in each case) were captured on streptavidin-coated flat-bottomed 96-well microtiter plates in 50µL volumes for 1 hour at room temperature. Plates were then washed 3 times with PBS and incubated with 50µL of human PfRH5-specific mAb for an hour at room temperature. The plates were washed 3 more times in PBS before the addition of 50µL of pentameric β-lactamase-tagged prey proteins (here, PfCyRPA, PfP113 and basigin) for a further hour at room temperature. All wells were subsequently washed twice with PBS-T and then twice with PBS before the addition of 150µL/well of the β-lactamase substrate nitrocefin. Absorbance readings were made at 485nm. All bait and prey proteins were expressed as fusion proteins N-terminal of rat

CD4 domains 3 and 4 (CD4d3+4), a biotin acceptor peptide and a 6His tag. Prey proteins were expressed with a C-terminal with a collagen oligomeric matrix protein (COMP) peptide to promote pentamerisation and a β-lactamase enzyme for quantification purposes.

2.2.5 SPR assay for PfRH5-basigin binding

Data were collected on a Biacore X100 (GE healthcare). Experiments were performed at 25°C in SPR running buffer (PBS + 0.005% Polysorbate-20, GE healthcare). Approximately 670RU of basigin was amine-coupled to a CM5 chip (GE healthcare) on flow cell 2 (Fc 2) using standard NHS/EDC chemistry. PfRH5-mAb complexes were made by mixing PfRH5 and mAb to a final concentration of 0.5µM PfRH5 and 1µM mAb in SPR running buffer. Complexes were injected over Fc 1 and Fc 2 at a flow rate of 10µL/min for 30s and the surface was regenerated with 10mM glycine pH 1.5 for at a flow rate of 10µL/min for 60s. Between experiments, one injection of 0.5µM PfRH5 was made to assess basigin degradation caused by regeneration. The immobilised basigin was a truncation containing immunoglobulin-like domains 1 and 2 (amino acids 22-205), expressed in *E. coli*, and purified by Ni^{2+} affinity chromatography with a 6His-tag (which was subsequently cleaved) and buffer-exchanged into HBS by SEC. All data used was reference subtracted from a non-immobilised flow cell (Fc 2-1). Binding values were measured manually in the Biacore X100 control software.

2.2.6 SPR assay for PfRH5-PfCyRPA binding

Data were collected on a Biacore X100 (GE healthcare). Experiments were performed at 25°C in SPR running buffer (PBS + 0.005% Polysorbate-20, GE healthcare). Mab was injected at a concentration of 20nM at a flow rate of 5µL/min for 35s over Fc 2 on a protein

A coated chip (GE healthcare). Next, PfRH5 was injected over Fc 1 and Fc 2 at a concentration of 50nM at a flow rate of 10µL/min for 120s before injecting PfCyRPA at a concentration of 1µM for 120s, also at a flow rate of 10µL/min. The PfCyRPA protein used was expressed as secreted protein from HEK293 cells and purified by c-tag affinity chromatography. The construct was based on the 3D7 sequence and comprised amino acids 29-362 with three mutations introduced to ablate N-linked glycosylation (S147A, T324A and T364A). All data used was reference subtracted from a non-immobilised flow cell (Fc 2-1). Binding values were measured manually in the Biacore X100 control software.

2.2.7 SPR assay for PfRH5-PfP113 binding

Data were collected on a Biacore X100 (GE healthcare). Experiments were performed at 37°C in SPR running buffer (PBS + 0.005% Polysorbate-20, GE healthcare). The whole experiment was run at a flow rate of 5µL/min. Approximately 1500RU of CAP reagent (GE healthcare) was captured on Fc 1 and Fc 2. On Fc 1, approximately 500RU of a biotinylated control CD4d3+4-tagged protein was immobilised. On Fc 2, each experiment consisted in capturing 1500RU of CAP reagent in an 80s injection, approximately 1800RU of PfP113-Nt in an 80s injection at 20µg/mL. After this, PfRH5-mAB complex (both at 1µM) was flowed over Fc 1 and Fc 2. Flow cell 2 was regenerated between experiments in a 110s injection of 6M guanidine + 250mM NaOH, as per the manufacturer's instructions. PfP113-Nt was expressed at the Sanger Institute (Cambridge, UK) by the Wright lab. PfP113-Nt was based on the 3D7 sequence and comprised amino acids 1-197 with one mutation introduced to ablate N-linked glycosylation (S186A). All data used was reference subtracted from a control-immobilised flow cell (Fc 2-1). Binding values were measured manually in the Biacore X100 control software.

2.2.8 Statistical analysis

Correlations between EC_{30} values from the GIA assay and were assessed by calculating the Spearman rho coefficient (R). This nonparametric test was chosen due to the small sample sizes and because of its ability to detect non-linear relationships. All data analysis was carried out in Prism 5.0 (GraphPad). The threshold for statistical significance (α) was set at 0.05 and *p*-values were two-tailed.

2.3 Chapter V methods

2.3.1 Epitope binning by BLI

Assays were carried out on an OctetRED384 (FortéBio) using streptavidin-coated biosensors (FortéBio) and black 96-well plates (Greiner). The biosensors followed a six-step sequential assay: Baseline (PBS, 30s), Protein immobilisation (neat supernatant, 120s), Wash (PBS, 60s), mAb1 binding (300nM mAb1, 120s), Wash (PBS, 60s), mAb2 binding (150nM mAb2, 120s). The PfRH5 protein sequences used here were based on the 3D7 reference sequence (amino acids 26-526) with mutations N39Q and N214Q to delete glycosylation sequons. The proteins also contained an AviTag™ biotin acceptor peptide followed by a Strep-Tag II™ at the 3' end of the PfRH5-coding sequence. The proteins were expressed as secreted proteins in HEK293F cells, co-expressed with the bacterial BirA biotin ligase for efficient site-specific biotinylation. 72 hours after transfection, supernatants were centrifuged and filtered to remove cell material and then extensively dialysed in PBS to remove free biotin. Mabs were diluted in PBS.

Data presentation

"Relative binding" shown in Figure 5.1 A shows data as shown in equation (1) below where "$Signal_{mAb2}$" was normalised for the amount of PfRH5 bound to the biosensor such that "$Signal_{mAb2}$" = raw nm shift in "mAb2 binding"/raw nm shift in "Protein immobilisation".

$$(1) \quad \text{Relative binding} = \frac{\text{Signal}_{\text{mAb2}} \text{ with mAb1 bound}}{\text{Signal}_{\text{mAb2}} \text{ alone}}$$

The correlation matrix was made in Microsoft Excel using the PEARSON function (see equation (2), below) by correlating binding profiles such that to calculate the Pearson product-moment correlation coefficient of R5.003 and R5.006, the "relative binding" column under R5.003 was correlated pairwise with the "relative binding" column under R5.006.

$$(2) \quad \text{Pearson (r)} = \frac{\sum_{i=1}^{n}(x_i - \bar{x})(y_i - \bar{y})}{\sqrt{\sum_{i=1}^{n}(x_i - \bar{x})^2}\sqrt{\sum_{i=1}^{n}(y_i - \bar{y})^2}}$$

2.3.2 PfRH5-Nt and PfRH5ΔNL ELISAs

Here an indirect ELISA was carried out by coating PfRH5-Nt or PfRH5ΔNL on Maxisorp flat-bottom 96-well ELISA plates (Nunc) at 2µg/mL in 50µL at 4°C overnight. Plates were washed twice with PBS-T and blocked with 200µL of Blocker™ Casein (Thermofisher) for 1 hour. Wells were then incubated with 1000ng/mL of mAb (or PfRH5-immunised rabbit serum diluted 1:100 for the PfRH5-Nt ELISA positive control) for approximately 45 minutes at room temperature then washed 4 times with PBS-T before the addition of 50µL of goat

anti-human gamma-chain alkaline phosphatase-conjugated secondary antibody (goat anti-mouse IgG alkaline phosphatase-conjugated secondary antibody for QA1) (both Sigma-Aldrich) for 45 minutes at room temperature. Wells were then washed 6 times with PBS-T and developed with 100µL of PNPP substrate at 1mg/mL (Sigma-Aldrich) and read on an Infinity F50 plate reader at 405nm (Tecan).

2.3.3 Peptide ELISAs

A set of sixty-two biotinylated 20-mer peptides of PfRH5 overlapping by 12 amino acids (see Appendix 2.2) were custom-synthesised (Mimotopes). The peptides were designed to be oriented and tethered by their N-terminal biotinylated linker peptide (biotin-SGSG) with the exception the first peptide which contained the biotinylated linker at its C-terminus to preserve potential binding activity to the most N-terminal residues. These peptides were coated to the bottom wells of a streptavidin-coated 96-well plate in 50µL. The next day wells were blocked with 200µL of Blocker™ Casein (Thermofisher) and washed five times with PBS-T. Bound mAbs were detected using an anti-human gamma-chain-specific alkaline phosphatase-conjugated secondary antibody (Sigma-Aldrich) or the mouse equivalent for QA1 in 50µL for 30 minutes at a dilution of 1:1000 in PBS and washed five times with PBS-T before being developed with 100µL of PNPP alkaline phosphatase substrate for 20 minutes and read at 405nm on an Infinite 50 plate reader (Tecan).

2.3.4 HDX-MS

Hydrogen-deuterium exchange mass spectrometry was performed using a Waters HDX platform composed of a liquid handling robotic setup (LEAP technologies) for sample preparation and a nano-Acquity UPLC coupled to a Synapt G2-Si (Waters) mass

spectrometer. Non-deuterated and deuterated samples were loaded by the robot. The apo PfRH5 protein or PfRH5-mAb complex was digested in-line using a pepsin-immobilized column at 20°C. The peptides generated from pepsin digestion were trapped on a micro peptide trap for 2 min for the removal of salts at a flow rate of 200µl/min and then separated using a C18 column with a linear gradient of 5–80% acetonitrile (CH_3CN) and water both supplemented with 0.1% formic acid for 12 min at flow rate of 40µL/min. The liquid chromatography temperature was set at 0°C to reduce back-exchange. Sequence coverage and deuterium uptake were analysed by using ProteinLynx Global Server (Waters) and DynamX (Waters) programmes, respectively. Peptide mapping was obtained by using nondeuterated samples in triplicates and only unique peptides present in all three data files were selected for deuterium uptake data analysis. Leucine enkephalin at a continuous flow rate of 5µL/min was sprayed as a lock mass for mass correction.

Peptide mapping

Apo RH5 protein digests provided a list of 2056 peptides, after applying several selection filters and manual inspection only ≈ 130 peptides were selected for analysis. These peptides provided >93% sequence coverage with many overlapping peptides.

HDX Labelling

Deuterated samples were prepared by 10-fold dilutions from 0.7µM of apo PfRH5 or PfRH5-mAb complex in deuterated buffer, the pH of the sample was brought down to 2.3 by adding 50% vol/vol 100mM HCl. The samples were labelled for 20 seconds, 10 minutes and 2 hours. All HDX-MS experiments were performed in duplicate.

2.3.5 X-ray crystallography protein complex preparation

The PfRH5ΔNL sequence used was based on the 3D7 reference sequence and comprised amino acids K140-K247 and N297-Q526 with two glycosylation sequons removed (T216A and T299A) as originally described by Wright *et al*[130]. The construct also contained a four-amino acid c-tag (EPEA) at the C-terminus. A stable *Drosophila* S2 cell line had been previously made as described previously[139]. *Drosophila* S2 cells were cultured in Ex-cell 420 serum-free medium (Sigma-Aldrich). An appropriate number of cells were grown and split to 8E6 cells/mL and incubated in an orbital shaking incubator at 25°C for 96-hours or until the cell density exceeded 6E7 cells/mL. After this cell supernatants were clarified by centrifugation at 2500g for 15 mins and filtered with a 0.22µm membrane. Optionally, if large volumes were harvested, supernatants were concentrated by TFF on a Pellicon device (Millipore) using a 10kDa molecular weight cut-off filter. The concentrate was typically filtered again before purification by affinity chromatography on a 10mL column packed with CaptureSelect c-tag affinity matrix (Thermofischer) on an ÄKTA Pure FPLC system (GE Healthcare). Wash steps were done with 20mM Tris, 150mM NaCl, pH 7.5 and protein was eluted with 20mM Tris, 2M $MgCl_2$. The protein eluate was then extensively dialysed into 20mM HEPES, 150mM NaCl, pH 7.5 using slide-A-Lyzer dialysis cassettes at room temperature. PfRH5ΔNL was rid of glycosylated contaminants by lectin chromatography by passing the dialysed protein over a HiTrap Con A 4B column (GE Healthcare) in a continuous loop for 30 mins. The protein was then subjected to limited proteolysis by the addition of endoproteinase gluC (New England Biolabs) at 1mg/mL in a 1:1000 final volume of protein solution. Antibody Fab fragments were generated by papain digestion and purified from Fc fragments with protein A using a Pierce Fab Preparation kit (Thermofischer) following the manufacturer's recommendations. Fab and PfRH5ΔNL were mixed at an approximate 1:1 ratio and methylated with 1M ABC and 1M formaldehyde following the

method of Walter *et al*[174]. Lysine methylation is a common strategy used to decrease the solubility of protein to encourage crystallisation. The complex was then concentrated to 1mL in an Amicon ultra spin filter (30kDa MW cut-off, Millipore) and separated and buffer-exchanged by SEC using a HiLoad 16/60 Superdex 200pg on an ÄKTA Purifier FPLC system (GE Healthcare) kept in a temperature-controlled cabinet at 4°C. The SEC column was equilibrated and run in 20mM HEPES, 150mM NaCl, pH 7.5. Fractionation resolution was 1.5mL. Fractions identified as containing Fab-PfRH5ΔNL complex were pooled and concentrated in an Amicon ultra spin filter (30kDa MW cut-off, Millipore) in a temperature controlled microfuge set at 4°C until the concentration reached 8-12mg/mL.

2.3.6 X-ray crystallography initial screens

The crystal-growing phase of crystallography is entirely empirical, with every protein and protein complex being susceptible to crystallising in different conditions. Because of this, at the beginning of every new PfRH5ΔNL-Fab complex, a broad set of sparse matrix screens were used to identify initial hit conditions. Sparse matrix screens were set up in a sitting drop vapour-diffusion set-up in 200nL drops composed of 50% 8-12mg/mL protein solution and 50% well solution using a Mosquito crystal liquid handling robot (TTP Labtech). Typically, screens in the conditions contained in 96-well JCGS+ (Molecular Dimensions), JCSG core suite IV (Qiagen), Proplex (Molecular Dimensions), PGA (Molecular Dimensions), PACT (Molecular Dimensions), Morpheus (Molecular Dimensions) and MIDAS (Molecular Dimensions) screens were set up at either 18°C, 4°C or both.

2.3.7 X-ray crystallography crystal optimisation

Once an initial hit condition was identified, crystals were optimised using a variety of standard methods. Grid screens centred on the initial hit condition were varied by precipitant, salt or protein concentration. In addition, to accelerate nucleation, drops were seeded by adding microcrystals generated by maceration of the initial crystals with a ceramic bead (Seed Bead, Hampton Research) by simple addition into the drop or by streak-seeding with a horse hair coated in crystal seeds. Commonly, additive screens such as Silver Bullets (Hampton Research) containing a wide range of chemicals were included as altrenative optimisation screens. Optimisation screen plates were either set up in MRC 2-subwell crystallisation plates (96-well format, Swisssci) in 250nL drops or in 15-well EasyXtal tools (Qiagen) in 1µL or 2µL drops.

2.3.8 X-ray crystallography crystal freezing

Crystals were "fished" using an appropriately-sized nylon loop (usually 50-300µm in diameter) under a standard light microscope and transferred into a mother liquor containing a cryoprotectant (MPD, glycerol, ethylene glycol, or low MW PEG), if necessary, and vitrified in liquid nitrogen. Crystals were frozen at the temperature which led to their growth.

2.3.9 SDS-PAGE and protein staining

Samples for SDS-PAGE were prepared by adding 20mM DTT in Laemmli buffer (BioRad) and incubating the samples at 99°C for 10 mins. SDS-PAGE was carried out in 26-well NuPAGE 4-12% gradient polyacrilamide gels (Thermofisher) run in MES buffer for 45 mins at 200V constant voltage. 8µL of Precision Plus Protein unstained protein standard with a 10-

250kDa MW range (BioRad) was used for MW estimation. Gels were then washed once in deionised H_2O and total protein staining was done with Quick Coomassie stain (Generon) by submerging the gel for 30 minutes and washing with several changes of deionised H_2O.

2.3.10 X-ray crystallography data collection and molecular replacement

Crystallography data were collected at Diamond Light Source (Harwell Science and Innovation Campus, UK) at beamline I04 (wavelength 0.97949Å) and data reduction was carried out by the CCP4 processing suite[175]. Molecular replacement is one available method for solving the phase problem which borrows starting phases from a related known structure with ≥40% sequence identity. The known search model is rotated and translated in the unit cell or the asymmetric unit to arrive at a solution, representing the best fit between the calculated diffraction data from the molecular-replaced model and the data from the unknown structure. Phaser[176] was used to Fab search models were made from PDB entry 5K9O for R5.016, 4HK0 for R5.015 and a composite of 3TNN and 4KQ3 for R5.004. Chain A of 4U0R was used as the search model for PfRH5ΔNL.

2.3.11 Assay of growth inhibitory activity (GIA)

As described in the Chapter IV methods.

2.3.12 Quantification of the concentration of PfRH5-specific antibody in purified IgG

The specific concentration of antibody binding to PfRH5 was determined using the standardised ELISA method described by Miura *et al*[177]. In these ELISAs, an identical dilution series of a "standard" serum sample is made on each plate. The hyperbolic

relationship between IgG concentration and OD_{405} can only be approximated to a straight line in a certain range of IgG concentrations, and test samples are diluted such that they yield OD values (at 405nm) that fall in this range. In this manner, the IgG concentration in a diluted serum or purified IgG sample can be interpolated, and the IgG concentration in the original sample back-calculated. The method, as described by Miura *et al*., allows for a relative comparison between samples by comparing "ELISA units"; the dilution at which a sample gives an OD_{405} of 1 when assayed on the antigen of interest. Previous work by the Draper group has established a link between arbitrary "ELISA units" and an absolute antibody concentration by calibration-free concentration analysis (CFCA) using a Biacore T200. The constant of proportionality between an ELISA unit and was measured at: 1 ELISA unit = 0.434µg/mL.

2.3.13 Statistical analysis

Vaccine groups were compared using the non-parametric Mann-Whitney U test. Nonlinear least-squares regression was used to approximate EC_{50} values; these were interpolated by fitting a four-parameter dose-response curve to the relationship between Log_{10}(dose, µg/mL)) and GIA (%). All data analysis was carried out in Prism 5.0 (GraphPad). The threshold for statistical significance (α) was set at 0.05.

2.4 Chapter VI methods

2.4.1 Assay of growth inhibitory activity (GIA)

As described in the Chapter IV methods.

2.5 Appendices

Appendix 2.1: Primer list for mAb Vγ, Vκ, Vλ amplification by PCR

	Primer name	5’ to 3’ sequence
1	5' L VH1	ACAGGTGCCCACTCCCAGGTGCAG
2	5' L VH3	AAGGTGTCCAGTGTGARGTGCAG
3	5' L VH4/6	CCCAGATGGGTCCTGTCCCAGGTGCAG
4	5' L VH5	CAAGGAGTCTGTTCCGAGGTGCAG
5	3' Cγ CH1	GGAAGGTGTGCACGCCGCTGGTC
6	5' L VK1/2	ATGAGGSTCCCYGCTCAGCTGCTGG
7	5' L VK3	CTCTTCCTCCTGCTACTCTGGCTCCCAG
8	5' L VK4	ATTTCTCTGTTGCTCTGGATCTCTG
9	3' CK 543	GTTTCTCGTAGTCTGCTTTGCTCA
10	5' L Vλ1	GGTCCTGGGCCCAGTCTGTGCTG
11	5' L Vλ2	GGTCCTGGGCCCAGTCTGCCCTG
12	5' L Vλ3	GCTCTGTGACCTCCTATGAGCTG
13	5' L Vλ4/5	GGTCTCTCTCSCAGCYTGTGCTG
14	5' L Vλ6	GTTCTTGGGCCAATTTTATGCTG
15	5' L Vλ7	GGTCCAATTCYCAGGCTGTGGTG
16	5' L Vλ8	GAGTGGATTCTCAGACTGTGGTG
17	3' Cλ	CACCAGTGTGGCCTTGTTGGCTTG
18	CPEC VH1/5/7	CTTTTTCTAGTAGCAACTGCAACCGGTGTACATTCCGAGGTGCAGCTGGTGCAG
19	CPEC VH3	CTTTTTCTAGTAGCAACTGCAACCGGTGTACATTCTGAGGTGCAGCTGGTGGAG
20	CPEC VH4	CTTTTTCTAGTAGCAACTGCAACCGGTGTACATTCCCAGGTGCAGCTGCAGGAG
21	CPEC VH3-23	CTTTTTCTAGTAGCAACTGCAACCGGTGTACATTCTGAGGTGCAGCTGTTGGAG
22	CPEC VH4-34	CTTTTTCTAGTAGCAACTGCAACCGGTGTACATTCCCAGGTGCAGCTACAGCAGTG
23	CPEC VH1–18	CTTTTTCTAGTAGCAACTGCAACCGGTGTACATTCCCAGGTTCAGCTGGTGCAG
24	CPEC VH1–24	CTTTTTCTAGTAGCAACTGCAACCGGTGTACATTCCCAGGTCCAGCTGGTACAG
25	CPEC VH3–9/30/33	CTTTTTCTAGTAGCAACTGCAACCGGTGTACATTCTGAAGTGCAGCTGGTGGAG
26	CPEC VH6–1	CTTTTTCTAGTAGCAACTGCAACCGGTGTACATTCCCAGGTACAGCTGCAGCAG
27	CPEC VH4–39	CTTTTTCTAGTAGCAACTGCAACCGGTGTACATTCCCAGCTGCAGCTGCAGGAG
28	CPEC VH3–33	CTTTTTCTAGTAGCAACTGCAACCGGTGTACATTCTCAGGTGCAGCTGGTGGAG
29	CPEC JH1/2/4/5	GATGGGCCCTTGGTCGACGCTGAGGAGACGGTGACCAG
30	CPEC JH3	GATGGGCCCTTGGTCGACGCTGAAGAGACGGTGACCATTG
31	CPEC JH6	GATGGGCCCTTGGTCGACGCTGAGGAGACGGTGACCGTG
32	CPEC VK1	CTTTTTCTAGTAGCAACTGCAACCGGTGTACATTCTGACATCCAGATGACCCAGTC
33	CPEC VK1-9/1-13	CTTTTTCTAGTAGCAACTGCAACCGGTGTACATTCAGACATCCAGTTGACCCAGTCT
34	CPEC VK1D-43/1-8	CTTTTTCTAGTAGCAACTGCAACCGGTGTACATTGTGCCATCCGGATGACCCAGTC
35	CPEC VK2	CTTTTTCTAGTAGCAACTGCAACCGGTGTACATGGGGATATTGTGATGACCCAGAC
36	CPEC VK2-28/2-30	CTTTTTCTAGTAGCAACTGCAACCGGTGTACATGGGGATATTGTGATGACTCAGTC
37	CPEC VK3-11/3D-11	CTTTTTCTAGTAGCAACTGCAACCGGTGTACATTCAGAAATTGTGTTGACACAGTC

38	CPEC VK3-15/3D-15	CTTTTTCTAGTAGCAACTGCAACCGGTGTACATTCAGAAATAGTGATGACGCAGTC
39	CPEC VK3-20/3D-20	CTTTTTCTAGTAGCAACTGCAACCGGTGTACATTCAGAAATTGTGTTGACGCAGTCT
40	CPEC VK4-1	CTTTTTCTAGTAGCAACTGCAACCGGTGTACATTCGGACATCGTGATGACCCAGTC
41	CPEC JK1/2/4	ATGGTGCAGCCACCGTACGTTTGATYTCCACCTTGGTC
42	CPEC JK3	ATGGTGCAGCCACCGTACGTTTGATATCCACTTTGGTC
43	CPEC JK5	ATGGTGCAGCCACCGTACGTTTAATCTCCAGTCGTGTC
44	CPEC JK150/3	ATGGTGCAGCCACCGTACGTCTGATTTCCACCTTGGTC
45	CPEC VL1	CTTTTTCTAGTAGCAACTGCAACCGGTTCCTGGGCCCAGTCTGTGCTGACKCAG
46	CPEC VL2	CTTTTTCTAGTAGCAACTGCAACCGGTTCCTGGGCCCAGTCTGCCCTGACTCAG
47	CPEC VL3	CTTTTTCTAGTAGCAACTGCAACCGGTTCTGTGACCTCCTATGAGCTGACWCAG
48	CPEC VL4/5	CTTTTTCTAGTAGCAACTGCAACCGGTTCTCTCTCSCAGCYTGTGCTGACTCA
49	CPEC VL6	CTTTTTCTAGTAGCAACTGCAACCGGTTCTTGGGCCAATTTTATGCTGACTCAG
50	CPEC VL7/8	CTTTTTCTAGTAGCAACTGCAACCGGTTCCAATTCYCAGRCTGTGGTGACYCAG
51	CPEC CL reverse	GGCTTGAAGCTCCTCACTCGAGGGYGGGAACAGAGTG

Appendix 2.2: List of biotinylated PfRH5 peptide 20-mers

1 : ENAIKKTKNQENQLTLLPIKGSG	23 : SGSGKCIAVDAFIKKIQETYDKVK	45 : SGSGKDLSDMTNILQQSELLLTNL
2 : SGSGNQENQLTLLPIKSTEEEKDD	24 : SGSGIKKIQETYDKVKSKCNDIKN	46 : SGSGILQQSELLLTNLNKKMGSYI
3 : SGSGLPIKSTEEEKDDIKNGKDIK	25 : SGSGDKVKSKCNDIKNDLIATIKK	47 : SGSGLTNLNKKMGSYIYIDTIKFI
4 : SGSGEKDDIKNGKDIKKEIDNDKE	26 : SGSGDIKNDLIATIKKLEHPYDIN	48 : SGSGGSYIYIDTIKFIHKEMKHIF
5 : SGSGKDIKKEIDNDKENIKTNNAK	27 : SGSGTIKKLEHPYDINNKNDDSYR	49 : SGSGIKFIHKEMKHIFNRIEYHTK
6 : SGSGNDKENIKTNNAKDHSTYIKS	28 : SGSGYDINNKNDDSYRYDISEEID	50 : SGSGKHIFNRIEYHTKIINDKTKI
7 : SGSGNNAKDHSTYIKSYLNTNVND	29 : SGSGDSYRYDISEEIDDKSEETDD	51 : SGSGYHTKIINDKTKIIQDKIKLN
8 : SGSGYIKSYLNTNVNDGLKYLFIP	30 : SGSGEEIDDKSEETDDETEEVEDS	52 : SGSGKTKIIQDKIKLNIWRTFQKD
9 : SGSGNVNDGLKYLFIPSHNSFIKK	31 : SGSGETDDETEEVEDSIQDTDSNH	53 : SGSGIKLNIWRTFQKDELLKRILD
10 : SGSGLFIPSHNSFIKKYSVFNQIN	32 : SGSGVEDSIQDTDSNHTPSNKKKN	54 : SGSGFQKDELLKRILDMSNEYSLF
11 : SGSGFIKKYSVFNQINDGMLLNEK	33 : SGSGDSNHTPSNKKKNDLMNRTFK	55 : SGSGRILDMSNEYSLFITSDHLRQ
12 : SGSGNQINDGMLLNEKNDVKNNED	34 : SGSGKKKNDLMNRTFKKMMDEYNT	56 : SGSGYSLFITSDHLRQMLYNTFYS
13 :	35 :	57 :

SGSGLNEKNDVKNNEDYKNVDYKN	SGSGRTFKKMMDEYNTKKKKLIKC	SGSGHLRQMLYNTFYSKEKHLNNI
14 : SGSGNNEDYKNVDYKNVNFLQYHF	36 : SGSGEYNTKKKKLIKCIKNHENDF	58 : SGSGTFYSKEKHLNNIFHHLIYVL
15 : SGSGDYKNVNFLQYHFKELSNYNI	37 : SGSGLIKCIKNHENDFNKICMDMK	59 : SGSGLNNIFHHLIYVLQMKFNDVP
16 : SGSGQYHFKELSNYNIANSIDILQ	38 : SGSGENDFNKICMDMKNYGTNLFE	60 : SGSGIYVLQMKFNDVPIKMEYFQT
17 : SGSGNYNIANSIDILQEKEGHLDF	39 : SGSGMDMKNYGTNLFEQLSCYNNN	61 : SGSGNDVPIKMEYFQTYKKNKPLT
18 : SGSGDILQEKEGHLDFVIIPHYTF	40 : SGSGNLFEQLSCYNNNFCNTNGIR	62 : SGSGDVPIKMEYFQTYKKNKPLTQ
19 : SGSGHLDFVIIPHYTFLDYYKHLS	41 : SGSGYNNNFCNTNGIRYHYDEYIH	
20 : SGSGHYTFLDYYKHLSYNSIYHKS	42 : SGSGNGIRYHYDEYIHKLILSVKS	
21 : SGSGKHLSYNSIYHKSSTYGKCIA	43 : SGSGEYIHKLILSVKSKNLNKDLS	
22 : SGSGYHKSSTYGKCIAVDAFIKKI	44 : SGSGSVKSKNLNKDLSDMTNILQQ	

Chapter III: Isolation and *in vitro* testing of PfRH5-specific monoclonal antibodies

3.1 Authorship statement

Dr. Sean Elias and Andrew Worth helped stain and sort the plasmablasts. Bernadeta Dadonaite and Francesca Donnellan amplified antibody genes, cloned plasmids, expressed antibodies and screened the supernatants in 3 of 11 plates under my supervision. Geneviève Labbé assisted by carrying out the RT-PCR and PCR1 of around half of the plates.

3.2 Introduction

Monoclonal antibodies (mAbs) are powerful tools in the biological sciences and have become both indispensable research workhorses and leading therapeutic agents. Due to their high affinities of interaction, their bivalent nature and their high specificity for their target, this class of biomolecules is among the most well understood both on levels genetic and proteomic. Classically, mAbs have been isolated from antibody-secreting immortalised B cells called hybridomas, usually derived from the fusion of mouse B cells with myeloma partner cells as described in the seminal work by Köhler and Milstein in the 1970s[178], work which earnt them co-receipt of a Nobel prize in 1984 with Niels Jerne. Various methods to isolate and express human monoclonal antibodies have since been developed, often more elaborate due to the increased difficulty in gaining access to human B cell-rich tissue

samples. Fully human hybridomas[179], EBV-immortalised human B cells[180], transgenic mice carrying a human antibody repertoire[181], proteomic methods[182,183], human V_H and V_L phage libraries[184] as well as the single-cell cloning methods[185,186] used in this chapter have all been developed with varying success. Importantly, the method I used preserves cognate HC/LC pairing which is crucial for preserving the binding properties of mAbs whose paratope matured as a unique HC/LC pair. Furthermore, this method was chosen for its technical tractability at medium scale with the material at my disposal. It also presented a unique opportunity to isolate human antibodies from an ongoing clinical trial of PfRH5 (VAC057) and therefore to study the humoral response to PfRH5 delivered as a vaccine using a human-compatible regime. Some important work has been done studying mouse mAbs to PfRH5, however, the information gained from mouse immune responses will be limited by intrinsic differences in immune system biology[187]. Differences in the antibody response to Dengue virus proteins[188] and Meningococcal proteins[189] have been reported before and there is no reason to believe this wouldn't extend to malaria proteins.

VAC057[171] was a 2015 first-in-human Phase Ia safety and immunogenicity clinical trial of PfRH5 (3D7 clone) which enrolled 24 healthy volunteers. Sixteen volunteers were vaccinated twice; once with $5x10^{10}$vp ChAd63 PfRH5 and once with $1x10^{8}$pfu (group 2B) or $2x10^{8}$pfu (group 2C) MVA PfRH5 following an 8-week prime-boost interval. Viral vectored vaccines involve the use of replication-deficient viruses carrying a heterologous expression cassette coding for the vaccine antigen of choice for ectopic expression from the muscle (deltoid) of vaccinees[190]. Classically, these viral vectors induce a strong T cell response but a relatively modest humoral response[191,192]. The use of viral-vectored vaccines serves to circumvent recombinant protein expression and purification to cGMP standards at scale, an attractive feature for often difficult-to-produce malaria proteins[138]. The specific aims of this chapter were to set up the methods necessary to isolate vaccine-specific mAbs, isolate a panel of

unique PfRH5-specific mAbs and to characterise the properties and identify the differences and similarities between mAbs in the panel.

3.3 Overview of the mAb isolation protocol

Broadly speaking, I followed the outline of the protocol by Smith *et al.* (2009)[186] with the exception of some PCR and cloning steps which were modified as discussed in in 3.3.2 and 3.3.3.

3.3.1 Plasmablast isolation

Classically, B cell activation by protein antigen occurs in response to crosslinking of B cell receptors on the B cell surface and T_{FH} cell co-stimulation with CD40L and IL-21 and/or IL-4. Upon activation, B cells follow one of two divergent fates dependent on the upregulation of different transcription factors. Either they commit to plasma cell differentiation (IRF-4, Blimp-1, XBP-1) or they remain in the B cell phenotype as quiescent memory B cells (mBC) (Bcl-6, Pax-5, IRF-8)[193]. Because terminally-differentiated long-lived plasma cells reside in the bone marrow, circulating plasmablasts are the most differentiated antibody-secreting cell type to which researchers have easy access. Plasmablasts are activated B cells in the process of terminal differentiation into plasma cells as well being a short-lived cell type in their own right[194]. Plasmablasts were isolated on the 7th day after boosting, a widely reported peak for peripheral blood antibody secreting cells (ASC)[195,196] including following malaria protein vaccination[191,197]. Phenotypic changes occur during the plasmablast maturation process like BCR downregulation, upregulation of CD38 and downregulation of B cell-specific marker CD20[193,198–201], as a result they can require a complex flow panel to sort. B cells were first

enriched from PBMC to increase their frequency when flow-sorting and to reduce non-specific staining. ASCs used for antibody cloning were sorted according to the panel described in Smith *et al.*: CD19+, CD20-, CD27^{hi}, IgG+ (if possible), CD38^{hi}.

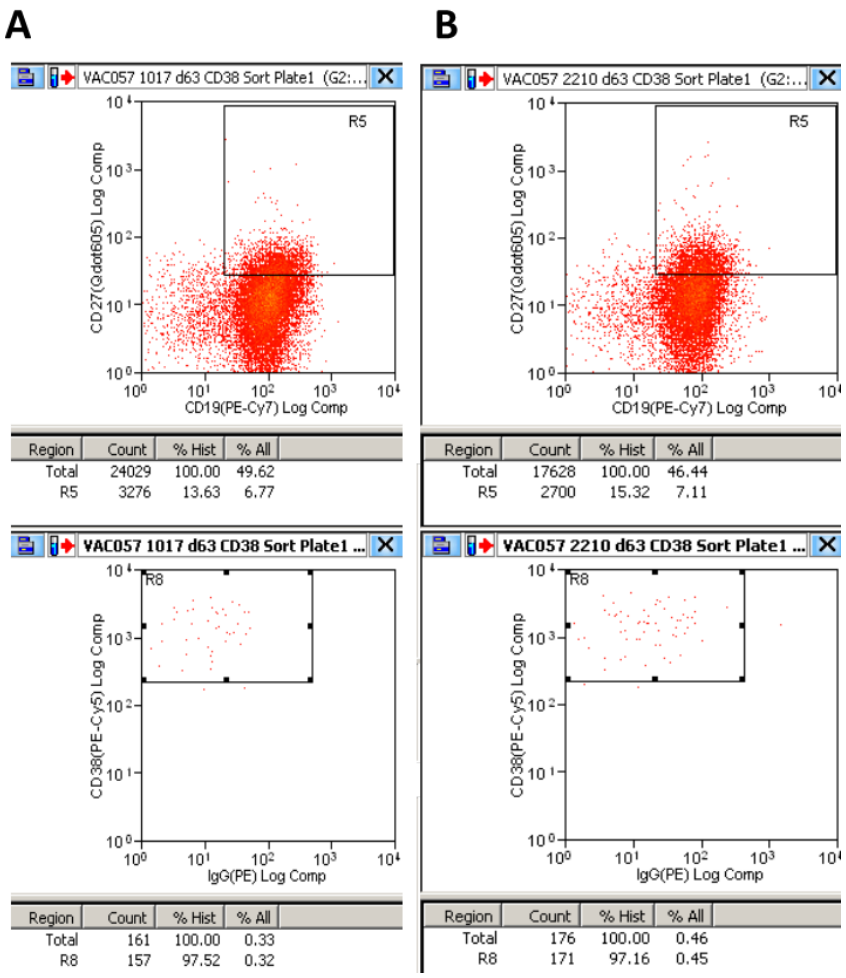

Figure 3.1: Scatter plots of CD38$^+$/IgG$^+$ peripheral blood plasmablasts. These data show staining and single-cell sorting for volunteers 1017 (A) and 2210 (B) 7 days after second immunisation (day 63).

In addition to plasmablast frequency having been low (≈ 0.4% of CD19$^+$ CD27$^+$ lymphocytes), plasmablast-phenotype cells were largely poorly stained with anti-IgG, suggesting one or a combination of early BCR downregulation, non-specific staining or a

significant proportion of non-IgG-secreting ASC (Figure 3.1). The small vaccine-induced ASC response, lack of definitive IgG staining along with the knowledge that only around 50% of sorted cells yielded a gamma-chain PCR product (see Figure 3.2) leads me to believe that many of the other cells sorted are in fact IgM-secreting vaccine-induced ASC or "background" (non-vaccine-induced) blood-borne $CD19^{+}$ $CD20^{-}$ $CD38^{hi}$ IgA B cells which are known to circulate in a steady state[202]. Typically between 50 and 200 $CD38^{hi}$ cells were sorted per volunteer donation (5 million cells) at day 63.

3.3.2 V_H/V_L gene amplification (PCR)

Amplifying variable region DNA from the two copies present in genomic DNA from a single cell would be a low success strategy. Luckily, the plasmablast stage in a B cell's lifecycle is highly active in terms of antibody secretion[203]; as a result the antibody-coding mRNA copy number exceeds the DNA copy number by orders of magnitude. A degenerate primer set originally designed by Tiller *et al.*[185] is intended to cover the allotype diversity observed at the annealing sites. A separate set was used here in both of the subsequent PCRs (RT-PCR/PCR1 and PCR2). In the RT-PCR, specific primers and reverse-transcriptase convert mRNA to cDNA from the leader sequence of the HC or LC ORF to the 5' end of Cγ, Cκ or Cλ. The next PCR (PCR1) amplifies this cDNA using the same primer set to generate sufficient template for the final, more specific cloning PCR which follows (PCR2). In PCR2 (Figure 3.2), a larger and more specific set of degenerate primers, still covering all variable exon family diversity, is designed to put the variable domain-coding region in frame with the plasmid ORF and add the 5' and 3' adjuncts necessary for cloning. Taking Figure 1.2 as an example, this PCR would amplify from the most 5' end of V_H13 to the most 3' end of J_H6 in the V_γ PCR. The primers were previously modified from the Tiller *et al.* list to include a 27bp

5’ and a 18bp (V_γ), 19bp (Vκ) or 22bp (Vλ) 3’ homology region with the insertion site flanks for CPEC (see materials and methods). With the exception of the reverse-transcription, all PCR extensions were carried out by a high-fidelity proofreading polymerase (Phusion HF) instead of *Taq* polymerase[186] in an effort to minimise errors introduced by PCR. With the PCR buffer composition, primer sequences and polymerase differing from the original PCR protocol, conditions needed to be re-optimised. High annealing temperatures and the addition of DMSO were necessary to achieve specific high-level amplification.

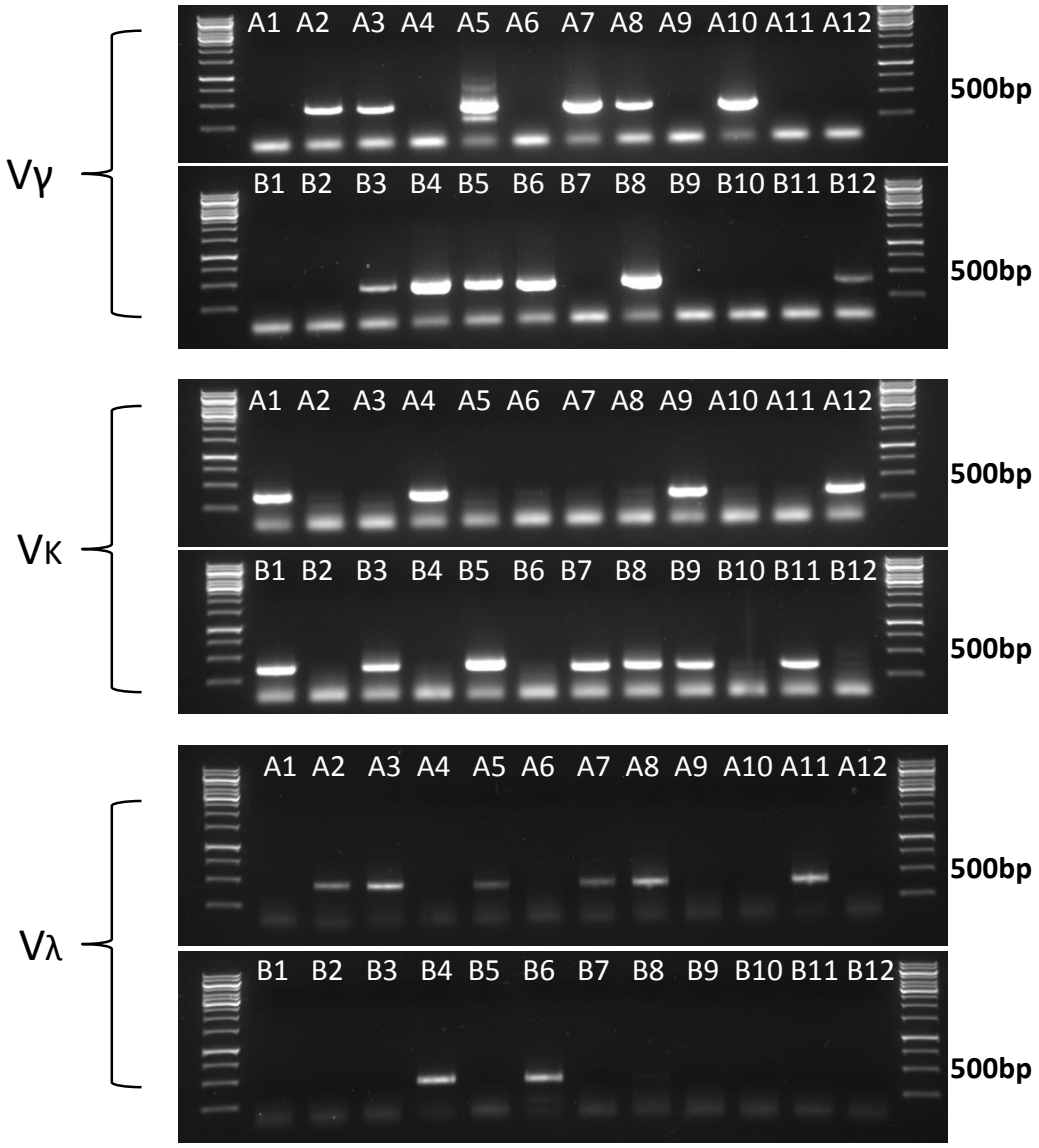

Figure 3.2: PCR amplification of Vγ, Vκ and Vλ exon inserts (PCR2). Each lane represents a PCR product from a single plasmablast. The expected size of the PCR amplicons was approximately 420bp for V_γ, 395bp for Vκ and 430bp for Vλ. Amplicons were run on a 1% agarose gel.

3.3.3 V_H/V_L gene cloning

Because we anticipated a large number of cloning reactions, in the interest of hands-on time saving and cost minimisation, a number of alternative cloning methods were considered such as sequence and ligation-independent cloning (SLIC)[204], Gibson assembly[205], Gateway cloning[206], circular polymerase extension cloning (CPEC)[207] and In-Fusion cloning[208]. The original Smith *et al.* protocol relied on tedious rounds of DNA digestion with restriction enzymes, gel electrophoresis and gel extraction to prepare the newly amplified V_H/V_L genes for cloning into a mammalian expression vector. CPEC was chosen as a cheap, fast and efficient alternative for cloning the variable genes. More recently, others have also adopted CPEC for cloning antibody variable exons into expression plasmids[209]. To increase the efficiency of cloning and keep the plasmid size relatively small, I opted to keep the HC and LC expression cassettes on separate plasmids (Figure 3.3). V_H exons were cloned in frame with an IgG1 constant domain, Vκ exons were cloned in frame with a Cκ constant domain and Vλ exons were expressed in frame with a Cλ2 constant domain.

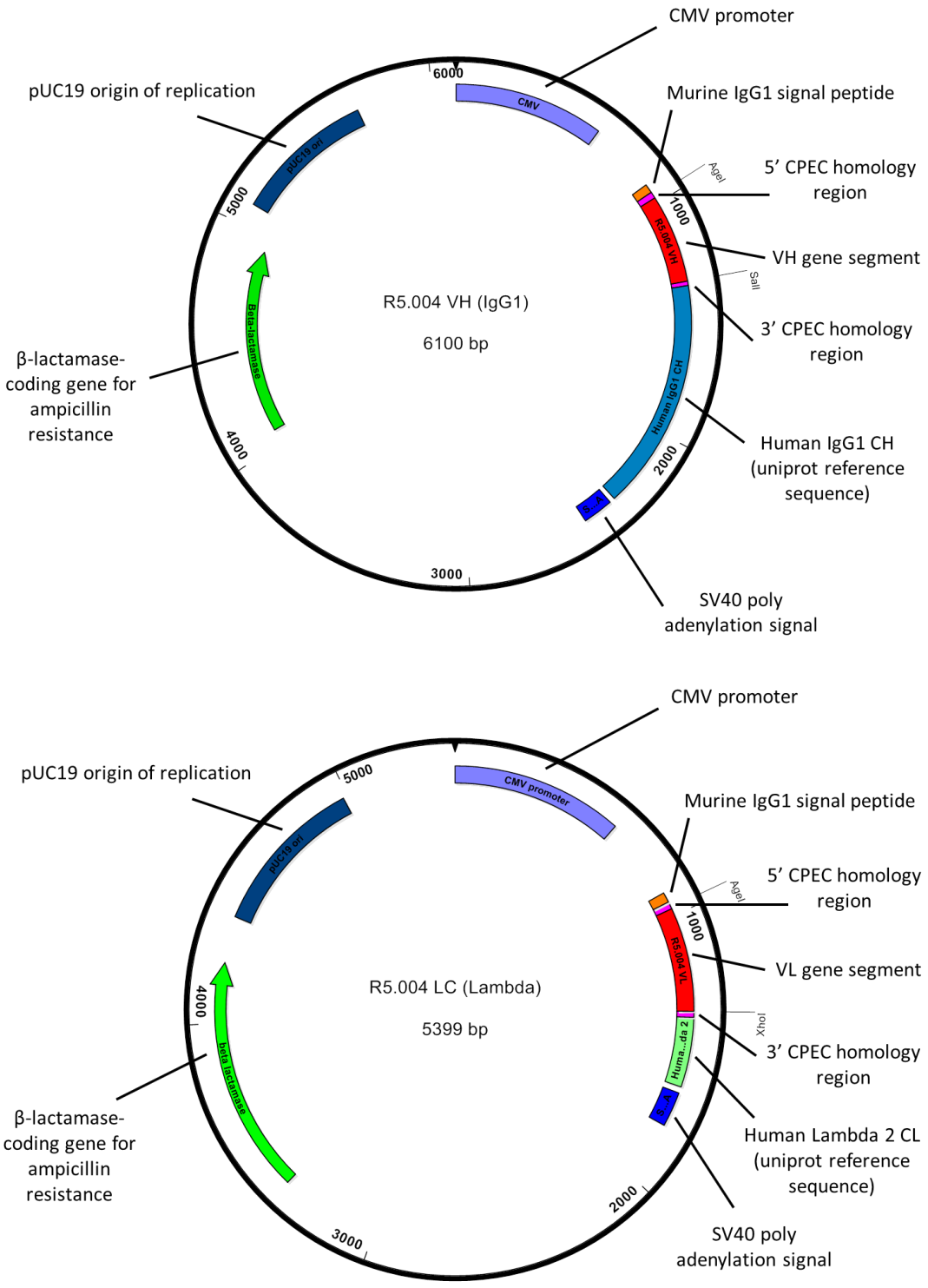

Figure 3.3: Plasmid maps of the expression plasmids used for recombinant mAb expression. The example maps used here are for the heavy chain (top) and light chain (bottom) of a mAb later named R5.004. Plasmids were obtained from the Wilson group[195].

In CPEC (Figure 3.4 A), an insert is amplified with a 15-30bp sequence at either end which is complementary to the ends of the vector into which one wishes to insert the gene, previously

opened with the appropriate restriction enzymes (AgeI-SalI for HC plasmids, AgeI-XhoI for Cλ plasmids and AgeI-BsiWI for Cκ plasmids). The insert and linearised vector are mixed and heated to 98˚C to denature complementary strands and generate single-stranded DNA. The temperature is then decreased following a slow ramp to below the melting temperature (Tm) of the overlapping sequences, with the aim that in the place of the sense and antisense strands of the vector annealing back together, the sense strand of the insert extremity will anneal with the vector antisense strand and vice-versa. The annealed complementary strands are then substrates for any DNA-dependent DNA polymerase and are thus extended by a high-fidelity proof-reading polymerase to complete the complementary strand of the plasmid leaving only a single nick on each strand. The product runs on a gel with two bands, as shown in Figure 3.4 B. The success of this process relies on the overlapping sequences having a high (60-70˚C) and very similar Tm. Once optimised, CPEC yielded correctly-assembled clones in around 90-95% of colonies (Figure 3.4 C).

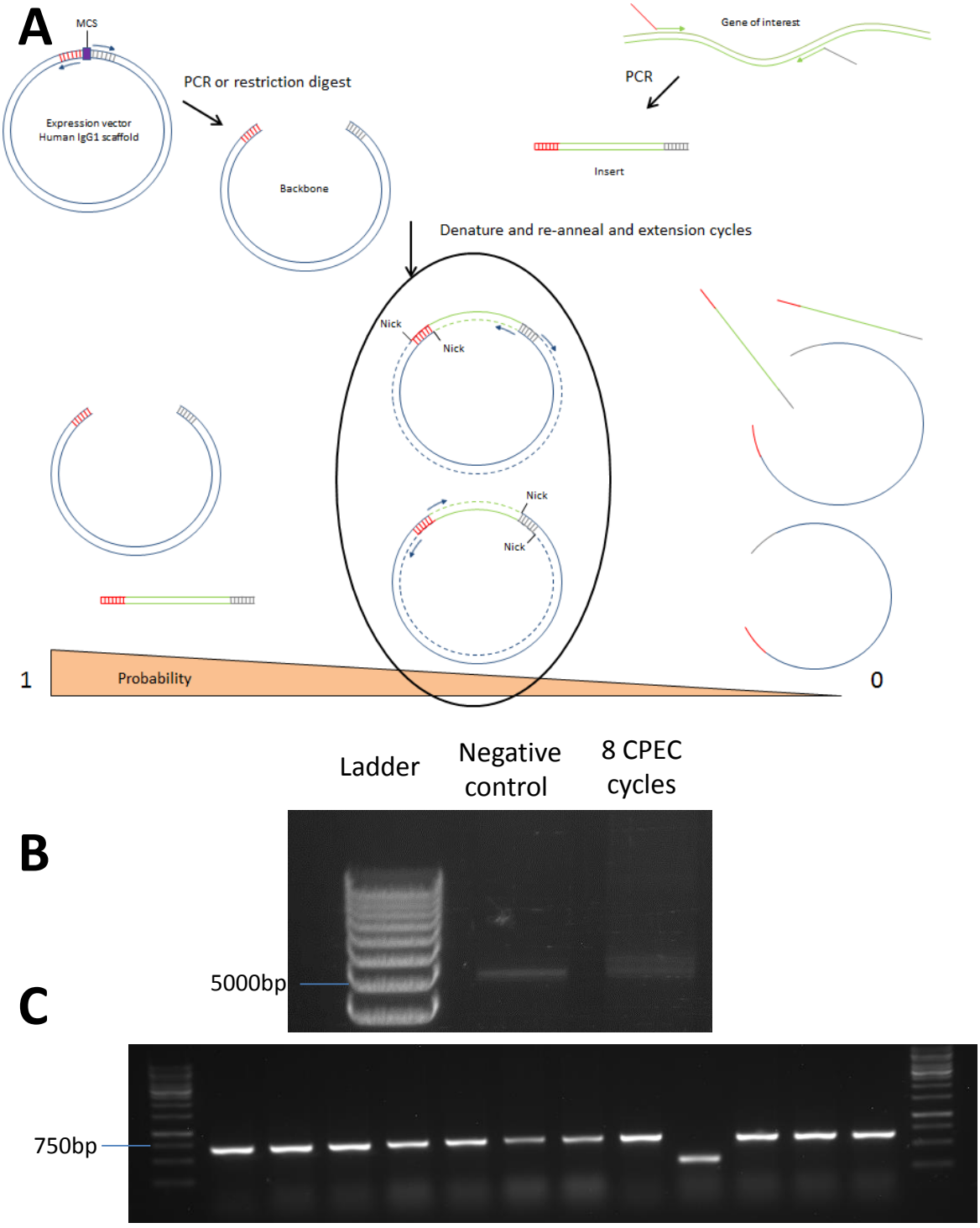

Figure 3.4: (A) Diagram of CPEC assembly cloning. (B) 0.7% agarose gel of linearised Cλ plasmid CPEC-assembled with water as a negative control (left) and linearised Cλ plasmid CPEC-assembled with a VL exon (right). The expected size of linear Cλ plasmid is 5019bp and 5399bp for the plasmid and insert. (C) PCR colony screen of Vγ exons in 12 CPEC-assembled HC colonies. The expected size of a successful assembly is ≈ 675bp.

3.3.4 Antibody expression and screening

Cognate HC- and LC-coding plasmids were co-transfected in adherent HEK293 cells using linear 25kDa polyethylenimine (PEI) in small volumes in single wells of a 96-well cell culture plate. HEK293 cells are known to readily express correctly-folded, correctly-glycosylated human antibodies in large quantities when transfected into these cells using PEI[210,211]. To test the presence of IgG secretion and PfRH5 specificity, I screened transfected HEK293 supernatants by ELISA (Figure 3.5 B). Unlike in the original Smith *et al.* protocol, in the interest of time and cost saving I chose not to sequence plasmids prior to transfection to check that a productive variable gene had been cloned in the correct reading frame. This led me to include an anti-human IgG sandwich ELISA in the screening process to confirm the presence of soluble human IgG expression from transfected cells (Figure 3.5 A).

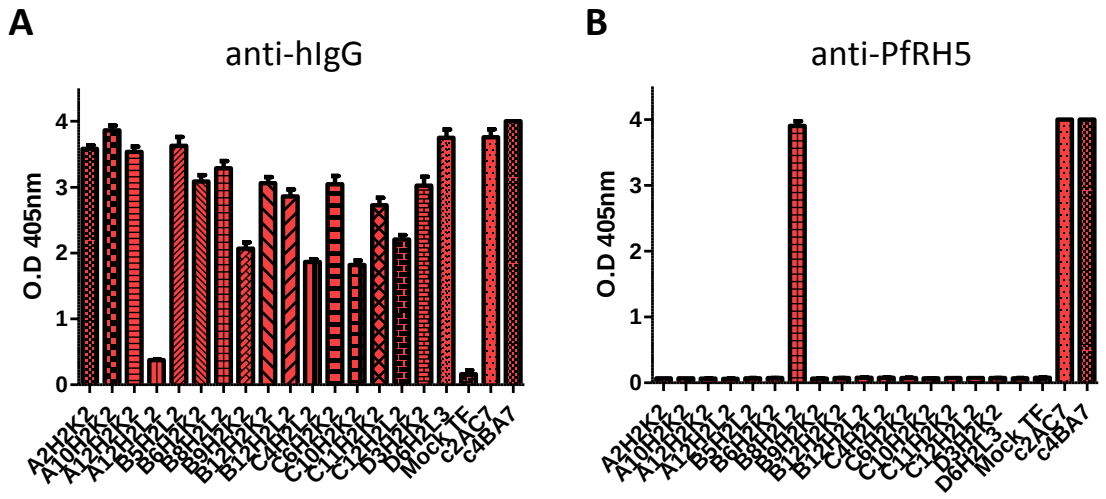

Figure 3.5: ELISA screen for PfRH5-reactivity. Panel A: Anti-human IgG sandwich ELISA showing IgG expression levels of 17 successfully cloned plasmids originating from plasmablasts isolated from volunteer 1019. Panel B: Indirect anti-PfRH5 ELISA showing a single positive clone. This clone corresponds to the subsequently renamed R5.004. A mock transfection (Mock TF) with no DNA and c2AC7/c4BA7 were included as negative and positive controls, respectively. Data shown are the average of three separately transfected wells, error bars are standard deviation.

3.4 Isolating mAbs from VAC057 in numbers

Sorted plates of ASC were initially cloned as and when they were available because the trial was ongoing, but as the trial progressed and more data were available PfRH5-specific ASC ELISPOTs and purified IgG *P. falciparum* growth inhibition assays were used to select plates sorted from volunteers with the best responses. Volunteers 2207 and 2209 were selected based on their high specific ASC response (Figure 3.6 A) and 2210 was selected based on the high inhibitory properties of their PfRH5-specific IgG (Figure 3.6 B). There is debate over whether plasmablast-derived IgG reflects serum IgG[212–214]. However, there was no obvious relationship between either of these selection criteria and the number of successfully cloned PfRH5-specific antibody genes (see Figure 3.6 and Table 3.1).

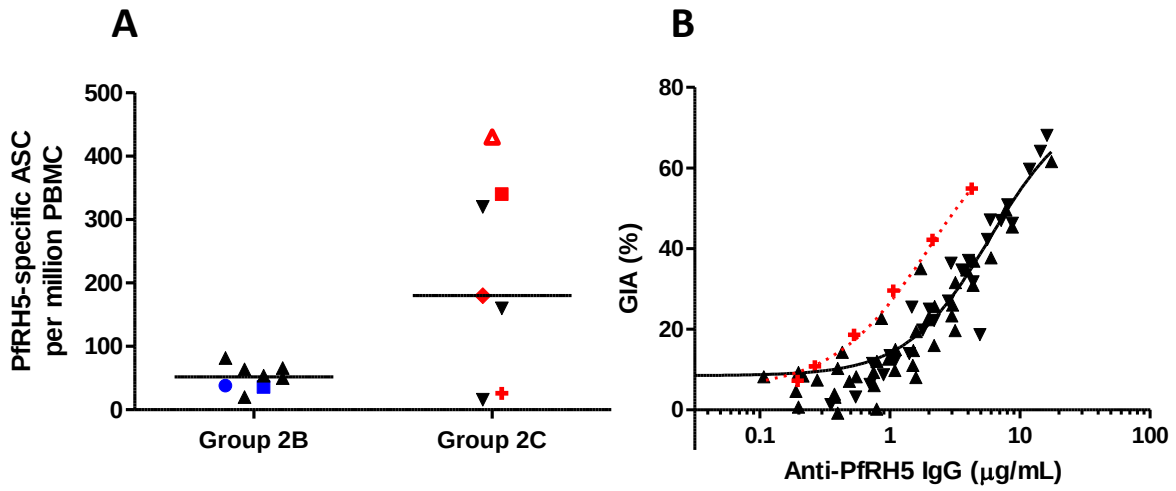

Figure 3.6: Volunteer selection criteria. (A) Number of PfRH5-specific ASC in PBMC in each volunteer separated by dose group. Blue and red data points represent volunteers from which antibody V_H/V_L cloning was attempted. The blue circle and blue square represent volunteers 1019 and 1012 respectively and the red triangle, red square, red diamond and red cross represent volunteers 2207, 2209, 1017 and 2210. (B) *P. falciparum* (3D7) growth inhibition curves showing neutralisation by PfRH5-specific IgG in all group 2B and 2C volunteers. Red crosses represent volunteer 2210. Figures adapted from data published in (Payne *et al.*[171]).

	Cloned	IgG expressed	PfRH5-specific
1012 plate 148	19	18	0
1012 plate 147	21	21	0
1019 plate 159	20	19	1
1019 plate 161	24	23	2
1019 plate 164	17	16	1
2207 plate 194	28	20	2
2207 plate 197	40	36	0
1017 plate 215	13	7	1
1017 plate 219	39	36	10
2209 plate 205	26	23	0
2210 plate 237	21	17	0
Success (%)	268/528 (**50.7**)	236/268 (**88.0**)	17/236 (**7.2**)

Table 3.1: Success rate at each bottleneck in the PfRH5-specific mAb isolation process. 268 out of a possible 526 (48 plasmablasts per plate) were successfully cloned into an expression vector, 236 out of 268 plasmid pairs expressed IgG and 17 of those 236 were PfRH5 binders.

In the work by Wrammert *et al.* where antibody variable regions genes were cloned using similar methods from volunteers vaccinated with Fluzone 2005-06 (Aventis Pasteur), a formulation containing four serotypes of inactivated influenza virus, haemagglutinin-specific plasmablasts constituted around 70% of the circulating ASC population at the peak of the response. The extremely high ASC response observed in their work can likely be attributed to the stimulation of a large pool of mBCs generated over the course of decades of exposure to influenza antigens, an advantage *P. falciparum*-naïve UK volunteers would not have benefitted from. On the other hand, their ASC population was highly pauci-clonal whereas ours was seemingly highly diverse given the size of the panel (Table 3.2/Figure 3.7).

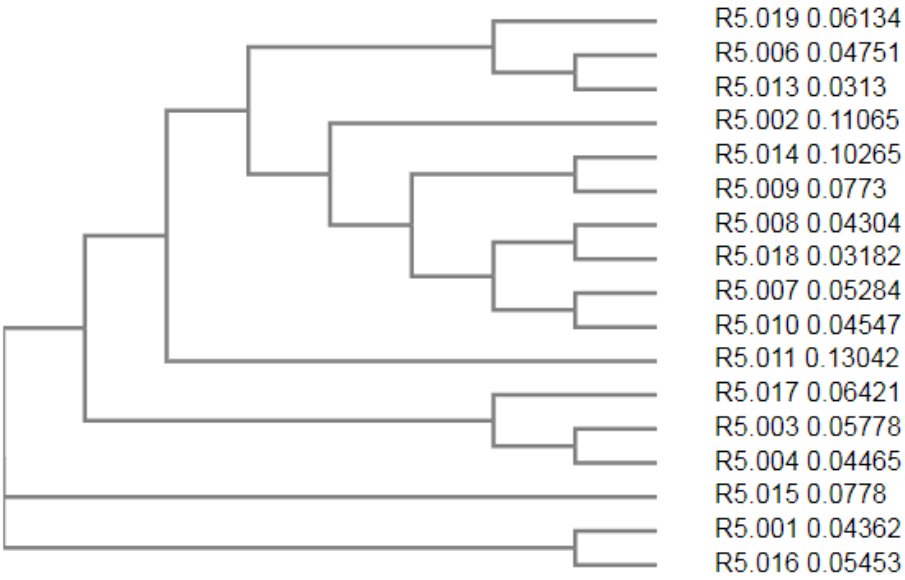

Figure 3.7: mAb cladogram. The cladogram was generated by NCBI's Clustal Omega after multiple sequence alignment of each mAb's V_γ exon. The numbers next to the mAb name indicate sequence similarity to the closest consensus sequence (node). Identical sequences would have values of 0.

The antibodies in this panel are distinct as evidenced by their differing variable region length and/or different use of V-gene exons (Table 3.2). The antibodies are genetically fairly close to germline, showing low levels of SHM suggesting low levels of germinal centre migration characteristic of an early extrafollicular response[193,215]. This paucity of SHM was also seen in anti-*Zaire ebolavirus* mAbs isolated from plasmablasts and mBC in response to protein delivered in the same vector, so could possibly be a feature of viral-vectored vaccination (internal communications, Draper group), or due to the number of immunisations or even a consequence of the 7 day post-boost time point chosen.

mAb	VR donor	Chain	Allele usage	% SHM
R5.001	1019	Heavy	IGHV1-18*04, IGHD4-17*01, IGHJ5*02	1.0 (3/296)
		Light	IGKV1D-16*01, IGKJ4*01	1.1 (3/278)
R5.002	1019	Heavy	IGHV3-49*04, IGHD1-20*01, IGHJ5*02	0.3 (1/301)
		Light	IGLV3-21*02, IGLJ2*01,IGLJ3*01	0.3 (1/288)
R5.003	1019	Heavy	IGHV1-69*01, IGHD3-22*01, IGHJ4*02	2.4 (7/293)
		Light	IGKV3-11*01, IGKJ2*01	2.1 (6/287)
R5.004	1019	Heavy	IGHV1-69*01, IGHD3-16*01, IGHJ3*02	2.4 (7/295)
		Light	IGLV1-44*01, IGLJ3*02	1.0 (3/294)
R5.006	2207	Heavy	IGHV4-39*01, IGHD6-13*01, IGHJ4*02	2.7 (8/298)
		Light	IGLV3-21*01, IGLJ2*01/IGLJ3*01	2.1 (6/290)
R5.007	2207	Heavy	IGHV3-7*02, IGHD3-16*01, IGHJ5*02	1.0 (3/292)
		Light	IGKV4-1*01, IGKJ1*01	3.0 (9/300)
R5.008	1017	Heavy	IGHV3-33*01, IGHD3-10*01, IGHJ4*02	2.4 (7/292)
		Light	IGKV1-39*01, IGKJ4*01	2.1 (6/287)
R5.009	1017	Heavy	IGHV3-23*04, IGHD3-22*01, IGHJ4*02	1.4 (4/295)
		Light	IGLV1-40*01, IGLJ3*02	1.0 (3/297)
R5.010	1017	Heavy	IGHV3-7*03, IGHD6-25*01, IGHJ6*02	1.4 (4/295)
		Light	IGLV3-21*02, IGLJ2*01/IGLJ3*01	1.1 (3/285)
R5.011	1017	Heavy	IGHV7-4-1*02, IGHD3-22*01, IGHJ4*02	1.0 (3/293)
		Light	IGLV3-21*02, IGLJ3*02	1.4 (4/289)
R5.013	1017	Heavy	IGHV4-39*01, IGHD3-3*01, IGHJ4*02	1.7 (5/297)
		Light	IGKV3-11*01, IGKJ3*01	1.8 (5/283)
R5.014	1017	Heavy	IGHV3-9*01, IGHD2-21*02, IGHJ4*02	1.4 (4/296)
		Light	IGLV1-44*01, IGLJ3*02	1.4 (4/294)
R5.015	1017	Heavy	IGHV1-2*04, IGHD3-10*01, IGHJ6*02	1.7 (5/295)
		Light	IGLV3-21*01, IGLJ2*01/IGLJ3*01	4.2 (12/288)
R5.016	1017	Heavy	IGHV1-18*01, IGHD3-9*01, IGHJ6*02	1.7 (5/296)
		Light	IGKV1-5*03, IGKJ2*01	3.6 (10/281)
R5.017	1017	Heavy	IGHV1-69*02, IGHD5-24*01 , IGHJ6*02	3.8 (11/291)
		Light	IGLV1-40*01, IGLJ3*02	0.3 (1/299)
R5.018	1017	Heavy	IGHV3-33*01, IGHD3-22*01, IGHJ4*02	1.7 (5/295)
		Light	IGKV1-39*01, IGKJ1*01	2.5 (7/284)
R5.019	1017	Heavy	IGHV4-31*01, IGHD3-3*01, IGHJ4*02	1.3 (4/298)
		Light	IGKV3-20*01, IGKJ2*04	1.7 (5/290)
c2AC7	Mouse	Heavy	IGHV5-15*02, IGHD2-4*01, IGHJ1*01	3.1 (9/295)
		Light	IGKV3-1*01, IGKJ1*01	3.4 (10/296)
c4BA7	Mouse	Heavy	IGHV1-87*01, IGHD1-3*01, IGHJ4*01	3.1 (9/292)
		Light	IGKV4-91*01, IGKJ4*01	2.1 (6/288)
c9AD4	Mouse	Heavy	IGHV5-15*02, IGHD2-4*01, IGHJ1*01	2.0 (6/295)
		Light	IGKV3-1*01, IGKJ1*01	3.4 (10/296)
QA1	Mouse	Heavy	IGHV5-4*02, IGHD2-1*01, IGHJ4*01	3.4 (10/296)
		Light	IGKV3-7*01, IGKJ2*01	2.4 (7/296)

Table 3.2: PfRH5 mAb panel list. For each antibody: the donor origin, the heavy and light chain variable exon usage and the percentage amino acid deviation from germline resulting from junctional diversity and somatic hypermutation. The genetic data were compiled using NCBI's IgBLAST[216]. Three chimeric (c2AC7, c4BA7 and c9AD4) and one fully mouse (QA1) monoclonal were included as they are frequently used as controls in various experiments due to their previous characterisation[127,130].

3.5 *In vitro* testing of the panel of PfRH5-specific mAbs

3.5.1 Binding to parasitic protein (dot blot)

To test whether these mAbs are able to bind PfRH5 expressed in parasites, a dot blot on schizont culture supernatant was carried out. The supernatant used came from 3D7 clone *P. falciparum* (identical to the PfRH5 vaccine used to elicit the mAbs) to maximise the likelihood of detecting binding. It has previously been shown that soluble PfRH5 exists in culture supernatant predominantly as a processed 45kDa form which is thought to be cleaved during the invasion process[134,217]. Quite surprisingly, all 17 mAbs bound PfRH5 from the supernatant (Figure 3.8) confirming the structural integrity of the vaccine and that these mAbs have the potential to bind live merozoites, in theory. Furthermore, this result indicates that none of these mAbs are likely to bind the most N-terminal 116 amino acids lacking from the processed 45kDa form[135].

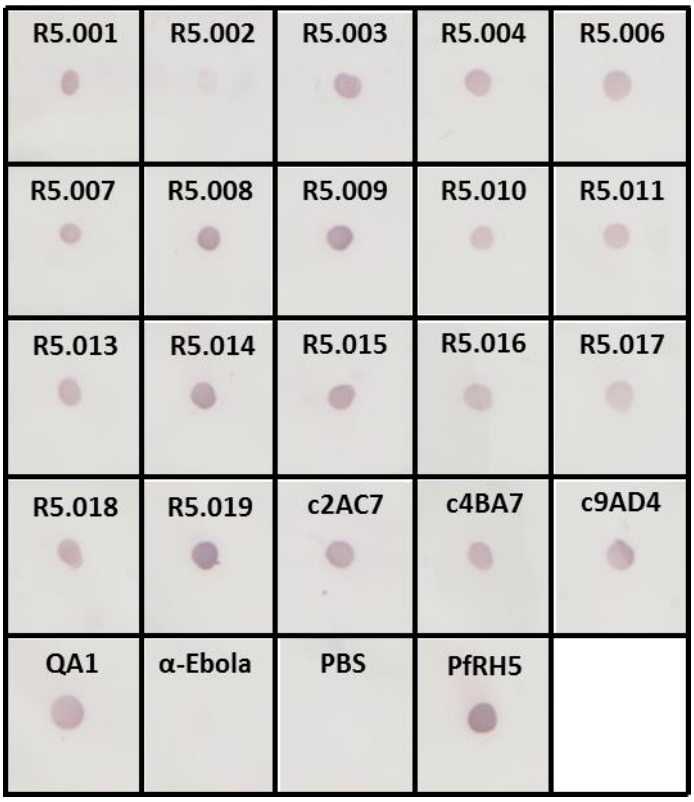

Figure 3.8: mAb binding to parasite-expressed PfRH5. A dot blot of all mAbs isolated in this work shows their binding to *P. falciparum*-derived PfRH5 (3D7 clone) from parasite culture supernatant. "α-Ebola" is an isotype-matched mAb reactive to *Zaire Ebolavirus* glycoprotein cloned and expressed using identical methods to the anti-PfRH5 mAbs.

3.5.2 Affinities and binding rate constants

The affinity of a ligand for its binding partner is one of its main functional characteristics. The affinity of a protein-protein interaction is expressed by the equilibrium dissociation constant K_D which has the unit M (mol L^{-1}) (Equation 3.2). This value represents the concentration of unbound A at which B is half-saturated in a simple 1:1 binding model (Equation 3.1). Perhaps more informatively, a chemical interaction can be described in terms of its kinetic rate parameters. These parameters describe the rate of change of complex formation at a given concentration of A and B (Equation 3.3). The K_D can also be expressed as the ratio of the association and dissociation rate constants K_{off} (or k_D) and K_{on} (or k_A) where

K_{on} is the rate of complex formation (unit M^{-1} s^{-1}) is and K_{off} (unit s^{-1}) is the fraction of complex decay.

$$(1) \quad [A] + [B] \underset{K\text{off}}{\overset{K\text{on}}{\rightleftharpoons}} [AB]$$

Equation (3.1): The propensity of two chemical elements to associate in a complex is described by two reaction rate constants K_{on} and K_{off}.

$$(2) \quad K_D = \frac{[A][B]}{[AB]} = \frac{K_{off}}{K_{on}}$$

Equation (3.2): The dissociation constant of the interaction between two interactants A and B where [A] is the concentration of A and [B] is the concentration of B and [AB] is the concentration of AB complex.

$$(3) \quad \frac{d[AB]}{dt} = K_{on}[A][B] - K_{off}[AB]$$

Equation (3.3): The rate of change of complex formation can be described simply by the concentrations of the interactants and the rate constants K_{on} and K_{off}, specific to a particular interaction.

High affinity antibodies are usually better neutralisers in many disease fields[218–222]. The importance of affinity and related kinetic rate parameters for merozoite invasion inhibition will be discussed further in Chapter IV. The affinities reported in Table 3.3 were calculated using Biacore X100 evaluation software using the calculated kinetic rate parameters and fitting to a 1:1 Langmuir binding model measured by SPR using an antibody-down approach on a protein A-coated chip (see Chapter II). The PfRH5 used runs as a single symmetrical peak by SEC, eluting at a similar time to 66.5kDa BSA (not shown) and runs at the correct molecular weight of approximately 60kDa by SDS-PAGE (Figure 3.9). As a result, PfRH5 can be viewed as monomeric and monodisperse, features important for measuring affinities using mass-sensitive means such as SPR[223].

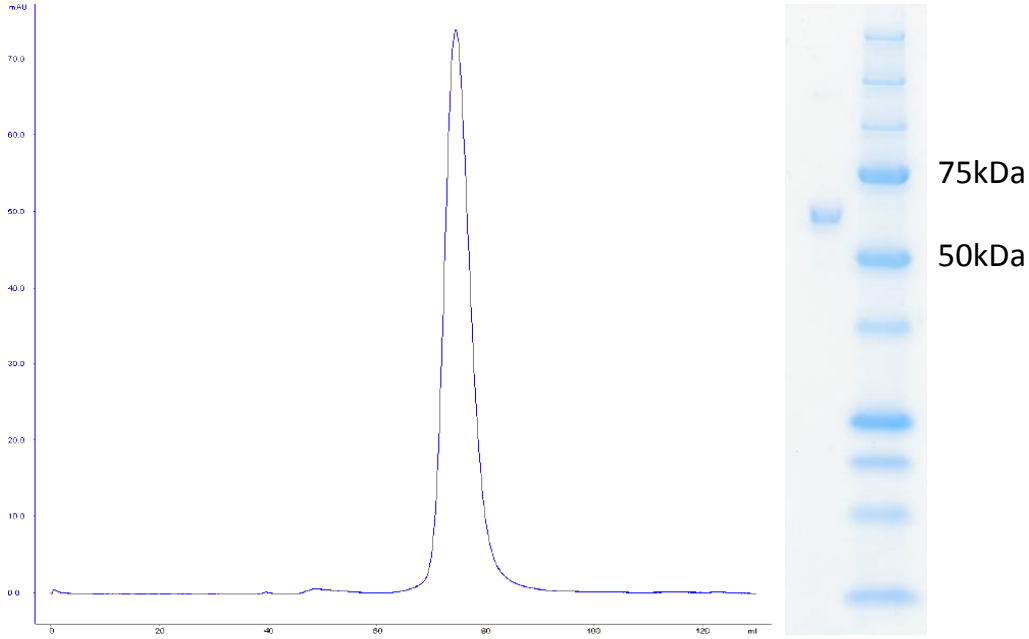

Figure 3.9: Recombinant PfRH5 quality. (Left) A_{280} trace of PfRH5 (3D7 clone) size exclusion chromatography on HiLoad Superdex 16/600 200pg column. (Right) PfRH5 in a reducing SDS-PAGE stained with a total protein stain. Estimated monomeric molecular weight 60.2kDa.

Despite the antibodies showing seemingly low levels of differences from germline (Table 3.2), the measured affinities were generally high but globally within the normal 10^{8}M < K_D < 10^{-12}M range for antibodies[224,225] (Figure 3.10, Table 3.3). R5.002 was the lowest affinity mAb in the panel, with an affinity in the mid-nanomolar range which is likely related to its V_L and V_H both having only a single amino acid substitution from germline (Table 3.2). At the other end of the spectrum, R5.014 has an affinity conservatively estimated in the low picomolar range owing to its exceptionally slow K_{off} (Table 3.3).

mAb	K_{on} ($M^{-1}s^{-1}$)	K_{off} (s^{-1})	K_D (M)
R5.001	1.02E+06	1.65E-03	1.62E-09
R5.002	3.86E+05	4.91E-03	1.27E-08
R5.003	1.70E+06	1.86E-03	1.09E-09
R5.004	1.71E+06	1.09E-03	6.36E-10
R5.006	6.77E+05	2.34E-04	3.46E-10
R5.007	3.78E+05	3.26E-04	8.63E-10
R5.008	7.22E+05	6.39E-04	8.86E-10
R5.009	5.12E+05	2.72E-04	5.31E-10
R5.010	7.83E+05	3.63E-04	4.63E-10
R5.011	1.61E+06	1.67E-05	1.03E-11
R5.013	7.73E+05	6.02E-05	7.79E-11
R5.014	3.15E+06	<2.91E-06	<9.21E-13
R5.015	6.29E+05	4.23E-05	6.73E-11
R5.016	1.14E+06	4.88E-04	4.28E-10
R5.017	1.44E+06	2.91E-04	2.01E-10
R5.018	4.25E+05	6.71E-06	1.58E-11
R5.019	3.07E+06	4.72E-04	1.54E-10
c2AC7	5.16E+06	1.62E-04	3.14E-11
c4BA7	5.89E+05	2.55E-05	4.33E-11
c9AD4	3.63E+06	5.04E-04	1.39E-10
QA1	2.95E+05	7.27E-04	2.46E-09

Table 3.3: Affinity and rate constant values for the panel of mAbs. The binding constant values of 17 human anti-PfRH5 mAbs were determined by SPR. Affinities and kinetic rate constants were calculated from 5 different concentration injections plus one replicate.

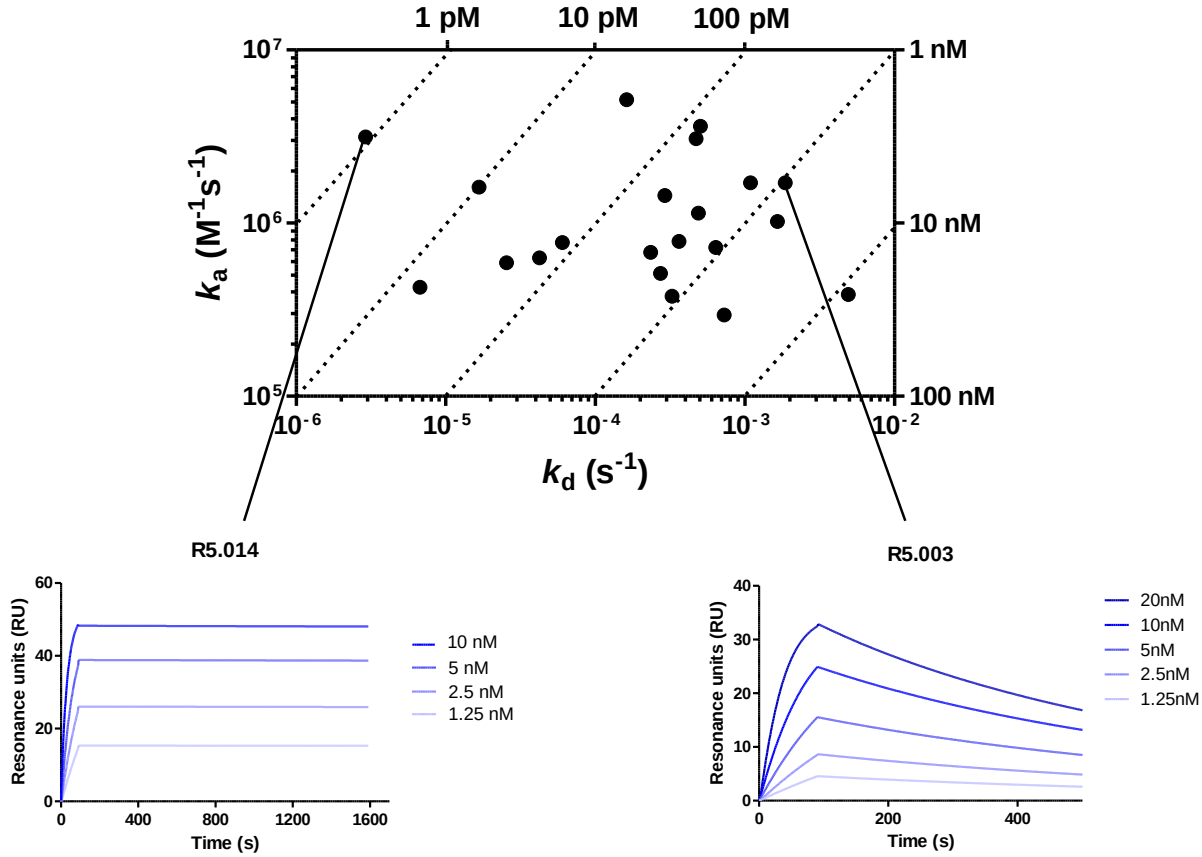

Figure 3.10: Isoaffinity plot of the panel of human mAbs. Points on any given diagonal have equal affinities. Multi-cycle kinetic SPR sensorgrams of two mAbs (R5.014 and R5.003) are shown as examples for illustration purposes. All data used here are taken from Table 3.3.

3.5.3 Binding capabilities to the most common natural PfRH5 polymorphisms

The primary sequence of PfRH5 is well conserved across strains relative to other *P. falciparum* invasion ligands such as PfAMA-1[226] and PfEBA-175[227]. Still, the five most common non-synonymous SNPs were investigated for their ability to influence the binding of this panel of human mAbs to PfRH5. These amino acid substitutions were: Y147H, H148D, S197Y, C203Y and I410M with global minor allele frequencies (MAF) of 0.174, 0.184, 0.164, 0.135 and 0.094 respectively (current as of August 2017 according to the catalogue of Genetic Variation in *P. falciparum* v4.0 compiled on MalariaGEN https://www.malariagen.net/data). It is worth clarifying that the minor allele is H at position

147, D at position 148, Y at position 197, M at position 410 and C at position 203; it just so happens that the reference sequence based on the 3D7 strain carries the minor allele coding for a cysteine at this position. These five polymorphisms were introduced by site-directed mutagenesis and the mAb-PfRH5 interaction strength measured in real-time by Bio-Layer Interferometry (BLI). None of the polymorphisms had any detectable effect on the binding of the panel of mAbs with the exception of R5.017 whose binding to PfRH5 was severely impaired by the bulkiness and/or hydrophobicity of the tyrosine sidechain in the 197Y variant (Figure 3.11).

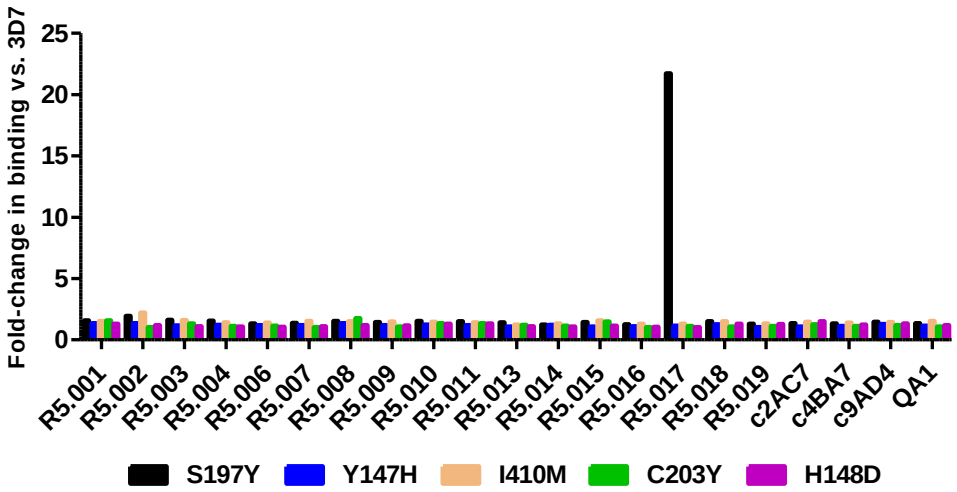

Figure 3.11: mAb binding to common PfRH5 polymorphisms. A bar chart shows the influence in binding of the mAb panel of the five most common PfRH5 non-synonymous SNPs expressed in fold-change relative to PfRH5 3D7 binding such that value = (3D7 binding)/(mutant binding). Data are representative of singlicate binding experiments.

3.5.4 Linear or conformational epitope binding

Linear or continuous epitopes are epitopes composed of a stretch of amino acids in the order of their primary sequence whereas conformational or discontinuous epitopes are formed of amino acids brought together in a protein's tertiary structure. Up to 90% of B-cell epitopes

are thought to be conformational[228]. All mAbs were assayed by ELISA against PfRH5 previously heat-denatured at 90°C for 10 mins. Of these, only R5.007 and c4BA7, a mAb previously shown to be able to bind a linear sequence of PfRH5 in a peptide[127], were able to bind the denatured PfRH5 (Figure 3.12). c2AC7 had also previously been shown to bind a conformational epitope[127].

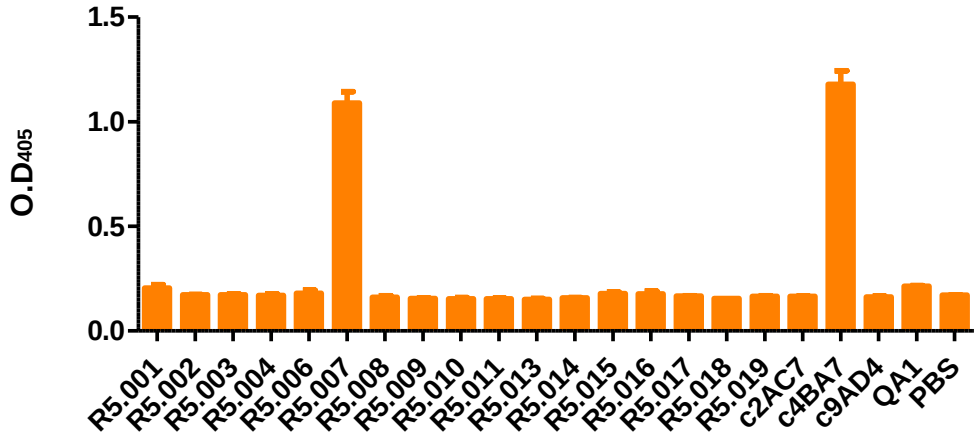

Figure 3.12: Testing the mAbs for linear epitope binding. Indirect ELISA showing the ability of the mAb panel to bind heat denatured PfRH5. Data are the mean of two replicate wells. Error bars are standard deviation.

The fact that most mAbs bind conformational epitopes is unsurprising but it does serve to confirm the integrity of the PfRH5 vaccine immunogen encoded by viral vectors and secreted *in situ*. This result also discounts epitope mapping by linear peptide arrays for all mAbs except R5.007.

3.6 Discussion

3.6.1 Generating the panel of anti-PfRH5 mAbs

The difficulty in isolating large numbers of vaccine-specific ASC resulted in a smaller-than-expected panel. The odds of discovering a super-potent bnAb like HIV's 35O22 which emerged from a 140,000 mBC screen[229] were thus not in my favour; despite this, the panel seemed to be fairly broad and proved informative beyond its small size (as will be shown in Chapters IV, V and VI). In an effort to enrich the proportion of PfRH5-specific plasmablasts sorted, attempts to stain the cells with fluorophore labelled monomeric or tetrameric PfRH5 were made but were fraught with low signal-to-noise and didn't ultimately lead to an improved gating strategy (data not shown). As mentioned before, plasmablasts are known to undergo BCR downregulation during their maturation process and could be devoid of the capability to bind antigen. Using successfully expressed antibody, ELISAs on lysed MVA virus showed a small proportion (≈ 10-15%) of reactive antibodies (data not shown). The other 80% antibodies unreactive to PfRH5 or MVA capsid proteins are of unknown specificity.

In the gene cloning process, some PCRs yielded no V_H amplicons (e.g B2 in Figure 3.2), likewise some PCRs yielded no V_L amplicons (e.g B10 in Figure 3.2). This could be explained by a variety of reasons including but not limited to:

- A cell-sorting or gating error (no cell or incorrect cell type)
- mRNA degradation
- Although the degenerate primers are designed to cover as much diversity as possible, some templates will inevitably be preferentially amplified at the annealing

temperature chosen. This can be observed in the different amplification efficiencies of certain PCR products (e.g V_H B8 vs. V_H B12 in Figure 3.2).

In some instances, the same well would generate a band in the Vκ and Vλ PCR (not shown in Figure 3.2). Theoretically B cells are unable to express Kappa and Lambda light chains simultaneously due to allelic exclusion, although on rare instances this has been seen[230]. This overlap is likely due to either a cell-sorting error (two B cells per well), mRNA carry-over from a different well or simply the promiscuity of certain degenerate V_L primers.

In the mAb screening process, some efforts were also made to reduce the chances of detecting false positive PfRH5-binding mAbs. After incubation with HEK293 supernatants, in total 8 washes in PBS-T were performed and around 1 hour of time passed. Although this probably all but eliminates spurious PfRH5 binding it would also likely reduce the chances of detecting the lowest affinity PfRH5-specific mAbs. Arguably low-affinity antibodies are of lesser value so milder washing protocols were not explored. The cell culture medium used for antibody expression was supplemented with ultra-low IgG FCS to reduce the chance of bovine IgG cross-reactivity in the ELISA. Lastly, affinity-purified alkaline phosphatase-conjugated anti-human gamma chain-specific secondary antibody was used for specific PfRH5 detection. Likewise, efforts were made to reasonably reduce false negatives. On each transfection plate, the plasmids coding for chimeric mouse anti-PfRH5 mAbs c2AC7 and c4BA7 were included. These two mAbs bind a conformational and a linear epitope, respectively[127]. c2AC7 consistently led to lower O.D values than c4BA7. In retrospect, this could be explained by the slower K_{off} of c4BA7 (see Table 3.3). However, this led us to question the integrity of polystyrene-adsorbed PfRH5. Mab binding to PfRH5 was measured by simple PfRH5-down indirect ELISA. The microwell plates used in this ELISA screen were NUNC ® Maxisorp™ polystyrene plates. These plates have high protein-binding properties, an important feature to increase the likelihood of allowing for bivalent antibody

binding. However the harsh binding conditions could theoretically compromise certain delicate conformational epitopes or selectively bind PfRH5 in certain orientations, potentially shielding a subset of epitopes from antibody accessibility[231,232]. To counter this, in later rounds of screening the supernatants were simultaneous screened on streptavidin-coated ELISA plates onto which biotinylated PfRH5 had been bound, however no differences were observed when compared to the PfRH5-down ELISA.

3.6.2 Anti-PfRH5 mAb binding characteristics

The mAb affinities described here are high relative to some studies on human mAbs[233], although as mentioned above, not exceptional. It must be noted that the data from Table 3.2 and Table 3.3 can be reconciled, low SHM does not necessarily mean low affinity[234]. It is firstly important to remain aware of protein-specific effects such as structurally rigid proteins typically being more likely to be subject to higher interaction affinities with ligands due to reduced entropic cost of binding[235,236]. PfRH5 is known to contain a highly-rigid core[130], against which all but one of these human mAbs are reactive to (see Chapter 4). The above-average affinities can also be explained by the selection process used here. It's likely that this panel is artificially enriched for high affinity/low K_{off} mAbs because of the potentially low concentration of mAb present in supernatants and the long incubation and multiple wash steps used in the ELISA screening assay.

MAbs c2AC7, c4BA7, c9AD4 and QA1 were included in many of the assays in this thesis because of their extensive characterisation in terms of binding characteristics[127,130] and growth inhibitory[127] properties. Some differences (although arguably relatively minor) in reported affinity values for these control mAbs can be noted between those published for parental mAbs[127]. Assuming we are measuring the same interaction exactly, there is inherent

variation between different measurements. In these two measurements, different operators and different machines were used, different assay setups on the chip (anti-mouse mAb capture vs. protein A), different protocols (single-cycle kinetics vs. multi-cycle kinetics), and different evaluation software were also used (Biacore T100 vs. Biacore X100). Although the previous work was performed to a high standard, the material available at the time was suboptimal. Of course SPR relies on the measurement of active protein; we now have purer and more heavily quality controlled[139] (Jin *et al*, in preparation) PfRH5 (Figure 3.9), with a 4 amino-acid tag compared to a 20.4kDa tag so less scope for spurious results and interference. Finally, with the exception of QA1, the three other control mAbs (c2AC7, c4BA7 and c9AD4) had since been chimerised and therefore had different constant domains, so it's a possibility that the interaction values had been altered in the process. Evidence for different constant domains influencing the affinity of an identical variable domain has been observed before[237].

In Figure 3.11, only one of 17 mAbs was found to be affected by one of 5 amino acid mutations. Whilst this assay is not geared for detecting subtle differences in affinity, it is believed to be easily sensitive enough to detect any affinity changes relevant to parasite growth inhibition. Not all variant positions are predicted to be surface exposed. Using the freely-available "findSurfaceResides.py" PyMOL script (which uses a 2.5Å rolling-ball model to identify solvent-exposed residues) and the previously published crystal structure of a PfRH5 truncation (PDB code: 4WAT), position 410 was not found to be surface-exposed and thus unlikely to affect the binding of any mAbs. The ablation in binding of R5.017 to S197Y is not only strongly supported by data but is also very plausible because of this mAbs' known *in vitro* competition with QA1, a mAb which binds a similar location to R5.017 (Chapter 4). In fact QA1 makes contact with S197 but with the main chain[130] so would be unlikely to be affected by the sidechain mutation.

In Figure 3.8, a dot blot was chosen over the more conventional immunofluorescence assay (IFA) for assaying mAb binding to parasitic PfRH5 in an attempt to avoid false-negatives. Indeed, given that mAbs by definition suffer from lower signal intensity than pAbs due to the 1:1 binding (at best) with PfRH5 and that aldehyde-reliant methods used for sample fixation are known to modify or hide some protein epitopes[238,239], a significant problem for assaying a panel of mAbs in which 16/17 bind conformationally sensitive epitopes.

Chapter IV: Merozoite-killing properties of anti-PfRH5 mAbs

4.1 Authorship statement

At the Jenner Institute the GIA assays are carried out by a dedicated research assistant to reduce user variability and maximise comparability of absolute growth inhibition values carried out in separate experiments over time. As a result the parasite culture, synchronisation and assay setup were carried out by Jennifer Marshall or her successor Dr. Doris Quinkert. Likewise, and to facilitate comparison of absolute growth inhibition data between labs around the world, selected assays were carried out at the GIA reference centre at the Laboratory of Malaria and Vector Research (LMVR), National Institute of Allergy and Infectious Diseases (NIAID) at the National Institute of Health (NIH) in the USA by Ababacar Diouf. Dr. Francis Galaway (Sanger Institute, Cambridge) conducted the AVEXIS blocking assays. The humanised mouse model was developed and housed at the Center for Infectious Disease Research (CIDR) in Seattle, USA and the passive transfer study was carried out by Dr. Lander Foquet.

4.2 Introduction

Following the isolation and initial characterisation of mAbs in Chapter III, the aim of Chapter IV was to begin establishing a link between function (growth inhibition) and the particular features of the mAbs. To this end, the potency of each mAb clone in terms of its ability to

inhibit invasion was determined. Assessing the neutralising capacity of the mAbs is firstly an essential characteristic of each mAb and secondly is knowledge essential for the determination of the neutralising epitopes of PfRH5, provided the mAbs' binding site is found. Antibodies exert their killing or growth-inhibitory function by mediating ADCC or complement-dependent cytotoxicity (CDC) or by sterically interfering with essential interactions. As mentioned in Chapter I, invasion-blocking vaccines attempt to induce antibodies with the specific function of interfering with essential protein-protein interactions on the merozoite surface. The GIA assay serves as a model to quantify the effect of this specific type of immunity and does not contain any immune cells or active complement, discounting any growth-inhibitory effect attributable to ADCC or CDC. The concept of the GIA assay is fairly simple. This assay is designed to quantify the change in parasite multiplication rate (PMR) of *P. falciparum* parasites over one growth cycle by measuring an endpoint activity of a plasmodial enzyme which closely correlates with parasite biomass. The GIA assay is specifically intended to measure the effect of invasion-blocking antibodies and can be viewed simply as an assay measuring the interference of merozoite attachment to uninfected RBCs. This assay does not purport to replicate physiological conditions; the haematocrit used is 1% instead of the physiological 45% (although in practice, the "apparent" haematocrit in the assay is much higher as all cells fall to the bottom of the wells under gravity); no lymphocytes or other cell types are present; complement activity is removed by heat-inactivation; and the static setup in no way mimics blood-flow through blood vessels. These factors raise questions over the validity of this assay as a correlate of protection for vaccine or drug screening purposes. As discussed in Chapter I, the GIA assay is not capable of measuring what is thought to be the mechanism of antibody-mediated NAI. However, it is measuring a conceptually-valid method of non-natural immunity which can be induced by vaccination. In this chapter, firstly the neutralisation potential of the mAbs against strains

carrying the homologous or a heterologous PfRH5 sequence were tested in the GIA assay and two were additionally tested in a humanised mouse model. Secondly, an initial investigation into whether neutralisation was correlated with different mAb binding parameters or with the disruption of certain protein-protein interactions which are known to occur with PfRH5 during invasion was conducted.

4.3 Growth inhibition of anti-PfRH5 human mAbs

4.3.1 Anti-PfRh5 mAbs in the GIA assay

The GIA of this set of mAbs spanned a broad range, from undetectable activity to high neutralisation activity in the same range as the most potent neutralising mAbs to PfRH5 described previously[127,141] or against any merozoite protein[132,240–245] (Figure 4.1 A). Furthermore, almost all mAbs were shown to be strain-transcending, a feature unique to PfRH5 within malaria invasion ligands (discussed in Chapter III). All mAbs, with the exception of R5.017, neutralised all six heterologous strains tested with relative potencies comparable to the homologous 3D7 strain (Figure 4.1 B). Relative to 3D7, the M-Camp strain was more refractory to antibody-mediated growth inhibition in a mAb-independent manner (i.e all mAbs were less potent) suggesting mechanistic or biological invasion differences in this strain. The neutralisation capacity of R5.017 was severely impaired in a strain-dependent manner in Cp845 and FVO strains, pointing to differences in the binding site of this mAb in these two strains. R5.017 was shown to have highly-reduced binding to the S197Y variant (see Chapter III). To investigate any causal link between this polymorphism and reduced *in vitro* growth inhibition, these parasite strains were sequenced at the genomic locus of PfRH5, specifically at the five positions in PfRH5 known to harbour

the five most common non-synonymous SNP. Table 4.1 summarises the outcome of the sequencing. Indeed FVO and Cp845 were the only two strains tested to carry the S197Y polymorphism. Furthermore this sequencing revealed that the six heterologous strains chosen cover all of the diversity of the five most common polymorphisms in PfRH5; increasing the likelihood of these mAbs being truly strains transcending.

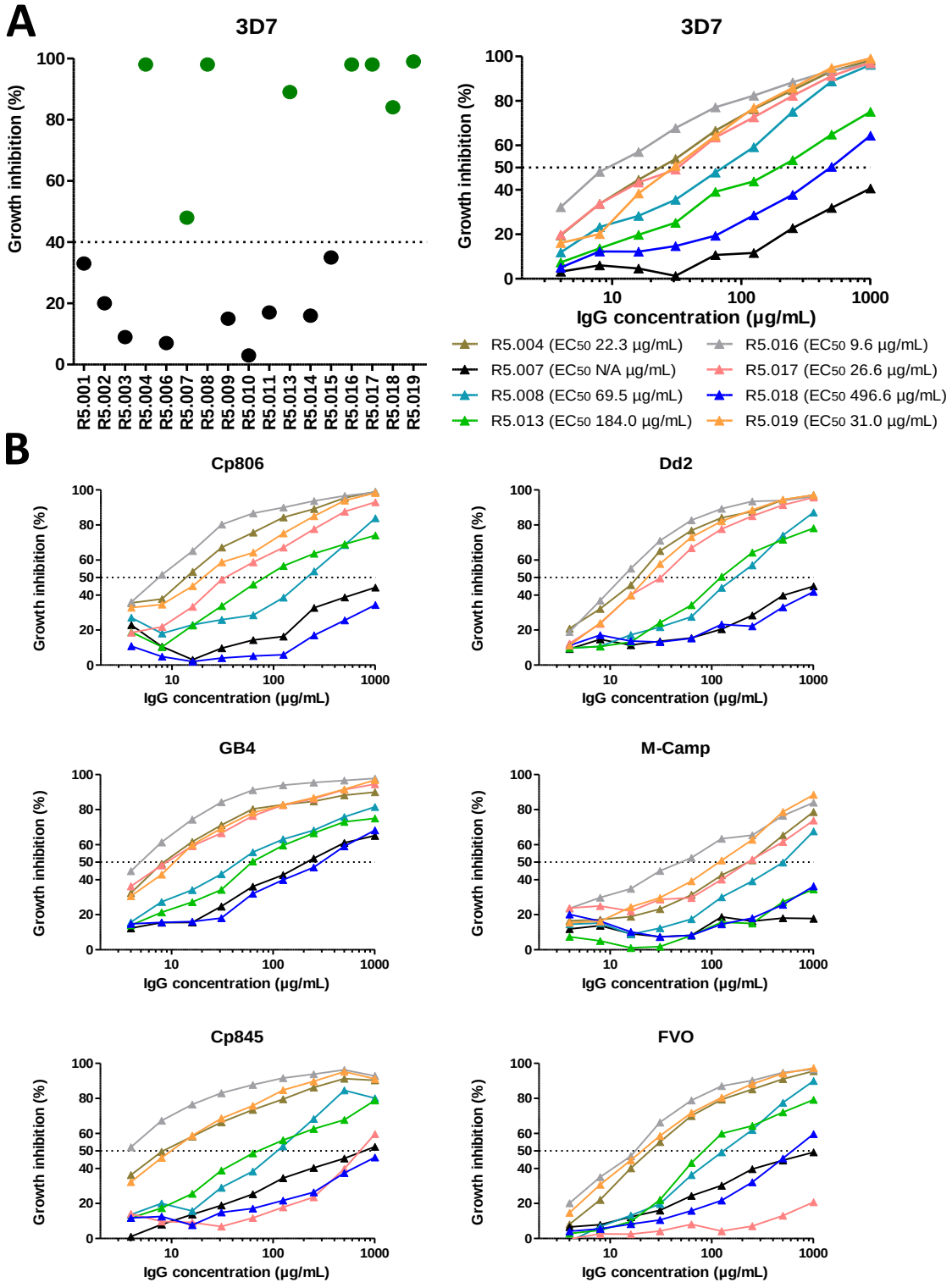

Figure 4.1: Growth inhibition of anti-PfRH5 mAbs. In (A), the left panel shows a high-concentration growth inhibition pre-screen of each mAb at 3000µg/mL, the right panel shows two-fold dilution series of the inhibitory mAbs identified from the pre-screen from 4µg/mL to 1000µg/mL. These assays were carried out using the homologous 3D7 *P. falciparum* clone. EC_{50} values reported are obtained by interpolation from a variable slope four-parameter curve on GraphPad Prism 5.0. (B) shows two-fold dilution series of the neutralising mAbs identified from the pre-screen against 6 heterologous *P. falciparum* strains from 4µg/mL to 1000µg/mL. All data are the mean of two replicate wells, error bars are not shown.

	147	148	197	203	410
3D7 (Lab-adapted clone)	Y	H	S	C	I
FVO (Lab-adapted line)	Y	H	**Y**	**Y**	I
Dd2 (Lab-adapted line, Indochina)	Y	H	S	C	**M**
GB4 (Lab-adapted line, Ghana)	Y	H	S	**Y**	I
M-Camp (Patient isolate, Malaysia)	Y	H	S	**Y**	I
Cp806 (Patient isolate, Cambodia)	**H**	**D**	S	**Y**	I
Cp845 (Patient isoate, Cambodia)	Y	H	**Y**	**Y**	I

Table 4.1: Table of amino acid variation at most five most polymorphic sites. Amino acids observed at the five most variable positions in PfRH5 sequenced from the seven strains used in the growth inhibition experiments in Figure 4.1. The geographical origin of the strains is in parentheses next to the strain name. Differences from the 3D7 reference sequence are highlighted in red.

4.3.2 mAb neutralisation of *P. falciparum* in a humanised mouse model

A newly-developed and as yet unpublished humanised mouse model for supporting *P. falciparum* malaria growth was made available to me at the Center for Infection Disease Research (CIDR, Seattle, USA). The model is based on the FRG mouse[246] on a NOD background (FRGN) supplied by Yecuris™. This mouse is a triple knockout for Fah-/-, RAG-/- and IL2rγ-/-. Fah knock-out causes liver disease when the drug NTBC (2-(2-nitro-4-trifluoromethylbenzoyl)-1,3-cyclohexanedione) is withdrawn, allowing for human hepatocyte xenografts; RAG knock out interferes with the recombination of TCR and BCR; and IL2rγ knock-out impairs immune function by deleting a mediator involved in multiple cytokine signalling pathways necessary for lymphocyte development. Further to this, mice are given daily intraperitoneal human RBC (hRBC) injections resulting in a 50-70% proportion of hRBC. Mice are further treated with clodronate and cyclophosphamide to reduce macrophage and neutrophil function. The resulting model is able to be engrafted with human hepatocytes and red blood cells which are maintained due to severe immunodeficiency. This group have also developed a transgenic *P. falciparum* strain based on NF54 carrying a luciferase reporter

gene under the control of a constitutive promoter, allowing for real-time visualisation and quantification of luminescence using an *in vivo* imaging system (IVIS).

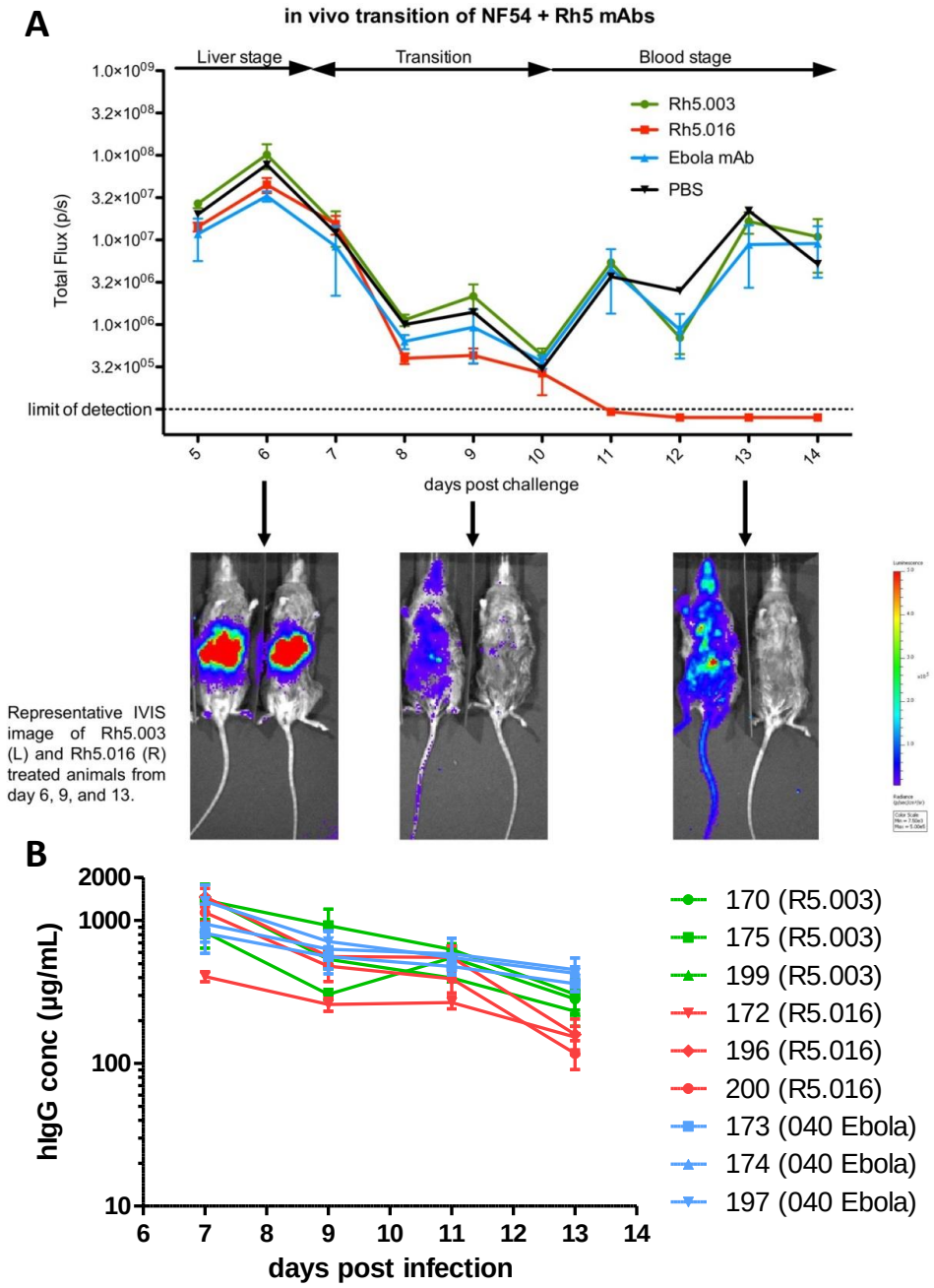

Figure 4.2: Passive transfer of anti-PfRH5 mAb into a humanised mouse model. FRGN mice were passively transferred mAb at 100mg/kg at day 7, coinciding with the beginning of the blood-stage transition. The transition phase refers to a low-signal phase between liver-stage infection and blood-stage where hepatocyte infection is lost and blood-stage parasitaemia is still low. In A, luciferase signal over time is plotted above and error bars are SEM of 3 mice in each group. In B, serum concentrations of human mAb were measured by ELISA at days 7, 9, 11 and 13 post-challenge. Data points are the mean, representative of duplicate wells in two separate experiments and error bars are SEM.

Seven days after sporozoite challenge, three mice in each of three groups were given an intravenous injection of non-neutralising PfRH5 mAb R5.003, neutralising PfRH5 mAb R5.016 or an isotype control mAb specific to *Zaire ebolavirus* glycoprotein (Figure 4.2 A). A further group of three mice were given PBS as controls. Results from days 10 to 14 show the establishment of a patent blood-stage infection in all groups except for the mice given neutralising mAb R5.016, whose luciferase signal was reduced to undetectable levels from day eleven until the end of the experiment. Serum concentrations of all mAbs were high, in the region of 1000µg/mL or more decreasing to 200-400µg/mL over the course of six days (Figure 4.2 B); concentrations which lead to 100% growth inhibition and 90% growth inhibition in GIA assays against the homologous 3D7 clone. These data provide important proof of concept that potent invasion-blocking mAbs identified *in vitro* are capable of clearing infection in a humanised *in vivo* model of infection against a *P. falciparum* parasite challenge.

4.3.3 Correlation between mAb kinetic rate constants and neutralisation

The quick invasion of RBCs by the merozoite poses an extra hurdle to overcome by vaccine-induced antibodies against the merozoite, in comparison to many other antibody-susceptible pathogens whose neutralising antibodies are afforded the time to reach equilibrium. Antibodies targeting invasion ligands such as PfAMA-1 or PfRH5 are required to reach maximal occupancy in a time-frame limited by the 20-70s invasion rate[61]. The evidence of the impact this has on growth inhibition is strong. For example, the difference in potency comparing an anti-basigin mAb to an anti-PfRH5 basigin-blocking mAb of a similar affinity is in the order of 60-fold (see Douglas *et al.*[127] and Figure 4.3 B). The growth inhibitory effect of mAb-mediated neutralisation in a GIA assay is related to the proportion of PfRH5

bound by mAb. From the observed rate of mAb-PfRH5 complex formation, described by the differential equation in Chapter III (Equation (3.3))[i], it is clear that in pre-equilibrium conditions where the concentration of complex [AB] is small relative to the concentrations of free mAb and PfRH5 [A] and [B] respectively, the term K_{off}[AB] is negligible. This means that at equal mAb concentrations [A] and equal amounts of PfRH5 available for binding [B] (same parasite density, same number of available PfRH5 molecules on each merozoite), [A] and [B] are constants; this means that the intrinsic interaction rate parameter K_{on} is largely responsible for the steepness of slope of complex formation in pre-equilibrium conditions (Figure 4.3 C, <80s).

[i] as a reminder, this equation is: $\frac{\mathrm{d[AB]}}{\mathrm{dt}} = K_{on}[\mathrm{A}][\mathrm{B}] - K_{off}[\mathrm{AB}]$

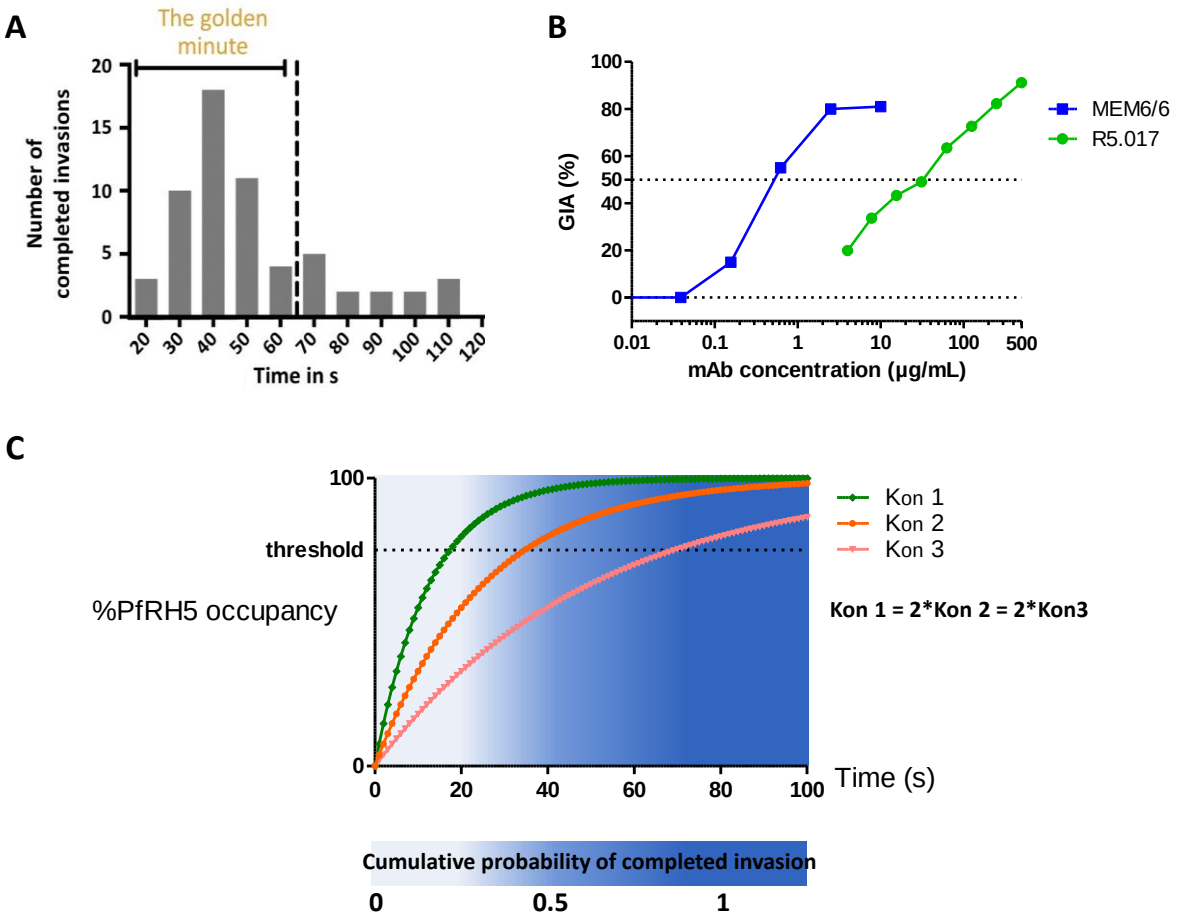

Figure 4.3: *Figure 4.3*: Fast merozoite invasion imposes a binding constraint. In panel A is a histogram adapted from Weiss *et al*.[61] showing the average invasion speed of merozoites in culture. Plotted in panel B is the growth inhibition of anti-basigin mAb MEM6/6 and basigin-blocking anti-PfRH5 mAb R5.017. These mAbs have similar affinities, 1.37E^{-10}M for MEM6/6[247] and 2.01E^{-10}M for R5.017 (see Chapter III) and therefore similar PfRH5 occupancy at equilibrium, by definition. In panel C is a theoretical plot of 3 mAbs at equal concentrations binding the same epitope on a merozoite at three two-fold increasing association-rates (K_{on}) showing increasing %PfRH5 occupancy, most markedly in pre-equilibrium conditions. The "threshold" line refers to the threshold number of PfRH5 molecules which need to be bound by mAb on a merozoite in order to lead to an abortive invasion event; here this threshold is set arbitrarily at 75%. The blue shaded area shows the cumulative probability of invasion of a merozoite in the absence of mAb, with probabilities based on the histogram in panel A.

The realisation that antibody association rate is important for invasion-blocking antibodies is not new[127,248]. In order to investigate whether the different neutralisation capabilities of these mAbs is related to different kinetics of binding, the rate and affinity constants of the human growth inhibitory mAbs and neutralising chimeric and mouse mAbs c2AC7, c9AD4 and QA1 were correlated with their potency of neutralisation. It seems there is a strong

correlation between the on-rate and neutralisation in neutralising mAbs (R= -0.9; *p*=0.0002) but no strong correlations were observed with the off-rate or the affinity constants (Figure 4.4). Therefore it is clear that the potency of neutralising anti-PfRH5 mAbs can be predicted from their intrinsic binding speed K_{on}. When non-neutralising mAb data are included (data not shown), none of the correlations are significant at $\alpha = 0.05$. Therefore, neutralisation cannot be predicted from the on-rate alone, only the potency of a mAb already known to inhibit invasion, indicating a more complex mechanism of neutralisation than simply rapid PfRH5 binding.

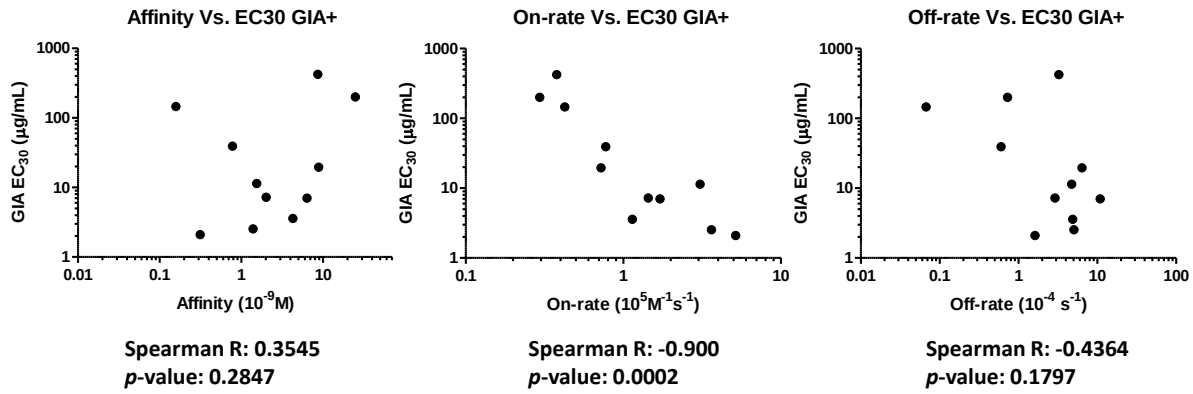

Figure 4.4: Correlations of the mAb kinetic binding constants with neutralisation. K_{on} (on-rate), K_{off} (off-rate) and K_D (affinity) were correlated with GIA (EC_{30}) of anti-PfRH5 mAbs. The 17 human mAbs, two chimeric mAbs (c2AC7, c9AD4) and one mouse mAb (QA1) were included to bolster the sample size of neutralising mAbs, their provenance being irrelevant here. EC_{30} was chosen as the neutralisation readout in order to include weaker-neutralising mAbs. The EC_{30} values were interpolated from Figure 4.1 A and kinetic values from Chapter III.

4.3.4 mAb-mediated interaction disruption between PfRH5 binding partners

Among the proteins which have been shown to interact with PfRH5 are: basigin, PfRIPR, PfCyRPA and PfP113. Antibodies raised to basigin, PfCyRPA and PfRIPR have all been reported to inhibit invasion *in vitro*. The common factor is that these three proteins all bind PfRH5 so it is possible that the mechanism of growth inhibition of antibodies directed to

these proteins is the disruption of their binding to PfRH5; this has already been confirmed to be the case with the RBC receptor basigin[129] but whether PfRH5-PfCyRPA, PfRH5-PfP113 or PfPfRH5-PfRIPR must necessarily occur in order for invasion to proceed is not currently known. Protein-protein interactions can often be viewed as switches, triggering the next step in a process of coordinated events. Answering the question of whether there are further essential interactions whose disruption can be exploited by antibody blockade would have significant consequences for PfRH5 vaccine design and could shed light on biological processes of merozoite invasion. Anti-PfRH5 mAbs present ideal tools for associating their mechanism of invasion inhibition with essential interaction blockade and beginning to understand where PfRH5 interacts with these proteins, provided the mAb epitopes can be located on PfRH5. It is currently unknown where PfCyRPA and PfRIPR bind to PfRH5.

As is the case with many cell-surface to cell-surface signalling events, the interactions measured so far between members of the PfRH5 invasion complex are generally weak, lying in the low μM range[129,130,135], meaning sensitive methods must be used to study their blockade. Despite its name, PfRIPR (Pf**R**H5-**I**nteracting **PR**otein) seems increasingly unlikely to directly bind to PfRH5, having been explicitly shown *not* to interact with PfRH5 both by Galaway *et al*.[135] and by the Draper group in unpublished experiments. Even if PfRIPR does interact with PfRH5 in their natural context, the inability to detect an interaction *in vitro* removes any possibility to set up an interaction-blocking assay. To study the ability of different mAbs to interfere with PfCyRPA, PfRIPR or basigin binding to PfRH5, two methods were used in an attempt to improve the reliability of results; AVEXIS, an avidity-enhanced plate-based assay using pentameric prey molecules[249], and SPR.

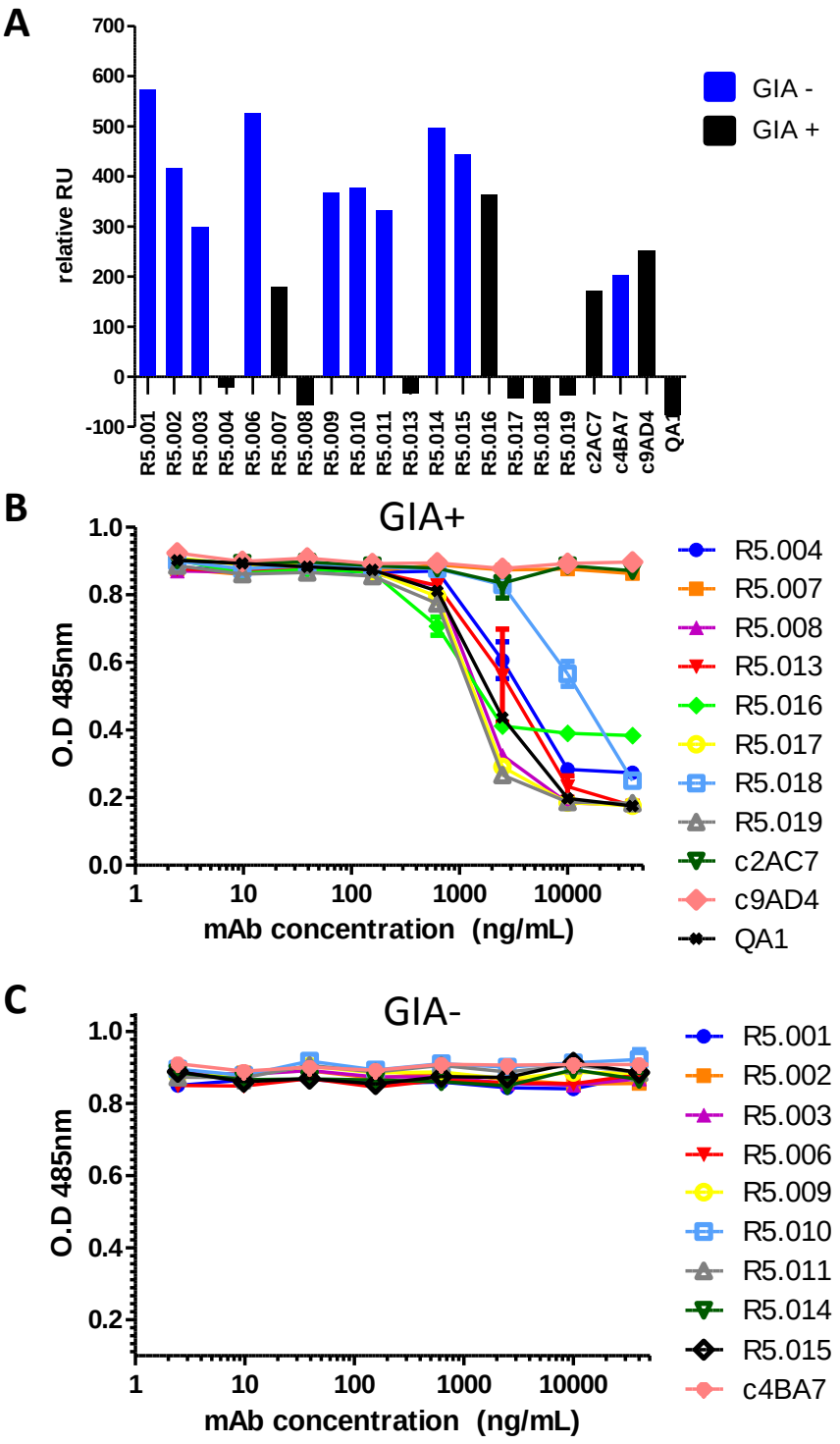

Figure 4.5: Neutralising mAbs block basigin binding to PfRH5. (A) SPR-based basigin-blocking assay. Neutralising mAbs are coloured in black and non-neutralising mAbs in blue. (B) AVEXIS-based basigin-blocking assay with neutralising mAbs. (C) AVEXIS-based basigin blocking assay with non-neutralising mAbs. Data in A are representative of one experiment for each mAb. Data points in B and C are mean of duplicate wells, error bars are SEM. An example of a positive basigin blockade and negative basigin blockade in the SPR assay can be found in Appendix 4.1 at the end of this chapter.

PfRH5-basigin interaction blockade

From the data in Figure 4.5, it is clear that a set of mAbs reliably block basigin binding *in vitro*. R5.004, R5.008, R5.013, R5.017, R5.018 and R5.019 consistently and strongly block basigin binding across both assays. There is conflict between the assays in Figure 4.5 A and B over whether R5.016 blocks basigin binding, although arguably in both assays R5.016 blocks basigin to a lower degree than the other basigin blocking mAbs mentioned above. c2AC7 and c9AD4 have previously been shown to be unable to block basigin binding by AVEXIS[127], however they may be part of an intermediate basigin-blocking phenotype which also includes R5.007, and c4BA7 in the SPR assay. In summary, basigin blockade does indeed appear to be a major mechanism of neutralisation for the majority of human mAbs isolated in this thesis. Interestingly, the three most potent anti-PfRH5 mAbs (c2AC7, c9AD4 and R5.016) in this work do not appear to interfere with basigin binding in this assay to the same extent as neutralising mAbs R5.004, R5.008, R5.013, R5.017, R5.018 and R5.019.

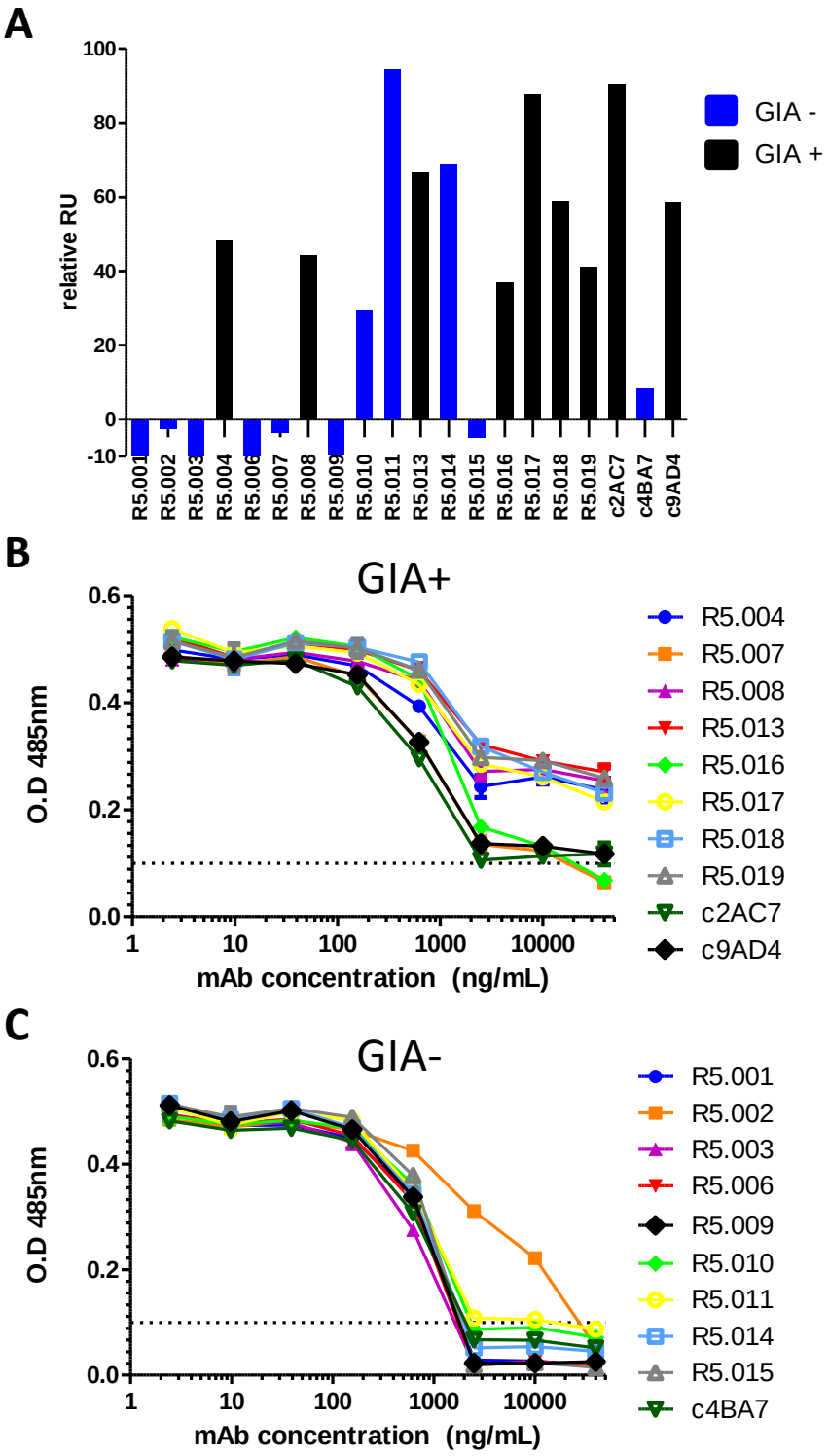

Figure 4.6: Non-neutralising mAbs do not block PfCyRPA binding to PfRH5. (A) SPR-based PfCyRPA blocking assay. Neutralising mAbs are coloured in black and non-neutralising mAbs in blue. (B) AVEXIS-based PfCyRPA blocking assay with neutralising mAbs. (C) AVEXIS-based PfCyRPA blocking assay with non-neutralising mAbs. Data in A are representative of one experiment for each mAb. Data points in B and C are mean of duplicate wells, error bars are SEM. An example of a positive and negative PfCyRPA blockade in the SPR assay can be found in Appendix 4.1 at the end of this chapter.

PfRH5-PfCyRPA interaction blockade

Data in Figure 4.6 show a set of mAbs with a definite ability to interfere with PfCyRPA binding to PfRH5 *in vitro*. R5.001, R5.002, R5.003, R5.006, R5.007, R5.009, R5.015 and c4BA7 clearly block PfCyRPA binding in both assays. Further to these, R5.010 blocks PfCyRPA binding in the AVEXIS assay in Figure 4.6 C and may show some lower-level interference in the SPR-based assay in Figure 4.6 A. R5.016, c2AC7 and c9AD4 appeared to block PfCyRPA in the AVEXIS assay but not the SPR assay. In the plate-based AVEXIS assay, all mAbs blocked PfCyRPA from binding PfRH5 to an extent, with a group consisting of R5.004, R5.008, R5.013, R5.017, R5.018 and R5.019; the group of mAbs identified as basigin-blocking in Figure 4.5 being the weakest blockers. The interface of PfRH5 which makes contact with PfCyRPA is not described in the literature so it is conceivable that an antibody is capable of blocking the binding of both proteins. In summary, in the SPR assay it is clear that there are two clear phenotypes: blockers (R5.001, R5.002, R5.003, R5.006, R5.007, R5.009, R5.015 and c4BA7) and non-blockers. In the AVEXIS assay, there are three phenotypes: “super-strong” blockers (R5.001, R5.003, R5.006, R5.009, R5014, R5.015 and c4BA7), “strong” blockers (R5.002, R5.007, R5.010, R5.011, R5.016, c2AC7 and c9AD4) and partial blockers (R5.004, R5.008, R5.013, R5.017, R5.018 and R5.019). Of the human mAbs, the clear PfCyRPA blockers to emerge from these experiments are: R5.001, R5.003, R5.006, R5.007, R5.009, R5.015 and potentially to a lesser degree R5.010 and R5.016. With the exception of R5.016, none of these mAbs show strong growth-inhibitory properties.

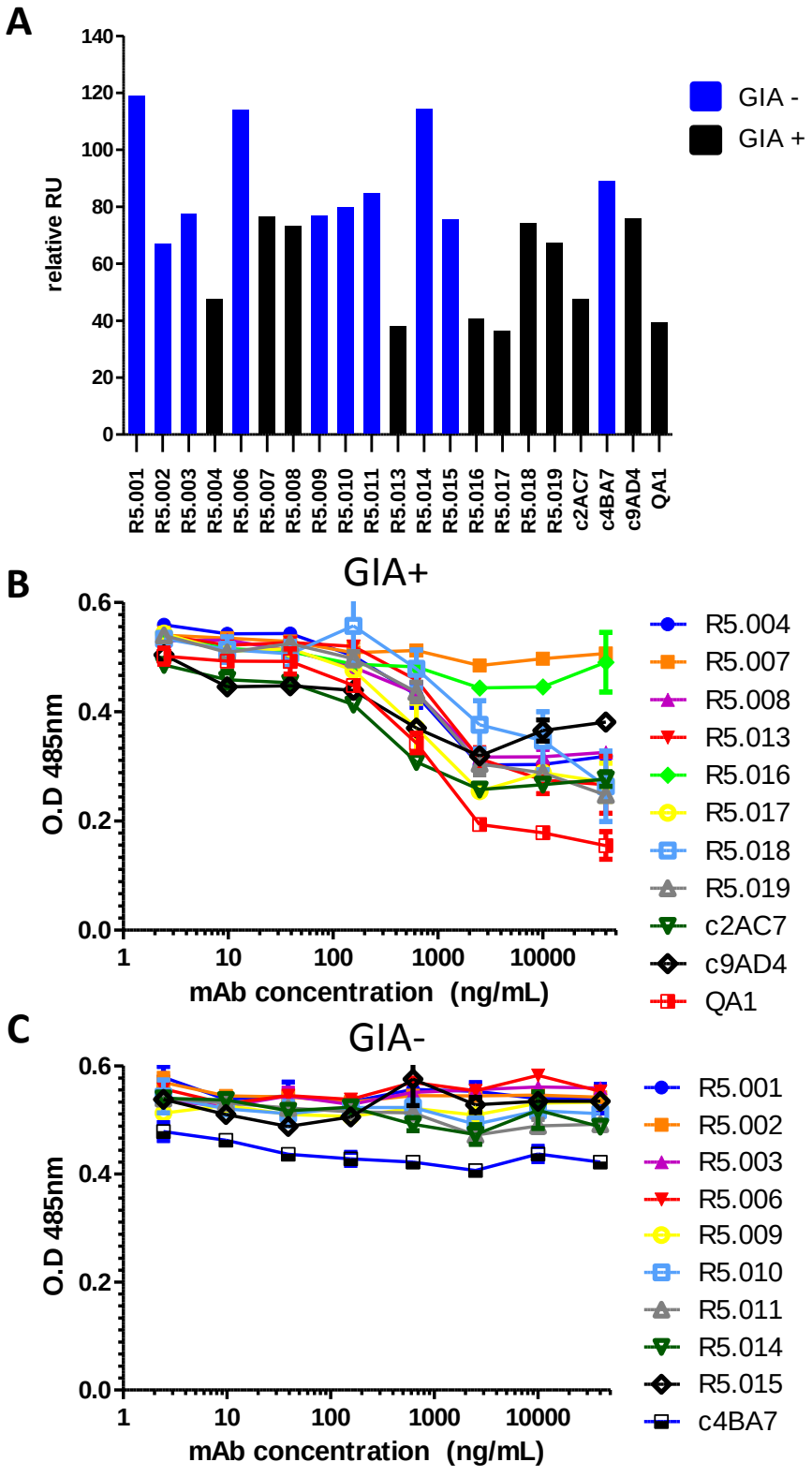

Figure 4.7: The relationship between PfP113-PfRH5 blocking and GIA is unclear. (A) SPR-based PfP113 blocking assay. Neutralising mAbs are coloured in black and non-neutralising mAbs in blue. (B) AVEXIS-based PfP113 blocking assay with neutralising mAbs. (C) AVEXIS-based PfP113 blocking assay with non-neutralising mAbs. Data in A are representative of one experiment for each mAb. Data points in B and C are mean of duplicate wells, error bars are SEM. An example of measurements of PfP113 binding in the SPR assay can be found in Appendix 4.1 at the end of this chapter.

PfRH5-PfP113 interaction blockade

As with basigin blocking, there is a separation in PfP113 blockade between neutralising mAbs and non-neutralising mAbs (with a few exceptions), in both types of assay although more obvious in the AVEXIS assay (Figure 4.7). However, unlike in the basigin-blocking assays, the binding was never completely abrogated by any mAb. None of the non-neutralising mAbs showed any blocking effect and neither did the neutralising mAbs R5.016 and R5.007 (interesting these two mAbs lie at both ends of the GIA spectrum). Across both assays, the mAbs which blocked the most PfP113 binding were: QA1, c2AC7, R5.017, R5.013 and R5.004. Again, R5.016 gave different answers between the two assay formats. At first glance, it may be tempting to suppose that the clear separation in PfP113 blocking phenotype between neutralising and non-neutralising mAbs may be causally linked with growth inhibition, though I believe this to be specious for reasons which will be discussed in section 4.4.5 of this chapter.

4.4 Discussion

Human mAbs elicited by human vaccination span a broad range of growth inhibition. Roughly half the mAbs produced in this work did not inhibit invasion detectably. As mentioned earlier, the most potent mAbs isolated here are comparable to the best anti-merozoite mAbs isolated before, in terms of invasion inhibition. Claims of ultra-high neutralizing human anti-merozoite mAbs have been described in one paper from the mid-1980s, however the neutralization claims are so extraordinary (70% growth inhibition at <50ng/mL of mAb binding an unidentified 195kDa protein[250]) relative to all published data since, they surely point to a misleading result either because the assay used is not comparable to modern growth inhibition assays or simply because of an error.

4.4.1 The GIA assay as a correlate of protection

In addition to the data from section 4.3.2, two studies point to a correlative link between activity in this assay and *in vivo* PMR reduction/protection of *P. falciparum* parasites and protection in *Aotus* monkeys[111,122]. A further study extended these findings for the protection of Rhesus macaques against *P. knowlesi*[251]. The threshold for protection, defined independently in both *Aotus* challenge studies mentioned before with antibodies to two different invasion ligands indicate ≥60% GIA at a serum dilution of 1:4 is correlative of protection. FVO strain parasites adapted to invade *Aotus* RBC and used in these studies causes disease in these monkeys, furthermore, this strain is known to invade *Aotus* RBC with similar efficiency to human RBC[252]. Furthermore, a recent blood-stage challenge of PfAMA-1 showed <60% GIA at a serum dilution of 1:4 and showed no protective efficacy[121], which is consistent with the non-human primate results. However because no challenge trial of invasion blocking antibodies in humans has been successful, it is unknown whether the threshold for protection in non-human primates is the same for humans.

4.4.2 Differing susceptibility of strains to neutralising anti-PfRH5 antibody

Significant genetic diversity is observed in natural infection with *P. falciparum*[253], making successful induced immunity extremely reliant on being "strain-transcending". Multiple genetically different but stable strains exist with slightly different phenotypes with respect to drug resistance[254] or invasion preferences[255,256]. For example, PfRH4 is not normally expressed in the W2mef strain where its function is replaced by PfEBA-175 (although it can be selectively upregulated upon loss of PfEBA-175 expression[257]), but is expressed on the 3D7 clone and relied upon for invasion[140,258]. Antibodies to PfRH5 have widely been claimed to be strain-transcending[55,125,127,129,259] which may well be true on a polyclonal level,

however, this is (predictably) not the case on a monoclonal level. Data here show that within this panel, R5.017 is not able to neutralise parasites which carry the S197Y mutation due to a significant loss of binding. Polymorphisms at sites of vulnerability need to be identified and considered when designing a vaccine as they form an easy escape from immune pressure. Sequence variation is not the only explanation for the differences in parasite neutralisation. MAb-independent effects are visible in Figure 4.1 B but plotted more visibly in Figure 4.8. There seem to be intrinsic differences in susceptibility to antibody or reliance on PfRH5, particularly M-Camp stands out as being more difficult to neutralise by targeting PfRH5 with these mAbs, and similarly GB4 appears to be consistently more susceptible to anti-PfRH5 mAb. In the case of R5.004, the EC_{50} is increased 25-fold between GB4 and M-Camp and 10-fold between homologous strain 3D7 and M-Camp (Figure 4.1). The reason for this is unknown; PfRH5 expression levels or invasion speeds may be different depending on the strain, shifting the amount of specific antibody needed to neutralise the parasite. Further investigation must be done to understand the reason for decreased susceptibility in strains such as M-Camp or increased susceptibility in strains such as GB4. Interestingly, the summary paper of VAC057[171], the trial from which these mAbs originate, shows that GB4 was indeed more susceptible to these polyclonal vaccine-induced IgG and that Cp806 was less susceptible, on the other hand. All other strain susceptibilities were similar to 3D7, including M-Camp. It could be that these differences are simply due to experimental anomalies or that neutralising polyclonal IgG is qualitatively different to neutralising mAb, a hypothesis which will become more plausible in Chapter VI.

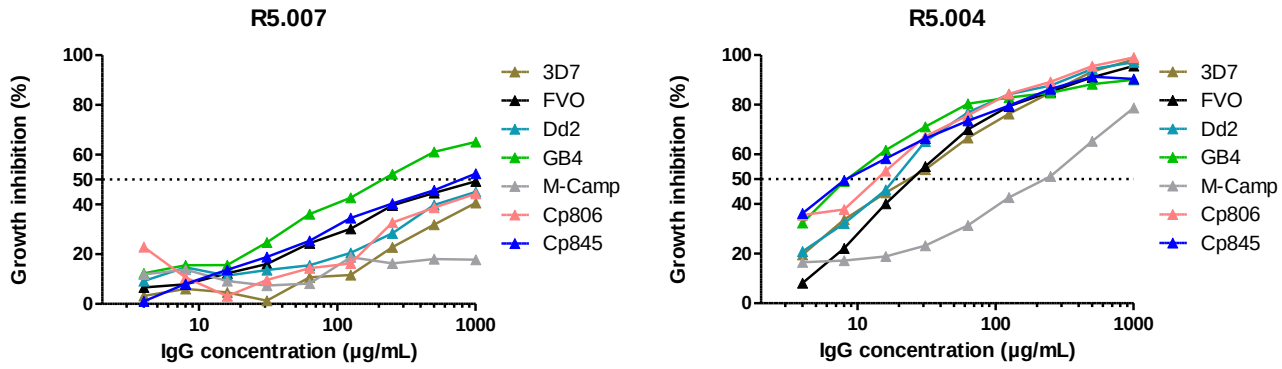

Figure 4.8: Two examples of strain-dependent neutralisation capacities of PfRH5 mAbs. The data shown here are adapted from Figure 4.1.

4.4.3 Correlation with association-rate

The sample sizes are small in the kinetic rate correlations as they were made with data from growth inhibitory mAbs only, given there were no data to suggest that any of the non-neutralising mAbs bound PfRH5 on the parasite. Moreover, because a mAb is so large with respect to PfRH5, (especially when taking into consideration that PfRH5 is thought to exist in a complex on the surface of the merozoite, further limiting the unoccluded surface of PfRH5 when carrying out its function), I supposed that any 150kDa mAb would be sufficient to inhibit basigin-binding through steric effects, as long as it is able to bind merozoite PfRH5. Data from Chapter VI show that indeed some non-neutralising mAbs are patently able to bind parasite, meaning that epitope-specificity is the major predictor of neutralisation and association-rate is the major correlate of potency among neutralising antibodies.

4.4.4 Passive transfer of mAbs into a humanised mouse model

The dose of mAb given to these mice (100mg/kg) is a high dose by any account and, had these mice not have been prohibitively expensive, a dose escalation study would have been done to give a closer approximation of the minimal concentration of R5.016 mAb needed for protection from challenge. The clinical relevance of this model is, although undoubtedly more predictive of human *in vivo* conditions than the GIA assay, by no means absolute. The average mouse haematocrit is very similar to that of humans[260] but only 50-70% of RBCs in these mice were human, the rest being mouse erythrocytes, known to be poorly invaded by human *P. falciparum* parasites[261]. Moreover, the amount of RBC rosetting and endothelial cytoadherence is unknown, important features of natural infection with the potential to reduce the potency of mAb activity. Cell-dependent[262] and complement-dependent[58] merozoite killing mediated by specific antibody has been reported before. If these killing mechanisms do indeed play a protective role in natural infection, they would almost certainly not be able to contribute in these immunodeficient mice. The presence of human complement protein C3 has been detected in the serum of these mice (Dr. Lander Foquet, personal communication), presumably originating from the xenografted hepatocytes. Although the concentration of human complement proteins is not thought to be functionally relevant, complement activity cannot be fully ruled out. The IgG serum half-life is much shorter than would be expected in a primate host. Murine neonatal Fc receptor (FcRn) is known to bind human IgG1[263] and FRGN mice are severely immunocompromised meaning that the clearance of foreign immune complexes would be expected to be slowed. It is not clear why the concentration of mAb dropped so quickly, although it could simply be explained by these mAbs having a large volume of distribution in these mice.

4.4.5 Basigin/PfCyRPA/PfP113 interaction blockade

Unquestionably, the causal link between PfRH5 interaction-blocking and growth inhibition is strongest for basigin. Blockade of the basigin-PfRH5 interaction has of course been described to inhibit growth when targeted by mAbs to both PfRH5 and basigin[127,129]. In this work, basigin blockade coherently explains the neutralising mechanism of all human anti-RH5 mAbs with the exception of R5.007 and R5.016.

Antibodies targeting PfCyRPA are known to have an inhibitory effect[131,133,241] but whether this is due to disrupting its interaction with PfRH5 was unknown before this work. PfCyRPA antibodies might block binding to PfRIPR[133,135,136], which was not studied here and is a plausible mechanism of growth inhibition of these antibodies, rather than PfRH5-PfCyRPA disruption. Although the Chen *et al*[132]. paper identified a PfCyRPA-reactive neutralising antibody which blocked binding to PfRH5, this does not mean that the antibody didn't also block PfRIPR binding to PfCyRPA, a possibility not explored by the authors. My data suggest mAbs binding to the PfCyRPA binding site on PfRH5 are not a major source of growth inhibition. R5.007 blocks PfCyRPA-binding *in vitro* and has modest growth inhibitory properties, similar to neutralising anti-PfCyRPA mAbs[131,241]discovered so far, although correlation does not imply causation. These data do not preclude that PfCyRPA-PfRH5 blockade from being a mechanism of growth inhibition; blocking this interaction by targeting PfCyRPA could be more effective.

PfP113 is known to bind the PfRH5 N-terminus[135], and although this N-terminus is intrinsically unstructured, it is possible that it preferentially adopts an N-terminal "upwards-pointing" conformation, making PfP113-binding susceptible to steric interference from mAbs binding close to the basigin-binding interface, thus co-correlating with basigin blockade, as observed here. Although no N-terminal anti-PfRH5 mAbs were isolated here (all human

mAbs bound the 45kDa shed PfRH5 in supernatant which lacks 15kDa at the N-terminus), a highly-potent N-terminal mAb was described previously[141] but it is not known whether it interferes with PfP113 binding. PfP113 is the only member of the PfRH5 invasion complex whose vaccine-induced polyclonal antibodies have no measureable growth inhibitory properties (unpublished data, Draper group), however this doesn't formally rule out its involvements in the invasion process as any hypothetical neutralising epitopes may not be temporally or spatially available for antibody binding during the invasion process. Moreover, PfP113 has since been reported not to exist on the merozoite surface[77], although again it is plausible that this protein simply isn't available for antibody-binding. More convincingly, the invasion phenotype of conditionally knocked-down PfP113 merozoites has been reported not to be impaired (Malaria Gordon Research Conference 2017).

I am aware of the limitations of the extent to which a protein-protein binding assay reflects the natural environment these proteins bind in on the merozoite. Different steric constraints imposed by binding partners, the plasticity of the plasma membrane and fluctuating local concentrations of various elements are all variables which cannot be easily mimicked in any of the assays reported here. In the SPR assay, the low affinities of certain binding partners call for the use of high concentrations which has a tendency to lead to high background binding. Furthermore, PfCyRPA and PfP113 did not retain sufficient activity after amine-coupling to the SPR chip to conduct reliable assays hence why each assay format was slightly different. One reason for the slight discordance in results between SPR and AVEXIS assays is explained by the fact that in the AVEXIS assay, detection is carried out by measuring the presence of a large pentameric probe whose access to PfRH5 epitopes is likely to be more severely restricted by antibody than the (mostly) monomeric interactions measured by SPR. Equally, pentameric interactions in the AVEXIS assay are likely to provide a more sensitive means of probing the disruption of these weak interactions than SPR. In summary, these data

support PfRH5-basigin blockade being the major contributor to vaccine-induced PfRH5 mAb-mediated growth inhibition; although small contributions to GIA may be provided by interfering with PfCyRPA and PfP113 binding to PfRH5; however from the work in this chapter, the evidence for it is weak.

The next chapter will extend the search for a correlate of neutralisation in these mAbs by identifying their binding location on PfRH5 by various epitope mapping techniques.

4.5 Appendices

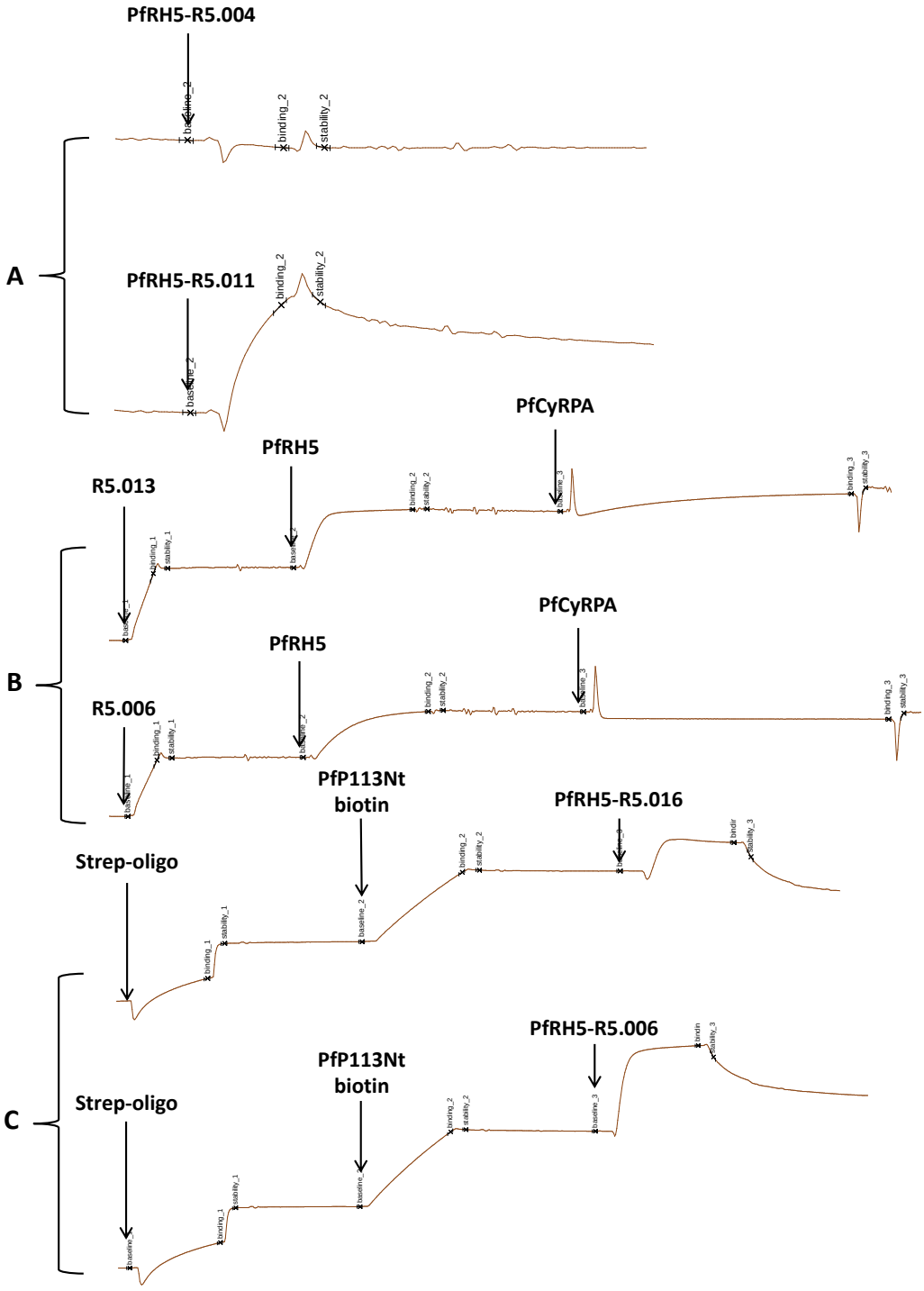

Appendix 4.1: Raw data used in basigin/PfCyRPA/PfP113 binding assays. These relate to Figure 4.5 A, Figure 4.6 A and Figure 4.7 A. (A) PfRH5-R5.004 complex or a PfRH5-R5.011 complex flowed over a chip with covalently-bound basigin. (B) PfCyRPA flowed over PfRH5 tethered to the protein A chip by R5.013 or R5.006. (C) PfRH5-R5.016 complex and PfRH5-R5.006 complex flowed over biotinylated PfP113Nt held onto the chip with oligonucleotide-conjugated streptavidin proteins. Here, data are reference-subtracted from a flow-cell coupled with an irrelevant protein tagged with identical tags to PfP113Nt (rat CD4d3+4 and His6tag).

Chapter V: Epitope mapping of the human mAbs

5.1 Authorship statement

HDX-MS experiments were set up jointly by Dr. Shahid Mehmood and me. Dr. Mehmood carried out the data processing. Antigen reversal and the associated GIAs were done at the LMVR by Ababacar Diouf. Jennifer Marshall did the GIAs with rabbit antibody at the Jenner Institute.

5.2 Introduction

The fine binding specificity of mAbs has been documented to have a large bearing on their neutralising properties in influenza virus[264], HIV[265], West Nile virus[266], RSV[267], Ebola virus[268], *Plasmodium vivax*[170], among many others. Determining the relative binding site of each mAb relative to one another is of great value in understanding the characteristics necessary for neutralisation of PfRH5 by mAbs, a major aim of this thesis. Supposing sufficient coverage of the molecule, if clonally-unrelated mAbs (as confirmed in Chapter III) bind similar locations on PfRH5 and have similar invasion inhibitory properties, this suggests the presence of multiple specific neutralising epitopes on PfRH5. Conversely, if this is not the case, that would suggest the ability of a mAb to inhibit growth is solely dependent on the number of PfRH5 molecules occupied, shifting the answer to "why does a mAb neutralise growth?" from a qualitative one to a quantitative one. This work also serves to group mAbs

based on similarity of binding site, allowing me to rationally choose mAbs to take forward for detailed binding analysis; work that isn't realistically feasible with seventeen different mAbs. Determining the absolute binding sites of mAbs of interest will allow us to make mechanistic predictions about growth inhibitory properties of certain mAbs, given that a PfRH5-basigin structure was solved in 2014, and of course serve as the basis for any potential rationally-based structural vaccine design. In this chapter, firstly relative binding sites of the mAbs were determined by sequential real-time binding assays and secondly the absolute binding locations of certain mAbs were investigated by ELISA, HDX-MS and X-ray crystallography. Throughout this chapter, to simplify orientation on the structure of the PfRH5ΔNL molecule, secondary structure features will be henceforth referred to by their number (e.g "helix 4" or "beta-strand 1"), a simple nomenclature system introduced in the first structural description of this protein[130] and illustrated below in Figure 5.1.

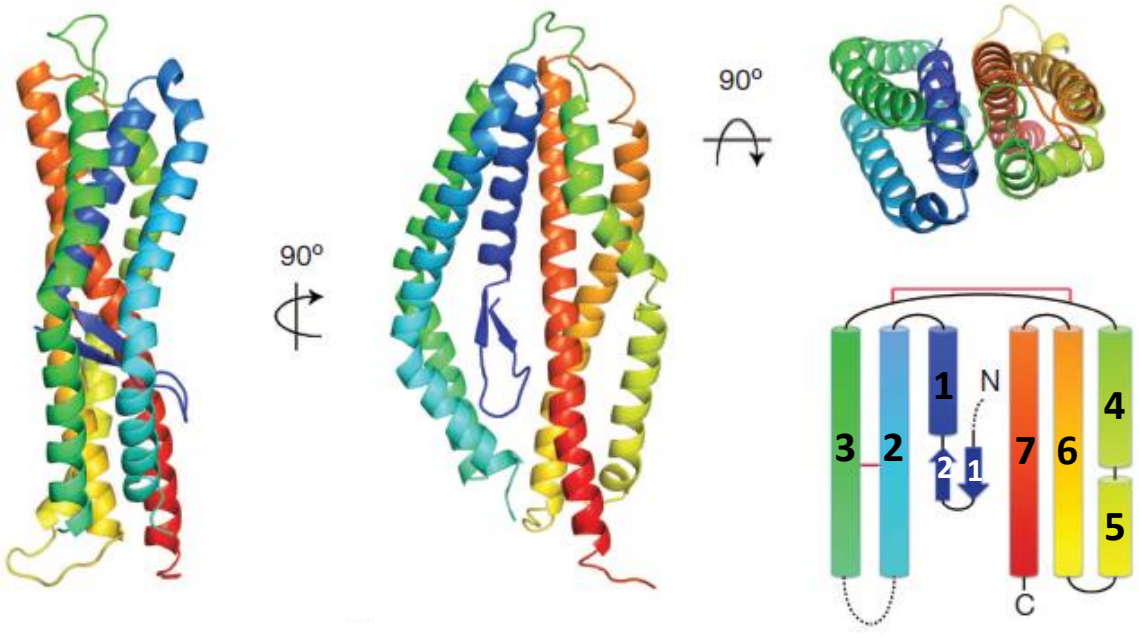

Figure 5.1: Structural feature nomenclature of PfRH5ΔNL. Alpha-helices (black numbers) and Beta-strands (white numbers) are likewise named according to their order in the primary sequence of PfRH5 from N- to C-terminus. Figure adapted from Wright *et al*[130].

5.3 Relative binding of the mAbs: Epitope binning

To determine the ability of each mAb to bind PfRH5 relative to one another, a sequential real-time binding assay was conducted where the binding of each mAb (mAb 2 in Figure 5.2) was measured in the presence of another pre-bound mAb (mAb 1 in Figure 5.2) and compared to the signal of mAb 2 binding PfRH5 alone. Stringent criteria were used to bin the relative binding into three phenotypes: 1) “blocking” if mAb 1 reduced the binding of mAb to 5% or less of its binding alone; 2) “non-blocking” if mAb 1 did not reduce the unencumbered binding of mAb 2 by more than 25%; and 3) “partially blocking” for values in between. The data were compiled in a “relative binding” matrix in Figure 5.2 A. The “relative binding” profile of each mAb was correlated with that of each other mAb to generate a correlation matrix in Figure 5.2 B. Relative binding profile correlations of 0.7 or above are highlighted in orange in Figure 5.2 B.

A

mAb 2

mAb 1	R5.001	R5.002	R5.003	R5.004	R5.006	R5.007	R5.008	R5.009	R5.010	R5.011	R5.013	R5.014	R5.015	R5.016	R5.017	R5.018	R5.019	2AC7NX	4BA7NX	9AD4NX	QA1
R5.001	0	0	0.642152	0.954113	0.789725	0.952053	0.951768	0.727439	0.893027	0.906644	0.752796	0.957276	0.495795	0.049707	0.701289	0.86404	0.897009	0.873174	0.871574	0.802856	0.841328
R5.002	0.380536	0.040336	0.384995	0.77155	0.3773	0.783765	0.800643	0.373171	0.660892	0.800341	0.577987	0.743963	0.264908	0.78481	0.776059	0.690899	0.810299	0.836836	0.751746	0.774991	0.919271
R5.003	0.65659	0	0	0.919371	0	0.905293	0.964228	0.047561	0.759203	0.970358	0.884049	0.955108	0	0.929299	0.850829	0.879023	0.838319	0.929462	1	0.998607	0.958984
R5.004	1	1	0.906466	0	0.953883	1	0.897508	0.846951	0.875704	0.955366	0	0.967492	0.84289	0.987959	0.152855	0.983907	0	1	0.837184	0.886799	0.307292
R5.006	0.789711	0	0	0.889544	0.015771	0.889153	0.85008	0.046951	0.757038	0.922317	0.828723	0.918266	0	0.919111	0.827256	0.77636	0.790231	0.873174	0.619559	0.815047	0.853516
R5.007	0.790506	0.586134	0.688796	0.763029	0.822461	0.048795	0.784164	0.7375	0.649632	0.878365	0.673926	0.819505	0.79396	0.817845	0.793002	0.676471	0.809163	0.823299	0	0.71543	0.711406
R5.008	0.790133	0.6543	0.787993	0.68323	0.721044	0.781174	0	0.821291	0.005755	0.948556	1	1	0.861698	0.947138	1	0	1	0.990648	0.800114	0.857143	0.642578
R5.009	0.682933	0	0.049987	0.679942	0.049638	0.778506	0.591884	0.010204	0.584631	0.912154	1	0.988141	0	0.880033	0.936331	0.394057	0.911103	0.950568	0.841234	0.853272	0.981439
R5.010	0.906933	0.756043	0.882693	0.858604	0.829369	0.87312	0	0.828737	0	0.003309	1	0.056812	0.760663	0.978362	0.996817	0	0.984648	0.982298	0.906339	0.931386	0.960557
R5.011	0.784	0.565486	0.847777	0.819876	0.797828	0.821931	0.920158	0.97187	0.004739	0	0.873169	0.038886	0.886957	0.942482	1	0.905039	0.951089	0.935204	0.782981	0.824068	1
R5.013	0.827733	0.778527	0.743029	0.137377	0.76758	0.908782	0.975916	0.952289	0.933311	0.943442	0	0.987865	0.895238	0.963298	0.006765	0.902455	0.027133	0.97328	0.87036	0.910978	0.280742
R5.014	0.771733	0.373806	0.781211	0.788089	0.735264	0.767831	0.922798	0.968009	0	0	0.904981	0	0.773085	0.908244	0.932352	0.861757	0.96894	0.917502	0.843518	0.826531	0.996133
R5.015	0.692566	0	0.025124	0.823627	0.125308	0.962939	0.901929	0.155452	0.848079	0.96091	0.970269	1	0	0.960534	0.981174	1	0.945316	0.955851	0.754032	0.909643	0.79041
R5.016	0	0.70901	0.700165	0.858985	0.810653	0.858727	0.981535	0.831776	0.863617	0.928216	0.967982	0.958922	0.707371	0.014572	0.958749	0.920936	0.881069	0	0.764401	0	0.851508
R5.017	0.98908	0.867061	0.80562	0.014143	0.885776	1	1	0.957944	0.848079	0.958778	0	1.016431	0.858971	1	0	1	0	1	1	0.994268	0.055105
R5.018	1	1	0.852562	0.837354	0.868534	0.951536	0.125154	0.891277	0.116962	0.928927	1	0.975353	0.878999	1	1	0	0.969103	0.974128	1	0.949427	0.665316
R5.019	0.952121	0.998523	0.790744	0	0.815271	0.942984	1	0.936137	0.890375	0.930348	0	0.987841	0.872601	0.956082	0	0.819685	0	0.993591	0.971774	0.938301	0
c2AC7	1	1	0.879339	0.910982	0.897167	0.934431	0.932704	0.917757	0.903755	0.936389	1	0.960237	0.818915	0.032787	1	0.781767	1	0	1	0	0.211507
c4BA7	0.765806	0.782951	0.84058	0.851134	0.84307	0.049623	0.819299	0.778515	0.823554	0.897797	0.816219	0.9366	0.776456	0.865499	0.927862	0.90689	0.807003	0.946168	0	0.843591	0.847391
c9AD4	0.891134	0.797377	0.797391	0.815217	0.804848	0.833935	0.786527	0.820221	0.776945	0.824124	0.875197	0.851761	0.774405	0.035038	0.880383	0.790503	0.812793	0	0.757787	0	0.30389
QA1	1	1	0.916842	0.014589	0.978158	0.986936	0.733288	0.868794	0.867414	0.925293	0	0.951536	0.816986	0.924409	0.141904	0.766117	0.308992	0.839558	1	0.796996	0

B

mAb 2

mAb 1	R5.001	R5.002	R5.003	R5.004	R5.006	R5.007	R5.008	R5.009	R5.010	R5.011	R5.013	R5.014	R5.015	R5.016	R5.017	R5.018	R5.019	2AC7NX	4BA7NX	9AD4NX	QA1
R5.001	1	0.558968	0.297855	-0.44693	0.224137	0.039971	-0.23787	0.247393	-0.16862	-0.0773	-0.30684	-0.06576	0.350491	0.518645	-0.29176	-0.19195	-0.35049	0.224128	0.108745	0.229317	-0.52043
R5.002	0.558968	1	0.858781	-0.51743	0.846204	0.012416	-0.16027	0.818759	-0.001	0.020412	-0.41654	0.047851	0.879592	-0.01383	-0.39685	-0.11201	-0.44901	-0.21319	0.094532	-0.22512	-0.6959
R5.003	0.297855	0.858781	1	-0.34187	0.982884	-0.07777	-0.175	0.968397	-0.2044	-0.26427	-0.30756	-0.24172	0.972951	-0.14059	-0.26491	-0.1176	-0.26467	-0.16253	0.023817	-0.20554	-0.46782
R5.004	-0.44693	-0.51743	-0.34187	1	-0.36647	-0.28957	-0.2118	-0.35988	-0.33835	-0.25283	0.937985	-0.27114	-0.39357	-0.39541	0.939035	-0.24302	0.944588	-0.31125	-0.28405	-0.31329	0.779385
R5.006	0.224137	0.846204	0.982884	-0.36647	1	-0.0868	-0.08977	0.960175	-0.08026	-0.16517	-0.35664	-0.14562	0.955706	-0.20755	-0.31815	-0.03373	-0.3085	-0.19512	-0.01021	-0.23485	-0.51068
R5.007	0.039971	0.012416	-0.07777	-0.28957	-0.0868	1	0.029014	-0.01565	0.053623	0.030516	-0.21208	0.068019	-0.10643	-0.05818	-0.28919	0.009732	-0.25069	-0.04844	0.940859	0.011985	-0.30597
R5.008	-0.23787	-0.16027	-0.175	-0.2118	-0.08977	0.029014	1	-0.05694	0.680479	0.190705	-0.38781	0.16202	-0.14673	-0.26505	-0.3836	0.965629	-0.38633	-0.22174	-0.06649	-0.19908	-0.2075
R5.009	0.247393	0.818759	0.968397	-0.35988	0.960175	-0.01565	-0.05694	1	-0.1926	-0.28481	-0.33416	-0.2607	0.978032	-0.14733	-0.31058	-0.01659	-0.3032	-0.16179	0.07772	-0.19802	-0.47818
R5.010	-0.16862	-0.001	-0.2044	-0.33835	-0.08026	0.053623	0.680479	-0.1926	1	0.730097	-0.48296	0.71672	-0.21152	-0.34537	-0.5072	0.66583	-0.50755	-0.29098	-0.07348	-0.25283	-0.48813
R5.011	-0.0773	0.020412	-0.26427	-0.25283	-0.16517	0.030516	0.190705	-0.28481	0.730097	1	-0.28077	0.994465	-0.22163	-0.17025	-0.32121	0.16154	-0.3289	-0.13921	-0.05005	-0.10779	-0.43775
R5.013	-0.30684	-0.41654	-0.30756	0.937985	-0.35664	-0.21208	-0.38781	-0.33416	-0.48296	-0.28077	1	-0.27771	-0.34568	-0.30878	0.98351	-0.40964	0.96776	-0.29846	-0.17605	-0.30859	0.740149
R5.014	-0.06576	0.047851	-0.24172	-0.27114	-0.14562	0.068019	0.16202	-0.2607	0.71672	0.994465	-0.27771	1	-0.19999	-0.17158	-0.32902	0.135476	-0.33754	-0.13025	-0.00915	-0.09955	-0.45597
R5.015	0.350491	0.879592	0.972951	-0.39357	0.955706	-0.10643	-0.14673	0.978032	-0.21152	-0.22163	-0.34568	-0.19999	1	-0.06535	-0.31409	-0.10349	-0.32581	-0.12779	-0.00354	-0.16968	-0.5044
R5.016	0.518645	-0.01383	-0.14059	-0.39541	-0.20755	-0.05818	-0.26505	-0.14733	-0.34537	-0.17025	-0.30878	-0.17158	-0.06535	1	-0.27392	-0.2099	-0.30839	0.866765	-0.02918	0.866756	0.046512
R5.017	-0.29176	-0.39685	-0.26491	0.939035	-0.31815	-0.28919	-0.3836	-0.31058	-0.5072	-0.32121	0.98351	-0.32902	-0.31409	-0.27392	1	-0.38843	0.978506	-0.28617	-0.25936	-0.30688	0.763441
R5.018	-0.19195	-0.11201	-0.1176	-0.24302	-0.03373	0.009732	0.965629	-0.01659	0.66583	0.16154	-0.40964	0.135476	-0.10349	-0.2099	-0.38843	1	-0.40688	-0.18215	-0.1218	-0.16483	-0.21671
R5.019	-0.35049	-0.44901	-0.26467	0.944588	-0.3085	-0.25069	-0.38633	-0.3032	-0.50755	-0.3289	0.96776	-0.33754	-0.32581	-0.30839	0.978506	-0.40688	1	-0.26425	-0.20374	-0.28193	0.753195
c2AC7	0.224128	-0.21319	-0.16253	-0.31125	-0.19512	-0.04844	-0.22174	-0.16179	-0.29098	-0.13921	-0.29846	-0.13025	-0.12779	0.866765	-0.28617	-0.18215	-0.26425	1	-0.03182	0.990411	0.161035
c4BA7	0.108745	0.094532	0.023817	-0.28405	-0.01021	0.940859	-0.06649	0.07772	-0.07348	-0.05005	-0.17605	-0.00915	-0.00354	-0.02918	-0.25936	-0.1218	-0.20374	-0.03182	1	0.036034	-0.30902
c9AD4	0.229317	-0.22512	-0.20554	-0.31329	-0.23485	0.011985	-0.19908	-0.19802	-0.25283	-0.10779	-0.30859	-0.09955	-0.16968	0.866756	-0.30688	-0.16483	-0.28193	0.990411	0.036034	1	0.140655
QA1	-0.52043	-0.6959	-0.46782	0.779385	-0.51068	-0.30597	-0.2075	-0.47818	-0.48813	-0.43775	0.740149	-0.45597	-0.5044	0.046512	0.763441	-0.21671	0.753195	0.161035	-0.30902	0.140655	1

C

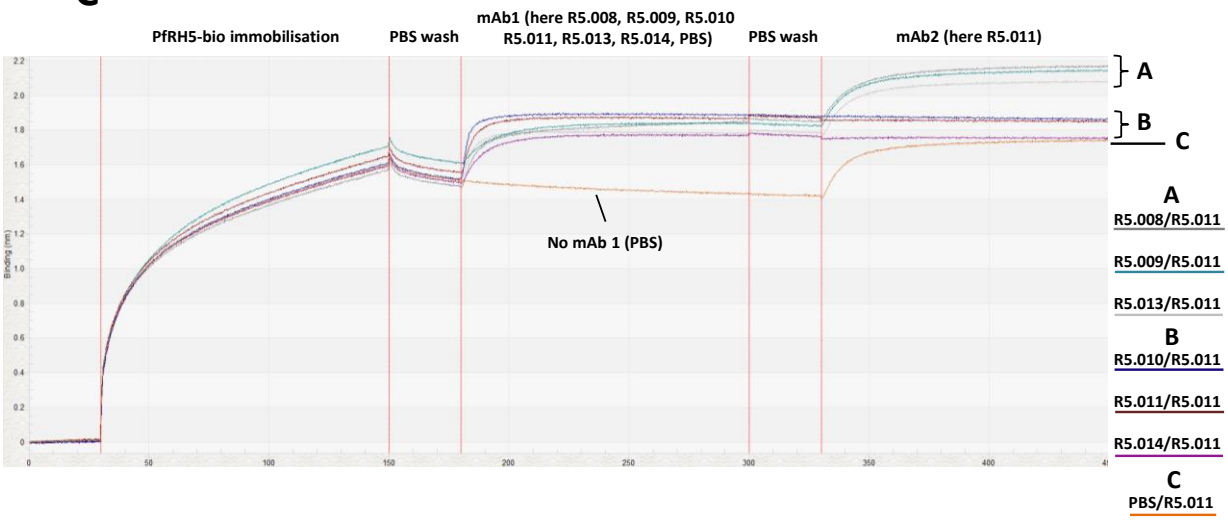

Figure 5.2: Competition matrix of mAbs binding to PfRH5 as sequential events. (A) Values represent fractional binding of mAb 2 in the presence of mAb 1 relative to mAb 2 binding to PfRH5 alone, termed "relative binding" here. Values >1 were normalized to 1 and negative values were likewise normalized to 0. Data were binned into 3 colours: green (non-blocking) if relative binding ≥0.75, pink (partially blocking) if relative binding <0.75 and ≥0.05 and red (blocking) if relative binding <0.05. (B) shows a Pearson product-moment correlation table which was made to correlate the binding profiles of every mAb against every other mAb in the panel to

identify members of the same epitope bin. Similar profiles were highlighted in orange with a cut-off of 0.70. (C) shows an example of the raw data used to derive relative binding.

The mAbs here generally clustered easily into separate epitope bins, with only R5.010 narrowly missing out on being simultaneously included in two epitope bins as only a small difference in correlation coefficient places R5.010 into the maroon bin rather than the olive bin (Figure 5.2 B). Seven distinct epitope bins were apparent with four containing neutralising mAbs (Figure 5.3). Given the size of PfRH5 and the size of an antibody "footprint", the presence of seven different epitope bins is indicative of fairly broad coverage from a panel of just seventeen randomly isolated mAbs. One member of each of the orange, green and yellow epitope bins contain a mAb (c9AD4, QA1 and c4BA7) whose binding site has been previously characterised on PfRH5. c9AD4 binds the top portion of helices 2 and 3 of PfRH5[130], QA1 binds the tip of the PfRH5 "kite" at the loops linking helices 3-4 and 6-7[130] and c4BA7 binds peptides present on a loop exiting the bottom of the "kite"[127,130]. It is reasonable to assume that members of any given bin bind overlapping or contiguous epitopes, a point which will be argued in the discussion of this chapter. This information suggests that there are two major neutralising epitope patches (orange and green, Figure 5.3 B) accessed by the human mAbs isolated here and they are likely occluding parts the tip of the "kite-like" structure of PfRH5. Furthermore, the neutralisation capacity of anti-PfRH5 mAbs seems to heavily depend on their binding location given that the correlation between binding location and neutralising activity is obviously strong.

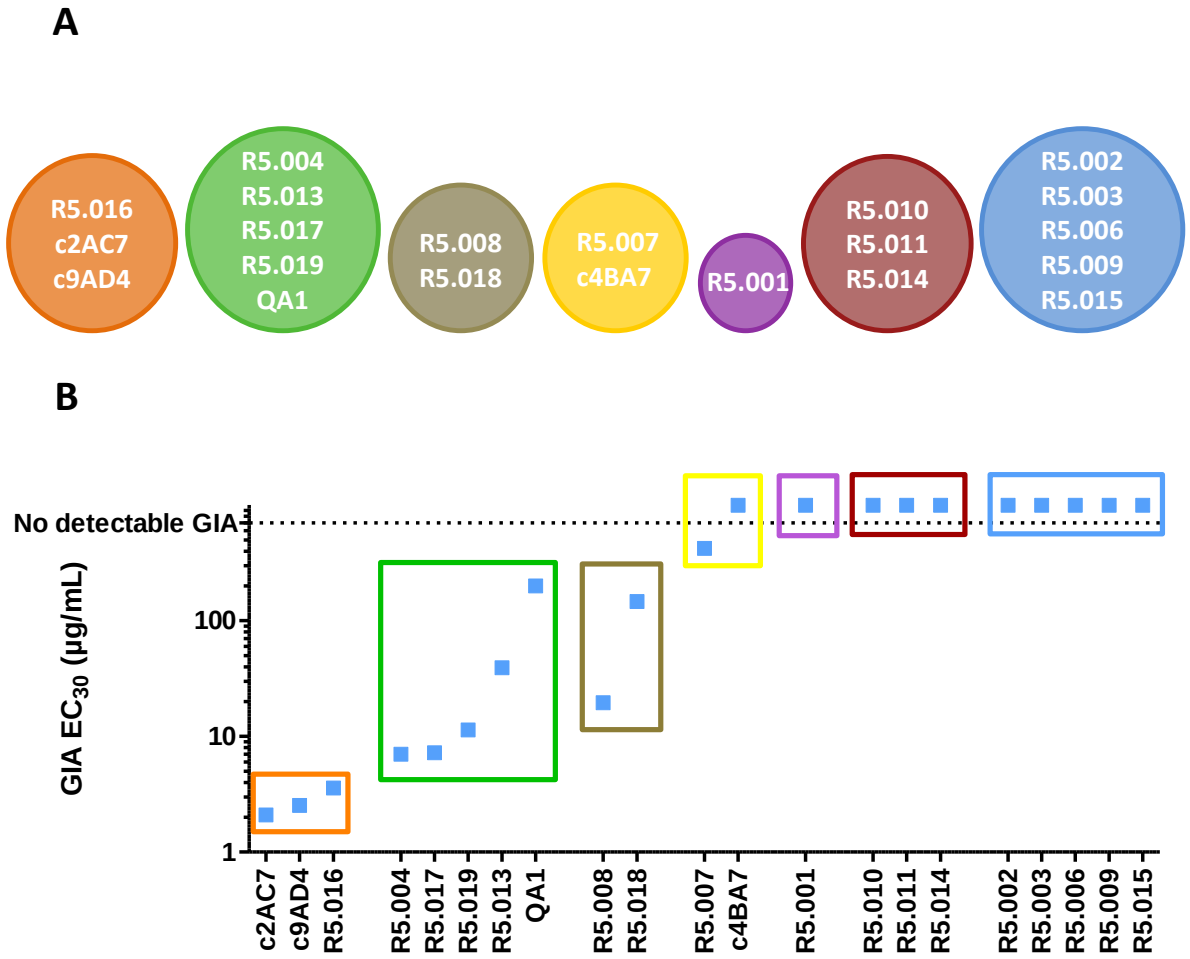

Figure 5.3: mAb epitope bins cluster by neutralisation phenotype. (A) Epitope bins as determined by a matrix of sequential binding assays. (B) Invasion inhibition (EC_{30}) of all mAbs ordered by epitope bin, represented by coloured boxes corresponding to the epitope bin colours in (A). The data used to construct the epitope bins are shown in Figure 5.2 and EC_{30} values are interpolated from growth inhibition data shown in Chapter IV.

5.4 Absolute binding of the mAbs on PfRH5

5.4.1 Mapping by ELISA

As reported by others, antibodies binding to the N-terminal portion of PfRH5 (which is cleaved at some point during the invasion process) have functional growth inhibition[135,141]. Assaying binding to PfRH5-Nt (amino acids E25-K140) serves to map the binding site to this section of amino acids. None of the human mAbs or indeed any chimeric mouse mAbs were able to bind this N-terminal portion of PfRH5; however PfRH5-Nt is recognised by polyclonal anti-PfRH5 antibody (Figure 5.4 A). The mAbs were also assayed against the crystallised form of PfRH5, PfRH5ΔNL to determine their suitability for inclusion in crystallographic trials; assaying binding to this protein also serves to map binding to amino acids K140-K247 and N297-Q526 as PfRH5ΔNL lacks M1-Y139 and N246-M296[130]. R5.007 and c4BA7 were both conspicuously unable to bind this protein (Figure 5.4 B) yet also unable to bind PfRH5-Nt, suggesting they bind between N246 and M296. Parental mouse mAb 4BA7 had previously been shown to bind peptides 28 and 29 (encompassing amino acids Y242-D269)[127] and thus would not be predicted to bind PfRH5ΔNL. This result was validated in Figure 5.4 C; R5.007 was found to bind the same two peptides as c4BA7. The canonical (overlapping) sequence is 250 DSYRYDISEEID 261, predicted to be included in a highly disordered 48-amino acid loop protruding from the base of the "kite-like" structure of PfRH5[130] between helices 2 and 3 (the 2-3 loop). This result also serves to confirm the clustering of R5.007 and c4BA7 into the same epitope bin, independently constructed from full-length PfRH5 binding (yellow bin, Figure 5.3 B). No other mAbs bound a peptide strongly in this assay (Figure 5.4 C, top panel). It must be noted that although this peptide array covers the whole PfRH5 sequence, the potential for false negatives is great as the assay is only capable of detecting binding of mAbs whose epitope is

both non-conformational and doesn't include a minimal binding region of more than 12 amino acids.

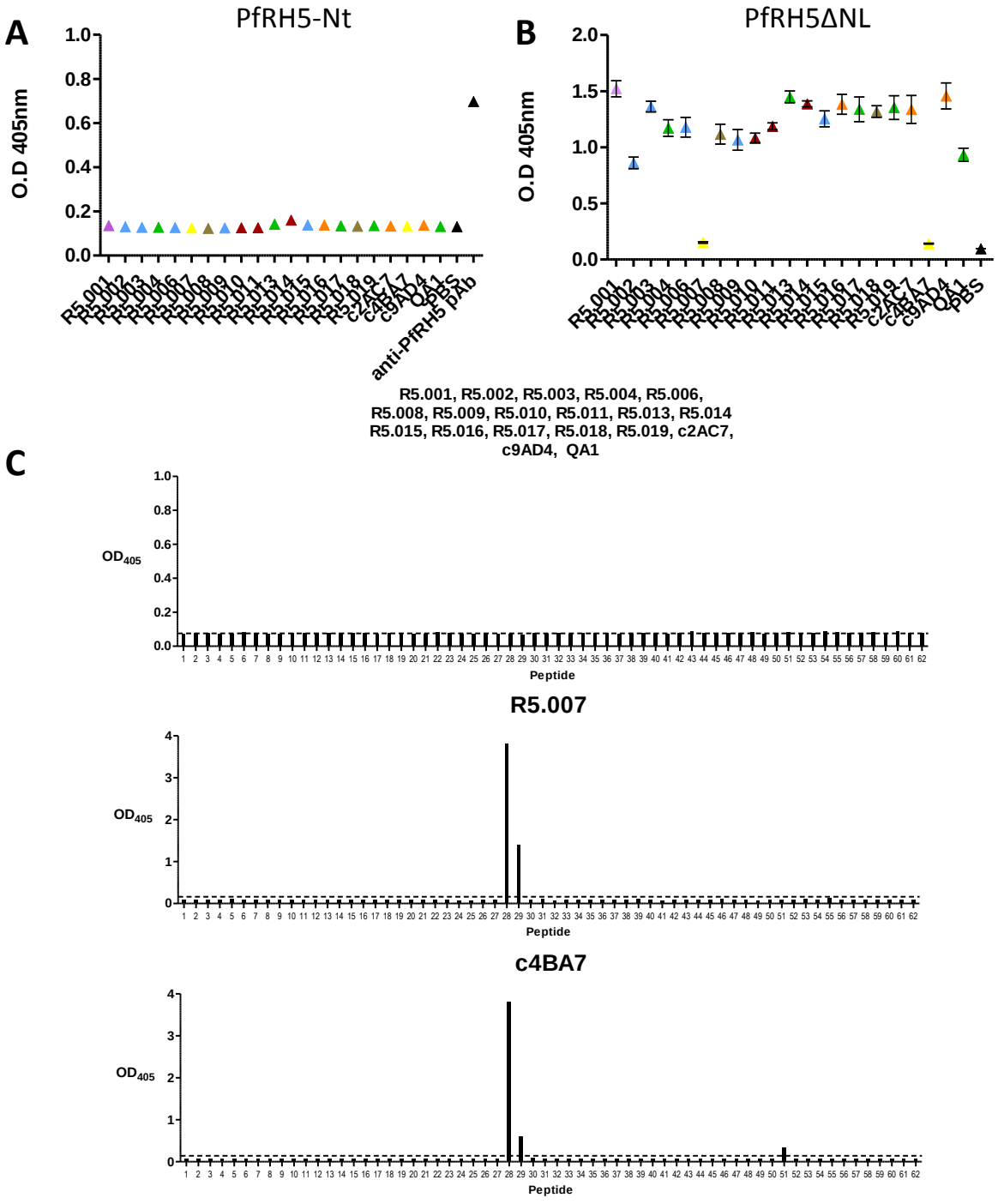

Figure 5.4: Mapping of mAb binding to PfRH5 truncations and overlapping peptides. (A) ELISA showing binding of anti-PfRH5 mAbs to PfRH5-Nt comprising the 117 most N-terminal amino acids of secreted PfRH5. The positive control, "anti-PfRH5 pAb" is purified IgG from a PfRH5-immunised rabbit. (B) ELISA showing binding of

anti-PfRH5 mAbs to PfRH5ΔNL, the truncation construct used for crystallisation studies. This construct lacks two unstructured domains (M1-Y139 and N248-M296). (C) ELISA showing binding to a set of sixty-two N-terminally tethered 20-mer peptides overlapping by 12 amino acids. In (A) data points are the mean of two replicate wells. In (B) data points are the mean of four replicate wells, error bars are SEM. The peptides in (C) were assayed in singlicate wells. All protein sequences are based on the 3D7 clone reference sequence.

5.4.2 Hydrogen-deuterium exchange mass spectrometry (HDX-MS)

HDX-MS is a technique often used in the study of protein confirmation and dynamics but which has more recently also found applications in probing the binding interfaces between protein complexes. HDX-MS experiments consist of measuring differences in protein deuterium uptake of a complex compared to the unbound protein (apo) when placed into a buffer containing deuterium oxide (D_2O) instead of H_2O. Main chain and side chain hydrogens (mainly amide, carboxyl, hydroxyl and amine), are in continual exchange with solvent hydrogens in a pH and temperature-dependent manner, however the exchange rate of these hydrogens is affected by local protein structure and solvent-excluded surface exchange is slowed or halted[269]. The more polar sidechains of amino acids exchange heteroatom-bound hydrogens several orders of magnitude faster than amide (main chain) hydrogens, meaning sidechain deuteration is almost completely lost in back-exchange in the time between labelling and ionisation. This feature means HDX-MS experiments essentially only measure changes in amide deuteration and that the degree of deuterium uptake is mostly sequence-independent with the exception of proline[270]. When proline is bound as an amide in a peptide bond its amide nitrogen has no hydrogen and is therefore invisible in HDX-MS experiments. PfRH5 only contains 7 prolines, sufficiently spaced to be unlikely to be contained on a single peptide and therefore unlikely to contribute to spurious protection. Briefly, samples are diluted in a solution containing >99.5% deuterated buffer for different lengths of time, subsequently quenched in a low-pH buffer to halt exchange, proteolytically degraded on a pepsin column and finally separated by liquid chromatography and the peptides analysed by

ESI-TOF MS. HDX-MS has many advantages; it allows data collection with full-length molecules over a wide range of pH and buffer conditions. This means that data generated by HDX-MS are highly representative of native, in solution interactions. HDX-MS also suffers from some sources of error. For instance, certain epitopes (particularly loops and epitopes lacking order) can exchange despite being solvent-occluded on one side by a binding partner. The resolution of this technique, like others relying on mass-spectrometry data[271], relies on the protein's intrinsic ability to be proteolytically digested into multiple overlapping peptides to a high degree of sequence coverage that are reliably detected by the mass analyser.

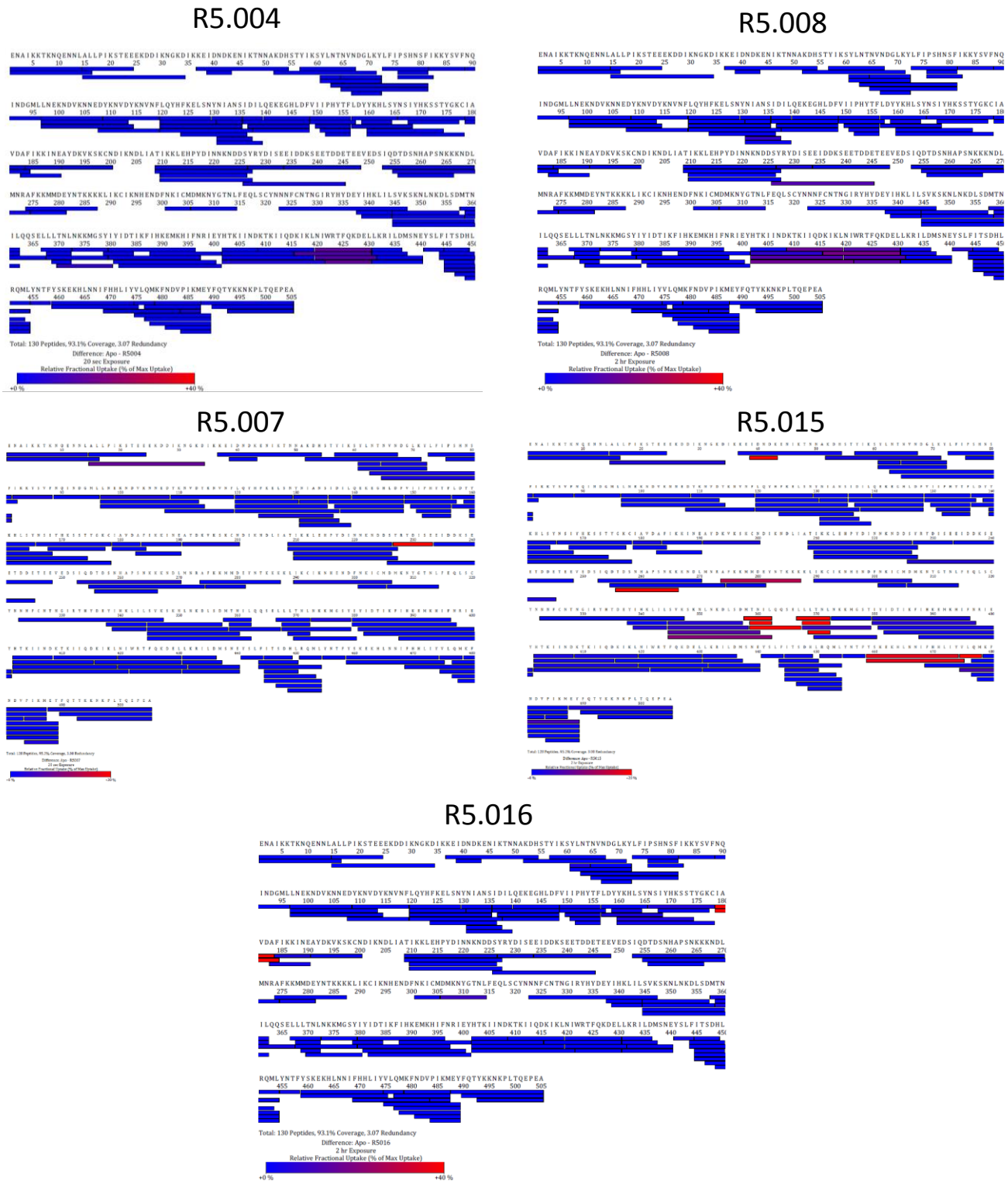

Figure 5.5: Protection of PfRH5 peptides when bound to mAb as measured by HDX-MS. Peptide protection was only deemed "real" if corroborated by protection of other overlapping peptides when available. Only the time-point with the highest signal-to-noise ratio is shown for each mAb (2h for R5.008, R5.015 and R5.016; 20s for R5.007 and R5.004). Recovered peptide coverage was at least 93.1% of the PfRH5 sequence, depending on the experiment. The sequence annotation here starts at E26, the most N-terminal residue predicted to exist after signal peptide cleavage during secretion. In the text I use the reference sequence numbering and thus +25 must be added to residue numbers to convert between this figure and the main text.

One mAb from each epitope bin (Figure 5.3) was complexed with full-length PfRH5 and run in an HDX-MS experiment, the results of which are shown in Figure 5.5. Protection was measured at three time-points: 20 seconds, 10 minutes and 2 hours. Experiments with mAbs R5.001 and R5.010 failed to return any reliably protected peptides (see Appendix 5.1) and the possible reasons for this will be addressed in the discussion. A set of overlapping peptides were protected by R5.004, protecting the sequence N445-L455 and mapping binding to the top of the PfRH5 "kite". The protection of this peptide is consistent with R5.004 blocking basigin binding to PfRH5, given basigin contacts PfRH5 at residues W447-T449[130]. Likewise, these data are consistent with R5.004 competing for an epitope on PfRH5 with QA1, whose light chain makes contact with the main chain of Q451 on PfRH5[130]. R5.008 protected similar peptides to R5.004 with the addition of the T435-L444 region which is, as with R5.004, consistent with R5.008's ability to block basigin (see Chapter IV, Figure 4.5). Later HDX-MS time points reveal a complete loss of protection for R5.004 but not for R5.008, confirming that R5.004 mostly binds the unstructured loop at the top of the diamond whereas R5.008 binds both the loop and the top of helix 6. R5.004 and R5.008 seem to protect an overlapping portion of a PfRH5 but appear to show only mild competition for binding (Figure 5.2 A). These data are entirely consistent with both R5.004 and R5.008 binding somewhat overlapping epitopes but with other contacts likely occurring in mutually exclusive areas as well.

R5.016 strongly protected peptide I204-F209 which concurs with its inability to bind PfRH5 simultaneously with chimeric mAb c9AD4 (which binds the top portion of helices 2 and 3 and makes contacts with A205 and F209[130]). R5.007 strongly protected peptide Y252-E258; this sequence is contained in the peptides bound in Figure 5.4 C and more particularly in the overlapping sequence R5.007 was predicted to bind above (250 DSYRYDISEEID 261). In light of the data supporting R5.007 binding to amino acids Y252-E258, the fact that the

overlapping peptide S251-E270 showed no protection will be attributed to an experimental anomaly. There were no previous data to locate the R5.015 epitope but in this experiment two major sections of overlapping peptides were protected; namely M383-L397 and Y486-L501. Fortunately, there is high peptide overlap at these areas, increasing the confidence in this result (Figure 5.5). The predicted residues involved in mAb binding to PfRH5 identified in these experiments are highlighted on the structure of PfRH5ΔNL in Figure 5.6.

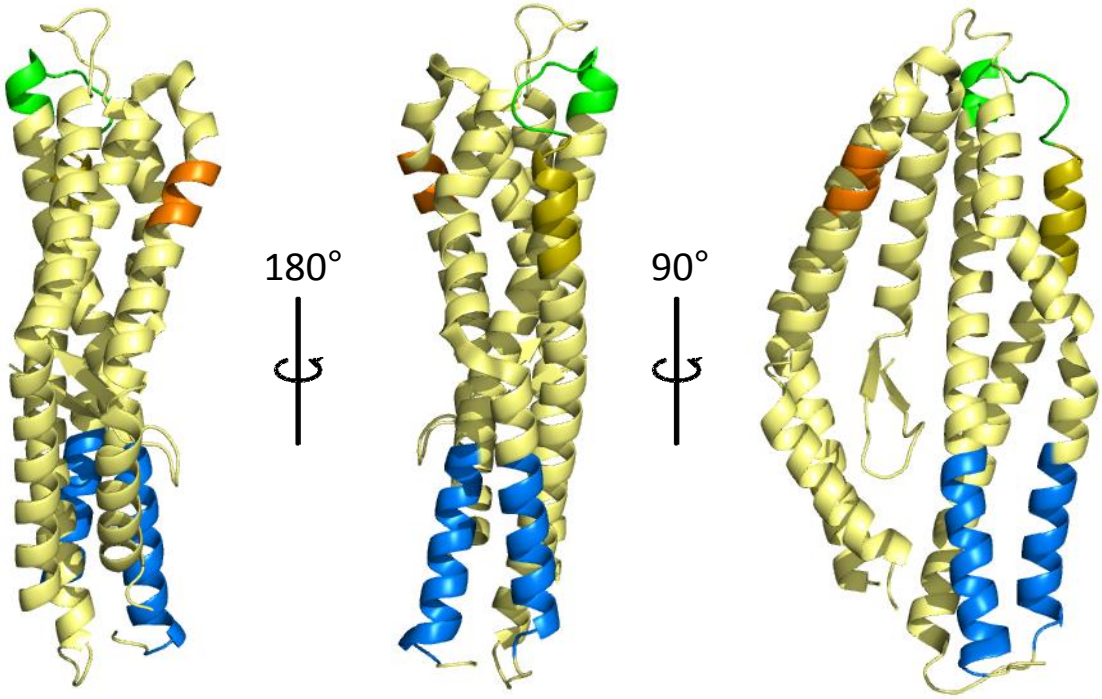

Figure 5.6: Location of protected peptides present in PfRH5ΔNL as determined by HDX-MS. Peptides protected by R5.004 are in green, R5.008 in olive, R5.016 in orange and R5.015 in blue. Note the green peptide was also protected by R5.008. The structure was made by highlighting amino acid sequences on chain A of PDB entry 4U0R in PyMOL. The HDX-MS peptide protection used to create this figure was derived from the data in Figure 5.5.

5.5 X-ray crystallography

X-ray crystallography is widely-regarded to be the gold standard for the structural characterisation of proteins. This method exploits the highly-ordered packing of molecules in a crystalline system and the short wavelength of X-rays. When the sample is exposed to highly-collimated coherent X-ray radiation, the rays undergo predictable elastic scattering upon contact with electrons clouds within the crystal. Most of the scattering deconstructively interferes to yield undetectable signal intensity, however in rare cases where atoms lie on lattice planes separated by a distance such that the path-length difference of incident light at a given angle is equal to an integer multiple of the X-ray wavelength, constructive interference occurs and discrete points of high-intensity diffracted radiation are recorded. The high-intensity spots are reflections of a diffraction pattern representing the crystal lattice in reciprocal-space. The reflection intensities are a function of the amplitude and the phase angle between diffracted waves and can be used to calculate so-called structure factors. A mathematical procedure called Fourier synthesis applied to the structure factors provides a real-space interpretation of the electron density of the molecule contained in the crystal.

5.5.1 Generation of samples for X-ray crystallography

A pipeline to obtain pure protein complex amenable to crystallisation has been previously used with success by Wright *et al.*[130] and so was adopted here. Briefly, PfRH5ΔNL was purified by C-tag affinity and concanavalin A lectin chromatography, buffer-exchanged into HEPES-buffered saline (HBS) and digested with endoproteinase GluC. In parallel, R5.004/R5.015/R5.016 antibodies were expressed from HEK293 cells, purified on protein G, digested with papain and depleted of Fc fragment with a mutated protein A incapable of

binding Fab. After this, two Fabs (R5.004/R5.016 and R5.015/R5.016) and PfRH5ΔNL were mixed at an approximate 1:1:1 molar ratio; the complex was methylated with dimethylamine borane complex (ABC) and subsequently concentrated and subjected to SEC as shown in Figure 5.7. Multiple peaks were visible by SEC. Eluting first was a high-MW species around 100kDa, identified as *Drosophila* midline fascilin, a contaminant known to co-purify from *Drosophila* S2 cells with C-tagged proteins (personal communications, Draper group). Eluting next were the PfRH5ΔNL/Fab peaks of which there were several distinct species, either represented by distinct peaks or a peak with a shoulder. These peaks were complexes containing both PfRH5ΔNL and Fab as shown by SDS-PAGE but it wasn't and still isn't clear which peak(s) contained one or both types of Fab due to equivalent gel mobility. The latest peak to elute was unbound Fab. As a precaution, the earliest-eluting peak was carried forward in both cases. I assume these multiple complex peaks represent complexes of PfRH5ΔNL with one or two Fabs of one or both types, and only the complexes with the largest differences in radius of gyration are resolved here. At the affinities and concentrations used here, the amount of complex bound with one Fab should be very low although it is possible that the endoproteinase treatment could have compromised the binding epitope for one or both of these Fabs in a fraction of PfRH5ΔNL molecules.

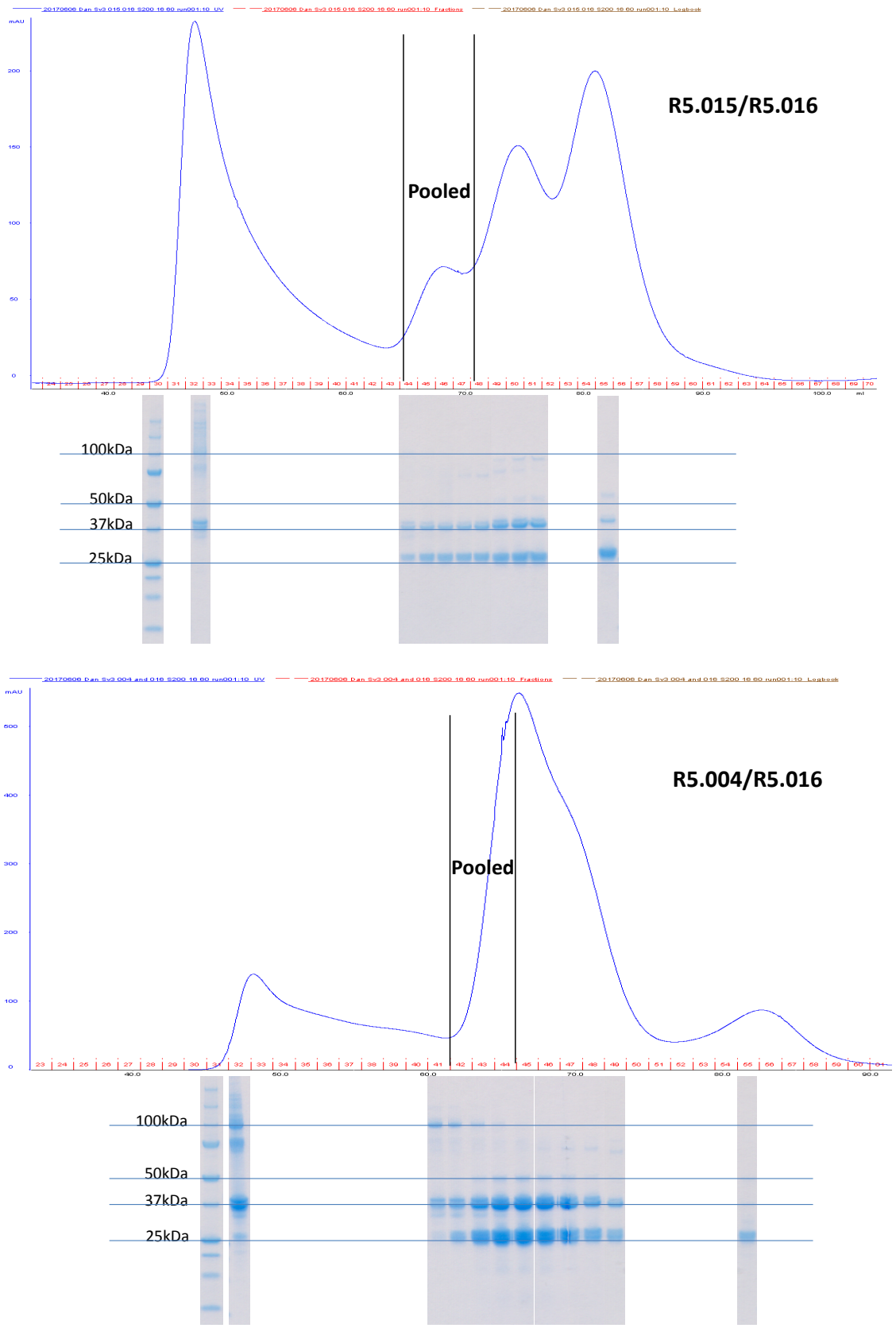

Figure 5.7: Protein complexes used for successful crystallisation. The top panel shows the SEC A_{280} trace of PfRH5ΔNL/R5.015/R5.016. Underneath is a total protein stain of the fractions aligned to their elution time. The lower panel shows the same data for PfRH5ΔNL/R5.004/R5.016. Expected MW: Fab 2(25kDa), PfRH5ΔNL (41kDa), Midline fascilin (100kDa).

Initial 96-well crystallisation screens were set up as 200nL sitting drops in PACT, PGA, JCSG+, MIDAS and Morpheus broad screens at both 4°C and 18°C. Crystallography is largely empirical and the conditions in the screens mentioned above are often selected on their previous success rate in large-scale crystallisation trials. Generally each condition contains one or several of: a salt, a precipitant and often a buffer as well to maintain a stable pH. For PfRH5ΔNL/R5.004/R5.016 the best-looking crystals grew as rod-like clusters in the 18°C JCSG+ screen in condition G8 (0.15M DL-malic acid, 20% PEG 3350) and for PfRH5ΔNL/R5.015/R5.016, the best-looking crystals grew in several wells as thick crystal clusters merging into a cube, the best of which grew in the 18°C PACT screen in condition F6 (0.2M sodium formate, 0.1M bis-tris propane pH 6.5, 20% PEG 3350). These initial hits were further optimised by crushing the crystals into seeds and including these in Silver Bullet 96-well additive screens (containing 80% of the initial hit condition and protein and 20% additive) in the hope of obtaining more highly-ordered crystals. In the case of PfRH5ΔNL/R5.004/R5.016, the additive screen did not yield many more crystals; the ones which did grow were of similar morphology to the parent crystal. In the case of PfRH5ΔNL/R5.015/R5.016, the additive screen yielded many large single crystals across several additive conditions. The best-looking crystals were frozen in the initial hit condition supplemented with 25% glycerol.

5.5.2 Data collection and processing

Crystallography data collection was carried out remotely at beamline I04 at the Diamond synchrotron (Harwell, UK). The highest-quality dataset for PfRH5ΔNL/R5.004/R5.016 was collected from the parent crystal and the best dataset for PfRH5ΔNL/R5.015/R5.016 was collected from a crystal supplemented with 20% of the Silver Bullet additive B8 (0.08% w/v

Ellipticine, 0.20% w/v Protamine sulfate salt, 0.20% w/v D-(+)-Trehalose dihydrate, 0.20% w/v 6-Phosphogluconic acid trisodium salt, 0.20% w/v D-(+)-Glucose, 0.02 M HEPES sodium pH 6.8). Summaries of the data collection are in Tables 5.1 and 5.2 In both cases, calculation of the Matthews coefficient showed the unit cell parameters were compatible with 140kDa of protein per asymmetric unit (the MW of PfRH5ΔNL is c. 41kDa and the MW of a Fab is c. 50kDa) with solvent contents within the expected range for protein crystals (30%-65%)[272].

	R5.004/R5.016	**R5.015**
Beamline	I04	I04
Wavelength	0.9795Å	0.9795Å
Space group	C 1 2 1	C 2 2 21
Omega start angle	290°	204°
Oscillation	0.2°	0.1°
Exposure time	0.2s	0.1s
Transmission	100%	100%
Images	900	1800

Table 5.1: PfRH5ΔNL-Fab co-complex data collection strategies used. Strategies shown are as recommended by EDNA from the CCP4 suite. Full 180° datasets were collected in both cases.

	R5.015/R5.016
Data reduction software	xia2
Space group	C 2 2 21
Unit cell dimensions (a, b, c)	97.74Å, 163.3Å, 176.82Å
Unit cell angles (α, β, γ)	90°, 90°, 90°
Resolution range	48.22Å-2.53Å (2.57Å-2.53Å)
Completeness	99.51% (99.33%)
CC-half	0.998 (0.569)
I/sigma(I)	11.94 (1.07)
R_{merge}	0.098 (1.842)
Multiplicity	6.7 (6.9)

	R5.004/R5.016
Data reduction software	Fast_DP
Space group	C 1 2 1
Unit cell dimensions (a, b, c)	232.76Å, 58.77Å, 118.45Å
Unit cell angles (α, β, γ)	90°, 106.10°, 90°
Resolution range	29.60Å-4.21Å (4.32Å-4.21Å)
Completeness	98.9% (91.3%)
CC-half	0.995 (0.791)
I/sigma(I)	6.70 (1.40)
R_{merge}	0.120 (0.652)
Multiplicity	3.3 (3.2)

Table 5.2: PfRH5ΔNL-Fab data processing summary. Data for the highest resolution shell are in brackets.

The structure of PfRH5ΔNL has been solved before, in complex with its RBC receptor basigin and two mAbs[130] as well as another PfRH5 truncation "PfRH5-C", lacking 15kDa at the N-terminus, as a monomer[273]. Furthermore, the mAbs are expressed as recombinant proteins so their sequences are known, enabling me to find highly homologous search models in the PDB. As a result, almost all the scattering mass could be accounted for with search models, so molecular replacement (MR) was the obvious choice for phasing. The search models in both cases were broken down into three rigid elements: PfRH5ΔNL, Fab V_H/V_L and Fab C_H/C_L. Fab fragment search models were reconstituted from heavy- and light-chains

bearing the most similarity based on a sequence search on the PDB. For R5.004, a composite of 3TNN and 4KQ3 was used, for R5.015 4HK0 was used and for R5.016 5K9O was used to generate search models. Large dissimilarities in sequence and unstructured loops which are likely to adopt sequence-independent conformations were removed from the search models, including the hypervariable loops of the Fabs. The search model for PfRH5ΔNL was simply chain A of 4U0R. MR was carried out straightforwardly using Phaser[176], yielding excellent scores for the final solution with the exception of R5.016 in one of the crystals (see Table 5.3). The molecular replacement failed to return a solution for the R5.016 search models in the PfRH5ΔNL/R5.015/R5.016 Patterson map and upon further inspection, electron density was lacking in the space R5.016 is known to bind meaning PfRH5ΔNL/R5.015/R5.016 crystals were in fact crystals of PfRH5ΔNL/R5.015 complex only.

	LLG	TFZ-score
PfRH5ΔNL/R5.004/R5.016	644	15.3
PfRH5ΔNL/R5.015	1492	34.4

Table 5.3: MR scores from Phaser. A translation function Z-score (TFZ-score) above 8 and a log-likelihood gain (LLG) above 100 are indicative of a highly-likely solution.

This is an ongoing structural biology project; as a result neither structure is complete at the time of writing this thesis. The dataset collected for PfRH5ΔNL/R5.015 is adequate and the model is currently in the course of being built, however the dataset collected for PfRH5ΔNL/R5.004/R5.016 is not of a high enough resolution to build an accurate model and further crystal optimisation is underway. However, the molecular replacement models generated below show the search models docked in to the actual electron density of the Fabs bound to PfRH5ΔNL and, although low-resolution, these data provide an accurate

representation of where these mAbs are bound. The Fab search models represented in the following Figures (Figure 5.8, Figure 5.9 and Figure 5.10) often lack CDR loops and show some discontinuity between the constant and variable domains as they were input separately to facilitate the MR process.

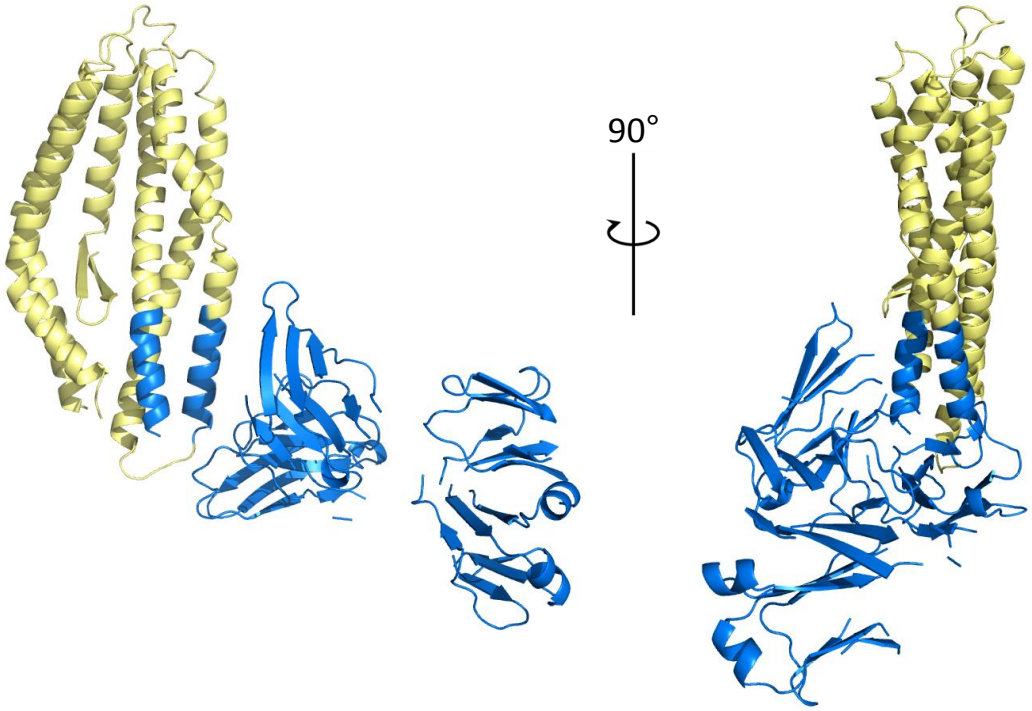

Figure 5.8: PfRH5ΔNL bound to R5.015 Fab. PfRH5ΔNL is shown in pale yellow and R5.015 Fab is shown in blue. The peptides protected by R5.015 in HDX-MS experiments are shown in blue on PfRH5ΔNL.

R5.015 binds the external interfaces of the lower portions of helices 5 and 7 (Figure 5.8). Here, crystallographic data agree well with the data obtained from HDX-MS experiments. R5.015, like all mAbs in the blue epitope bin, is able to block PfCyRPA binding to PfRH5. Likewise, R5.007 also blocks PfCyRPA binding and has been shown to bind a peptide proximal to the C-terminus of helix 2 found on the 2-3 loop (Figure 5.4 C). Importantly, helix 2 kinks towards helix 7, bringing the sequence bound by R5.007 close to the C-terminal end of helix 7 which is bound by R5.015. From these data, it seems reasonable to predict the C-

terminus of helix 7, with some involvement of the 2-3 loop, is likely to be implicated in the binding interface between PfRH5 and PfCyRPA. A contribution from helix 5 in PfCyRPA binding cannot be excluded.

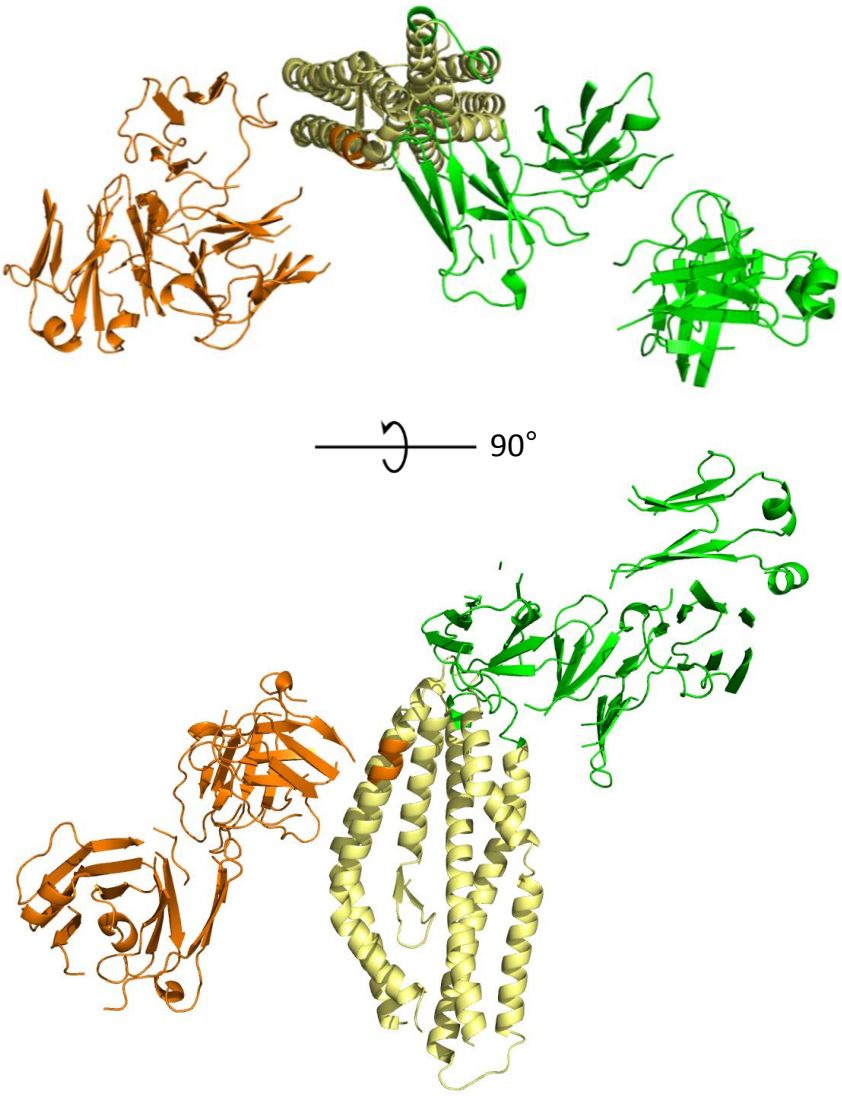

Figure 5.9: PfRH5ΔNL bound to R5.004 and R5.016 Fabs. PfRH5ΔNL is shown in pale yellow, R5.004 Fab is shown in green and R5.016 Fab is shown in orange. The peptides protected by R5.004 and R5.016 in HDX-MS experiments are shown on PfRH5ΔNL in green and orange respectively.

R5.004 binds PfRH5 essentially in the same region as basigin[130], at the top of the "kite" (Figure 5.9). The peptide protected by R5.004 in HDX-MS experiments is not directly contacted by the current incomplete R5.004 variable domain search model but examination of the current electron density maps suggest that the V_H CDRs which make contact with the N445-L455 sequence and these will be visualised in subsequent building and refinement steps. These crystallographic data strongly support R5.004's ability to block basigin binding, compete with QA1 and protect sequence N445-L455 from solvent exchange by HDX-MS. R5.016 binds towards the N-terminus of helix 2; again this is in concordance with I204-F209 being solvent protected by HDX-MS and with R5.016 competing for binding with c9AD4 which binds residues on the upper half of helices 2 and 3[130]. The angle of incidence of R5.016 Fab relative to PfRH5ΔNL is different from that of 9AD4[130]. One might suppose that only the V_H or V_L is involved in binding here, hence why the protected sequence is only 6 amino acids long despite the whole zone surrounding the Fab being α-helix or 3_{10}-helix.

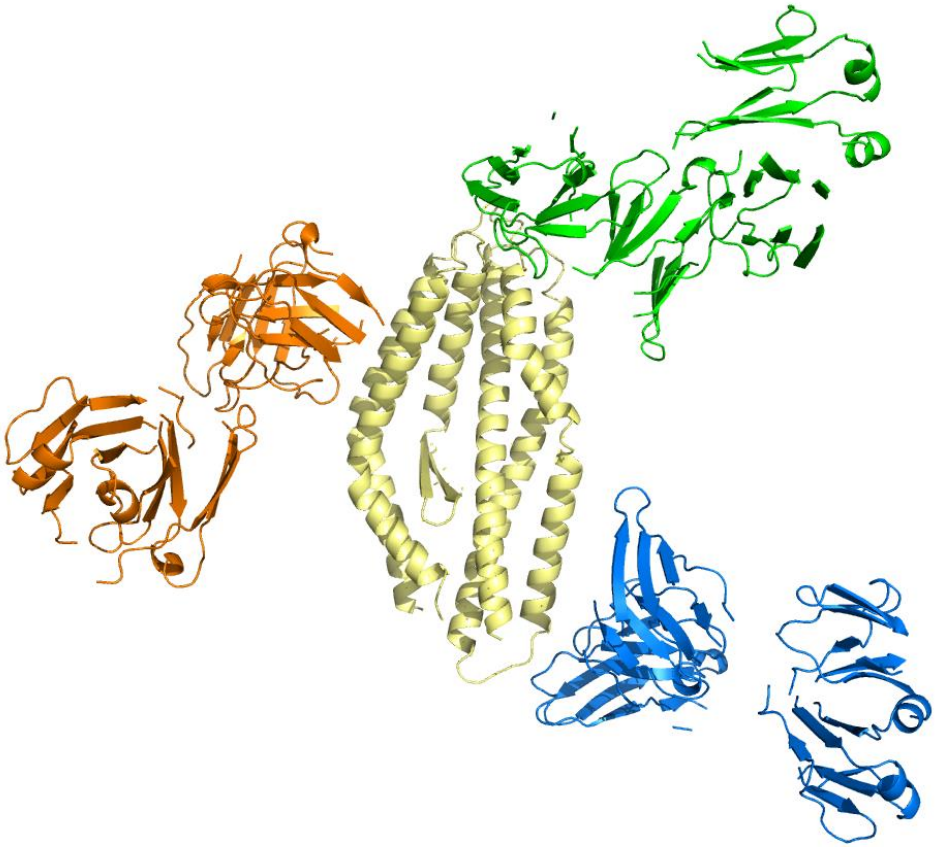

Figure 5.10: Representation of PfRH5ΔNL bound by R5.004, R5.015 and R5.016 Fabs. A composite of the structures in Figures 5.8 and 5.9 showing the search models for R5.004 (green), R5.015 (blue) and R5.016 (orange) in the positions where R5.004, R5.015 and R5.016 are bound to PfRH5ΔNL (yellow) is shown here. This figure was made by aligning PfRH5ΔNL in both structures in PyMOL.

Figure 5.10 is a consolidation of the crystallographic data from this chapter, simultaneously showing the putative binding sites of R5.004, R5.015 and R5.016. Each Fab, coloured according to its respective epitope bin, can be loosely construed as representing a similar binding site to that of the mAbs contained in their epitope bin and by extension ten of the seventeen human mAbs described in this thesis. This last claim would of course require validation with auxiliary data from small-angle X-ray scattering (SAXS), for example.

5.6 Assessing the merit of PfRH5ΔNL as a vaccine

Further to the realisation that sixteen of seventeen human mAbs (and the 7 best neutralisers of the 8 neutralising mAbs) bound PfRH5ΔNL, I sought to investigate what contribution to overall growth inhibition this fraction of antibodies had in the context of whole-PfRH5 vaccination elicited polyclonal antibody. To measure the impact depleting this fraction of Ab, human polyclonal antibody induced by full-length PfRH5 vaccination was incubated with high concentrations of PfRH5 or PfRH5ΔNL protein and the pre-depletion and post-depletion GIA was assessed. In every volunteer, the pre-incubation of vaccine-induced PfRH5-specific antibodies with PfRH5ΔNL was functionally equivalent to the addition of full-length PfRH5 (Figure 5.11 A). Furthermore, in all cases except for volunteer 1014, growth inhibition was entirely reversed by the addition of either protein, suggesting that all neutralising epitopes relevant to growth inhibition are contained in the truncated PfRH5ΔNL protein construct. By extension, as PfP113 is known to bind PfRH5 at the N-terminus which is absent in PfRH5ΔNL, these data show that antibodies with the theoretical capacity to block PfP113 binding, although clearly present (Figure 5.11 B), are not relevant to growth inhibition here.

5.6.1 Antigen-reversal GIA

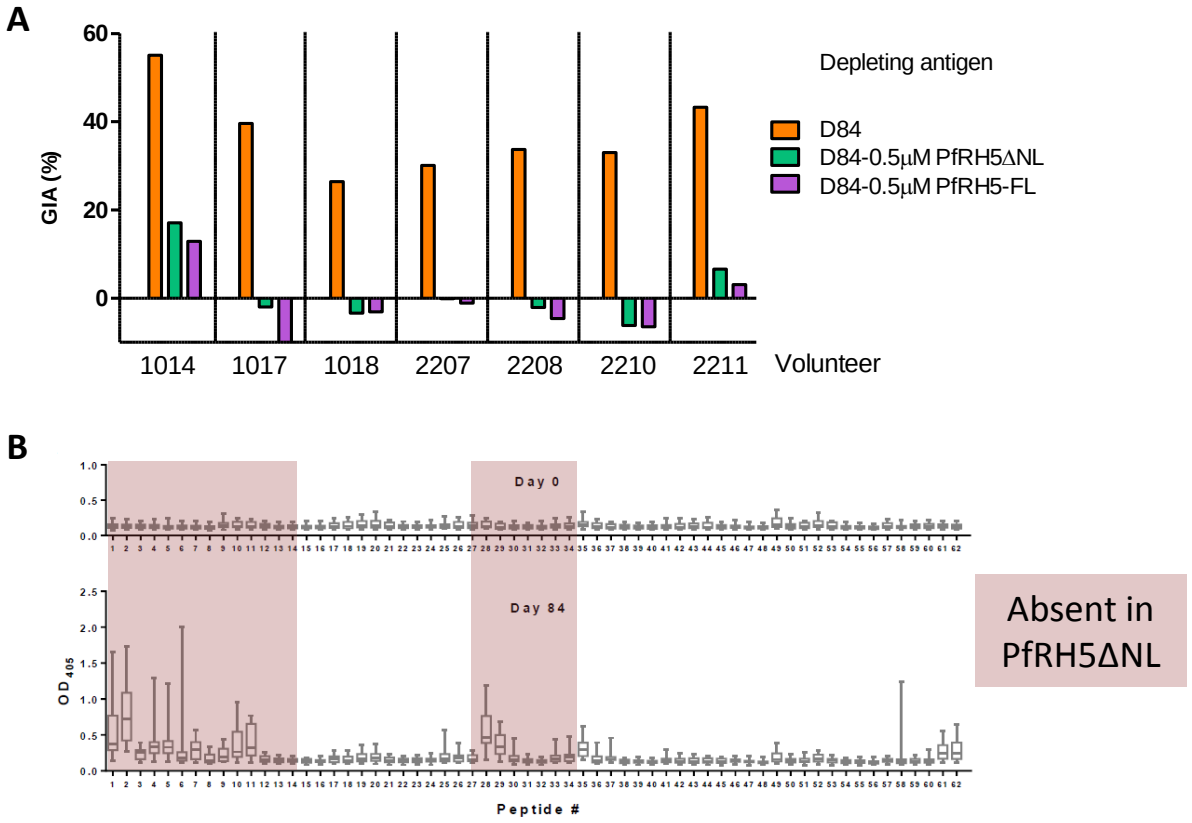

Figure 5.11: Antigen-reversal GIA with full-length PfRH5 or PfRH5ΔNL. Panel A shows the effect on GIA of adding 0.5µM (≈ 30µg/mL for PfRH5-FL and ≈ 40µg/mL for PfRH5ΔNL) of PfRH5 or PfRH5ΔNL to polyclonal antibody raised by full-length PfRH5 vaccination. Volunteers 1014, 1017, 2207, 2208, 2210 and 2211 were enrolled in VAC057. The D84 IgG starting concentration was adjusted to give 30-50% GIA. Background (pre-immune IgG GIA) was subtracted from all values for each volunteer. Panel B is adapted from Payne *et al*.[171] and shows the ELISA response to overlapping PfRH5 peptides of a pool (n=16) of pre-immune sera (Day 0, top) and immune sera (Day 84, bottom) from VAC057. The red shaded areas show the sections of protein missing from PfRH5-FL to make PfRH5ΔNL.

From these data, I postulated that the loops removed from PfRH5 to yield PfRH5ΔNL at best play no role in modulating the immune response to PfRH5 and at worst are immunologically deleterious. Possible mechanisms for this include actual steric interference/epitope obstruction similar to the glycan shield of HIV gp120[274], or immune diversion by immunodominance such as that observed in influenza whereby haemagglutinin-specific antibodies are preferentially raised to the variable head and not the conserved stem[275]. A

strong immune response to the N-terminus of PfRH5, in addition to diverting immune system resources, could plausibly lead to the emergence of antagonistic antibodies which interfere with the binding of neutralising antibodies to other parts of PfRH5. To investigate the effect of these portions of protein on the antibody response to PfRH5, a head-to-head preclinical vaccine trial was conducted in rabbits (Figure 5.12).

5.6.2 Rabbit immunisation experiment

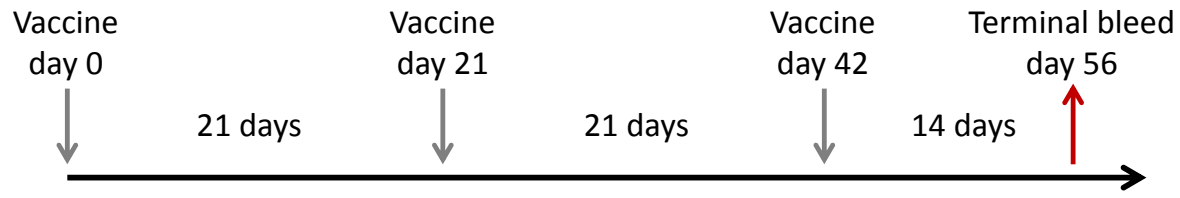

	PfRH5 FL (3D7) c-tag	PfRH5ΔNL (3D7) c-tag
Number of rabbits (NZL white)	6	6
Immunogen MW	60.2kDa	41.2kDa
Adjuvant	Addavax	Addavax
Dose/vaccination	486pmol (29.2µg)	486pmol (20µg)
Schedule	3 vaccines 3 weeks apart	3 vaccines 3 weeks apart
Route	intramuscular	intramuscular

Figure 5.12: PfRH5 and PfRH5ΔNL vaccine schedule and plan.

Two groups of six rabbits were immunised with equimolar doses of full length PfRH5 (PfRH5FL) or PfRH5ΔNL based on the same strain sequence, purified with the same affinity tag, administered using an identical regime, delivered by the same route and formulated in the same adjuvant (Figure 5.12).

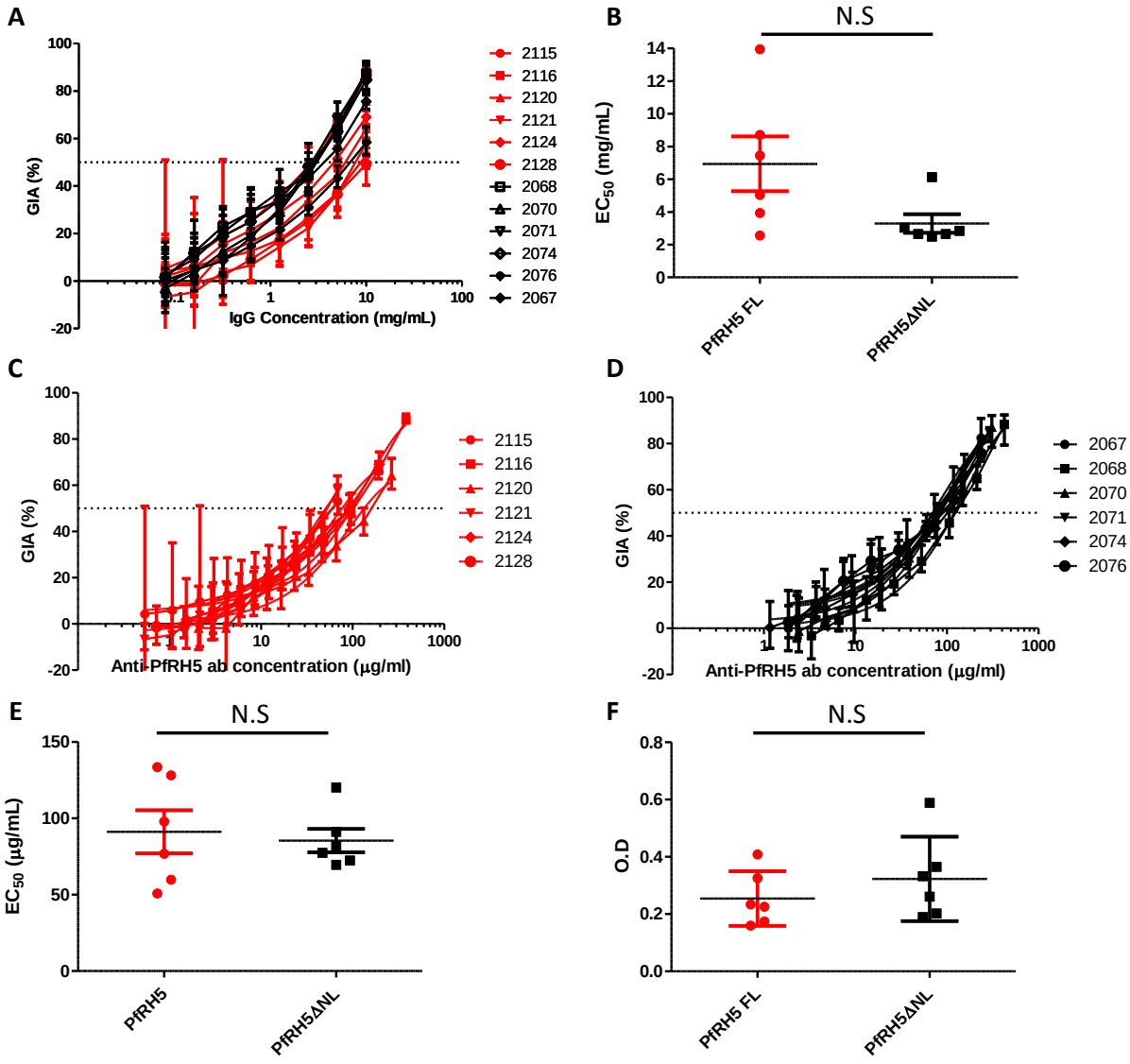

Figure 5.13: PfRH5ΔNL is marginally more immunogenic but elicits identical antibody quality to PfRH5FL vaccination. All data plotted in red represents rabbits in the PfRH5 full-length group and black data points represent PfRH5ΔNL data points. Panel A shows GIA of a dilution series of purified IgG, concentration-adjusted and starting at 10mg/mL, from all twelve rabbits in the experiment. Panels B and E show a comparison of EC_{50} values of total IgG and PfRH5-specific IgG, respectively. Panels C and D show individual rabbit purified IgG dilution series plotted as a function of PfRH5-specific IgG. Panel F shows ELISA reactivity to PfRH5 plotted as raw optical density at 405nm of 10,000-fold dilutions of sera. Here, each data point is representative of duplicate wells across three separate ELISAs. Pre-immune serum from each rabbit was also tested for growth inhibition; all were negative (data not shown). EC_{50} values in panels B and E were interpolated from four-parameter curves fitted by non-linear regression analysis. Data points in A, C and D are average of 3 replicate wells, error bars are mean and standard deviation. Statistical tests between means in in B, E and F were found to be non-significant at α=0.05 by a Mann Whitney rank-sum test. Error bars in B, E and F show mean and standard deviation.

Purified IgG from the PfRH5ΔNL group is slightly more potent on average (Figure 5.13 A).

The PfRH5FL vaccination group showed significant variation in inducing antibodies with

GIA, in contrast to the PfRH5ΔNL group where all six rabbits responded comparably (Figure 5.13 B). Notably, one rabbit from the PfRH5FL group responded poorly, a risk heightened by the use of outbred animals. Next, analysis of the "quality" of immune response was conducted by comparing the relative potencies of the fraction of antibody specific to the immunogen (Figure 5.13 C-E). Manifestly, the PfRH5-specific antibodies in both groups were equally potent in a GIA assay, on average. This result confirms that all the relevant neutralising epitopes on PfRH5 are present in the PfRH5ΔNL construct. Figure 5.13 F sought to explain the small difference in total IgG potency observed in panel A; indeed panel F shows that PfRH5-specific antibody titers were marginally higher in the PfRH5ΔNL group.

5.7 Discussion

Taken together, data in this chapter show that human vaccine-induced antibodies probably access several mutually-exclusive epitopes on PfRH5. Two major epitope "patches", orange and green accessed by R5.016 and R5.004 respectively, are probably the main contributors to invasion-blocking inhibition with possible contributions from a third more weakly neutralising epitope patch (yellow) accessed by R5.007. The binding sites of R5.004, R5.007, R5.015 and R5.016 have been characterised with high confidence. The general binding site for PfCyRPA on PfRH5 has been proposed for the first time, mapping to the same face of PfRH5 but at the opposite end to which basigin binds, at the bottom of the PfRH5ΔNL "kite". Equally, in this work, PfRH5ΔNL was shown to contain all the epitopes which elicit antibodies contributing measurably to growth inhibition and a PfRH5ΔNL vaccine elicits antibodies of the same potency as vaccination with full-length PfRH5.

5.7.1 Epitope binning and ELISAs

The epitope bins described in this chapter are likely to represent mAbs accessing overlapping or contiguous epitopes. With one-on-one mAb competition, it is clear that when two 150kDa proteins compete for binding to a 60kDa protein, there is ample opportunity to interpret binding inhibition as being caused either by epitopes overlapping, (i.e that the two mAbs share PfRH5 amino acids critical for binding) or caused by steric clashes of two mAbs when bound. In the format used here, the degree of inhibition of a mAb (mAb 2) binding to PfRH5 whilst another mAb (mAb 1) is already bound is measured. The binding profile of each mAb (consisting of the relative inhibition caused by every other mAb) is then correlated with the binding profile of every other mAb. If the correlation exceeds a certain cut-off, then and only then are two mAbs included in the same epitope bin. For example, R5.001 and R5.016 compete for binding in a one-on-one format (Figure 5.2 A) yet they are inhibited to different degrees with respect to c2AC7, c9AD4 or R5.009, for example, making their binding profile correlation coefficient fall below the threshold (0.51<0.70). My interpretation is that some of the inhibition seen when binding two mAbs to PfRH5 is due to epitope overlap and some is due to steric clashes by other regions of the antibody; the larger the panel of mAbs, the more likely it becomes that binding profile correlations will point to epitope overlap because epitope overlap will always result in inhibition whereas the particular Fc or Fab orientation will only inhibit a subset of mAbs binding at a different epitope. The epitope bins could be further refined by using Fab or smaller single-chain variable fragment (ScFv) constructs to eliminate steric inhibition to a degree, although arguably all types of inhibition, steric or otherwise, are relevant for interpreting immunological interference between mAbs in growth inhibition assays (see Chapter IV) and, by extension between vaccine-induced antibodies. In my view, the epitope binning format used here is a reliable, but approximate, way of determining relative binding sites of mAbs, and the epitope bins described here have proved

exceptionally good correlates in predicting which mAbs inhibit invasion (Figure 5.3 B) or inhibit the interaction of PfRH5 binding partners (see Chapter IV also). The fact that no mAbs bind the PfRH5-Nt is consistent with them all binding parasite-derived shed PfRH5 which is mostly a 45kDa cleaved fragment lacking 15kDa from the N-terminus. It is slightly surprising that none of the seventeen mAbs isolated here target the 134 amino acid unstructured stretch at the N-terminus, especially as it is clear that antibodies to this region are elicited by vaccination in the VAC057 trial[171]. The latest investigations do not find a difference in immunogenicity between structured epitopes and unstructured epitopes, globally speaking[276]. Still, it is possible that differences in immunogenicity between ordered and disordered epitopes exist on a protein-specific basis, with one relevant report of a *P. falciparum* merozoite surface protein (PfMSP-2) being notably more immunogenic in its ordered domains relative to its unstructured regions[277].

5.7.2 Determining mAb binding sites on PfRH5 by HDX-MS

Two mAbs, R5.001 and R5.010 did not strongly protect any peptides, despite knowledge of their binding to the PfRH5ΔNL core portion of PfRH5 (Figure 5.4 B) which does not include the major regions of disorder. It is possible for unstructured loops to be ligand-bound and exchange with solvent, provided the non-occluded face is sufficiently solvent-exposed. PfRH5ΔNL is known to be highly rigid and ordered, having been predicted to be ordered *in silico* and because previously-characterised co-crystals of PfRH5ΔNL bound to mAb or basigin had main chain RMSDs below 1Å[130]. Nevertheless, there are two surface-exposed regions in PfRH5ΔNL which are not known epitopes of other mAbs in this panel and which lack secondary structure; meaning is it conceivable that exchange could still occur. These regions are a 20-amino acid peptide preceding β-strand 1 at the N-terminus (of PfRH5ΔNL)

and the 29 most C-terminal amino acids of PfRH5; these regions having not been resolved in the crystal structure either because they were proteolytically trimmed and/or not resolved due to high B-factors. R5.010 did weakly protect a set of overlapping peptides covering the sequence N156-I163, although these data should not be trusted in the absence of bolstering evidence because several other overlapping peptides showed no protection (Appendix 5.1). Still, a mAb or Fab binding N156-I163 could conceivably sterically interfere with R5.008 binding, explaining the discordance observed between their mutually exclusive binding yet opposite abilities to block basigin *in vitro* and cause invasion inhibition (see Chapter IV).

5.7.3 Determining mAb binding sites on PfRH5 by X-ray crystallography

Significant effort was expended in trying to obtain co-crystals of sufficient quality to precisely define the binding location of a number of mAbs. Dozens of 96-well condition screens were set up and hundreds of crystals were shot at the synchrotron. In addition to the PfRH5ΔNL/R5.015/R5.016 and PfRH5ΔNL/R5.004/R5.016 complex screens which yielded useable datasets, broad condition screens of PfRH5ΔNL/R5.008, PfRH5ΔNL/R5.004, PfRH5ΔNL/R5.016, PfRH5ΔNL/R5.011, PfRH5ΔNL/R5.004/R5.015 and PfRH5ΔNL/R5.008/R5.016 complexes were also attempted. The reasons for failure were varied; in some cases no crystals grew, in other cases the crystal was not sufficiently ordered to generate datasets <6-7Å in resolution. In the case of PfRH5ΔNL/R5.011, PfRH5ΔNL/R5.004 and PfRH5ΔNL/R5.016 crystals of Fab alone grew and generally resulted in the collection of useless sub-2Å datasets; possibly due to the complex being disrupted by chemical elements in certain screen conditions. At the time of writing, more crystals are being grown in an attempt to obtain higher resolution data for the PfRH5ΔNL/R5.004/R5.016 complex; additionally attempts to grow crystals of

PfRH5ΔNL/R5.011/R5.004 and PfRH5ΔNL/R5.011/R5.008 are currently ongoing. SAXS data were also gathered this summer at the European Synchrotron Radiation Facility (ESRF, Grenoble, France) for PfRH5 apo, PfRH5-R5.001, PfRH5-R5.004, PfRH5-R5.007, PfRH5-R5008, PfRH5-R5.010, PfRH5-R5.015 and PfRH5-R5.016. SAXS provides low-resolution information (10-30Å) about the general shape and size of a protein or protein complex in solution. These datasets have not been processed yet but could serve to complement low-resolution information from crystals once that route has been exhausted.

5.7.4 Alternative epitope mapping strategies

Determining the binding interface in protein-protein interactions can be highly informative and as such, many techniques for epitope mapping exist. Many were considered but ultimately not attempted for this work due to a variety of reasons:

NMR spectroscopy is a popular technique for structurally characterising proteins in solution under strong magnetic fields. NMR spectroscopy experiments rely on measuring the activity of NMR-active atomic nuclei under high-frequency magnetic fields. This activity is sensitive to local chemical environments, providing information on the location of NMR nuclei within a molecule. NMR requires the use of isotope-labelled atoms which typically limits the expression host to bacteria, although mammalian cell[278] and insect cell[279] labelling has been described. PfRH5 expresses without too much difficulty in both systems[126,139]. However the size and complexity of PfRH5-Fab complexes precludes it from all but the most cutting-edge NMR techniques. Large proteins (>30kDa) tumble slowly in solution leading to fast signal decay and high signal-to-noise ratios, and the high complexity of large proteins creates a huge number of signals which leads to peak overlap even in 2-dimensional NMR techniques. In the past 15 years or so, advances have been made to accommodate larger proteins in NMR,

notably with the refinement of 3- and 4-dimentional NMR with multiple isotope labelling in conjunction with advanced TROSY NMR spectroscopy[280] methods, among others. Still, high molecular weight NMR spectroscopy techniques are not widely used and require a lot of time, specialist equipment (≥900kHz magnet) and even more specialist expertise to solve even one structure in atomic detail.

Alanine scanning is an attractive method consisting of the precise and high-throughput detection of changes in binding in response to sequential mutation to alanine at all amino acid positions on a protein. Alanine scanning requires the protein be amenable to high-throughput, reliable expression even with potentially sensitive amino acid side chains being replaced by a methyl group. Although PfRH5 has been expressed in various constructs in several expression hosts, it is still a sensitive protein and difficult to express as full-length protein outside of *Drosophila* S2 cells, which are not optimised for small-volume culture and transfection. Furthermore, alanine scanning has several inherent drawbacks; it relies on binding to be detectably sensitive to only one amino acid substitution and furthermore, mutations to alanine can result in protein structural changes when replacing a bulky sidechain residue, leading to false positive detection. This method was investigated but eventually deemed prohibitively expensive, with a quote for 50,000$ per 384 mutations.

Single-particle cryo-electron microscopy has become a hot technique over the past few years (in fact the pioneers of this technique were recently awarded the 2017 Nobel prize for chemistry), allowing the determination of solvated protein at sub-8Å resolution without the requirement of growing crystals. Conceptually, this technique is simple: protein solution is flash-frozen at cryogenic temperatures and subjected to transmission EM electron bombardment resulting in thousands of single-molecule images which can be merged and averaged to yield high-resolution structures, provided adequate sample preparation and computational capacity. Increased radiation damage and weak electron scattering due to low-

density cross sections in smaller proteins are the major factors limiting the application of this technique to smaller proteins[281] (although rare exceptions exist[282]). PfRH5-Fab complexes lie at the very limit at which this technique is useful, with resulting data, if any, very likely to be both hard-fought and low-resolution.

5.7.5 Assessing the potency of PfRH5ΔNL vaccine-induced antibodies

Unfortunately, in this experiment, the EC_{50} values of total IgG as well as PfRH5-specific antibody were higher to that of two previously-conducted rabbit studies with PfRH5 in this lab[125,140] delivered by viral vectors, but in the same range as other previous results where rabbits were immunised with recombinant PfRH5 protein and viral vectors in a separate study[139]. Still, the purpose of this experiment was to compare PfRH5FL and PfRH5ΔNL as fairly as possible to determine a) whether all the neutralising epitopes are indeed contained in PfRH5ΔNL and b) whether the disordered regions removed for crystal studies played any role in immune interference or diversion and both of these questions were answered. PfRH5ΔNL vaccination did seem to reduce the variability and was slightly more immunogenic and therefore can be tentatively viewed as an "improved" immunogen although these differences may well disappear in larger sample sizes. Even if these differences are real, the improvements are not substantial enough to warrant further investigation and development. More rational avenues must be explored on the vaccine front to increase the immune response quality in response to PfRH5 vaccination.

Vaccination, even with a single protein typically leads to the appearance of multiple activated B cell clones in the blood. The mechanism leading to the generation of antibodies in the polyclonal response begins with a BCR binding an antigen, a process decidedly independent of other BCR binding events, with ample opportunity to lead not only to many very different

clones but also many similar clones. The interplay between the different functions mediated by different mAbs binding as well as their ability to bind simultaneously or indeed not, has the capacity to lead to effects not seen at the monoclonal level. A first attempt at investigating polyclonal-specific effects is carried out in Chapter VI.

5.8 Appendices

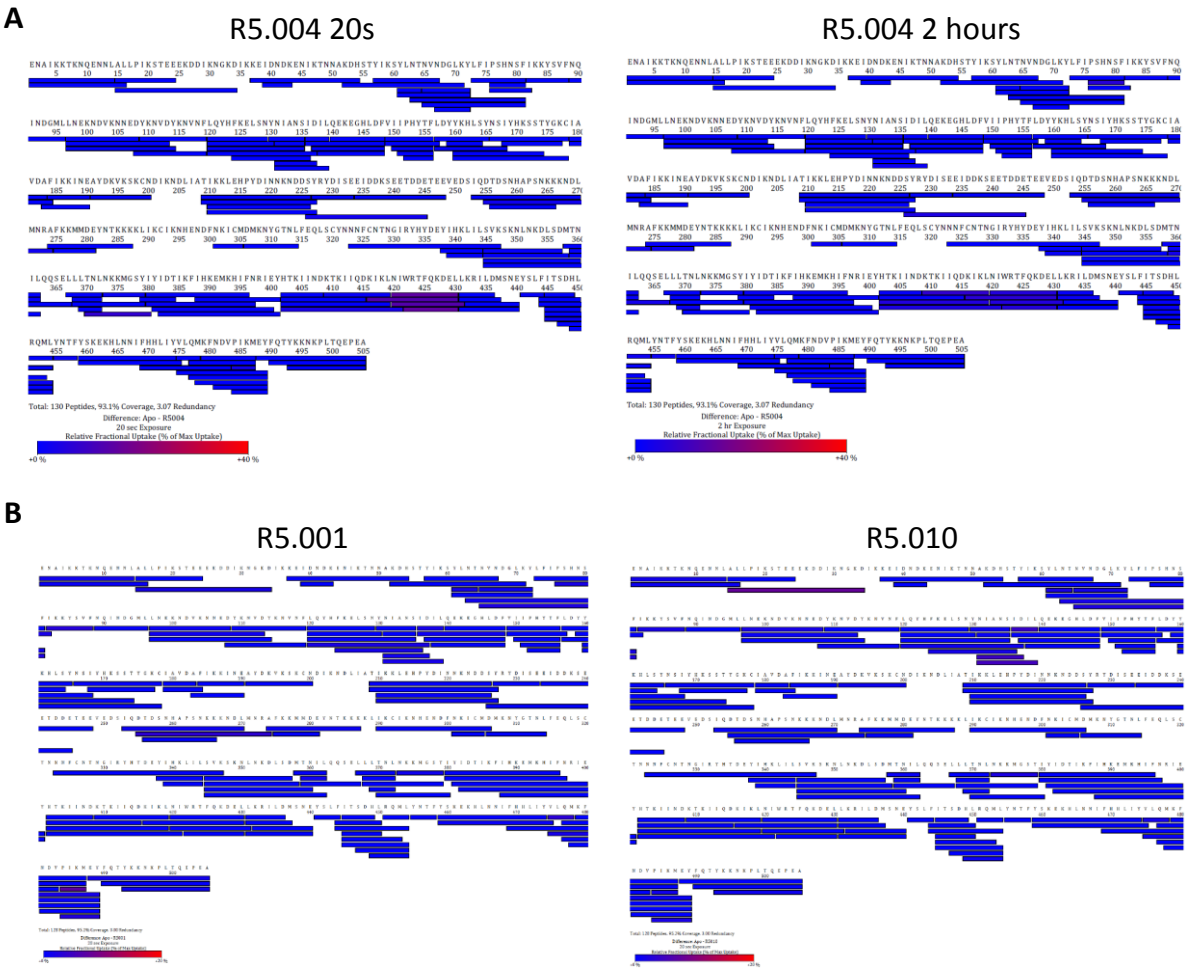

Appendix 5.1: Supplementary HDX-MS data. (A) R5.004 protection all but disappears in longer measurements, likely due to incomplete shielding of the protein backbone, likely reflecting the binding of an unstructured region. (B) No peptides were reliably protected by either R5.001 or R5.010 (20s time point shown here) although a weak hint of protection in some overlapping peptides is visible in the region of N156-I163 for R5.010.

Chapter VI: Functional interactions between PfRH5 mAbs

6.1 Authorship statement

As mentioned in earlier chapters, GIA assays are carried out by a dedicated research assistant at the Jenner Institute. Dr. Doris Quinkert carried out all assays below. Experimental design, sample preparation and data analysis, interpretation and presentation were done by me.

6.2 Introduction

In vitro studies in Chapter V measured binding interdependencies between the mAbs. In many instances mAbs which competed for PfRH5 binding were functionally similar (similar neutralisation phenotype). There were, however, a few instances in which mAbs competed for binding yet had significantly different neutralisation phenotypes. Namely, the R5.008/R5.010 pair and the R5.016/R5.001 pair fitted this description. I sought to investigate whether *in vitro* binding inhibition translated to functional interference of growth inhibition. In doing so, I inadvertently discovered signs of cooperativity between mAbs binding PfRH5 leading to synergistic combinations. Polyclonal antibody raised by vaccination is composed of multiple different mAb clones; however their combined activity is not necessarily the sum of their individual actions. Antibodies, like any drug, have the potential to interact functionally through various means. An initial investigation into signs of synergy or

antagonism within this panel of seventeen mAbs is carried out here, generating information crucial for judging the importance of PfRH5 epitopes with respect to vaccine design.

6.3 Synergy, antagonism and cooperativity

6.3.1 Definitions

- Synergy can loosely be defined as the combined effect of two or more drugs which is greater than could be predicted, *a priori*, from their individual effects alone.

- The same definition applies to functional antagonism when the combined effects are smaller than could be predicted, *a priori*, from individual drug effects alone. In this chapter, "antagonism" will specifically refer to the effect produced by a molecule fitting the pharmacological definition of an antagonist:
  "In pharmacology, antagonists have affinity but no efficacy for their cognate receptors, and binding will disrupt the interaction and inhibit the function of an agonist at receptors".

- Cooperativity (which can be positive or negative) will refer to the concept of synergy and antagonism which arises from a combination of agents targeting the same protein. A more formal definition of cooperativity is: "Cooperativity is the interaction process by which binding of a ligand to one site on a macromolecule (enzyme, receptor, etc) influences binding at a second site." Cooperativity requires a minimum of three components, at least one of which must be multivalent. I will use the term "anti-cooperativity" to describe effects which lead to the loss of cooperativity without leading to true antagonism.

- Additivity occurs when the combined effect of the drugs can be predicted, *a priori*, from their individual effects alone. Defining the predicted effect of combinations of drugs above which "synergy" takes place is typically done using three different but equally valid models, those of Gaddum, Bliss and Loewe. Gaddum's non interaction or "highest single agent" (HSA) is the least complicated model of "additivity" where the highest effect at a given concentration of either of the drugs is the baseline above or below which synergy and antagonism are defined. Intuitively, this definition of synergy states simply that a combination is synergistic if that combination exceeds the effect of the most effective single drug alone used in the combination. Two drugs are synergistic according to Gaddum if Equation 6.1 is satisfied.

$$\mathbf{Effect}_{\mathbf{P+Q}} > \mathbf{max}\left(\mathbf{Effect}_{\mathbf{P}}, \mathbf{Effect}_{\mathbf{Q}}\right)$$

Equation 6.1: If the effect of a combination of drugs P and Q exceeds that of the most effective drug in the combination, at its concentration used in the combination, then synergy occurs according to Gaddum's definition.

Bliss' definition of independent action (Bliss additivity) arises naturally from the definition of the joint probability of independent events; i.e the probabilities of invasion in the presence of drug P or drug Q alone. In this model, each Bliss additive drug in a combination is acting as if the other drug was not present. The expected effect of a combination of two drugs obeying Bliss additivity is given by Equation 6.2.

$$\mathbf{GIA}_{\mathbf{bliss}} = \mathbf{GIA}_{\mathbf{P}} + \mathbf{GIA}_{\mathbf{Q}}(\mathbf{1} - \mathbf{GIA}_{\mathbf{P}}) = \mathbf{GIA}_{\mathbf{P}} + \mathbf{GIA}_{\mathbf{Q}} - (\mathbf{GIA}_{\mathbf{P}} \times \mathbf{GIA}_{\mathbf{Q}})$$

Equation 6.2: GIA_{bliss} denotes the expected effect of a combination of two additive drugs P and Q whose effects alone are denoted by GIA_P and GIA_Q, respectively. Note that here, GIA is a fraction and not a percentage.

Whilst Bliss additivity yields a point estimate of the effect of a combination, Loewe dose-equivalence (Loewe additivity) accounts for differently shaped dose-response curves between drugs P and Q in its estimate of combination effects. A combination of drugs are additive according to Loewe's definition if they satisfy the equation shown in Equation 6.3.

$$\frac{\mathbf{D_p}}{\mathbf{D_P}} + \frac{\mathbf{D_q}}{\mathbf{D_Q}} = \mathbf{1}$$

Equation 6.3: Two drugs P and Q are said to be Loewe additive if the doses of two drugs P and Q necessary to achieve a certain effect are the same when administered alone or in combination. D_P and D_Q are the doses of drug required to achieve a specific effect (X% inhibition for example) when administered alone and D_p and D_q are the doses of drug necessary to achieve the same effect (X%) when administered in combination.

The Loewe model does not require independent drug actions and even supposes a degree of dependence between the drugs[283–285], making it better-suited to synergy arising from cooperative events, in theory. That said, it is not clear to me whether two drugs which independently inhibit interactions on a nexus protein mediating multiple functions through these interactions, are classed as acting independently. Choosing which model best fits observed data is only straightforward if a certain amount of information relating to the drug-target interaction is known[284] and if "synergy" is adequately defined. The choice of model to describe the effects observed in this chapter is extraneous in this instance because in the following sections, the cooperativity and antagonism described are caused by mAbs which are inert in the GIA assay. This means that any increase or decrease in activity caused by a combination including a non-neutralising mAb should be referred to as true synergy or antagonism under any of these definitions.

6.4 Antagonism between mAbs (immune interference by reduction of neutralisation)

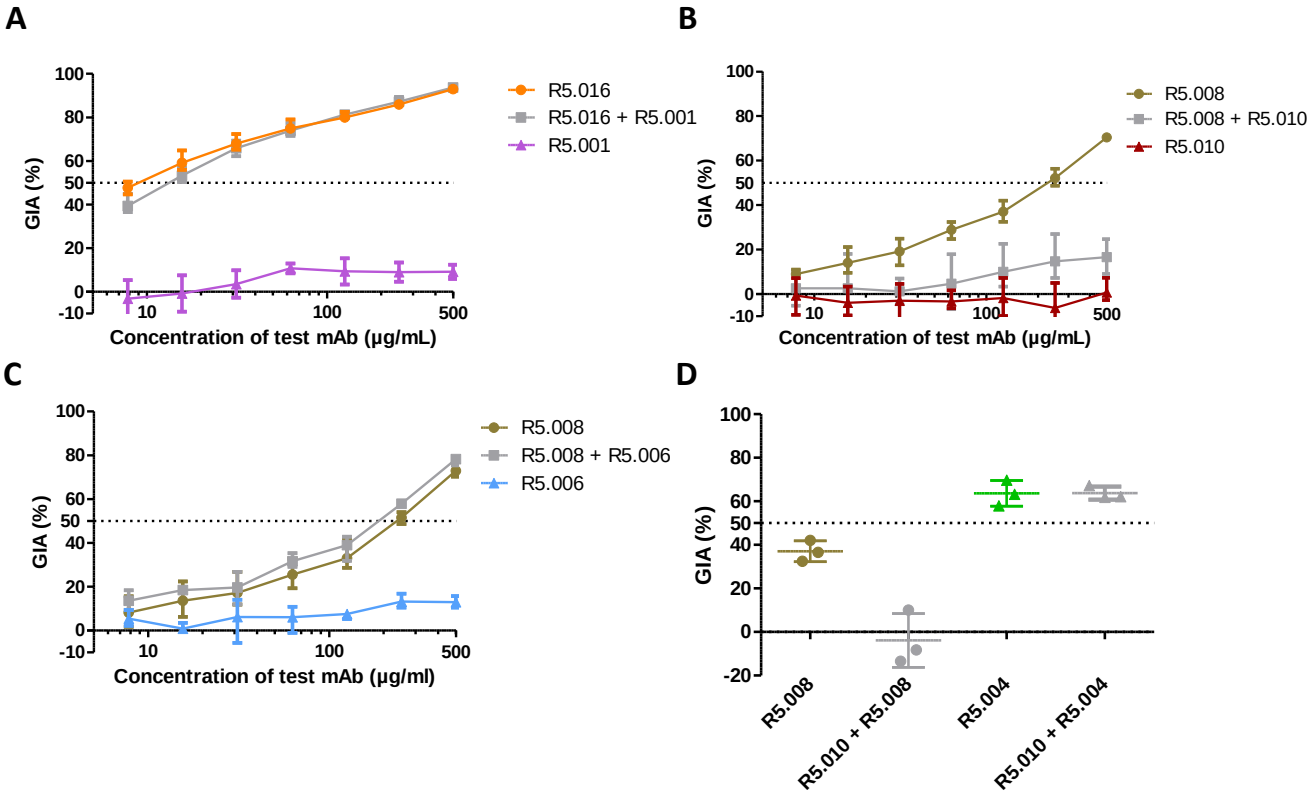

Figure 6.1: Functional interference between mAbs is specific and cannot always be predicted from *in vitro* studies. Panel A shows R5.016 alone, R5.001 alone and a combination of R5.016 and competing antibody R5.001. Panel B shows dilution series of R5.008 alone, R5.010 alone and a combination of R5.008 and competing antibody R5.010. Panel C shows a dilution series of R5.008 alone, R5.006 alone and a combination of R5.008 and non-competing antibody R5.006. In each of these cases, the grey lines represent a dilution series of R5.016 (A) or R5.008 (B and C) in 500µg/mL of R5.001 (A) or R5.010 (B) or R5.006 (C) such that each concentration of growth inhibitory mAb in the grey curves is in the presence of 500µg/mL of non-inhibitory mAb. Panel D shows growth inhibitory antibody R5.008 in the presence and absence of its competing antibody R5.010 and growth inhibitory antibody R5.004 in the presence and absence of non-competing R5.010. The concentration of each mAb is 125µg/mL such that for R5.008 and R5.004 the total concentration of mAb is 125µg/mL and in the R5.008 + R5.010 and R5.004 + R5.010 mixes, the total mAb concentration is 250µg/mL. The dilution curves in panels A, B and C are average of three replicate wells, error bars are SEM. In panel D three replicate wells are represented; data shown are the mean and error bars are standard deviation.

As expected, the GIA of R5.008 is abrogated in the presence of a competing mAb (R5.010, Figure 6.1 B) and is unaffected by the presence of a non-competing mAb (R5.006, Figure 6.1 C). Interestingly, R5.016 was unaffected by the presence of a mAb known to compete for

binding on PfRH5 *in vitro*, with R5.016 performing similarly in an excess of R5.001 as it did alone in terms of growth inhibition (Figure 6.1 A). R5.004 is the most potent of a group of mAbs which all bind a similar area, all of which likely contribute significantly to GIA within anti-PfRH5 pAb. R5.004 and R5.008 are likely to bind a similar area as they protect overlapping peptides by HDX-MS (see Chapter V), both inhibit basigin binding, additionally they show mild competition for binding to PfRH5 (see Chapter IV). Figure 6.1 D shows that R5.004 is unaffected by the presence of an equimolar quantity of R5.010 whereas R5.008 GIA is completely abrogated when mixed with the same ratio of R5.010, indicating that this antagonism is specific to R5.008-like[i] antibodies only and thus R5.010 is by no means a universal antagonist of mAb-mediated growth inhibition, as would have been predicted from *in vitro* studies.

[i] "R5.008-like antibodies" will specifically refer to the set of hypothetical antibodies which bind the exact same epitope with any affinity.

6.5 Cooperativity between mAbs

6.5.1 Positive cooperativity between mAbs

Cooperative effects were observed with combinations of mAbs targeting PfRH5; a surprising and serendipitous phenomenon which arose from testing for antagonism. This was equally surprising because in each case, one of the mAbs in the synergistic mix was functionally inert in the GIA assay. Figure 6.2 A shows that the growth inhibition of a combination of R5.011 and R5.016 is greater than that of R5.016 alone despite R5.011 being essentially unable to inhibit growth even at high concentrations (see Figure 4.1 A in Chapter IV and Figure 6.2 C). To determine whether other mAbs were able to act in this way, R5.014 and R5.010 were also tested on the basis that they belong to the same epitope bin as R5.011 (maroon). R5.014, the most similar mAb to R5.011 (binding profile correlation coefficient 0.99) was also able to synergise with R5.016 whereas another highly similar mAb, R5.010 (binding profile correlation coefficient 0.71) was not. R5.015, a highly-different mAb to R5.011 (binding profile correlation coefficient -0.22) was also unable to synergise, suggesting that a specific R5.011-like interaction must occur to mediate the synergistic effect (Figure 6.2 B). In Figure 6.2 C, a high concentration of R5.011 is present at every concentration of R5.016 in the grey curve, in an effort to determine the maximal synergy observed at different concentrations of R5.016 and therefore different ratios of R5.016/R5.011. Synergy occurs at all concentrations of R5.016 tested here and the maximal increase in growth inhibition occurs at around 30µg/mL of R5.016 where the effect of adding 500µg/mL of non-inhibitory R5.011 is equivalent to increasing the concentration of R5.016 10-fold.

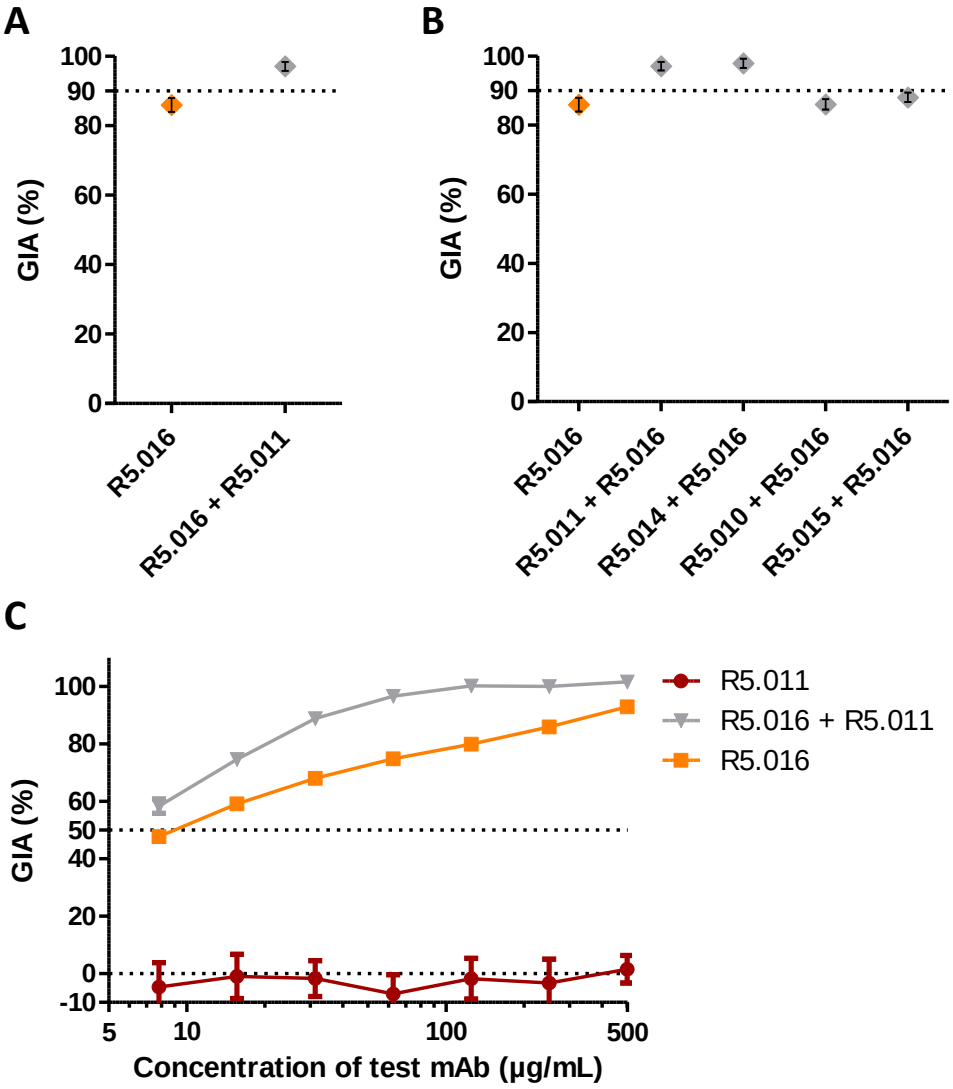

Figure 6.2: R5.011 and R5.014 have a synergistic neutralising effect in combination with R5.016. Panel A shows 150µg/mL of R5.016 alone and 150µg/mL of R5.016 in combination with 150µg/mL of R5.011. Panel B shows 150µg/mL of R5.016 alone or in combination with 150µg/mL of R5.011, R5.014, R5.010 and R5.015. Panel C shows a dilution series of R5.011 alone, a dilution series of R5.016 alone or a dilution series of R5.016 in the presence of 500µg/mL of R5.011. Plotted on the x-axis is the concentration of the test mAb, i.e the concentration of R5.011 in the maroon data, the concentration of R5.016 in the orange data and the concentration of R5.016 in the grey data. In the grey data R5.016 is the test mAb and R5.011 is the influencing mAb. At every concentration of R5.016 in the grey data, there is 500µg/mL of R5.011. Data shown is the mean of 3 replicate wells, error bars are standard deviation.

6.5.2 R5.011-mediated cooperativity applies to all neutralising mAbs but not non-neutralising mAbs

R5.011-mediated synergy applies to all mAbs with neutralising capabilities; however R5.011 does not confer neutralising capabilities to non-neutralising mAbs (Figure 6.3). This provides

an early suggestion that the addition of R5.011 is not qualitatively changing growth inhibition, and that it is simply increasing the occupancy of the neutralising mAbs. The growth inhibition in the presence of a 1:1 ratio of R5.011 at 150µg/mL of R5.007, R5.018, R5.013, R5.008 and R5.019 was increased by 40-50%. The other mAbs see smaller increases in absolute % GIA because the GIA of the combination reaches ≈ 100%. These mAbs are known to bind disparate epitopes, yet they are affected to similar degrees. This means that one epitope is unlikely to be preferentially over-exposed as compared to another due to the presence of R5.011 by the displacement of another (unknown) protein binding to PfRH5, for instance.

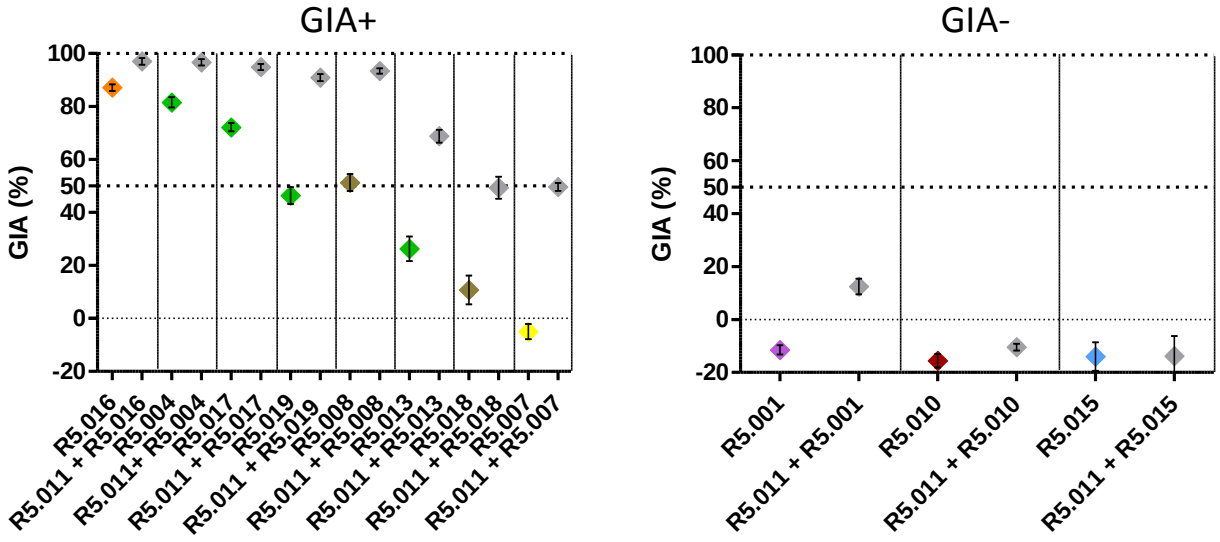

Figure 6.3: Cooperativity occurs when adding R5.011 with neutralising mAbs but not non-neutralising mAbs. Data points are coloured according to their epitope bin (see Chapter V), all combinations are in grey. Plotted on the left-hand graph are all human neutralising mAbs (R5.016, R5.004, R5.017, R5.019, R5.008, R5.013, R5.018 and R5.007) alone at a concentration of 150µg/mL or supplemented with 150µg/mL of R5.011. Plotted on the right-hand graph are human non-neutralising mAbs R5.001, R5.010 and R5.015 alone at a concentration of 150µg/mL or supplemented with 150µg/mL of R5.011. All grey data points represent 300µg/mL of total IgG, 150µg/mL of neutralising mAb and 150µg/mL of R5.011. Data shown are the mean of 3 replicate wells, error bars are standard deviation.

6.5.3 Testing for inhibition of cooperativity (anti-cooperativity) between mAbs

In light of: 1) the data in sections 6.5.1, and 6.5.2 showing enhancement by mAbs R5.011 and R5.014; 2) the data from Chapter V showing that R5.010 competes with R5.011 and R5.014 *in vitro*; and 3) given that all three of these mAbs patently bind PfRH5 on the merozoite due to their functional interactions with neutralising mAbs, I investigated whether R5.010 is able to reverse cooperativity as well as inhibit R5.008 function.

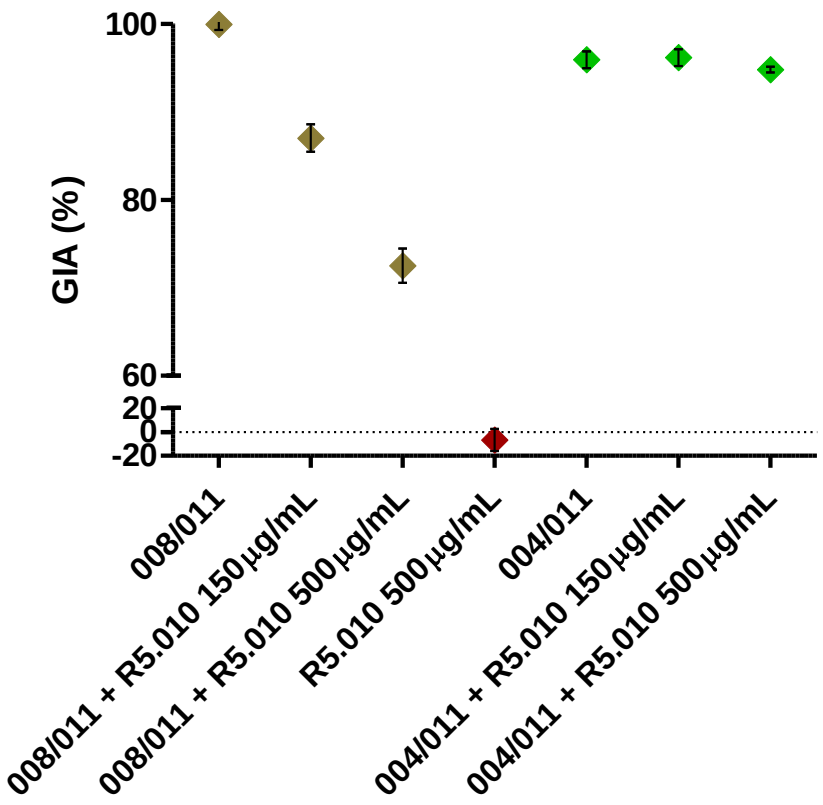

Figure 6.4: R5.010 does not interfere with R5.011 on the merozoite. Olive data points represent 200µg/mL R5.008 and 150µg/mL R5.011 plus the indicated concentration of R5.010 shown in the legend. Green data points represent 70µg/mL R5.004 and 150µg/mL R5.011 plus the indicated concentration of R5.011 shown in the legend. The marron data point represents only 500µg/mL R5.010, as indicated in the legend. "008/011" indicates the presence of R5.008 and R5.011; likewise "004/011" indicates the presence of R5.004 and R5.011. Data points show mean of 3 replicate wells, error bars are standard deviation.

There is a decrease in GIA as R5.010 is added to the R5.008 + R5.011 combination but not when it is added to the R5.004 + R5.011 combination (Figure 6.4), suggesting that the decrease in GIA observed in the R5.008 + R5.010 + R5.011 mix is entirely attributable to R5.010 competing for binding to PfRH5 with R5.008. The lack of R5.004-mediated GIA reversal under R5.011-enhanced conditions indicates that R5.010 and R5.011 are in fact not competing for binding to PfRH5 on the merozoite, despite this being the case *in vitro* (see Chapter V). The efficiency of R5.010 GIA reversal of R5.008 GIA is lessened under R5.011-enhanced conditions. In Figure 6.1 D, an equal quantity of R5.010 was able to entirely reverse the GIA of R5.008. Here, a 3.3-fold excess of R5.010 does not reverse R5.008 GIA entirely.

6.5.4 Cooperativity and antagonism in the polyclonal response to PfRH5

In an attempt to explore the role played by R5.011-like antibodies and R5.010-like antibodies in vaccine-induced polyclonal antibody to PfRH5, increasing concentrations of these mAbs were mixed with a given concentration of PfRH5-immune IgG raised in one of the rabbits (2115) from the immunisation experiment in Chapter V.

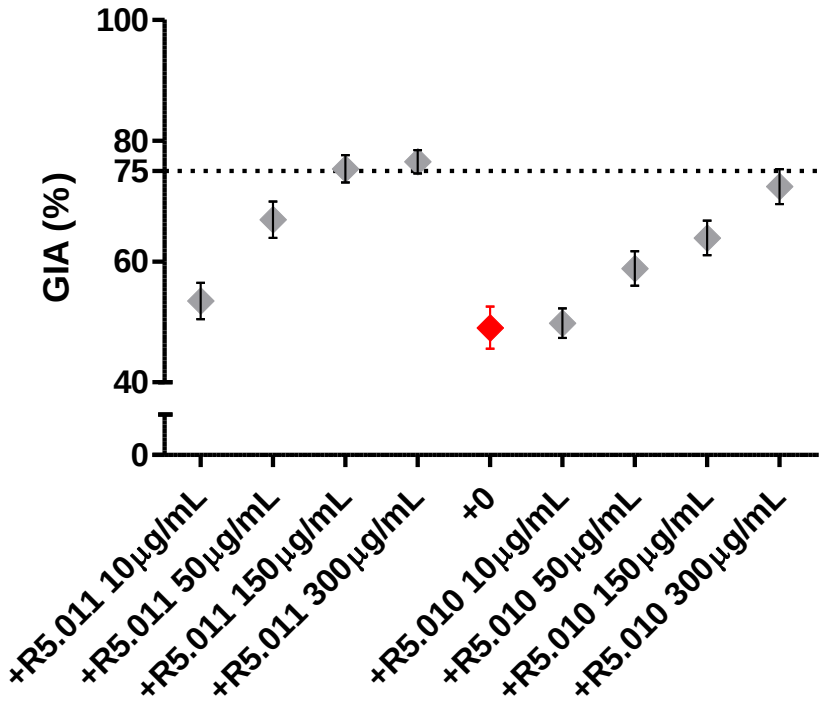

Figure 6.5: R5.011 and R5.010 both increase the potency of PfRH5-immune pAb. Each data point represents 7mg/mL of anti-PfRH5 pAb from rabbit 2115 (see Chapter V) and the x-axis indicates what has been included in addition. The red data point representss just 7mg/mL of PfRH5-immune pAb and all grey data points represent the indicated concentration of R5.010 or R5.011 mAb as well. Data points are the mean of 3 replicate wells, error bars are standard deviation.

The inclusion of increasing concentrations of R5.011 increases the potency of anti-PfRH5 pAb up to a value X, with 150µg/mL<X<300µg/mL. Interestingly, increasing concentrations of R5.010 also increased the potency of PfRH5-immune pAb (clearly less efficiently than R5.011, however) indicating a qualitative difference in the action of R5.010 in combination with mAb compared to its action in pAb (Figure 6.5).

6.6 Investigating the mechanisms of cooperativity

6.6.1 R5.011 potentiates the effect of neutralising mAb in a combination but it does not gain neutralising capacity *per se*

When R5.004 or R5.016 are kept at different constant concentrations, the addition of increasing concentrations of R5.011 in each case only enhances growth inhibition up to a concentration of ≈ 200µg/mL (Figure 6.6). Firstly, this shows that the maximal R5.011-mediated synergy occurs from ≈ 200µg/mL upwards meaning irrespective of the neutralising mAb/R5.011 ratio, introducing concentrations of R5.011 above 200µg/mL is of no benefit. Secondly, the fact that the maximal amount of R5.011-mediated enhancement is dependent only on the concentration of R5.011 (and not on the concentration of neutralising mAb), suggests that R5.011 is indeed potentiating the neutralising effect of R5.004/R5.016 rather than the converse (R5.004/R5.016 allowing R5.011 to have an effect which is not permitted in their absence). These data confirm the data in pAb from Figure 6.5 showing that 150µg/mL<X<300µg/mL of R5.011 did not further enhance growth inhibition.

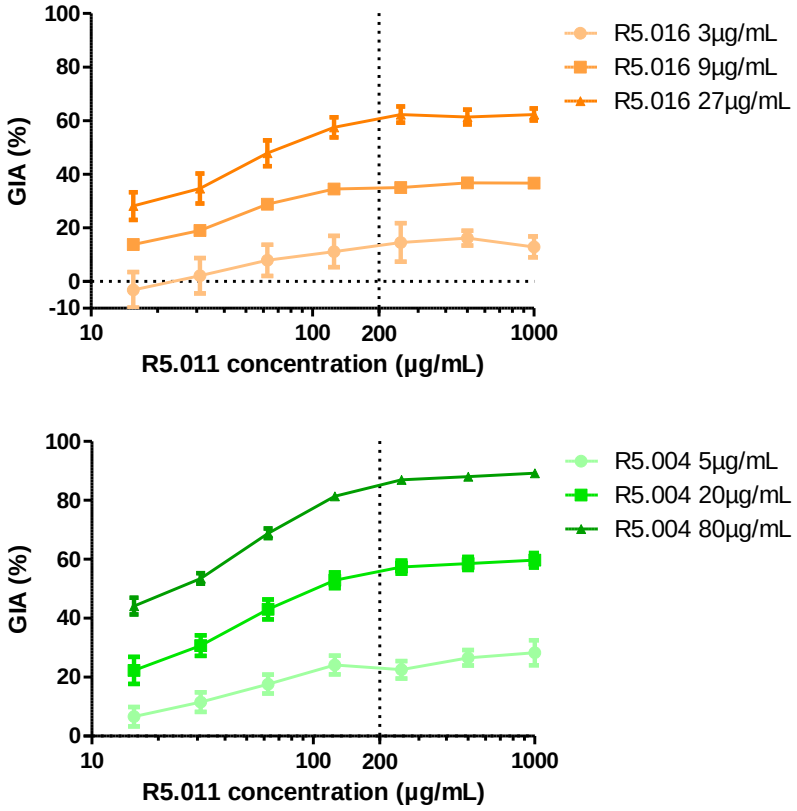

Figure 6.6: R5.011 does not substitute neutralising mAb within a combination; it potentiates the effect of neutralising mAb and not the converse. Three different concentrations of R5.016 (top) and R5.004 (bottom) were used and R5.011 was titrated into the assay. At every point in any given curve is a constant concentration of neutralising mAb (R5.004 or R5.016). Data shown are the mean of 3 replicate wells, error bars are standard deviation.

6.6.2 R5.011 does not require bivalency to carry out its cooperative function

R5.011 Fab is cooperative to the same degree as the intact bivalent mAb (Figure 6.7, Appendix 6.1 A). This result confirms that R5.011 enhancement is not related to the bivalent properties of IgG such as crosslinking PfRH5 or Fc-mediated properties such as C1q recruitment. This also shows that the increased steric volume of a whole 150kDa mAb relative to a 50kDa Fab is not beneficial for the mechanism of cooperativity here. The enhancement of R5.008 by R5.011 is striking; the GIA of a combination containing 80µg/mL of R5.008 and 80µg/mL of R5.011 is equivalent to that of 500µg/mL of R5.008 alone (equivalent to a 6-7 fold increase in R5.008 concentration or equivalent to 3-fold decrease in

total mAb concentration for the same GIA). The difference in potency between R5.011 + R5.008 and R5.011Fab + R5.008 is precisely two-fold (see Appendix 6.1 A). This offers precious extra information; namely that R5.011 mAb binds monovalently. The reason R5.011 mAb is equivalent to an exact two-fold decrease in GIA relative to R5.011 Fab is because IgG has a valency of two. Monovalently-bound R5.011 is removing the second Fab arm "from solution" and restricting it from binding a second site whereas free Fab is allowed to bind independently, leading to a two-fold increase in free concentration of R5.008 binding site.

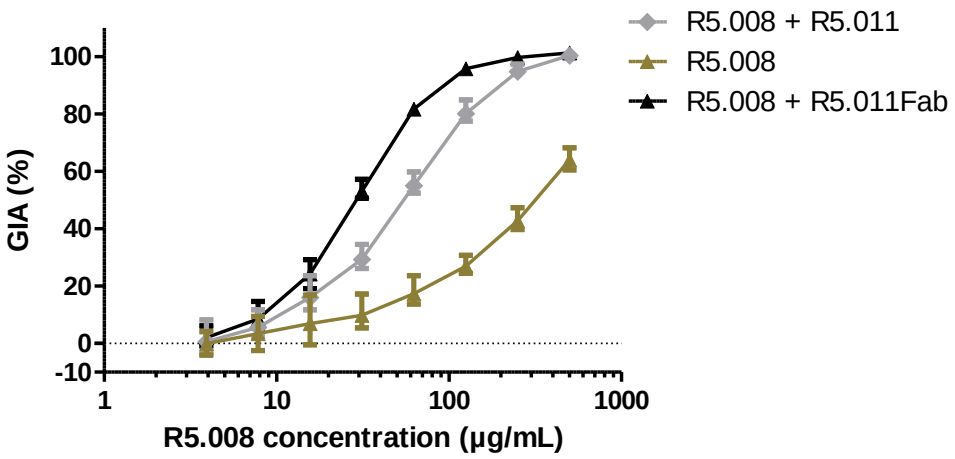

Figure 6.7: R5.011-enhancement of growth inhibition does not require bivalency. The molar concentration of binding sites is the same between Fab and mAb. Strictly-speaking the concentration of Fab plotted is 2/3 multiplied by the value on the x-axis (because the MW of a Fab is 50kDa and the MW of a mAb is 150kDa). All combinations are diluted as equimolar mixes in terms of binding sites (for example at x=500µg/mL, the R5.008+R5.011Fab curve contains 500ug/mL of R5.008 + 333.3µg/mL of R5.011 and R5.008+R5.011 contains 500µg/mL of R5.008 and 500µg/mL of R5.011). Data shown are the mean of 3 replicate wells, error bars are standard deviation.

6.6.3 Fab-mediated neutralisation is different from its parental neutralising mAb

Understanding the mechanism of cooperativity will require a basic understanding of antibody-mediated neutralisation under non-cooperative conditions. Little is known about the state of the PfRH5 invasion complex during invasion or the sequence of events that leads to invasion. PfRH5 neutralisation by mAb blocking basigin binding is conceptually simple, but bivalency of IgG leads to potentially complex binding events. To study this, GIA assays were carried out with Fab and parental mAb. These data show that mAb is a better neutraliser than Fab at low concentrations, a situation which is reversed at higher concentrations (Figure 6.8 A). The same pattern is observed with R5.008 and R5.016 mAb and Fab (Appendix 6.2). My interpretation relies on PfRH5 coming together as a dimer at a susceptible point in the invasion process. Hints of PfRH5 multimerising on the merozoite surface have been suggested by others[130,135], although with poor experimental evidence. According to the proposed model in Figure 6.8 B, mAb neutralisation alone is leading to a degree of self-inhibition, tentatively estimated at 50% as a way of showing that when the left-hand Fab of an IgG molecule is bound there is 0% inhibition of another IgG binding the second PfRH5 in the dimer but when the right-hand Fab is bound, another mAb is 100% prevented from binding the second PfRH5 in the dimer. This would average out to 50% in large numbers of complexes and begin to explain why the R5.004 mAb dilution series has such a shallow slope compared to Fab. When a mAb is bound to the dimer, the bound site is 100% occluded from basigin binding; however, a further proportion of basigin (arbitrarily 30% in Figure 6.8 B) is also prevented from binding to the second PfRH5 in the dimer when whole mAb is bound, due to its steric bulk. This accounts for mAb being more potent than Fab at low concentrations. When Fab is used in a GIA, the situations is much simpler; each bound Fab is 100% occluding basigin binding to that site and 0% at the second site on the other PfRH5 in the dimer; thus equally bound Fab on one half of the dimer does not impede binding of

another Fab to the second PfRH5 in the dimer. This explains why the Fab dose-response curve takes the shape of a classic sigmoid curve when Fab is used and why high concentrations of Fab lead to higher total PfRH5 occupancy (GIA) than mAb (because there is no self-inhibition of binding on the dimer).

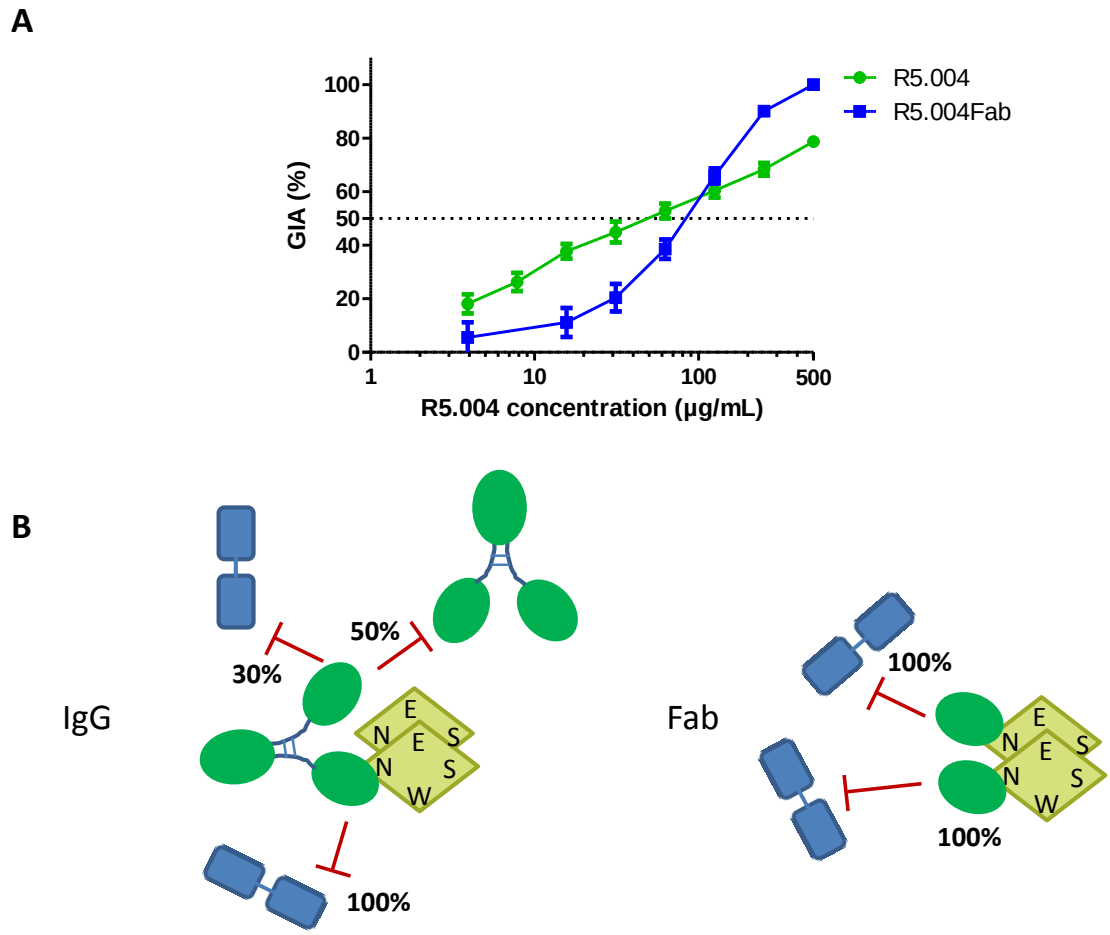

Figure 6.8: Fab neutralisation is fundamentally different from that of parental mAb. Panel A shows the GIA of a dilution series of R5.004 (green) and R5.004 Fab (blue) over a concentration range of 3.9 to 500µg/mL. The concentration of Fab plotted here is adjusted to reflect the number of binding sites in the equivalent concentration of mAb shown on the x-axis. The molar concentration of binding sites is the same between Fab and mAb. Strictly-speaking the concentration of Fab plotted is 2/3 multiplied by the value on the x-axis (because MWFab ≈ 50kDa and MWmAb ≈ 150kDa). Panel B shows a proposed model which fits the data in panel A. The green ovals connected by blue lines are R5.004 mAb, the blue dimers are basigin and the yellow diamonds represent PfRH5. The letters N, E, S and W are abbreviations for the cardinal points as a way of orienting the PfRH5 dimer. Red lines with percentages show an estimate of inhibition. In A, data shown are the mean of 3 replicate wells, error bars are standard deviation.

6.6.4 The neutralisation phenotype of R5.004/R5.008 changes in the presence of R5.011

When R5.011 is included in a mix with R5.004 Fab or mAb, the GIA curve shape becomes identical to R5.004 Fab alone; i.e a "normal" sigmoidal dose-response curve characteristic of a 1:1 binding event. Appendix 6.1 B shows the exact 2-fold discrepancy between the grey and the black curves, meaning that a purely monovalent binding event is happening in the grey data (R5.004 mAb and R5.011 mAb), whereby only one Fab in the IgG is blocking basigin binding and the other is being actively removed from solution *and* not blocking basigin binding. My interpretation is that the mAb self-inhibition of R5.004 mAb is removed when R5.011 is present, as well as the additional steric interference of bound R5.004 mAb with basigin binding to the unbound PfRH5 in the dimer (i.e the 30% basigin blocking and 50% mAb blocking are both lost from Figure 6.8 B). I believe R5.011 is spatially separating PfRH5 molecules and preventing them from dimerising, leading to fractionally slower invasion time due to reduced avidity of the PfRH5-basigin interaction caused by a higher proportion of monomeric PfRH5 interacting with basigin than in the absence of R5.011 (Figure 6.9 B). This model is consistent with all data shown in Figure 6.9 A.

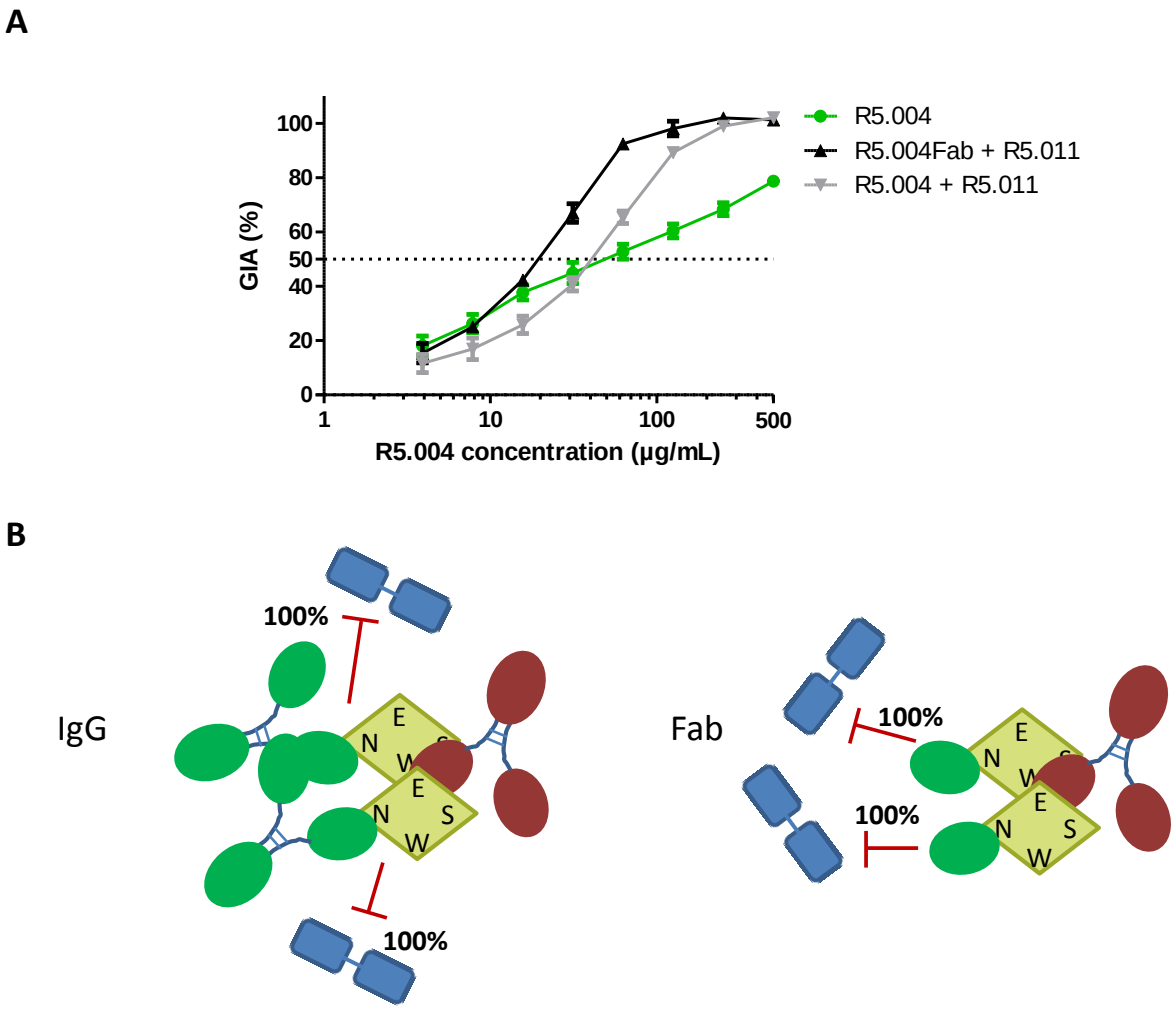

Figure 6.9: Fab neutralisation is qualitatively identical to parental mAb when mixed with R5.011. Panel A shows the GIA of a dilution series of R5.004 mAb (green) over a concentration range of 3.9 to 500µg/mL. The grey and black lines represent R5.004 mAb + R5.011 mAb and R5.004 Fab + R5.011 mAb respectively. Both mixes (grey and black) contain an equimolar quantity of R5.004 binding sites. As before, the concentration of Fab plotted here is adjusted to reflect the number of binding sites in the equivalent concentration of mAb shown on the x-axis. The molar concentration of binding sites is the same between Fab and mAb. Strictly-speaking the concentration of Fab plotted is 2/3 multiplied by the value on the x-axis (because MWFab ≈ 50kDa and MWmAb ≈ 150kDa). Panel B shows a predicted model which fits the data in panel A. The green ovals connected by blue lines are R5.004 mAb, the maroon ovals connected by blue lines are R5.011 mAb, the blue dimers are basigin and the yellow diamonds represent PfRH5. The letters N, E, S and W are abbreviations for the cardinal points as a way of orienting the PfRH5 dimer. Red lines with percentages show an estimate of inhibition. In A, data shown are the mean of 3 replicate wells, error bars are standard deviation.

6.7 Discussion

In the current work, mAbs with synergistic and antagonistic properties seem to arise under normal circumstances following PfRH5 vaccination and were easily identified in a panel of just seventeen mAbs. R5.016 in the presence of an equal amount of R5.011 reaches 80% invasion inhibition at a neutralising antibody concentration 10-fold lower than R5.016 alone and at a total antibody concentration 5-fold lower than R5.016 alone (EC_{80}(R5.016+R5.011) = 100µg/mL (of which 50µg/mL is R5.016); EC_{80}(R5.016) = 500µg/mL). This occurs despite there being no difference in EC_{50} between R5.016 alone or in combination with R5.011 (Figure 6.10), raising questions about how the potency of mAb invasion inhibition should be reported. These mAbs, despite possessing no neutralising activity by themselves, are likely to play an important role in skewing the overall effect of complex pools of polyclonal antibody. The mechanism(s) by which the reported cooperativity occurs is clearly complex.

6.7.1 Antagonism

Immune interference in the form of antagonism between antibodies binding the same merozoite protein has been described previously in the field of blood-stage malaria vaccines with antibodies specific for PfMSP-1. Indeed a set of mAbs have been shown to negatively interfere with a class of neutralising mAbs which prevent PfMSP-1 processing from PfMSP-1_{42} to PfMSP-1_{19} and PfMSP-1_{33}[115]. These antibodies are known to be elicited both by recombinant PfMSP-1 protein vaccination and in response to natural infection[115,286].

Fortunately the association rates within competing mAb pairs were very similar (1.02E6 vs. 1.14E6 for R5.001 and R5.016 respectively and 7.22E5 vs. 7.83E5 for R5.008 and R5.010 respectively, see Chapter III), making equimolar mixes of these mAbs “fair” comparisons.

The mechanism of antagonism between the R5.008/R5.010 competition pair is readily explained by the fact that they are unable to bind simultaneously *in vitro* (Chapter V) and therefore the obvious explanation is that these mAbs are unable to bind concurrently due to epitope overlap or other steric clashes. It is my understanding that the affinity of an antibody for its target is weakly dependent on the nature of the target epitope, and thus the affinities of the mAbs in this panel have little bearing on the affinity of mAbs that *could* be raised to the same epitope. In spite of this, the functional contribution of R5.008-like antibodies to growth inhibition is still likely to be low as other basigin-blocking antibodies are able to bind simultaneously. R5.016 was unaffected by the presence of R5.001 even in large molar excesses, despite competing for PfRH5 binding *in vitro* and having similar association-rate constants. It is my assumption that R5.001 is incapable (or very poorly able) to bind PfRH5 on the parasite in the context of invasion due to its epitope being spatially occluded by other members of the PfRH5 invasion complex or rendered inaccessible when PfRH5 is in the proximity of a plasma membrane rather than in solution. This would explain its inability to inhibit invasion on its own and likewise its inability to interfere with growth inhibition caused by R5.016. Given that the R5.016 epitope is available for binding, I am confident that the R5.001 binding site is distinct and that *in vitro* competition is attributable to steric effects from the non-bound Fab components of the antibodies. It is also possible that R5.016 and R5.001 bind an overlapping epitope with different angles of incidence, leading to different growth inhibition profiles; however the fact that R5.001 and R5.016 segregate to different epitope bins in competitive binding studies (see Chapter V) suggests that the former explanation is more likely.

In light of the evidence for functional synergy mediated by R5.011-like and R5.014-like mAbs, the detrimental function of R5.010 was predicted to be greater than simply inhibiting the action of R5.008-like mAbs in polyclonal anti-PfRH5 antibody, given that R5.010

binding also precludes the binding of R5.014-like and R5.011-like antibodies *in vitro* (see Chapter V). Results in Figures 6.4 and 6.5 show that R5.010 does not preclude R5.011-like antibodies from binding to a merozoite-bound PfRH5 and that in fact, the inclusion of R5.010 in polyclonal vaccine-induced antibody is beneficial. Because R5.010 does not have cooperative properties of its own, my interpretation of Figure 6.5 is that although R5.010 is not anti-cooperative on its own, it is in fact able to inhibit the binding of truly anti-cooperative antibodies which exist in the polyclonal pool. If this interpretation were to be correct, it would point to the growth inhibitory properties of polyclonal vaccine-specific IgG being in a constant state of tug-of-war between cooperativity and immune interference. Supposing truly anti-cooperative sites could be located on PfRH5, an engineered PfRH5 immunogen could be designed to selectively include the minimal binding epitope of neutralising (R5.016-like, R5004-like) and cooperative (R5.011-like, R5.014-like) mAbs whilst carrying mutations to selectively exclude binding of antagonistic (R5.010-like) and anti-cooperative (should they exist).

6.7.2 Cooperativity

In the field of blood-stage immunity, evidence for synergy between anti-merozoite antibodies has been described before, although only among mixes of polyclonal antibodies specific for two or more distinct proteins. Particularly, antibodies to PfRH5 and PfCyRPA[133], antibodies to PfRH5 and PfRH4[140], antibodies to PfRAMA and PfRH5/PfCyRPA[287], antibodies to PfRH5 and PfRAMA/PfMSRP5[287] and antibodies to the trio of PfRH2, PfAARP and a fragment of PfEBA-175[288] have been previously described as being synergistic combinations. The basis for the synergy observed in these cases is unknown. Whatever the mechanism, it is surely different from the cooperativity described here as two or more proteins (possibly)

involved in different stages of the invasion process were subject to *neutralising* antibody targeting in the examples cited above.

The contribution of cooperativity in vaccine-induced polyclonal antibody

The cooperativity between PfRH5 mAbs could begin to explain the disconnect observed between the median potency of PfRH5-specific mAb (median $EC_{50} \approx 500\mu g/mL$ in the work here, assuming this panel is representative of vaccine-induced pAb) and PfRH5-specific pAb ($EC_{50} \approx$ 8-10μg/mL, see Payne *et al.*[171]). It is of course possible that PfRH5-specific pAb contains rare ultra-potent clones which are contributing significantly to the observed growth inhibition. In my view this is unlikely as it would require these hypothetical clones to access an unknown ultra-susceptible epitope patch not bound by any of the mAbs generated in this work, or previously generated PfRH5-specific mAbs in mice[127,141]. Alternatively, the hypothetical "super-clone" would need to possess an incredibly high association-rate; unlikely, as some of the mAbs described here are already approaching the limits of what is commonly-observed, with little scope for a plausible mechanism of high on-rate B-cell selection *in vivo*[289]. It is my view that cooperativity of the kind described in this chapter explains the increased potency of polyclonal PfRH5 antibody relative to mAb more readily than the presence of ultra-high potency clones. Data from Figure 6.5 tend to agree with this view; increasing the ratio of R5.011-like Ab/total anti-PfRH5 Ab appears to increase antibody potency. This indicates that either:

-Cooperative R5.011-like Ab are not reliably elicited by full-length PfRH5 vaccination (this is unlikely as a panel of seventeen identified two such mAbs in humans).

-The concentration of R5.011-like mAbs naturally-elicited from full-length PfRH5 vaccination is too low to lead to detectable changes in growth inhibition.

-R5.011-like mAbs are reliably elicited at functionally-relevant concentrations however their binding is not allowed due to the action of anti-cooperative mAbs which collectively exist at a concentration which partially or totally negates the effect of R5.011-like mAbs.

R5.010 does not have the same mAb enhancement capabilities as R5.011 and R5.014 as shown by data in Figures 6.1 D and 6.4 yet in polyclonal antibody, R5.010 appears to have a cooperative role (Figure 6.5). My only explanation for this is that R5.010 is somehow, on balance, favouring the action of cooperative mAbs; presumably by competing with the binding of mAbs which are deleterious to cooperativity from the polyclonal pool of clones. This interpretation favours the third option mentioned above and points to a complex interplay between neutralising, inert, cooperative and anti-cooperative mAbs in the pool of antibody clones naturally elicited by vaccination with full-length PfRH5.

The mechanism of anti-PfRH5 mAb cooperativity

Recently, cooperativity between non-neutralising mAbs and neutralising mAbs has been described in HIV[290,291] and Ebola[292] virus as well as *Neisseria meningitidis* neutralisation. Generally, mechanisms of synergy are poorly understood and technically difficult to study. Initially, attempts to determine whether the synergy observed in this chapter is related in mechanism to mAb synergy previously described in the literature were explored.

- A major factor of *N. meningitidis* virulence is the activity of Factor H binding protein (fHbp). The cooperativity between some mAbs directed to fHbp in the presence of complement[293] is well understood in this instance[294]. If mAbs are able to bind simultaneously in such an orientation that their Fc portions are able to be simultaneously bound by the classical complement pathway activator C1q, then cooperativity is observed due to CDC. Indeed C1q is essentially unable to bind a

single IgG Fc ($K_D \approx 100\mu M$) but this binding is increased up to 10,000-fold in the presence of multiple Fc portions in close proximity[295]. The synergy described in this chapter is unlikely to be due to complement activation because the GIA assay only contains 10% human serum (≈ 7µg/mL of C1q) which is previously heat-inactivated. It is possible that the full complement cascade need not proceed to MAC formation for growth inhibition as it is conceivable that C1q (a ≈ 410kDa hexamer) binding alone could cause a significant steric effect in the delicate context of PfRH5-basigin binding. The realisation that C1q is indeed heat-labile[296] and that the cooperativity observed here applies even in the context of Fab (Figures 6.7 and 6.9) definitively rules out C1q binding as a mechanism of cooperativity.

- Another conceivable mechanism of cooperativity is R5.011 leading to increased avidity in the context of neutralising mAb binding by artificially crosslinking two PfRH5 molecules. This model was proposed in the 1980s to explain the higher affinity for mixtures of mAb binding to distinct sites on human chorionic gonadotropin compared to the mAbs' affinities alone[297]. Again, this model breaks down in the face of the data in Figures 6.7 and 6.9 showing Fab-mediated cooperativity is equally as potent as mAb cooperativity.
- Models whereby R5.011 is mediating cooperativity or synergy by interfering with a distinct essential process to the neutralising mAbs isolated in this thesis such as PfRIPR or PfCyRPA binding or PfRH5-N-terminus processing are very difficult to reconcile with the fact that R5.011 causes no measurable growth inhibition even at high concentrations (see Chapter IV and Figure 6.2 C).

All data interpretation in this chapter relies on Fab retaining the same monovalent affinity as its parental mAb, a very reasonable assumption given the body of data showing this is often the case[298–301], and on PfRH5 forming dimers or higher order homocomplexes at some point

during invasion. The data supporting this latter assumption are weak but this has been proposed twice before: once because of the complementarity of basigin packing in crystal complexes[130], and again due to the tetrameric assembly of the PfRH5 binding protein PfP113[135]. The cooperativity model proposed here whereby R5.011-like and R5.014-like antibodies delay invasion by decreasing PfRH5 dimerisation, allowing neutralising antibodies to reach higher PfRH5 fractional occupancies on the merozoite is by no means definite. A model whereby R5.011 increases the affinity of neutralising mAb by inducing a conformational change at the single protein level is unlikely. Superficially, this seems implausible as every crystal structure of PfRH5, unbound, bound to basigin and bound to two different mAbs show <1Å RMSD values, consistent with a rigid PfRH5 core; furthermore multiple disparate epitopes (R5.004 and R5.007 epitopes for example) are enhanced by R5.011. However, if R5.011 binding was regulating the state of PfRH5 protein exposure at the population level, this would also fit the data shown in this chapter. Unfortunately, measuring these transient conformational changes and/or small changes in affinity between mAb and PfRH5 would be difficult to determine experimentally. Likewise, proving that R5.011 delays the invasion process is unlikely to be straightforward. Concentrations at which R5.011 begins to have a measurable effect on neutralising mAb GIA (approximately ≥15µg/mL) are already orders of magnitude above the K_D (K_D R5.011 = 1E-11M so 15µg/mL is ≈ 10,000-fold above the K_D) and therefore the occupancy at these concentrations at equilibrium would be >99%. The time to reach equilibrium and therefore >99% occupancy is predicted to require only approximately 22s at 15µg/mL according to the empirically-derived formula for the time taken for mAb-target interactions to reach equilibrium is given in Equation 6.4. As discussed in Chapter IV, antibodies to PfRH5 are unlikely to reach equilibrium before merozoite invasion is complete, especially at modest antibody concentrations, meaning that the relatively moderate difference in GIA caused by the addition

of R5.011 is likely due to a very small increase in PfRH5 exposure time. Because R5.011 does not seem to alter the fraction of successful invasion events (the readout of this being GIA) and because the delay in invasion time is likely to be very small, confirming that R5.011 slows the invasion process will be difficult to verify experimentally using direct methods such as microscopy.

$$T_{eq} \approx \frac{3.5}{(K_{on} \times [mAb]) + K_{off}}$$

Equation 6.4: The time needed to reach equilibrium (T_{eq}) for antibody binding can be roughly approximated by the above formula where K_{on} is the association-rate constant, K_{off} is the dissociation-rate constant and [mAb] is the concentration of mAb. This formula was taken from Björkelund *et al*.[302]

Data in Figure 6.4 show that the ability of R5.010 to reverse R5.008-mediated GIA is decreased when in combination with R5.011. Given that the R5.010 + R5.011 combination has no GIA (Figure 6.3), the explanation for this could be that bound R5.010 competes with two (or more) R5.008 mAbs bound to adjacent PfRH5 molecules, a situation which is lost when R5.011 separates PfRH5 molecules. Alternatively, if R5.011 binding stabilises a conformation which is preferentially bound by R5.008 and not R5.010, the effect of R5.008 (neutralisation) would be more apparent than the effect of R5.010 (antagonism). Without resorting to wild unsupported speculation, I have no answer for this result.

For the sake of clarity, insights into the mechanism of cooperativity were illustrated only with mAb R5.004 in sections 6.6.2, 6.6.3 and 6.6.4. These investigations were extended to R5.008 and R5.016 (Figure 6.10) and were also consistent with the model proposed above. By all accounts, R5.008 in Figure 6.10 A appears to behave very similarly to R5.004, which is consistent with them both binding a similar epitope on PfRH5. There were, however, notable differences between R5.004/R5.008 and R5.016. For instance, in Figure 6.10 B, the grey

curve is identical to R5.016 alone (orange) at low concentrations which is not the case for the black curve (R5.016 Fab + R5.011). This could be interpreted as R5.016 offering a degree of extra basigin blocking by the non-bound Fab portion of mAb compared to R5.004 (arbitrarily 30% in Figure 6.8 B), possibly explaining why R5.016 mAb is more potent than R5.004 mAb in the first instance but also why this extra shielding appears to persist even when R5.011 is acting. It is reassuring that R5.016 cooperativity shows differences to R5.004 cooperativity as they were shown to bind different parts of PfRH5 and lie in different planes when bound (see Chapter V). On the other hand it is not clear that R5.016 is growth inhibitory because of interference with basigin binding to PfRH5 so I am cautious of over-interpreting these GIA data, something I may already be guilty of.

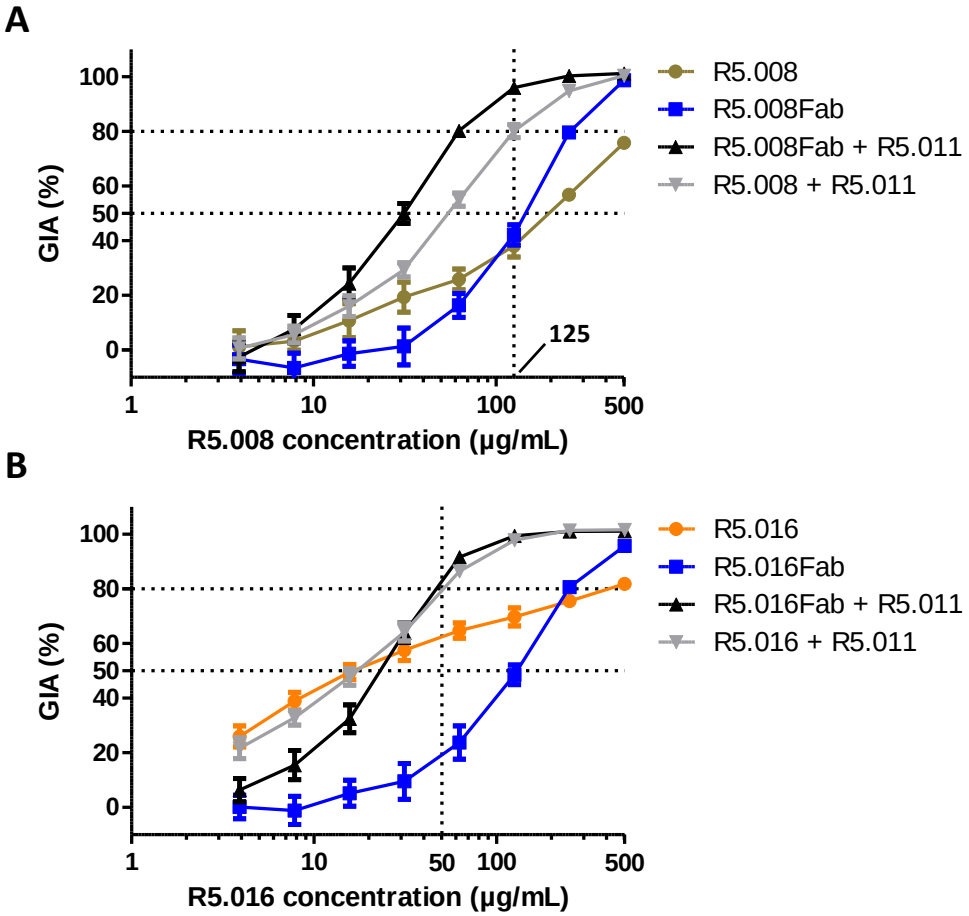

Figure 6.10: The neutralisation patterns of R5.008 and R5.016 by neutralising Fab or mAb or their combination with R5.011 can be explained by the same cooperativity model as described in section 6.6.4. Assay setup and the data presentation is identical to that shown in Figures 6.8 A and 6.9 A. Dotted lines illustrate differences in EC_{50} and EC_{80} between the mAbs and mAb fragment combinations.

The implications of the cooperativity, anti-cooperativity and antagonism between PfRH5 mAbs are likely to be consequential for vaccine design. These data suggest that synergy is a major factor in the potency of polyclonal antibody raised to PfRH5 and therefore the antigen minimisation trend based on keeping only overtly "neutralising" epitopes may be counter-productive. Likewise, the presence of R5.010-like mAbs is seemingly undesirable. More effort must be made to understand the basis of synergy and antagonism and their actual effect in polyclonal antibody if meaningful attempts to engineer a PfRH5-based immunogen are made.

6.8 Appendices

	A			B	
Concentration (µg/mL)	R5.008 mAb + R5.011 mAb	R5.008 mAb + R5.011 Fab		R5.004 mAb + R5.011 mAb GIA	R5.004 Fab + R5.011 mAb
500	100.41	101.38		102.09	101.29
250	94.88	99.78		98.96	102.00
125	80.13	95.86		89.26	98.05
62.5	55.05	81.72		65.39	92.46
31.2	29.35	53.02		40.70	66.92
15.6	16.07	24.27		25.81	42.26
7.8	5.69	8.57		16.94	25.10
3.9	0.61	2.03		11.58	15.36

Appendix 6.1: Two-fold mAb/Fab GIA discrepancies. The two-fold difference in Fab compared to parental mAb offers information on molecular interactions. Data shown are average GIA (of 3 replicates), with cells highlighted proportionally to the values contained within them. Data in A show the grey and black curves in Figure 6.7 and data in B show the grey and black curves in Figure 6.9 A. There is an almost perfect 2-fold concentration discrepancy between the two adjacent columns in A and in B, the reason for which is explained in the main body of text.

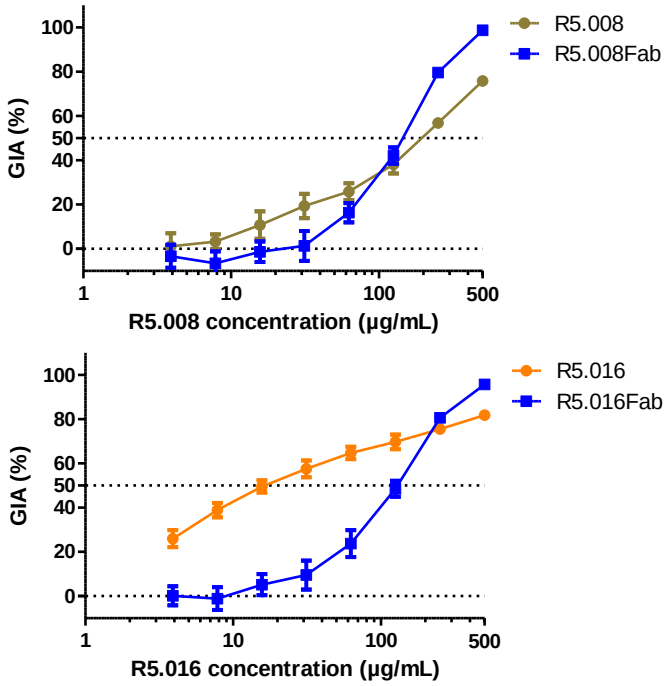

Appendix 6.2: The R5.008/R5.016 Fab/mAb neutralisation patterns reflect what is seen with R5.004. GIA of a dilution series of R5.008 mAb (olive, top graph) and R5.008 Fab (blue, top graph) and R5.016 mAb (orange, bottom graph) and R5.016 Fab (blue, bottom graph) over a concentration range of 3.9 to 500µL/mL. The concentration of Fab plotted here is adjusted to reflect the number of binding sites in the equivalent concentration of mAb shown on the x-axis. The molar concentration of binding sites is the same between Fab and mAb. Strictly-speaking the concentration of Fab plotted is 2/3 multiplied by the value on the x-axis (because MWFab ≈ 50kDa and MWmAb ≈ 150kDa).

Chapter VII: Conclusions and future directions

7.1 Summary of output

The isolation of seventeen human mAbs, here, is to my knowledge the first report of fully-human mAbs specific for PfRH5. Furthermore, these mAbs were elicited in response to a human-compatible vaccine, shedding some light on the immune response raised by full-length PfRH5 vaccination. The work here has made important advances in understanding the nature of an effective antibody response targeting this protein—a necessary first step in designing a new PfRH5-based immunogen likely to elicit a superior immune response to the native, full-length protein.

7.1.1 Establishment of a pipeline for isolating vaccine-induced human mAbs

The establishment of a pipeline for reliably isolating antibody-coding genes from the peripheral B cells of vaccinated individuals became a 6-month exercise in testing different reagents and PCR troubleshooting and optimisation, despite a published protocol being widely available[186]. The introduction of the cheaper and more streamlined CPEC as the method of choice for cloning these genes into expression vectors was worthwhile in my opinion, despite having had to redesign and re-order the whole set of degenerate primers for PCR2.

Since, over a hundred mAbs have been made to different vaccine immunogens such as PfAMA-1, PvDBP and *Zaire Ebolavirus* glycoprotein. Given the utility, versatility and clinical potential of mAbs, this pipeline is likely to remain a key methodology used in many subsequent clinical trials conducted by the Draper group. A more immunogenic vaccine/adjuvant/delivery method as well as a successful antigen-specific plasmablast detection method (all of which the Draper group is currently working on) would see this pipeline become significantly more time-efficient and less onerous.

7.1.2 Information from the panel

A summary of the information resulting from the isolation of seventeen human monoclonal antibodies binding PfRH5 can be found in the bullet points below:

- The work here replicated the potency of the most potent anti-PfRH5 mAbs reported previously with R5.016 which has an EC_{50} in the 10-15µg/mL range; a value which could be close to the limit of what is achievable by a single mAb elicited naturally from vaccination.

- A proportion of PfRH5-reactive mAbs raised in response to human vaccination are not able to inhibit parasite growth appreciably by themselves *in vitro*.

- The antibody response to PfRH5 is cross-strain neutralising at the polyclonal level but not necessarily at the monoclonal level. This thesis showed that antibodies which are reliant on binding to any of the five most frequent amino acid polymorphisms do not

significantly contribute to neutralisation in vaccine-induced pAb, given the ability of pAb to neutralise comparably across strains known to carry these mutations.

- Data in this thesis confirmed and complemented information that was already made available by Douglas *et al.*[127] and Wright *et al.*[130] from a smaller panel of antibodies; namely, that potently-neutralising antibodies access two major epitopes which lie at the top of the PfRH5 diamond. One of these lies at the basigin-binding interface and another on the "north-western" face comprising helices 2 and 3. This work further identified the R5.007 binding site at the bottom of the diamond as a weakly-neutralising epitope (although significantly more potent in combination with R5.011, see sections 4.3.1 and 6.5.2). This epitope had not been previously identified as relevant for neutralisation.

- In humans, the vast majority of the neutralising antibodies are directed to the ordered core of PfRH5 and not the major disordered regions. Despite the PfRH5 being supposedly tethered by its N-terminus and the existence of potent N-terminal mAbs to PfRH5[141], it seems that in pAb raised to full-length PfRH5, these play a minor (see R5.007) role in growth inhibition or do not occur frequently in humans.

- PfCyRPA binds PfRH5 toward the bottom of the "kite" with likely involvement of helix 7 and the 2-3 loop. However, antibodies directed to this zone of PfRH5 are weakly or not inhibitory.

- Cooperativity and antagonism are both features of the polyclonal response to PfRH5 and this might also be the case for many other proteins. These functional effects

operating at the polyclonal level are unlikely to be rare and surely play an important role in influencing the potency of vaccine-induced pAb.

7.2 Future directions

7.2.1 Prospects for PfRH5 as a target for blood-stage immunity

For PfRH5, a second Phase I trial based on full-length PfRH5 delivered in a protein-in-adjuvant formulation (AS01B) is currently underway with significantly improved immunogenicity and comparable antibody quality (personal communications, Draper group). This safety and immunogenicity trial is due to be followed by an efficacy trial in the form of a blood-stage controlled human malaria infection (CHMI). Given the leading status of PfRH5 in the blood-stage malaria vaccine field (with PfRIPR a close second), the outcome of this upcoming clinical trial is likely to have important consequences for the future of blood-stage vaccines. As mentioned several times in this work, arguably the main advantage of blood-stage vaccines over malaria vaccines to other stages of the lifecycle is that they do not require sterile protection to be efficacious; in fact, to an extent, the less efficacious a blood-stage vaccine is, the more it should benefit from infection. In the case of many merozoite antigens, repeated exposure by infection engenders high levels of specific IgG (e.g PfMSP-1, PfAMA-1 or PfEBA-175) which could lead to a boosting effect of vaccine-induced mBC. In the case of a PfRH5, which is poorly immunogenic in the context of natural infection, infection-induced boosting may be negligible. Nevertheless, a further benefit from the concurrent but suboptimal development of NAI (which would apply to a PfRH5-based vaccine) is the development of antibodies acquired to antigens known to synergise with PfRH5 (PfRH4, PfCyRPA, PfAARP, etc) and which could contribute small additional protective effects.

Furthermore, PfRIFINs and PfEMP-1 are both protein families involved in mediating rosetting[45] and vascular adhesion[44]. The acquisition of antibodies to these proteins from natural infection should lead to synergistic effects by reducing rosetting, thus affording more time for vaccine-induced antibody to bind *and* lead to additive effects from reducing the parasite burden by promoting splenic clearance of iRBC. In short, a PfRH5 vaccine need not be highly effective *per se*, just highly protective (against death and severe malaria) to be a successful intervention. The issue with these projected benefits is that there are few opportunities to measure the magnitude of their effect before late-stage clinical trials. *In vitro* assays are not suited to replicate dynamic natural infection in the blood-stage, characterised by the aforementioned rosetting and vascular adhesion; and Phase II trials in malaria-naïve individuals only represent end-point efficacy with no realistic contribution from infection-induced immunity. Without longitudinal vaccine studies, the true extent of these effects will be difficult to assess.

It may be the case that targeting PfRH5 alone will never lead to a truly efficacious vaccine with long-term protection but it is likely to feature in a multi-component, multi-stage vaccine, the only type of vaccine with a realistic chance of long-term protection according to most experts in the field today[303–306]. For this reason, the drive to improve the immune response to PfRH5 is just as urgent.

7.2.2 Modulating cooperativity and antagonism

In some ways the relatively small size of the panel of mAbs was a blessing in disguise. There is a limit to what experiments are tractable with large panels of mAbs. A larger panel of mAbs would have meant discarding or prioritising some mAbs over others earlier in the characterisation process due to superficially similar performances in neutralisation or growth inhibition assays, or epitope binning assays, thus missing out on some important subtleties.

Antagonism

Antagonism has been seen before in antibody responses to the merozoite protein PfMSP-1, as mentioned in section 6.7.1. These antagonistic antibodies pre-exist in populations where malaria transmission is high and are raised by recombinant PfMSP-1 vaccination. Importantly, elucidation of the binding site of neutralising antibodies and antagonistic antibodies permitted the design of mutated PfMSP-1 proteins which preferentially binds neutralising antibodies over antagonistic antibodies[307]. Despite this, there has been so sign of an improved PfMSP-1 vaccine candidate; presumably these failed to have an effect on elicited antibody quality. One explanation for this could be that there are multiple sites of neutralisation on PfMSP-1[308], each of which could have its own contribution to growth inhibition and its own subset of antagonistic antibodies. This means that inhibiting antagonism would have a reduced effect if neutralisation was proceeding via alternate antibody-mediated mechanisms simultaneously and independently.

It is not clear whether PfRH5 will ultimately benefit from immunogen design to limit or ablate antagonistic effects from vaccine-induced antibody. In my opinion, there are more encouraging signs on this front for PfRH5 given that basigin blockade is thought to be the main contributor to growth inhibition and that anti-cooperative mAbs (should they exist and be readily elicited by normal PfRH5 vaccination) are likely to have a highly deleterious effect in polyclonal IgG. The presence of pre-existing antibody targeting merozoite antigens in malaria-endemic populations raises serious questions about blood-stage vaccines in general. Fortunately, PfRH5 is the target of relatively low levels of antibody in natural infection (compared to PfMSP-1, in any case). Furthermore, the target age-group of blood-stage vaccines are young children with lower IgG titers and crucially lower malaria exposure than adults therefore lower merozoite-specific antibody levels, mitigating potential antagonistic effects arising from infection-induced antibody. The problem of vaccine-induced antagonism,

on the other hand, is a major problem which must be addressed at the preclinical immunogen design stage.

Cooperativity

Cooperativity of the kind described in Chapter VI, as far as I am aware, has not been described in malaria proteins before. More experiments are required to determine the importance of cooperative effects within anti-PfRH5 pAb and the extent to which this can be increased by vaccination. However, enhancing PfRH5 cooperativity seems conceptually more worthwhile than enhancing synergy between PfRH5 and PfRH4 IgG[140], for example, because the increase in efficacy is more likely to translate across different strains. PfRH5/PfRH4 synergy is known not to occur against the FVO strain[140], observation that is likely to extend to all strains not normally reliant on PfRH4, such as W2mef[258] and likely many more wild strains.

7.2.1 PfRH5 vaccine design

PfRH5 is immunogenic as a vaccine in humans (Payne *et al.*[171] and Draper group personal communications), giving it hope as a viable vaccine candidate. Antigen minimisation (see Figure 1.8) was the strategy borne in mind at the beginning of this project but immunisation experiment in Chapter V showed that trivial antigen minimisation will not be effective and that there are hurdles to overcome before improving on full-length PfRH5 protein vaccination. Data from Chapter VI showed that simply defining epitopes to which overtly neutralising antibodies bind as "important" is likely to be a suboptimal strategy in designing an improved PfRH5 immunogen. The R5.011 and R5.010 binding sites are of high interest and attempts to crystallise R5.011 and R5.010 with PfRH5ΔNL are ongoing. The

contribution of R5.011-like cooperative antibodies to growth inhibition within polyclonal IgG must be evaluated. If their importance is a great as suggested by the data in this thesis, a thorough investigation into the abundance and effect of anti-cooperative antibodies must be carried out. If cooperativity between neutralising and non-neutralising mAbs features in humoral responses to other pathogen proteins, and there are indications it does[291,292], then the blind antigen minimisation paradigm based on single-epitope scaffolds requires a re-think.

7.2.2 Viral vectored mAb delivery

In recent years the concept of "vectored immuno-prophylaxis" or VIP has been described[309,310]. To-date this approach has primarily utilised an adeno-associated virus (AAV) vector to deliver a mAb or antibody-like immunoadhesins, which are expressed *in situ* from virally-transduced cells following intramuscular immunisation. An attractive approach, the added flexibility of vectored delivery allows vaccinologists to circumvent several limitations of naturally-elicited antibodies which may be undesirable or suboptimal such as size or valency. Furthermore, some protective clones may arise infrequently or in low amounts following conventional vaccination; a particularly relevant application is in HIV where bnAbs can take years to arise[311] because of their complex CDRs necessitating high levels of SHM. Because the genetic material for any antibody can be expressed in situ by AAV, exceptionally tight-binding, affinity-enhanced mAbs could be delivered .Various *in vitro* and *in silico* antibody variable region affinity maturation technologies are now well-established and available for affinity enhancement, with sometimes impressive results[312–314]. Similarly and perhaps more relevantly, techniques relying both on rational design and directed evolution for specifically enhancing the association-rates of antibodies for their target epitopes have also been used to great effect[315,316].

In the case of PfRH5, it may be that Fabs, camelid nanobodies, single-chain variable fragments (ScFvs) or any other small protein construct would show sufficiently reduced antagonism from interfering antibodies to outweigh the loss in half-life conferred by Fc in whole IgG molecules.

Mouse models would suggest that it may be easier to elicit high concentrations of specific clones for long periods of time by AAV delivery rather than in response to a vaccine[317]; whether these high concentrations and impressive longevity can be translated into humans remains to be determined. As things stand it isn't clear that mAb delivery is an efficient way of protecting against the blood-borne form of malaria. A highly-neutralising PfRH5 mAb has been passively transferred in monkeys prior to an *Aotus*-adapted FVO *P. falciparum* challenge (Douglas *et al.*, manuscript in preparation and personal communications). A dose of 33mg/kg was insufficient for protection but 100mg/kg was successful, although serum mAb levels were in the order of hundreds of μg/mL, much higher than can be achieved by vaccination. Setting aside the possibility of escape mutants, it may be that efficient neutralisation by targeting PfRH5 requires cooperativity between different clones of mAb, of the type observed in this thesis. Using vectored delivery, specific combinations of cooperative mAbs could be delivered, with no chance of observing vaccine-induced antagonistic or anti-cooperative antibodies, leading to a theoretically higher potency of response than could be achieved with one mAb.

Currently, I am expressing bispecific, dual variable domain immunoglobulin (DVD-Ig) mAbs with specificity for the R5.016 or R5.004 binding site and the R5.011 binding site in an attempt to exploit cooperative effects with a single molecule. Conceptually, this type of strategy has several advantages: 1) it could be delivered by a single AAV rather than two; 2) it could reduce the scope for escape mutants[318] and 3) efficacy should be increased, particularly at lower concentrations as the binding of one arm of the DVD-Ig would raise the

local concentration of the second arm, hopefully leading to increased occupancy compared to two independent binding events by separate mAbs.

7.3 Final remarks

Thousands of years of co-evolution have led the *P. falciparum* merozoite to exquisite adaptation to its host, and, as a result, has become an exceptionally difficult beast to tame. Vaccinology has largely built its success on empirical methods and heuristics. Tackling the most difficult pathogens such as HIV, malaria and tuberculosis will require a thorough understanding of pathogenic biological processes, innovative approaches and 21st century techniques. With a resounding lack of highly-susceptible merozoite targets on the horizon, investigations such as these, aiming to enhance the potency of response to existing targets will become increasingly important to the future of malaria vaccinology. I am hopeful that some of the information generated in this thesis can be built on and used to target PfRH5 with greater effect.

References

1. Sandin, S., Öfverstedt, L. G., Wikström, A. C., Wrange, Ö. & Skoglund, U. Structure and flexibility of individual immunoglobulin G molecules in solution. *Structure* **12,** 409–415 (2004).

2. Roux, K. H., Strelets, L. & Michaelsen, T. E. Flexibility of human IgG subclasses. *J Immunol* **159,** 3372–3382 (1997).

3. Chudasama, V., Maruani, A. & Caddick, S. Recent advances in the construction of antibody-drug conjugates. *Nat. Chem.* **8,** 114–9 (2016).

4. Tonegawa, S. Somatic generation of antibody diversity. *Nature* **302,** 575–581 (1983).

5. Elhanati, Y. *et al.* Inferring processes underlying B-cell repertoire diversity. *Philos. Trans. R. Soc. Lond. B. Biol. Sci.* **370,** 15115 (2015).

6. Pieper, K., Grimbacher, B. & Eibel, H. B-cell biology and development. *J. Allergy Clin. Immunol.* **131,** 959–971 (2013).

7. Sutherland, C. J. *et al.* Two Nonrecombining Sympatric Forms of the Human Malaria Parasite Plasmodium ovale Occur Globally. *J. Infect. Dis.* **201,** 1544–1550 (2010).

8. Sachs, J. D. & Malaney, P. The economic and social burden of malaria. *Nature* **415,** 680–685 (2002).

9. Rosenberg, R., Burge, R. & Schneider, I. An estimation of the number of malaria sporozoites ejected by a feeding mosquito. *Trans. R. Soc. Trop. Med. Hyg.* **84,** 209–212 (1990).

10. Sidjanski, S. & Vanderberg, J. P. Delayed migration of Plasmodium sporozoites from the mosquito bite site to the blood. *Am. J. Trop. Med. Hyg.* **57,** 426–429 (1997).

11. Ponnudurai, T., Lensen, A. H. W., Vangemert, G. J. A., Bolmer, M. G. & Meuwissen, J. Feeding behavior and sporozoite ejection by infected *Anopheles stephensi*. *Trans. R. Soc. Trop. Med. Hyg.* **85,** 175–180 (1991).

12. SHIN, S. C. J., VANDERBERG, J. P. & TERZAKIS, J. A. Direct Infection of Hepatocytes by Sporozoites of Plasmodium berghei. *J. Protozool.* **29,** 448–454 (1982).

13. Prudêncio, M., Rodriguez, A. & Mota, M. M. The silent path to thousands of merozoites: the Plasmodium liver stage. *Nat. Rev. Microbiol.* **4,** 849–56 (2006).

14. Manzoni, G. *et al.* Plasmodium P36 determines host cell receptor usage during sporozoite invasion. *Elife* (2017).

15. Alexis Kaushansky, Alyse N. Douglass, Nadia Arang, V. V., Nicholas Dambrauskas, Heather S. Kain, L. S. A. & D. Noah Sather, S. H. I. K. Malaria parasites target the hepatocyte receptor EphA2 for successful host infection. **350,** 1089–1092 (2015).

16. Sturm, A. *et al.* Manipulation of host hepatocytes by the malaria parasite for delivery into liver sinusoids. *Science* **313,** 1287–90 (2006).

17. Klein, E. Y. Antimalarial drug resistance: A review of the biology and strategies to delay emergence and spread. *Int. J. Antimicrob. Agents* **41,** 311–317 (2013).

18. Triglia, T. *et al.* Identification of Proteins from Plasmodium falciparum That Are Homologous to Reticulocyte Binding Proteins in Plasmodium vivax. *Infect. Immun.* **69,** 1084–1092 (2001).

19. Chotivanich, K. *et al.* Parasite Multiplication Potential and the Severity of Falciparum Malaria Sasithon Pukrittayakamee , Sornchai Looareesuwan and Nicholas J . White Published by : Oxford University Press Stable URL : http://www.jstor.org/stable/30111445 Parasite Multiplicati. **181,** 1206–1209 (2000).

20. Cowman, A. F. & Crabb, B. S. Invasion of red blood cells by malaria parasites. *Cell* **124,** 755–766 (2006).

21. Lamour, S. D., Straschil, U., Saric, J. & Delves, M. J. Changes in metabolic phenotypes of Plasmodium falciparum in vitro cultures during gametocyte development. *Malar. J.* **13,** 468 (2014).

22. Eichner M Molineaux L, Collins WE, Jeffery GM, Dietz K, D. H. H. Genesis, sequestration and survival of Plasmodiumfalciparum gametocytes: parameter estimates from fitting a model to malaria therapy data. *Trans R Soc Trop Med Hyg* **95,** 497–501 (2001).

23. Kafsack, B. F. C., Rovira-graells, N., Clark, T. G. & Bancells, C. A transcriptional switch underlies commitment to sexual development in human malaria parasites. *Nature* **507,** 248–252 (2014).

24. Regev-Rudzki, N. *et al.* Cell-cell communication between malaria-infected red blood cells via exosome-like vesicles. *Cell* **153,** 1120–1133 (2013).

25. Billker, O., Shaw, M. K., Margos, G. & Sinden, R. E. The roles of temperature, pH and mosquito factors as triggers of male and female gametogenesis of Plasmodium berghei in vitro. *Parasitology* **115 (Pt 1,** 1–7 (1997).

26. Martin, S. K. Affecting of in Vitroâ € ” Cultivated Plasmodium Gametocytes. *Changes* **49,** 25–29 (1993).

27. Rosenberg, R. & Rungsiwongse, J. The number of sporozoites produced by individual malaria oocysts. *Am. J. Trop. Med. Hyg.* **45,** 574–577 (1991).

28. Olivier, M., Van Den Ham, K., Shio, M. T., Kassa, F. A. & Fougeray, S. Malarial Pigment Hemozoin and the Innate Inflammatory Response. *Front. Immunol.* **5,** 1–10 (2014).

29. Shio, M. T., Kassa, F. A., Bellemare, M. J. & Olivier, M. Innate inflammatory response to the malarial pigment hemozoin. *Microbes Infect.* **12,** 889–899 (2010).

30. Schofield, L. & Hackett, F. Signal transduction in host cells by a glycosylphosphatidylinositol toxin of malaria parasites. *J. Exp. Med.* **177,** 145–53 (1993).

31. Schofield, L. & Grau, G. E. Immunological processes in malaria pathogenesis. *Nat. Rev. Immunol.* **5,** 722–735 (2005).

32. Clark, I. A., Alleva, L. M., Budd, A. C. & Cowden, W. B. Understanding the role of inflammatory cytokines in malaria and related diseases. *Travel Med. Infect. Dis.* **6,** 67–81 (2008).

33. Lyke, K. E. *et al.* Serum Levels of the Proinflammatory IL-8 , IL-10 , Tumor Necrosis Factor Alpha , and IL-12 (p70) in Malian Children with Severe Plasmodium falciparum Malaria and Matched Uncomplicated Malaria or Healthy Controls. *Infect. Immun.* **72,** 5630–5637 (2004).

34. Day, N. P. *et al.* The prognostic and pathophysiologic role of pro- and antiinflammatory cytokines in severe malaria. *J. Infect. Dis.* **180,** 1288–1297 (1999).

35. Nemeth, E. *et al.* IL-6 mediates hypoferremia of inflammation by inducing the synthesis of the iron regulatory hormone hepcidin. *J. Clin. Invest.* **113,** 1271–1276 (2004).

36. Grigorakaki, C., Morceau, F., Chateauvieux, S., Dicato, M. & Diederich, M. Tumor necrosis factor alpha-mediated inhibition of erythropoiesis involves GATA-1/GATA-2 balance impairment and PU.1 over-expression. *Biochem. Pharmacol.* **82,** 156–166 (2011).

37. Miller, L. H., Baruch, D. I., Marsh, K. & Doumbo, O. K. The pathogenic basis of malaria. *Nature* **415,** 673–679 (2002).

38. Modiano, D. *et al.* Severe malaria in Burkina Faso: Influence of age and transmission level on clinical presentation. *Am. J. Trop. Med. Hyg.* **59,** 539–542 (1998).

39. Dal-Bianco, M. P. *et al.* High prevalence of asymptomatic Plasmodium falciparum infection in Gabonese adults. *Am. J. Trop. Med. Hyg.* **77,** 939–42 (2007).

40. Cohen, S., McGregor, I. & Carrington, S. Gamma-Globulin and Aquired Immunity to Human Malaria. *Nature* **192,** 733–737 (1961).

41. Hoffman, S. L. *et al.* Naturally Acquired Antibodies to Sporozoites do not Prevent Malaria : Vaccine Development Implications Mutuma Mugambi Published by : American Association for the Advancement of Science Stable URL : http://www.jstor.org/stable/1699461 REFERENCES Linked ref. (1987).

42. Sedegah, M. *et al.* Naturally acquired CD8 + cytotoxic T lymphocytes against the Plasmodium falciparum circumsporozoite protein . Information about subscribing to The Journal of Immunology is online at : Plasmodium fakiparum CIRCUMSPOROZOITE PROTEIN ’. *J. Immunol.* **149,** 966–971 (1992).

43. Leech, J. of a Family of Variable Proteins on Infected Erythrocytes. **168,** (1988).

44. Turner, L. *et al.* Severe malaria is associated with parasite binding to endothelial protein C receptor. *Nature* **498,** 502–5 (2013).

45. Goel, S. *et al.* RIFINs are adhesins implicated in severe Plasmodium falciparum malaria. *Nat. Med.* **21,** 314–317 (2015).

46. Makhtar Niang, Amy Kristine Bei, Kripa Gopal Madnani, Shaaretha Pelly, Selasi Dankwa, Usheer Kanjee, Karthigayan Gunalan, Anburaj Amaladoss, K. P. Y. & Ndeye Sakha Bob, Benoit Malleret, , Manoj Duraisingh, and P. R. P. The variant STEVOR protein of Plasmodium falciparum is a red cell binding protein important for merozoite invasion and rosetting. *Cell Host Microbe* **16,** 81–93 (2014).

47. Winter, G. *et al.* SURFIN is a polymorphic antigen expressed on Plasmodium falciparum merozoites and infected erythrocytes. *J. Exp. Med.* **201,** 1853–63 (2005).

48. Bull, Peter C., Lowe, B. Parasite antigens on the infected red cell surface are targets for naturally acquired immunity to malaria. *Nat. Publ. Gr.* **4,** 623–6 (1998).

49. Hviid, L. & Salanti, A. VAR2CSA and protective immunity against pregnancy-associated Plasmodium falciparum malaria. *Parasitology* **134,** 1871–1876 (2007).

50. Salanti, A. *et al.* Evidence for the involvement of VAR2CSA in pregnancy-associated malaria. *J. Exp. Med.* **200,** 1197–1203 (2004).

51. Frank, M. *et al.* Frequent recombination events generate diversity within the multi-copy variant antigen gene families of Plasmodium falciparum. *Int. J. Parasitol.* **38,** 1099–1109 (2008).

52. Claessens, A. *et al.* Generation of Antigenic Diversity in Plasmodium falciparum by Structured Rearrangement of Var Genes During Mitosis. *PLoS Genet.* **10,** (2014).

53. Tran, T. M. *et al.* Naturally acquired antibodies specific for plasmodium falciparum reticulocyte-binding protein homologue 5 inhibit parasite growth and predict protection from malaria. *J. Infect. Dis.* **209,** 789–798 (2014).

54. Osier, F. H. A. *et al.* Breadth and magnitude of antibody responses to multiple Plasmodium falciparum merozoite antigens are associated with protection from clinical malaria. *Infect. Immun.* **76,** 2240–2248 (2008).

55. Patel, S. D. *et al.* Plasmodium falciparum merozoite surface antigen, PfRH5, elicits detectable levels of invasion-inhibiting antibodies in humans. *J. Infect. Dis.* **208,** 1679–1687 (2013).

56. Joos, C. *et al.* Clinical protection from falciparum malaria correlates with neutrophil respiratory bursts induced by merozoites opsonized with human serum antibodies. *PLoS One* **5,** (2010).

57. Kumaratilake, L. M., Ferrante, A., Jaeger, T. & Rzepczyk, C. M. Effects of cytokines, complement, and antibody on the neutrophil respiratory burst and phagocytic response to Plasmodium falciparum merozoites. *Infect. Immun.* **60,** 3731–3738 (1992).

58. Boyle, M. J. *et al.* Human antibodies fix complement to inhibit plasmodium falciparum invasion of erythrocytes andare associated with protection against malaria. *Immunity* **42,** 580–590 (2015).

59. Xin-Li, P. & Horii, T. Complement-mediated killing of Plasmodium falciparum erythrocytic schizont with antibodies to the recombinant serine repeat antigen (SERA). *Vaccine* **16,** 1299–1305 (1998).

60. Kennedy, A. T. *et al.* Recruitment of Factor H as a Novel Complement Evasion

Strategy for Blood-Stage Plasmodium falciparum Infection. *J. Immunol.* 1501581 (2015). doi:10.4049/jimmunol.1501581

61. Weiss, G. E., Crabb, B. S. & Gilson, P. R. Overlaying Molecular and Temporal Aspects of Malaria Parasite Invasion. *Trends Parasitol.* **32,** 284–295 (2016).

62. Riglar, D. T. *et al.* Super-resolution dissection of coordinated events during malaria parasite invasion of the human erythrocyte. *Cell Host Microbe* **9,** 9–20 (2011).

63. Cowman, A. F., Berry, D. & Baum, J. The cellular and molecular basis for malaria parasite invasion of the human red blood cell. *J. Cell Biol.* **198,** 961–971 (2012).

64. Hermsen, C. C. *et al.* Glutamate-rich protein (GLURP) induces antibodies that inhibit in vitro growth of Plasmodium falciparum in a phase 1 malaria vaccine trial. *Vaccine* **25,** 2930–2940 (2007).

65. Chiu, C. Y. H. *et al.* Antibodies to the Plasmodium falciparum Proteins MSPDBL1 and MSPDBL2 Opsonize Merozoites, Inhibit Parasite Growth, and Predict Protection from Clinical Malaria. *J. Infect. Dis.* **212,** 406–415 (2015).

66. O'Donnell, R. a *et al.* Antibodies against merozoite surface protein (MSP)-1(19) are a major component of the invasion-inhibitory response in individuals immune to malaria. *J. Exp. Med.* **193,** 1403–1412 (2001).

67. Blackman, M. J., Scott-Finnigan, T. J., Shai, S. & Holder, a a. Antibodies inhibit the protease-mediated processing of a malaria merozoite surface protein. *J. Exp. Med.* **180,** 389–393 (1994).

68. Cowman, A. F. *et al.* Functional analysis of proteins involved in Plasmodium falciparum merozoite invasion of red blood cells. *FEBS Lett.* **476,** 84–88 (2000).

69. Holder, A. A. *et al.* A malaria merozoite surface protein (MSP1)-structure, processing and function. *Memorias do Instituto Oswaldo Cruz* **87 Suppl 3,** 37–42 (1992).

70. Das, S. *et al.* Processing of Plasmodium falciparum Merozoite Surface Protein MSP1 Activates a Spectrin-Binding Function Enabling Parasite Egress from RBCs. *Cell Host Microbe* **18,** 433–444 (2015).

71. Dasgupta, S. *et al.* Membrane-wrapping contributions to malaria parasite invasion of the human erythrocyte. *Biophys. J.* **107,** 43–54 (2014).

72. Gao, X., Gunalan, K., Yap, S. S. L. & Preiser, P. R. Triggers of key calcium signals during erythrocyte invasion by Plasmodium falciparum. *Nat. Commun.* **4,** 2862 (2013).

73. Weiss, G. E. *et al.* Revealing the Sequence and Resulting Cellular Morphology of Receptor-Ligand Interactions during Plasmodium falciparum Invasion of Erythrocytes. *PLoS Pathog.* **11,** 1–25 (2015).

74. Stubbs, J. *et al.* Molecular mechanism for switching of P. falciparum invasion pathways into human erythrocytes. *Science* **309,** 1384–1387 (2005).

75. Lamarque, M. *et al.* The RON2-AMA1 interaction is a critical step in moving junction-dependent invasion by apicomplexan parasites. *PLoS Pathog.* **7,** (2011).

76. Beeson, J. G. *et al.* Merozoite surface proteins in red blood cell invasion, immunity and vaccines against malaria. *FEMS Microbiol. Rev.* **40,** 343–372 (2016).

77. Cowman, A. F., Tonkin, C. J., Tham, W.-H. & Duraisingh, M. T. The Molecular Basis of Erythrocyte Invasion by Malaria Parasites. *Cell Host Microbe* **22,** 232–245 (2017).

78. Baruch, D. I. *et al.* Immunization of Aotus monkeys with a functional domain of the Plasmodium falciparum variant antigen induces protection against a lethal parasite line. *Proc. Natl. Acad. Sci. U. S. A.* **99,** 3860–3865 (2002).

79. Pombo, D. J. *et al.* Immunity to malaria after administration of ultra-low doses of red cells infected with Plasmodium falciparum. *Lancet* **360,** 610–617 (2002).

80. Peyerl-Hoffmann, G. *et al.* Genetic diversity of Plasmodium falciparum and its relationship to parasite density in an area with different malaria endemicities in West Uganda. *Trop. Med. Int. Heal.* **6,** 607–613 (2001).

81. Read, A. F. & Taylor, L. H. The Ecology of Genetically Diverse Infections. *Science (80-.).* **292,** 1099–1101 (2001).

82. Gupta, S., Snow, R. W., Donnelly, C. A., Marsh, K. & Newbold, C. Immunity to non-cerebral severe malaria is acquired after one or two infections. *Nat. Med.* **5,** 340–343 (1999).

83. Cham, G. K. K. *et al.* Sequential, ordered acquisition of antibodies to Plasmodium falciparum erythrocyte membrane protein 1 domains. *J. Immunol.* **183,** 3356–63 (2009).

84. Elias, S. C. *et al.* Assessment of immune interference, antagonism, and diversion following human immunization with biallelic blood-stage malaria viral-vectored vaccines and controlled malaria infection. *J. Immunol.* **190,** 1135–47 (2013).

85. Sheehy, S. H. *et al.* ChAd63-MVA-vectored Blood-stage Malaria Vaccines Targeting MSP1 and AMA1: Assessment of Efficacy Against Mosquito Bite Challenge in Humans. *Mol. Ther.* **20,** 2355–2368 (2012).

86. Forbes, E. K. *et al.* Europe PMC Funders Group Combining Liver- and Blood-Stage Malaria Viral Vectored Vaccines : Investigating Mechanisms of CD8 + T cell Interference1. **187,** 3738–3750 (2012).

87. Lau, C. K. Y. *et al.* Structural conservation despite huge sequence diversity allows EPCR binding by the pfemp1 family implicated in severe childhood malaria. *Cell Host Microbe* **17,** 118–129 (2015).

88. S., H. The New England Journal of Medicine Downloaded from nejm.org at the Bodleian Libraries of the University of Oxford on March 20, 2016. For personal use only. No other uses without permission. From the NEJM Archive. Copyright © 2010 Massachusetts Medical So. *N. Engl. J. Med.* **315,** 601–606 (1986).

89. Doolan, D. L., Houghten, R. A. & Good, M. F. Location of human cytotoxic T cell epitopes within a polymorphic domain of the Plasmodium falciparum circumsporozoite protein. *Int Immunol* **3,** 511–516 (1991).

90. Mordmüller, B. *et al.* Supplementary Sterile protection against human malaria by

chemoattenuated PfSPZ vaccine. *Nature* **1,** 1 (2017).

91. Khusmith, S., Sedegah, M. & Hoffman, S. L. Complete protection against Plasmodium yoelii by adoptive transfer of a CD8+ cytotoxic T-cell clone recognizing sporozoite surface protein 2. *Infect. Immun.* **62,** 2979–2983 (1994).

92. Epstein, J. E. *et al.* Live Attenuated Malaria Vaccine Designed to Protect Through Hepatic $CD8^+$ T Cell Immunity. *Science (80-.).* **334,** 475–80 (2011).

93. Hoffman, S. L. *et al.* Sporozoite Vaccine Induces Genetically Restricted T Cell Elimination of Malaria from Hepatocytes and W . Ripley Ballou Published by : American Association for the Advancement of Science Stable URL : http://www.jstor.org/stable/1704001 REFERENCES Linked re. *Science (80-.).* 1078–1081 (1989).

94. Hodgson, S. H. *et al.* Evaluation of the efficacy of ChAd63-MVA vectored vaccines expressing circumsporozoite protein and ME-TRAP against controlled human malaria infection in malaria-naive individuals. *J. Infect. Dis.* **211,** 1076–1086 (2015).

95. Bojang, K. A. *et al.* Efficacy of RTS,S/AS02 malaria vaccine against Plasmodium falciparum infection in semi-immune adult men in The Gambia: A randomised trial. *Lancet* **358,** 1927–1934 (2001).

96. Olotu, A. *et al.* Four-year efficacy of RTS,S/AS01E and its interaction with malaria exposure. *N. Engl. J. Med.* **368,** 1111–20 (2013).

97. Garçon, N., Heppner, D. G. & Cohen, J. Development of RTS,S/AS02: a purified subunit-based malaria vaccine candidate formulated with a novel adjuvant. *Expert Rev. Vaccines* **2,** 231–238 (2003).

98. Dinglasan, R. R. *et al.* Disruption of Plasmodium falciparum development by antibodies against a conserved mosquito midgut antigen. *Proc. Natl. Acad. Sci. U. S. A.* **104,** 13461–13466 (2007).

99. Zhang, G. *et al.* Anopheles midgut FREP1 mediates plasmodium invasion. *J. Biol. Chem.* **290,** 16490–16501 (2015).

100. Hillyer, J. F. Invertebrate Immunity. **708,** 316 (2010).

101. April M. Clayton, Yuemei Dong, and G. D. The Anopheles innate immune system in the defense against malaria infection. *J. Innate Immun.* **6,** 169–181 (2014).

102. Pradel, G. Proteins of the malaria parasite sexual stages: expression, function and potential for transmission blocking strategies. *Parasitology* **134,** 1911–1929 (2007).

103. Wu, Y. *et al.* Phase 1 trial of malaria transmission blocking vaccine candidates Pfs25 and Pvs 25 formulated with montanide ISA 51. *PLoS One* **3,** (2008).

104. Wickramarachchi, T., Devi, Y. S., Mohmmed, A. & Chauhan, V. S. Identification and characterization of a novel Plasmodium falciparum merozoite apical protein involved in erythrocyte binding and invasion. *PLoS One* **3,** (2008).

105. Wåhlin, B. *et al.* Human antibodies to a Mr 155,000 Plasmodium falciparum antigen efficiently inhibit merozoite invasion. *Proc. Natl. Acad. Sci. U. S. A.* **81,** 7912–7916

(1984).

106. Egan, A. F., Burghaus, P., Druilhe, P., Holder, A. A. & Riley, E. M. Human antibodies to the 19kDa C-terminal fragment of Plasmodium falciparum merozoite surface protein 1 inhibit parasite growth in vitro. *Parasite Immunol.* **21,** 133–139 (1999).

107. Pan, W. *et al.* Fusion of Two Malaria Vaccine Candidate Antigens Enhances Product Yield, Immunogenicity, and Antibody-Mediated Inhibition of Parasite Growth In Vitro. *J. Immunol.* **172,** 6167–6174 (2004).

108. Chen, E., Paing, M. M., Salinas, N., Sim, B. K. L. & Tolia, N. H. Structural and Functional Basis for Inhibition of Erythrocyte Invasion by Antibodies that Target Plasmodium falciparum EBA-175. *PLoS Pathog.* **9,** (2013).

109. Anders, R. F. *et al.* Immunisation with recombinant AMA-1 protects mice against infection with Plasmodium chabaudi. *Vaccine* **16,** 240–247 (1998).

110. Stowers, A. W. *et al.* Vaccination of monkeys with recombinant Plasmodium falciparum apical membrane antigen 1 confers protection against blood-stage malaria. *Infect. Immun.* **70,** 6961–6967 (2002).

111. Douglas, A. D. *et al.* A PfRH5-based vaccine is efficacious against heterologous strain blood-stage plasmodium falciparum infection in Aotus monkeys. *Cell Host Microbe* **17,** 130–139 (2015).

112. Escalante, a a, Lal, a a & Ayala, F. J. Genetic polymorphism and natural selection in the malaria parasite Plasmodium falciparum. *Genetics* **149,** 189–202 (1998).

113. Volkman, S. K. Excess Polymorphisms in Genes for Membrane Proteins in Plasmodium falciparum. *Science (80-.).* **298,** 216–218 (2002).

114. Policy, S. D. & Conway, D. J. Strong diversifying selection on domains of the Plasmodium falciparum apical membrane antigen 1 gene. *Genetics* **158,** 1505–1512 (2001).

115. Guevara Patiño, J. A., Holder, A. A., McBride, J. S. & Blackman, M. J. Antibodies that inhibit malaria merozoite surface protein-1 processing and erythrocyte invasion are blocked by naturally acquired human antibodies. *J. Exp. Med.* **186,** 1689–1699 (1997).

116. Mitchell, G. H. A merozoite vaccine effective against Plasmodium knowlesi malaria. *Nature* **248,** 81–82 (1974).

117. O'Donnell, R. a, Saul, a, Cowman, a F. & Crabb, B. S. Functional conservation of the malaria vaccine antigen MSP-119across distantly related Plasmodium species. *Nat. Med.* **6,** 91–95 (2000).

118. Ogutu, B. R. *et al.* Blood stage malaria vaccine eliciting high antigen-specific antibody concentrations confers no protection to young children in Western Kenya. *PLoS One* **4,** (2009).

119. Sirima, S. B. *et al.* A phase 2b randomized, controlled trial of the efficacy of the GMZ2 malaria vaccine in African children. *Vaccine* **34,** 4536–4542 (2016).

120. Sagara, I. *et al.* A randomized controlled phase 2 trial of the blood stage AMA1-C1/Alhydrogel malaria vaccine in children in Mali. *Vaccine* **27,** 3090–3098 (2009).

121. Payne, R. O. *et al.* Demonstration of the blood-stage plasmodium falciparum controlled human malaria infection model to assess efficacy of the p. falciparum apical membrane antigen 1 Vaccine, FMP2.1/AS01. *J. Infect. Dis.* **213,** 1743–1751 (2016).

122. Singh, S. *et al.* Immunity to recombinant Plasmodium falciparum merozoite surface protein 1 (MSP1): Protection in Aotus nancymai monkeys strongly correlates with anti-MSP1 antibody titer and in vitro parasite-inhibitory activity. *Infect. Immun.* **74,** 4573–4580 (2006).

123. Miura, K. *et al.* Comparison of Biological Activity of Human Anti-Apical Membrane Antigen-1 Antibodies Induced by Natural Infection and Vaccination. *J. Immunol.* **181,** 8776–8783 (2008).

124. Raj, D. K. *et al.* Antibodies to PfSEA-1 block parasite egress from RBCs and protect against malaria infection. **344,** 871–877 (2014).

125. Douglas, A. D. *et al.* The blood-stage malaria antigen PfRH5 is susceptible to vaccine-inducible cross-strain neutralizing antibody. *Nat. Commun.* **2,** 601 (2011).

126. Sony Reddy, K. *et al.* Bacterially expressed full-length recombinant Plasmodium falciparum RH5 protein binds erythrocytes and elicits potent strain-transcending parasite-neutralizing antibodies. *Infect. Immun.* **82,** 152–164 (2014).

127. Douglas, A. D. *et al.* Neutralization of Plasmodium falciparum Merozoites by Antibodies against PfRH5. *J. Immunol.* **192,** 245–258 (2014).

128. Chiu, C. Y. H. *et al.* Association of antibodies to Plasmodium falciparum reticulocyte binding protein homolog 5 with protection from clinical malaria. *Front. Microbiol.* **5,** 1–8 (2014).

129. Cecile Crosnier. Basigin is a receptor essential for erythrocyte invasion. **480,** 534–537 (2012).

130. Wright, K. E. *et al.* Structure of malaria invasion protein RH5 with erythrocyte basigin and blocking antibodies. *Nature* **515,** 427–430 (2014).

131. Favuzza, P. *et al.* Structure of the malaria vaccine candidate antigen CyRPA and its complex with a parasite invasion inhibitory antibody. *Elife* **6,** 1–21 (2017).

132. Chen, L. *et al.* Structural basis for inhibition of erythrocyte invasion by antibodies to plasmodium falciparum protein CyRPA. *Elife* **6,** 1–15 (2017).

133. Reddy, K. S. *et al.* Multiprotein complex between the GPI-anchored CyRPA with PfRH5 and PfRipr is crucial for Plasmodium falciparum erythrocyte invasion. *Proc. Natl. Acad. Sci.* **112,** 1179–1184 (2015).

134. Chen, L. *et al.* An egf-like protein forms a complex with pfrh5 and is required for invasion of human erythrocytes by plasmodium falciparum. *PLoS Pathog.* **7,** (2011).

135. Galaway, F. *et al.* P113 is a merozoite surface protein that binds the N terminus of Plasmodium falciparum RH5. *Nat. Commun.* **8,** 14333 (2017).

136. Volz, J. C. *et al.* Essential Role of the PfRh5/PfRipr/CyRPA Complex during Plasmodium falciparum Invasion of Erythrocytes. *Cell Host Microbe* **20,** 60–71 (2016).

137. Birkholtz, L.-M. *et al.* Heterologous expression of plasmodial proteins for structural studies and functional annotation. *Malar. J.* **7,** 197 (2008).

138. Mehlin, C. *et al.* Heterologous expression of proteins from Plasmodium falciparum: Results from 1000 genes. *Mol. Biochem. Parasitol.* **148,** 144–160 (2006).

139. Hjerrild, K. A. *et al.* Production of full-length soluble Plasmodium falciparum RH5 protein vaccine using a Drosophila melanogaster Schneider 2 stable cell line system. *Sci. Rep.* **6,** 30357 (2016).

140. Williams, A. R. *et al.* Enhancing Blockade of Plasmodium falciparum Erythrocyte Invasion: Assessing Combinations of Antibodies against PfRH5 and Other Merozoite Antigens. *PLoS Pathog.* **8,** (2012).

141. Ord, R. L. *et al.* A malaria vaccine candidate based on an epitope of the Plasmodium falciparum RH5 protein. *Malar. J.* **13,** 326 (2014).

142. Zenonos, Z. A. *et al.* Basigin is a druggable target for host-oriented antimalarial interventions. *J. Exp. Med.* **212,** 1145–51 (2015).

143. Igakura, T. *et al.* A Null Mutation in Basigin, an Immunoglobulin Superfamily Member, Indicates Its Important Roles in Peri-implantation Development and Spermatogenesis. *Dev. Biol.* **194,** 152–165 (1998).

144. Lee, C. L. *et al.* Identification of CD147 (basigin) as a mediator of trophoblast functions. *Hum. Reprod.* **28,** 2920–2929 (2013).

145. Igakura, T. *et al.* Roles of Basigin, a Member of the Immunoglobulin Superfamily, in Behavior as to an Irritating Odor, Lymphocyte Response, and Blood–Brain Barrier. *Biochem. Biophys. Res. Commun.* **224,** 33–36 (1996).

146. Deeg, H. J. *et al.* Treatment of steroid-refractory acute graft-versus-host disease with anti-CD147 monoclonal antibody ABX-CBL. *Blood* **98,** 2052–2059 (2001).

147. Roush, S. W. & Murphy, T. V. Historical comparisons of morbidity and mortality for vaccine-preventable diseases in the United States. *JAMA* **298,** 2155–2163 (2007).

148. Fenner, F. A successful eradication campaign. Global eradication of smallpox. *Rev. Infect. Dis.* **4,** 916–930 (1982).

149. Hanley, K. A. The double-edged sword: How evolution can make or break a live-attenuated virus vaccine. *Evolution (N. Y).* **4,** 635–643 (2011).

150. Macadam, A. J. *et al.* Reversion of the attenuated and temperature-sensitive phenotypes of the sabin type 3 strain of poliovirus in vaccinees. *Virology* **172,** 408–414 (1989).

151. Kew, O. M., Sutter, R. W., de Gourville, E. M., Dowdle, W. R. & Pallansch, M. A. Vaccine-Derived Polioviruses and the Endgame Strategy for Global Polio Eradication. *Annu. Rev. Microbiol.* **59,** 587–635 (2005).

152. Chanock, R. M., Jensen, K. & Parrott, R. H. Respiratory Syncytial Virus Disease in Infants. **89,** 422–434 (1969).

153. Delany, I., Rappuoli, R. & Seib, K. L. Vaccines, reverse vaccinology, and bacterial pathogenesis. *Cold Spring Harb. Perspect. Med.* **3,** (2013).

154. Plotkin, S. A. Vaccines: Correlates of Vaccine- Induced Immunity. *Clin. Infect. Dis.* **47,** 401–409 (2008).

155. Liao, H. *et al.* Founder Virus. **496,** 469–476 (2013).

156. Van Regenmortel, M. H. V. Basic research in HIV vaccinology is hampered by reductionist thinking. *Front. Immunol.* **3,** 1–19 (2012).

157. Zhang, L. *et al.* A rationally designed TNF-α epitope-scaffold immunogen induces sustained antibody response and alleviates collagen-induced arthritis in mice. *PLoS One* **11,** 1–15 (2016).

158. McLellan, J. S. *et al.* Design and characterization of epitope-scaffold immunogens that present the motavizumab epitope from respiratory syncytial virus. *J. Mol. Biol.* **409,** 853–866 (2011).

159. Pierce, B. G. *et al.* Structure-Based Design of Hepatitis C Virus Vaccines that Elicit Neutralizing Antibody Responses to a Conserved Epitope. *J. Virol.* JVI.01032-17 (2017). doi:10.1128/JVI.01032-17

160. Jardine, J. G. *et al.* Priming a broadly neutralizing antibody response to HIV-1 using a germline-targeting immunogen. *Science (80-.).* **349,** 156–161 (2015).

161. Jardine, J. *et al.* Rational HIV Immunogen Design to Target Specific Germline B Cell Receptors. *Science (80-.).* **340,** 711–716 (2013).

162. Scheid, J. F. *et al.* Antibodies That Mimic CD4 Binding. *Science (80-.).* **333,** 1633–1637 (2012).

163. Leaver-Fay, A. *et al.* Rosetta3: An object-oriented software suite for the simulation and design of macromolecules. *Methods Enzymol.* **487,** 545–574 (2011).

164. Masignani, V. *et al.* Vaccination against Neisseria meningitidis using three variants of the lipoprotein GNA1870. *J. Exp. Med.* **197,** 789–99 (2003).

165. Scarselli, M. *et al.* Rational Design of a Meningococcal Antigen Inducing Broad Protective Immunity. *Sci. Transl. Med.* **3,** 91ra62-91ra62 (2011).

166. Lanzavecchia, A., Frühwirth, A., Perez, L. & Corti, D. Antibody-guided vaccine design: Identification of protective epitopes. *Curr. Opin. Immunol.* **41,** 62–67 (2016).

167. Sampath, S. *et al.* Glycan Masking of Plasmodium vivax Duffy Binding Protein for Probing Protein Binding Function and Vaccine Development. *PLoS Pathog.* **9,** (2013).

168. Campeotto, I. *et al.* One-step design of a stable variant of the malaria invasion protein RH5 for use as a vaccine immunogen. *Proc. Natl. Acad. Sci.* **114,** 998–1002 (2017).

169. Coley, A. M. *et al.* Structure of the malaria antigen AMA1 in complex with a growth-inhibitory antibody. *PLoS Pathog.* **3,** 1308–1319 (2007).

170. Chen, E. *et al.* Broadly neutralizing epitopes in the Plasmodium vivax vaccine candidate Duffy Binding Protein. *Proc Natl Acad Sci U S A* **113,** 6–11 (2016).

171. Payne, R. O. *et al.* Human vaccination against RH5 induces neutralizing antimalarial antibodies that inhibit RH5 invasion complex interactions. **2,** 1–19 (2017).

172. William Trager, J. B. J. Cultivation of malaria parasites. *Nature* **273,** 621–622 (1978).

173. Miura, K. *et al.* Anti-apical-membrane-antigen-1 antibody is more effective than anti-42-kilodalton-merozoite-surface-protein-1 antibody in inhibiting Plasmodium falciparum growth, as determined by the in vitro growth inhibition assay. *Clin. Vaccine Immunol.* **16,** 963–968 (2009).

174. Walter, T. S. *et al.* Lysine Methylation as a Routine Rescue Strategy for Protein Crystallization. *Structure* **14,** 1617–1622 (2006).

175. Winn, M. D. *et al.* Overview of the CCP4 suite and current developments. *Acta Crystallogr. Sect. D Biol. Crystallogr.* **67,** 235–242 (2011).

176. McCoy, A. J. *et al.* Phaser crystallographic software. *J. Appl. Crystallogr.* **40,** 658–674 (2007).

177. Miura, K. *et al.* Development and characterization of a standardized ELISA including a reference serum on each plate to detect antibodies induced by experimental malaria vaccines. *Vaccine* **26,** 193–200 (2008).

178. Köhler, G. & Milstein, C. Continuous cultures of fused cells secreting antibody of predefined specificity. *Nature* **256,** 495–497 (1975).

179. Olsson, L. & Kaplan, H. S. Human-human hybridomas producing monoclonal antibodies of predefined antigenic specificity. *Proc. Natl. Acad. Sci. U. S. A.* **77,** 5429–31 (1980).

180. Winger, L., Winger, C., Shastry, P., Russello, A. & Longenecker, M. Efficient generation in vitro , from human peripheral blood cells , of monoclonal Epstein-Barr virus transformants producing specific antibody to a variety of antigens without prior deliberate immunization. **80,** 4484–4488 (1983).

181. Lee, E.-C. *et al.* Complete humanization of the mouse immunoglobulin loci enables efficient therapeutic antibody discovery. *Nat. Biotechnol.* **32,** 356–63 (2014).

182. Boutz, D. R. *et al.* Proteomic identification of monoclonal antibodies from serum. *Anal. Chem.* **86,** 4758–4766 (2014).

183. Wine, Y. *et al.* Molecular deconvolution of the monoclonal antibodies that comprise the polyclonal serum response. *Proc. Natl. Acad. Sci. U. S. A.* **110,** 2993–8 (2013).

184. McCafferty, J., Griffiths, a D., Winter, G. & Chiswell, D. J. Phage antibodies: filamentous phage displaying antibody variable domains. *Nature* **348,** 552–554 (1990).

185. Tiller, T. *et al.* Efficient generation of monoclonal antibodies from single human B cells by single cell RT-PCR and expression vector cloning. *J. Immunol. Methods* **329,** 112–124 (2008).

186. Smith, K., Garman, L. & Wrammert, J. Rapid generation of fully human monoclonal antibodies specific to a vaccinating antigen. *Nat. Protoc.* **4,** 372–384 (2009).

187. Mestas, J. & Hughes, C. C. W. Of Mice and Not Men: Differences between Mouse and Human Immunology. *J. Immunol.* **172,** 2731–2738 (2004).

188. Wahala, W. M. P. B. & de Silva, A. M. The human antibody response to dengue virus infection. *Viruses* **3,** 2374–2395 (2011).

189. Ala'Aldeen, D. A. A. *et al.* Immune Responses in Humans and Animals to Meningococcal Transferrin-Binding Proteins : Implications for Vaccine Design. **62,** 2984–2990 (1994).

190. Ewer, K. J. *et al.* Viral vectors as vaccine platforms: From immunogenicity to impact. *Curr. Opin. Immunol.* **41,** 47–54 (2016).

191. Hodgson, S. H. *et al.* Combining Viral Vectored and Protein-in-adjuvant Vaccines Against the Blood-stage Malaria Antigen AMA1: Report on a Phase 1a Clinical Trial. *Mol. Ther.* **22,** 1–13 (2014).

192. Sheehy, S. H. *et al.* Phase Ia Clinical Evaluation of the Plasmodium falciparum Blood-stage Antigen MSP1 in ChAd63 and MVA Vaccine Vectors. *Mol. Ther.* **19,** 2269–2276 (2011).

193. Nutt, S. L., Hodgkin, P. D., Tarlinton, D. M. & Corcoran, L. M. The generation of antibody-secreting plasma cells. *Nat. Rev. Immunol.* **15,** 160–171 (2015).

194. Chu, V. T. & Berek, C. The establishment of the plasma cell survival niche in the bone marrow. *Immunol. Rev.* **251,** 177–188 (2013).

195. Wrammert, J. *et al.* Rapid cloning of high-affinity human monoclonal antibodies against influenza virus. *Nature* **453,** 667–71 (2008).

196. Blanchard-rohner, G., Pulickal, A. S., Zijde, C. M. J. Der, Snape, M. D. & Pollard, A. J. Brief report Appearance of peripheral blood plasma cells and memory B cells in a primary and secondary immune response in humans IgG-PC IgA-PC IgM-PC IgG-MC. *Vaccine* **114,** 4998–5002 (2009).

197. Elias, S. C. *et al.* Analysis of human B-cell responses following ChAd63-MVA MSP1 and AMA1 immunization and controlled malaria infection. *Immunology* **141,** 628–644 (2014).

198. Wirths, S. & Lanzavecchia, A. ABCB1 transporter discriminates human resting naive B cells from cycling transitional and memory B cells. *Eur. J. Immunol.* **35,** 3433–3441 (2005).

199. Odendahl, M. *et al.* Generation of migratory antigen-specific plasma blasts and mobilization of resident plasma cells in a secondary immune response. *Blood* **105,** 1614–1621 (2005).

200. Jourdan, M. *et al.* and plasma cells including detailed phenotypic and molecular An in vitro model of differentiation of memory B cells into plasmablasts and plasma cells including detailed phenotypic and molecular characterization. **114,** 5173–5181 (2014).

201. Kaminski, D. A., Wei, C., Qian, Y., Rosenberg, A. F. & Sanz, I. Advances in human B cell phenotypic profiling. *Front. Immunol.* **3,** 1–15 (2012).

202. Mei, H. E. *et al.* Blood-borne human plasma cells in steady state are derived from mucosal immune responses. **113,** 2461–2469 (2009).

203. Oracki, S. A. *et al.* Plasma cell development and survival. *Immunol Rev* **237,** 140–159 (2010).

204. Li, M. Z. & Elledge, S. J. Harnessing homologous recombination in vitro to generate recombinant DNA via SLIC. *Nat. Methods* **4,** 251–256 (2007).

205. Gibson, D. G. *et al.* Enzymatic assembly of DNA molecules up to several hundred kilobases. *Nat. Methods* **6,** 343–5 (2009).

206. Hartley, J. L., Temple, G. F. & Brasch, M. A. DNA Cloning Using In Vitro Site-Specific Recombination. *Genome Res.* **10,** 1788–1795 (2000).

207. Quan, J. & Tian, J. Circular polymerase extension cloning. *Methods Mol. Biol.* **1116,** 103–117 (2014).

208. Isaacs, S. N. Vaccinia Virus and Poxyvirology. *Life Sci.* **531,** 588 (2009).

209. Kivi, G. *et al.* HybriFree: a robust and rapid method for the development of monoclonal antibodies from different host species. *BMC Biotechnol.* **16,** 2 (2016).

210. Backliwal, G. *et al.* Rational vector design and multi-pathway modulation of HEK 293E cells yield recombinant antibody titers exceeding 1 g/l by transient transfection under serum-free conditions. *Nucleic Acids Res.* **36,** (2008).

211. Jäger, V. *et al.* High level transient production of recombinant antibodies and antibody fusion proteins in HEK293 cells. *BMC Biotechnol.* **13,** 52 (2013).

212. Halliley, J. L. *et al.* NIH Public Access. *Vaccine* **28,** 3582–3587 (2011).

213. Slifka, M. K., Antia, R., Whitmire, J. K. & Ahmed, R. Humoral immunity due to long-lived plasma cells. *Immunity* **8,** 363–372 (1998).

214. Wang, X. *et al.* Circulating memory B cells and plasmablasts are associated with the levels of serum immunoglobulin in patients with ulcerative colitis. *J. Cell. Mol. Med.* **20,** 804–814 (2016).

215. Godoy-Lozano, E. E. *et al.* Lower IgG somatic hypermutation rates during acute dengue virus infection is compatible with a germinal center-independent B cell response. *Genome Med.* **8,** 23 (2016).

216. Ye, J., Ma, N., Madden, T. L. & Ostell, J. M. IgBLAST: an immunoglobulin variable domain sequence analysis tool. *Nucleic Acids Res.* **41,** 34–40 (2013).

217. Baum, J. *et al.* Reticulocyte-binding protein homologue 5 - An essential adhesin involved in invasion of human erythrocytes by Plasmodium falciparum. *Int. J. Parasitol.* **39,** 371–380 (2009).

218. Puschnik, A. *et al.* Correlation between Dengue-Specific Neutralizing Antibodies and Serum Avidity in Primary and Secondary Dengue Virus 3 Natural Infections in

Humans. *PLoS Negl. Trop. Dis.* **7,** 1–8 (2013).

219. Rosenfeld, R. *et al.* Improved antibody-based ricin neutralization by affinity maturation is correlated with slower off-rate values. *Protein Eng. Des. Sel.* 1–7 (2017). doi:10.1093/protein/gzx028

220. Steckbeck, J. D. *et al.* Kinetic Rates of Antibody Binding Correlate with Neutralization Sensitivity of Variant Simian Immunodeficiency Virus Strains Kinetic Rates of Antibody Binding Correlate with Neutralization Sensitivity of Variant Simian Immunodeficiency Virus Strains †. **79,** 12311–12320 (2005).

221. Kostolanský, F. *et al.* The strong positive correlation between effective affinity and infectivity neutralization of highly cross-reactive monoclonal antibody IIB4, which recognizes antigenic site B on influenza A virus haemagglutinin. *J. Gen. Virol.* **81,** 1727–1735 (2000).

222. Bachmann, M. F. The Role of Antibody Concentration and Avidity in Antiviral Protection. *Science (80-.).* **276,** 2024–2027 (1997).

223. van der Merwe, P. a & Barclay, a N. Analysis of cell-adhesion molecule interactions using surface plasmon resonance. *Curr. Opin. Immunol.* **8,** 257–261 (1996).

224. Almeida, P. *Proteins: Concepts in Biochemistry*. (Garland Science, 2016).

225. Houk, K. N., Leach, A. G., Kim, S. P. & Zhang, X. Binding Affinities of Host-Guest, Protein-Ligand, and Protein-Transition-State Complexes. *Angew. Chemie - Int. Ed.* **42,** 4872–4897 (2003).

226. Healer, J. *et al.* Allelic polymorphisms in apical membrane antigen-1 are responsible for evasion of antibody-mediated inhibition in Plasmodium falciparum. *Mol. Microbiol.* **52,** 159–168 (2004).

227. Binks, R. H. *et al.* Population genetic analysis of the Plasmodium falciparum erythrocyte binding antigen-175 (eba-175) gene. *Mol. Biochem. Parasitol.* **114,** 63–70 (2001).

228. Haste Andersen, P., Nielsen, M. & Lund, O. Prediction of residues in discontinuous B-cell epitopes using protein 3D structures. *Protein Sci.* **15,** 2558–67 (2006).

229. Huang, J. *et al.* Broad and potent HIV-1 neutralization by a human antibody that binds the gp41–gp120 interface. *Nature* **515,** 138–142 (2014).

230. Sauter, H. & Paige, C. J. Detection of normal B-cell precursors that give rise to colonies producing both kappa and lambda light immunoglobulin chains. *Proc. Natl. Acad. Sci. U. S. A.* **84,** 4989–93 (1987).

231. Shabanova, I. N., Terebova, N. S. & Sapozhnikov, G. V. XPS study of the influence of minute additions of carbon metal-containing nanoforms on the polymer structure. *J. Electron Spectros. Relat. Phenomena* **195,** 43–47 (2014).

232. Kleijn, J. & Norde, W. The adsorption of proteins from aqueous solution on solid surfaces. *Heterog. Chem. Rev.* 157–172 (1995).

233. Poulsen, T. R. *et al.* Limits for Antibody Affinity Maturation and Repertoire

Diversification in Hypervaccinated Humans. *J. Immunol.* **187,** 0–0 (2011).

234. Poulsen, T. R., Meijer, P.-J., Jensen, A., Nielsen, L. S. & Andersen, P. S. Kinetic, affinity, and diversity limits of human polyclonal antibody responses against tetanus toxoid. *J. Immunol.* **179,** 3841–3850 (2007).

235. Thorpe, I. F. & Brooks, C. L. Molecular evolution of affinity and flexibility in the immune system. *Proc. Natl. Acad. Sci. U. S. A.* **104,** 8821–8826 (2007).

236. Reddy, S. B. *et al.* Differences in affinity of monoclonal and naturally acquired polyclonal antibodies against Plasmodium falciparum merozoite antigens. *BMC Microbiol.* **15,** 133 (2015).

237. Casadevall, A. & Janda, A. Immunoglobulin isotype influences affinity and specificity. *Proc. Natl. Acad. Sci. U. S. A.* **109,** 12272–3 (2012).

238. Battifora, H. Assessment of antigen damage in immunohistochemistry: The vimentin internal control. *Am. J. Clin. Pathol.* **96,** 669–671 (1991).

239. Werner, M., Chott, A., Fabiano, A. & Battifora, H. Effect of Formalin Tissue Fixation and Processing on Immunohistochemistry. *Am. J. Surg. Pathol.* **24,** 1016 (2000).

240. Aniweh, Y., Gao, X., Gunalan, K. & Preiser, P. R. PfRH2b specific monoclonal antibodies inhibit merozoite invasion. *Mol. Microbiol.* **102,** 386–404 (2016).

241. Pluschke, G. *et al.* Antigen CyRPA as Candidate Malaria Vaccine -Infected Mice Designates the falciparum Plasmodium Passive Immunoprotection of Passive Immunoprotection of Plasmodium falciparum-Infected Mice Designates the CyRPA as Candidate Malaria Vaccine Antigen. *J. Immunol.* **188,** 6225–6237 (2012).

242. Maskus, D. J. *et al.* Characterization of a novel inhibitory human monoclonal antibody directed against Plasmodium falciparum Apical Membrane Antigen 1. *Sci. Rep.* **6,** 39462 (2016).

243. Moreno, R. *et al.* Rhoptry-associated protein 1-binding monoclonal antibody raised against a heterologous peptide sequence inhibits Plasmodium falciparum growth in vitro. *Infect. Immun.* **69,** 2558–2568 (2001).

244. Collins, C. R. *et al.* Fine mapping of an epitope recognized by an invasion-inhibitory monoclonal antibody on the malaria vaccine candidate apical membrane antigen 1. *J. Biol. Chem.* **282,** 7431–7441 (2007).

245. Schofield, L. *et al.* A rhoptry antigen of Plasmodium falciparum contains conserved and variable epitopes recognized by inhibitory monoclonal antibodies. *Mol. Biochem. Parasitol.* **18,** 183–195 (1986).

246. Azuma, H. *et al.* Robust expansion of human hepatocytes in Fah−/−/Rag2−/−/Il2rg−/− mice. *Nat. Biotechnol.* **25,** 903–910 (2007).

247. Koch, C. *et al.* T cell activation-associated epitopes of CD147 in regulation of the T cell response, and their definition by antibody affinity and antigen density. *Int. Immunol.* **11,** 777–786 (1999).

248. SAUL, A. Kinetic constraints on the development of a malaria vaccine. *Parasite*

Immunol. **9,** 1–9 (1987).

249. Kerr, J. S. & Wright, G. J. Avidity-based Extracellular Interaction Screening (AVEXIS) for the Scalable Detection of Low-affinity Extracellular Receptor-Ligand Interactions. *J. Vis. Exp.* 1–8 (2012). doi:10.3791/3881

250. Schmidt-ullrich, B. Y. R., Brown, J. & Whittle, H. ANTIBODIES TO THE SECRETING STAGE ANTIGEN Erythrocytes infected with Plasmodium schizonts , as well as the merozoites released by these cells , bear surface proteins of Mr 195 , 000-250 , 000 , depending on the parasite species (1-9). These proteins and. **163,** 179–188 (1986).

251. Mahdi Abdel Hamid, M. *et al.* Vaccination with Plasmodium knowlesi AMA1 formulated in the novel adjuvant co-vaccine HT^{TM} protects against blood-stage challenge in rhesus macaques. *PLoS One* **6,** (2011).

252. Kaneko, O., Soubes, S. C. & Miller, L. H. Plasmodium falciparum: invasion of Aotus monkey red blood cells and adaptation to Aotus monkeys. *Exp. Parasitol.* **93,** 116–119 (1999).

253. Thaithong, S. *et al.* Clonal diversity in a single isolate of the malaria parasite Plasmodium falciparum. *Trans. R. Soc. Trop. Med. Hyg.* **78,** 242–5 (1984).

254. Guiguemde, W. A. *et al.* Chemical genetics of Plasmodium falciparum. **465,** 311–315 (2010).

255. Baum, J., Pinder, M. & Conway, D. J. Erythrocyte invasion phenotypes of *Plasmodium falciparum* in The Gambia. *Infect. Immun.* **71,** 1856–63 (2003).

256. Duraisingh, M. T. *et al.* Phenotypic variation of Plasmodium falciparum merozoite proteins directs receptor targeting for invasion of human erythrocytes. *EMBO J.* **22,** 1047–1057 (2003).

257. Reed, M. B. *et al.* Targeted disruption of an erythrocyte binding antigen in Plasmodium falciparum is associated with a switch toward a sialic acid-independent pathway of invasion. *Proc. Natl. Acad. Sci.* **97,** 7509–7514 (2000).

258. Tham, W. H. *et al.* Antibodies to reticulocyte binding protein-like homologue 4 inhibit invasion of Plasmodium falciparum into human erythrocytes. *Infect. Immun.* **77,** 2427–2435 (2009).

259. Bustamante, L. Y. *et al.* A full-length recombinant Plasmodium falciparum PfRH5 protein induces inhibitory antibodies that are effective across common PfRH5 genetic variants. *Vaccine* **31,** 373–379 (2013).

260. Schlager, G. & Weibust, R. S. Selection for hematocrit percent in the house mouse. *J Hered* **67,** 295–299 (1976).

261. Klotz, F. W., Chulay, J. D., Daniel, W. & Miller, L. H. Invasion of mouse erythrocytes by the human malaria parasite, Plasmodium falciparum. *J. Exp. Med.* **165,** 1713–1718 (1987).

262. Bouharoun-Tayoun, H., Oeuvray, C., Lunel, F. & Druilhe, P. Mechanisms underlying the monocyte-mediated antibody-dependent killing of Plasmodium falciparum asexual

blood stages. *J. Exp. Med.* **182,** 409–418 (1995).

263. Ober, R. J., Radu, C. G., Ghetie, V. & Ward, E. S. Differences in promiscuity for antibody-FcRn interactions across species: implications for therapeutic antibodies. *Int. Immunol.* **13,** 1551–1559 (2001).

264. Whittle, J. R. R. *et al.* Broadly neutralizing human antibody that recognizes the receptor-binding pocket of influenza virus hemagglutinin. *Proc. Natl. Acad. Sci.* **108,** 14216–14221 (2011).

265. Kwong, P. D. *et al.* Structure of an HIV gp120 envelope glycoprotein in complex with the CD4 receptor and a neutralizing human antibody. *Nature* **393,** 648–659 (1998).

266. Nybakken, G. E. *et al.* Structural basis of West Nile virus neutralization by a therapeutic antibody. *Nature* **437,** 764–769 (2005).

267. McLellan, J. S. *et al.* Structure-Based Design of a Fusion Glycoprotein Vaccine for Respiratory Syncytial Virus. *Science (80-.).* **342,** 592–598 (2013).

268. Murin, C. D. *et al.* Structures of protective antibodies reveal sites of vulnerability on Ebola virus. *Proc. Natl. Acad. Sci.* **111,** 17182–17187 (2014).

269. Blout, E. R., de Lozé, C. & Asadourian, A. The Deuterium Exchange of Water-soluble Polypeptides and Proteins as Measured by Infrared Spectroscopy. *J. Am. Chem. Soc.* **83,** 1895–1900 (1961).

270. Bai, Y., Milne, J. S., Mayne, L. & Englander, S. W. Primary Structure Effects on Peptide Group Hydrogen Exchange. **17,** 75–86 (2012).

271. Back, J. W., De Jong, L., Muijsers, A. O. & De Koster, C. G. Chemical cross-linking and mass spectrometry for protein structural modeling. *J. Mol. Biol.* **331,** 303–313 (2003).

272. Matthews, B. W. X-ray Crystallographic Studies of Proteins. *Annu. Rev. Phys. Chem.* **27,** 493 (1976).

273. Chen, L. *et al.* Crystal structure of PfRh5, an essential P. falciparum ligand for invasion of human erythrocytes. *Elife* **3,** 1–10 (2014).

274. Scanlan, C. N., Offer, J., Zitzmann, N. & Dwek, R. A. Exploiting the defensive sugars of HIV-1 for drug and vaccine design. *Nature* **446,** 1038–1045 (2007).

275. Mallajosyula, V. V. A. *et al.* Influenza hemagglutinin stem-fragment immunogen elicits broadly neutralizing antibodies and confers heterologous protection. *Proc. Natl. Acad. Sci.* **111,** E2514–E2523 (2014).

276. Macraild, C. A., Richards, J. S., Anders, R. F. & Norton, R. S. Antibody Recognition of Disordered Antigens. *Structure* **24,** 148–157 (2016).

277. MacRaild, C. A. *et al.* Conformational dynamics and antigenicity in the disordered malaria antigen merozoite surface protein 2. *PLoS One* **10,** 1–18 (2015).

278. Klein-seetharaman, J. Isotope Labeling in Mammalian Cells. *Methods Mol. Biol.* **831,** 1–13 (2012).

279. Saxena, K. Isotope Labeling in Insect Cells. *Methods Mol. Biol.* **831,** 1–16 (2012).

280. Fernández, C. & Wider, G. TROSY in NMR studies of the structure and function of large biological macromolecules. *Curr. Opin. Struct. Biol.* **13,** 570–580 (2003).

281. Glaeser, R. M. & Hall, R. J. Reaching the information limit in cryo-EM of biological macromolecules: Experimental aspects. *Biophys. J.* **100,** 2331–2337 (2011).

282. Banerjee, S. *et al.* 2.3 A resolution cryo-EM structure of human p97 and mechanism of allosteric inhibition. *Science (80-.).* **351,** 871–875 (2016).

283. Lehár, J. *et al.* Synergistic drug combinations tend to improve therapeutically relevant selectivity. *Nat. Biotechnol.* **27,** 659–666 (2009).

284. Baeder, D. Y., Yu, G., Hozé, N., Rolff, J. & Regoes, R. R. Antimicrobial combinations: Bliss independence and Loewe additivity derived from mechanistic multi-hit models. *Philos. Trans. R. Soc. B Biol. Sci.* **371,** 20150294 (2016).

285. Berenbaum, M. . What is synergy? *Pharmacol. Rev.* **41,** 93–141 (1989).

286. Nwuba, R. I. *et al.* The Human Immune Response to Plasmodium falciparum Includes Both Antibodies That Inhibit Merozoite Surface Protein 1 Secondary Processing and Blocking Antibodies. *Infect. Immun.* **70,** 5328–5331 (2002).

287. Bustamante, L. Y. *et al.* Synergistic malaria vaccine combinations identified by systematic antigen screening. *Proc. Natl. Acad. Sci.* 201702944 (2017). doi:10.1073/pnas.1702944114

288. Pandey, A. K. *et al.* Identification of a potent combination of key plasmodium falciparum merozoite antigens that elicit strain-transcending parasite-neutralizing antibodies. *Infect. Immun.* **81,** 441–451 (2013).

289. Foote, J. & Eisen, H. N. Kinetic and affinity limits on antibodies produced during immune responses. *Proc. Natl. Acad. Sci. U. S. A.* **92,** 1254–6 (1995).

290. Santra, S. *et al.* Human Non-neutralizing HIV-1 Envelope Monoclonal Antibodies Limit the Number of Founder Viruses during SHIV Mucosal Infection in Rhesus Macaques. *PLoS Pathog.* **11,** 1–38 (2015).

291. Horwitz, J. A. *et al.* Non-neutralizing Antibodies Alter the Course of HIV-1 Infection In Vivo. *Cell* **170,** 637–648.e10 (2017).

292. Howell, K. A. *et al.* Cooperativity Enables Non-neutralizing Antibodies to Neutralize Ebolavirus. *Cell Rep.* **19,** 413–424 (2017).

293. Beernink, P. T. *et al.* Fine antigenic specificity and cooperative bactericidal activity of monoclonal antibodies directed at the meningococcal vaccine candidate factor H-binding protein. *Infect. Immun.* **76,** 4232–4240 (2008).

294. Malito, E. *et al.* Neisseria meningitidis factor H-binding protein bound to monoclonal antibody JAR5: implications for antibody synergy. *Biochem. J.* **473,** 4699–4713 (2016).

295. Duncan, a R. & Winter, G. The binding site for C1q on IgG. *Nature* **332,** 738–740

(1988).

296. Lozada, C. *et al.* Identification of C1q as the heat-labile serum cofactor required for immune complexes to stimulate endothelial expression of the adhesion molecules E-selectin and intercellular and vascular cell adhesion molecules 1. *Proc. Natl. Acad. Sci. U. S. A.* **92,** 8378–8382 (1995).

297. Moyle, W. R., Anderson, D. M. & Ehrllcht, P. H. A circular antibody-antigen complex is responsible for increased affinity shown by mixtures of monoclonal antibodies to human A CIRCULAR ANTIBODY-ANTIGEN COMPLEX I. *J. Immunol.* **131,** 1900–1905 (1983).

298. Goncalvez, A. P., Purcell, R. H. & Lai, C. J. Epitope determinants of a chimpanzee Fab antibody that efficiently cross-neutralizes dengue type 1 and type 2 viruses map to inside and in close proximity to fusion loop of the dengue type 2 virus envelope glycoprotein. *J Virol* **78,** 12919–12928 (2004).

299. Cummins, M. *et al.* Kinetic Characterization of a Panel of High-Affinity Monoclonal Antibodies Targeting Ricin and Recombinant Re-Formatting for Biosensor Applications. *Antibodies* **3,** 215–231 (2014).

300. Culp, T. D., Spatz, C. M., Reed, C. A. & Christensen, N. D. Binding and neutralization efficiencies of monoclonal antibodies, Fab fragments, and scFv specific for L1 epitopes on the capsid of infectious HPV particles. *Virology* **361,** 435–446 (2007).

301. Padiolleau-Lefevre, S. *et al.* Expression and detection strategies for an scFv fragment retaining the same high affinity than Fab and whole antibody: Implications for therapeutic use in prion diseases. *Mol. Immunol.* **44,** 1898–1906 (2007).

302. Björkelund, H., Gedda, L. & Andersson, K. Avoiding false negative results in specificity analysis of protein-protein interactions. *J. Mol. Recognit.* **24,** 81–89 (2011).

303. Tran, T. M., Portugal, S., Draper, S. J. & Crompton, P. D. Malaria Vaccines: Moving Forward After Encouraging First Steps. *Curr. Trop. Med. Reports* **2,** 1–3 (2015).

304. Hill, A., Biswas, S., Draper, S. & Rampling, T. Towards a multi-antigen multi-stage malaria vaccine. *Malar. J.* **Conference,** S7 (2014).

305. Osier, F. H. *et al.* New antigens for a multicomponent blood-stage malaria vaccine. *Sci. Transl. Med.* **6,** 247ra102-247ra102 (2014).

306. Boes, A. *et al.* Analysis of a multi-component multi-stage malaria vaccine candidate-tackling the cocktail challenge. *PLoS One* **10,** 1–20 (2015).

307. Uthaipibull, C. *et al.* Inhibitory and blocking monoclonal antibody epitopes on merozoite surface protein 1 of the malaria parasite Plasmodium falciparum. *J. Mol. Biol.* **307,** 1381–1394 (2001).

308. Moss, D. K. *et al.* Plasmodium falciparum 19-kilodalton merozoite surface protein 1 (MSP1)-specific antibodies that interfere with parasite growth In Vitro can inhibit MSP1 processing, merozoite invasion, and intracellular parasite development. *Infect. Immun.* **80,** 1280–1287 (2012).

309. Deal, C. *et al.* Vectored antibody gene delivery protects against Plasmodium

falciparum sporozoite challenge in mice. *Proc. Natl. Acad. Sci.* **111,** 12528–12532 (2014).

310. Johnson, P. R. *et al.* Vector-mediated gene transfer engenders long-lived neutralizing activity and protection against SIV infection in monkeys. *Nat. Med.* **15,** 901–906 (2009).

311. Haynes, B. F. & Verkoczy, L. Host Controls of HIV Neutralizing Antibodies. *Science (80-.).* **344,** 588–589 (2014).

312. Lippow, S. M., Wittrup, K. D. & Tidor, B. Computational design of antibody-affinity improvement beyond in vivo maturation. *Nat. Biotechnol.* **25,** 1171–1176 (2007).

313. Boder, E. T., Midelfort, K. S. & Wittrup, K. D. Directed evolution of antibody fragments with monovalent femtomolar antigen-binding affinity. *Proc. Natl. Acad. Sci.* **97,** 10701–10705 (2000).

314. Votsmeier, C. *et al.* Femtomolar Fab binding affinities to a protein target by alternative CDR residue co-optimization strategies without phage or cell surface display. *MAbs* **4,** 341–348 (2012).

315. Fukunaga, A. & Tsumoto, K. Improving the affinity of an antibody for its antigen via long-range electrostatic interactions. *Protein Eng. Des. Sel.* **26,** 773–780 (2013).

316. Wu, H. *et al.* Ultra-potent antibodies against respiratory syncytial virus: Effects of binding kinetics and binding valence on viral neutralization. *J. Mol. Biol.* **350,** 126–144 (2005).

317. Balazs, A. B. *et al.* Antibody-based protection against HIV infection by vectored immunoprophylaxis. *Nature* **481,** 81–84 (2011).

318. Wang, J. *et al.* A Human Bi-specific Antibody against Zika Virus with High Therapeutic Potential. *Cell* **171,** 229–241 (2017).